EJA

European Journal of Anatomy

Volume 28 - Number 4 July 2024

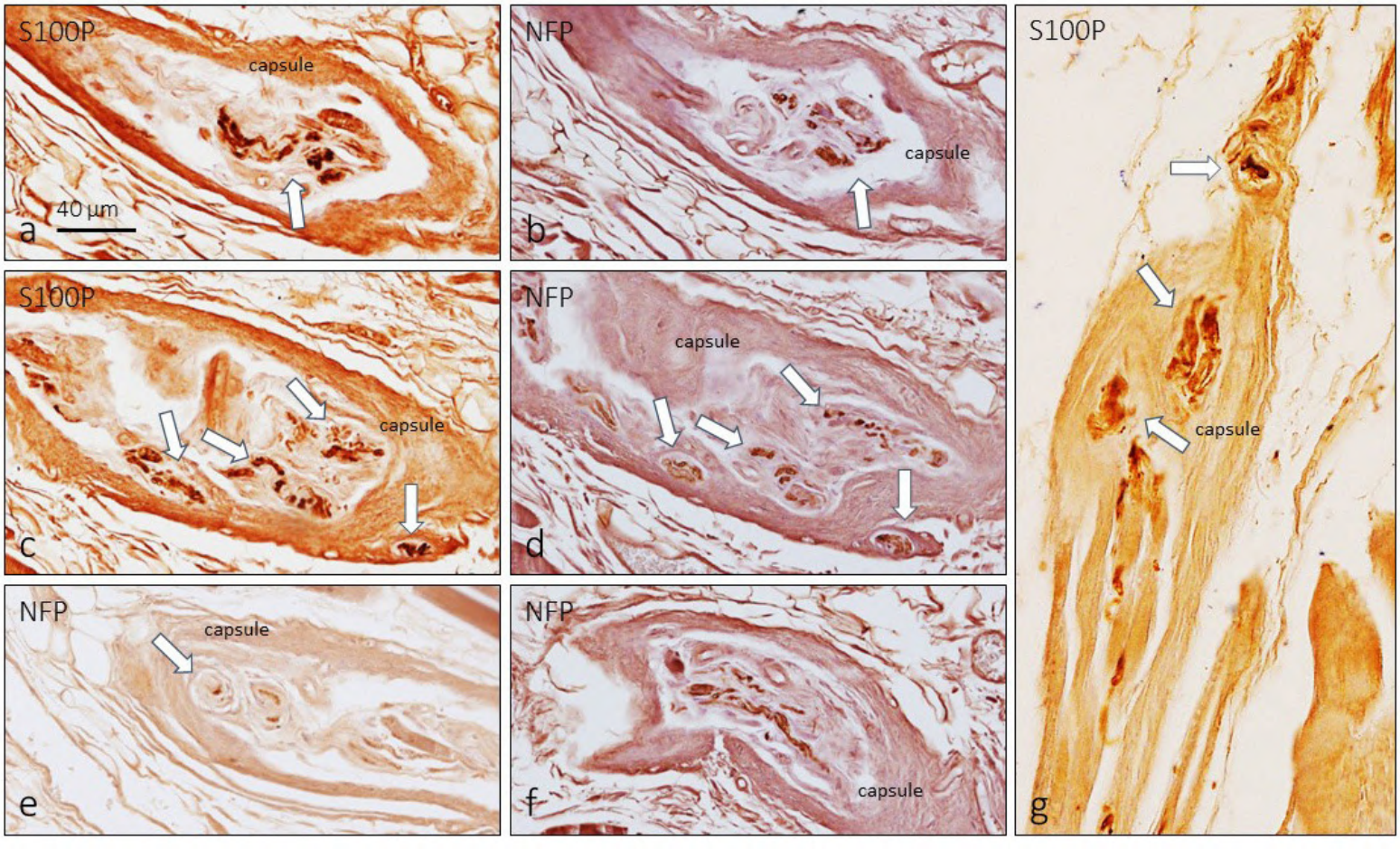

Indexed in:

CLARIVATE
- JCR:2020
- Q4 (21/23)
- I.F. J.C.I.: 0.19

DIALNET

EMBASE / Excerpta Medica

SCOPUS
- SJCR: 2020
- Q4 (31/39)
- I.F.: 0.162

Emerging Sources Citation Index

LATINDEX. Catálogo v1.0 (2002-2017)

Official Journal of the Spanish Society of Anatomy

Published by: **LOKI & DIMAS**

www.eurjanat.com

EJA
European Journal of Anatomy

Volume 28 - Number 4 July 2024

ORIGINAL ARTICLES

CASE REPORTS

REVIEW

Enhancing surgical expertise: 3D anatomy's role in residency programs

Arthur Defay[1], Jean Picquet[1], Henri-Dominique Fournier[2,3], Xavier Papon[1,2], Florian Bernard[2,3,4]

[1] *Vascular and Thoracic Surgery Department, University Hospital Angers, 49100, France*

[2] *Laboratory of Anatomy – Medical School –Angers, France*

[3] *Department of Neurosurgery, University Hospital, Angers, France*

[4] *CRCINA, UMR 1232 INSERM/CNRS and EA7315 team, Angers, France*

SUMMARY

Current virtual reality (VR) technology allows for the creation of instructional video formats that incorporate three-dimensional (3D) stereoscopic footage. Combined with 3D anatomic dissection, any surgical procedure or pathology can be represented virtually to supplement anatomical learning and surgical preoperative planning. The aim of this study was to evaluate the impact of virtual reality anatomical teaching. A prospective case-control study was performed. After a prerequisite anatomical knowledge assessment, participants were randomized in two groups: stereoscopic anatomical teaching program versus classic teaching with anatomical and surgical books of thoracic brachial outlet syndrome, and its related anatomy. Then, students completed a written anatomical test to assess their basic knowledge in vascular anatomy. Pre- and post-test performances were analyzed with independent t-tests for total score assessing basic anatomical knowledge, anatomical relationships and clinical inference.

Before performing the teaching, the 20 students included were homogenous in term of total exam mark in abdominal aorta (mean 78,78% vs 76,34%) and carotid artery evaluations (mean 78,57% vs 74,76%). After the course, there statistical differences ($p<0,05$) between the stereoscopic-3D.video group (n= 10, 90%) and classical-teaching group concerning the total exam mark, descriptive anatomy, anatomical relationships and clinical inference skills. All the students thought this method seemed indispensable to their anatomical training course (100%). The teaching video with 3D stereoscopy seems to be a useful and complementary teaching tool that is approved by the residents themselves. In a future study, it will be necessary to evaluate the contribution of this teaching in the long term.

Key words: Pedagogy – Vascular Surgery – Anatomy – 3D – Simulation

INTRODUCTION

Human anatomy is one of the fundamental disciplines of the medical curriculum. Its teaching combines lectures, dissections and commented illustrations and texts since the sixteenth centu-

Corresponding author:
Bernard Florian, MD. Department of Neurosurgery, CHU Angers, 49100, France. Laboratory of Anatomy, Medical School, 49100 Angers, France. Phone: +033680353917. E-mail: bernardflorian.bf@gmail.com

Submitted: November 6, 2023. **Accepted:** December 5, 2023

https://doi.org/10.52083/SOPF6039

ry and the work of Andreas Vesalius (Cobolet et al., 2014). 500 years later, teaching this specialty is a delicate undertaking. Almost all the anatomical learning is provided in the early stage of the medical curriculum (Bernard et al., 2020a). The students learn the basics without any clinical and surgical experience. At the beginning of residency, a second anatomical course is required to learn and practice surgery, such as vascular surgery. This includes a refresher course on surgical and clinical based-anatomy.

The recent growth of digital technologies offers new perspectives for medicine and the clinical follow-up of patients (Bernard et al., 2021; Satava et al., 1995), surgeries and surgical anatomical teaching (Bernard et al., 2019; Bernard et al., 2020b). Students can now view videos in 3D with their smartphones. The use of 3D stereoscopy is better than 2D to stimulate the student's visuospatial cognition (Bernard et al., 2018b; 2020b) and to learn anatomy (Bogomolova et al., 2020). We have shown in a previous study that this technology helps medical students to better understand anatomical relationships and clinical inference (Bernard et al., 2020a). The ability for students to visualize in 3D anywhere enables us to offer digital anatomo-surgical course tutorials on the go and challenge previous ways of accessing anatomical knowledge. In order to obtain certified anatomy videos, we undertook their production with residents, as well as anatomical and vascular teachers. These videos have been added as an extra tool to traditional teaching methods since 2016 at the University of Angers. The objective of this study is to evaluate the pedagogical value of 3D stereoscopic video compared to the traditional study method during residency.

In order to learn surgical anatomy, residents need to assist senior surgeons as often as possible. The repetition allows him/her to increase his/her mental representation of the surgery (Gimm et al., 2019; Sosa et al., 2007). Then, he/she can learn in the anatomical and/or simulation centre and perform surgeries step-by-step with the help of a mentor over a period of time (Scott et al., 2008). This teaching method is good, and many surgeons have been successfully trained this way. However, it has its limits, such as the need to find a "mentor" (Solorzano et al., 2010), to be in a reference university centre or to attend conferences with hidden costs (Miahi et al., 2019; Palazzo et al., 2016). Moreover, the increase of the number of residents accepted in the vascular surgery residency program raises the training issue, particularly as surgeries are scarce (too many residents for few surgeries). As a result, we have developed an anatomo-surgical 3D teaching program that can be displayed in a virtual-reality, mobile and web application. This application can be used in a pre-operative context. The aim of this study was to compare this approach to a traditional teaching method.

MATERIAL AND METHODS

Study design and population

This study is a prospective study conducted between September 2020 and June 2021. The study population is composed of surgical residents from the Faculty of Medicine in Angers and Nantes (France). All participating residents received anatomical instruction and dissection study during their medical curriculum.

3D stereoscopic clinical based anatomical video

A 3D video with French commentaries was developed to teach the anatomy of the thoracic brachial outlet, explaining its syndrome and its surgical treatment (available at https://youtu.be/UdmakWf7us4, supplemental video material 1). It could be watched via a 3D television, smartphone or virtual reality headsets in a VR, mobile and web app (AKIVI, Anatomical Knowledge in Virtual Immersion, www.AKIVI.fr). We set up a pedagogical committee to provide anatomical content that met the requirements of the first years of vascular surgery training. A resident (AD, first author) was also involved in the creation of this pedagogical resource at each step to meet students' and teachers' requirements.

Study protocol

Before the beginning of the session, the residents were divided into 2 main groups by randomization in order to minimize selection bias (Fig. 1). All the students in the study had previ-

ously completed cadaver dissection over a period of two weeks. The "video group" learnt from a 3D stereoscopic video and the "traditional methods group" or "book group" studied a selection of reference books. Before the teaching session, both groups completed an anatomical quiz to evaluate their knowledge of vascular surgical anatomy (Supplemental Materials 1 through 8). Two groups were subjected to different learning methods for a duration of 3 hours each. The first group, referred to as the "Video Group", engaged in learning through a 3D stereoscopic video, offering a potentially more immersive educational experience. Conversely, the "Traditional Methods Group (Book Group)", utilized a selection of reference books, adhering to conventional text-based learning approaches (*Atlas d'anatomie humaine*, Elsevier-Masson, 2021; Chaikof and Cambria, 2014; *Gray's Atlas d'anatomie humaine*, Elsevier-Masson, 2021). Both groups received an equal amount of study time, facilitating a comparative analysis of the effectiveness of immersive versus traditional

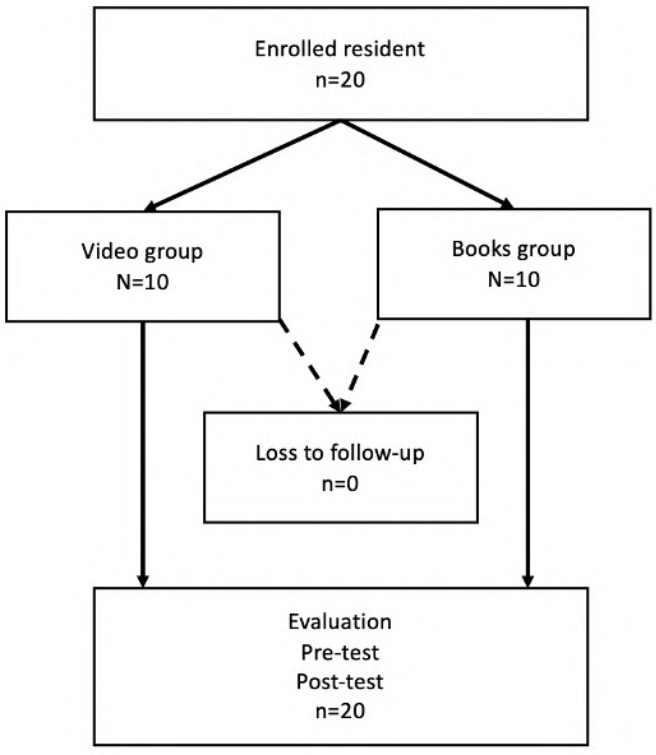

Fig. 1.- Cohort recruitment flowchart.

Table 1. Evaluation criteria for the video by residents using a Likert scale.

Q1	Do you find this teaching method easy to use
Q2	Does this teaching method seem similar to practicing it according to you
Q3	The possibility of reviewing the videos is a positive aspect of this method
Q4	The possibility of seeing dissections outside an anatomy laboratory is a positive point of this method
Q5	The possibility to see 3-dimensional dissections and to see the relationships and depth between organs is a positive aspecy of this method
Q6	The ability to see the surgery with commentary from the surgeon's point of view is a positive aspect of this method
Q7	Does this method (visible on mobile, computer, virtual reality glasses) seem indispensable to you in your anatomical training course
Q8	"I learned more with the help of the 3D video than during the practical dissection work dissection".
Q9	"I preferred virtual visualizations to cadaver dissections".

learning methods. Then, the students answered questions about the thoracic brachial outlet one month later. The video group also completed a satisfaction questionnaire about the 3D experience (Table 1). This quiz was not mandatory for the students. By agreeing to take it, the students agreed to participate in the study. Each student was evaluated individually.

3D students feedback

After watching the video, the students in the video group completed a 5-point Likert scale evaluation form ("strongly disagree", "somewhat agree", "don't know", "somewhat agree" and "strongly agree"). They also had the opportunity to select positive and negative aspects of the video.

Knowledge evaluated	Questions	Type
Descriptive anatomy	Q1 – Legend 1 = Internal carotid artery	R/W
	Q2 – Legend 2 = Common carotid artery	R/W
	Q3 – Legend 3 = External carotid artery	R/W
	Q4 – Legend 4 = Vagus nerve	R/W
	Q5 – Legend 5 = Inferior thyroid artery	R/W
	Q6 - Legend 1 = Internal carotid artery	R/W
	Q7 - Legend 2 = Sternocleidomastoid muscle	R/W
	Q8 - Legend 3 = Homohyoid muscle	R/W
	Q9 - Legend 4 = External carotid artery	R/W
	Q10 - Legend 5 = Common Carotid artery	R/W
Anatomical relationships	Q11 - The carotid bifurcation corresponds to the division of the common carotid artery into the internal and external carotid arteries.	R/W
	Q12 - The carotid bifurcation is located above the sternocleidomastoid muscle.	R/W
	Q13 - The sternocleidomastoid muscle divides the cervical region into an anterior and a lateral region.	R/W
	Q14 - The carotid bifurcation is located at the level of the 3rd cervical vertebra.	R/W
	Q15 - The right and left carotid bifurcations are similar.	R/W
	Q16 - The carotid bifurcation is located in a triangular muscle space.	R/W
	Q17 - The sternocleidomastoid, homohyoid and digastric muscles help to identify the carotid bifurcation.	R/W
	Q18 - The external carotid artery is anteromedial to the carotid bulb.	R/W
	Q19 - The internal carotid artery is posterolateral to the carotid bulb.	R/W
	Q20 - The four previous propositions are correct.	R/W
	Q21 - The internal carotid artery has an extracranial and intracranial course.	R/W
	Q22 - The internal carotid does not have any collaterals in its cervical portion.	R/W
	Q23 - The internal carotid artery vascularises the cervico-facial region.	R/W
	Q24 - The superior thyroid artery is a collateral branch of the internal carotid.	R/W
	Q25 - The internal carotid artery arises from the carotid bulb.	R/W
	Q26 - The internal jugular vein is located laterally to the carotid axis.	R/W
	Q27 - The thyro-lingual-facial venous trunk is a branch of the external jugular vein.	R/W
	Q28 - The X nerve or vagus nerve is anterior to the vascular axis of the neck.	R/W
	Q29 - The XII nerve or hypoglossal nerve may cross anteriorly to the carotid bifurcation.	R/W
	Q30 - The carotid glomus is dissected to release the origin of the internal carotid artery.	R/W
Reasoning, physiopathology, clinical outcomes	Q31 - Carotid massage can lead to syncope.	R/W
	Q32 - The carotid bifurcation is an area of curage in cancers of the cervical region.	R/W
	Q33 - A carotid murmur may be related to carotid stenosis.	R/W
	Q34 - Internal carotid surgery is indicated for internal carotid stenosis greater than 70%.	R/W
	Q35 - Angioscanner and echodoppler are examinations to assess carotid stenosis.	R/W
	Q36 - Carotid clamping during endarterectomy may damage the vagus nerve.	R/W
	Q37 - Carotid dissection above the bifurcation may damage the hypoglossal nerve.	R/W
	Q38 - As the hypoglossal nerve passes posteriorly and medially, it may be injured in the event of carotid clamping.	R/W
	Q39 - The presence of intracranial collaterals of the internal carotid artery allows carotid clamping to be performed with clinical or paraclinical monitoring of cerebral perfusion.	R/W
	Q40 - Postoperative haematoma after endarterectomy may be due to the presence of small perforating branches emerging from the common carotid artery	R/W
	Q41 - Preoperatively for an endarteriectomy, it is necessary to ensure that the patient is on antiplatelet therapy, that he has had two paraclinical imaging examinations (ultrasound, CT and/or MRI), as well as an ENT examination to look for vocal cord paralysis.	R/W
	Q42 - Surgically the posterior belly of the digastric muscle borders the carotid region above.	R/W

Supplemental material 1. Anatomical evaluation of carotid artery. R/W: right/wrong items.

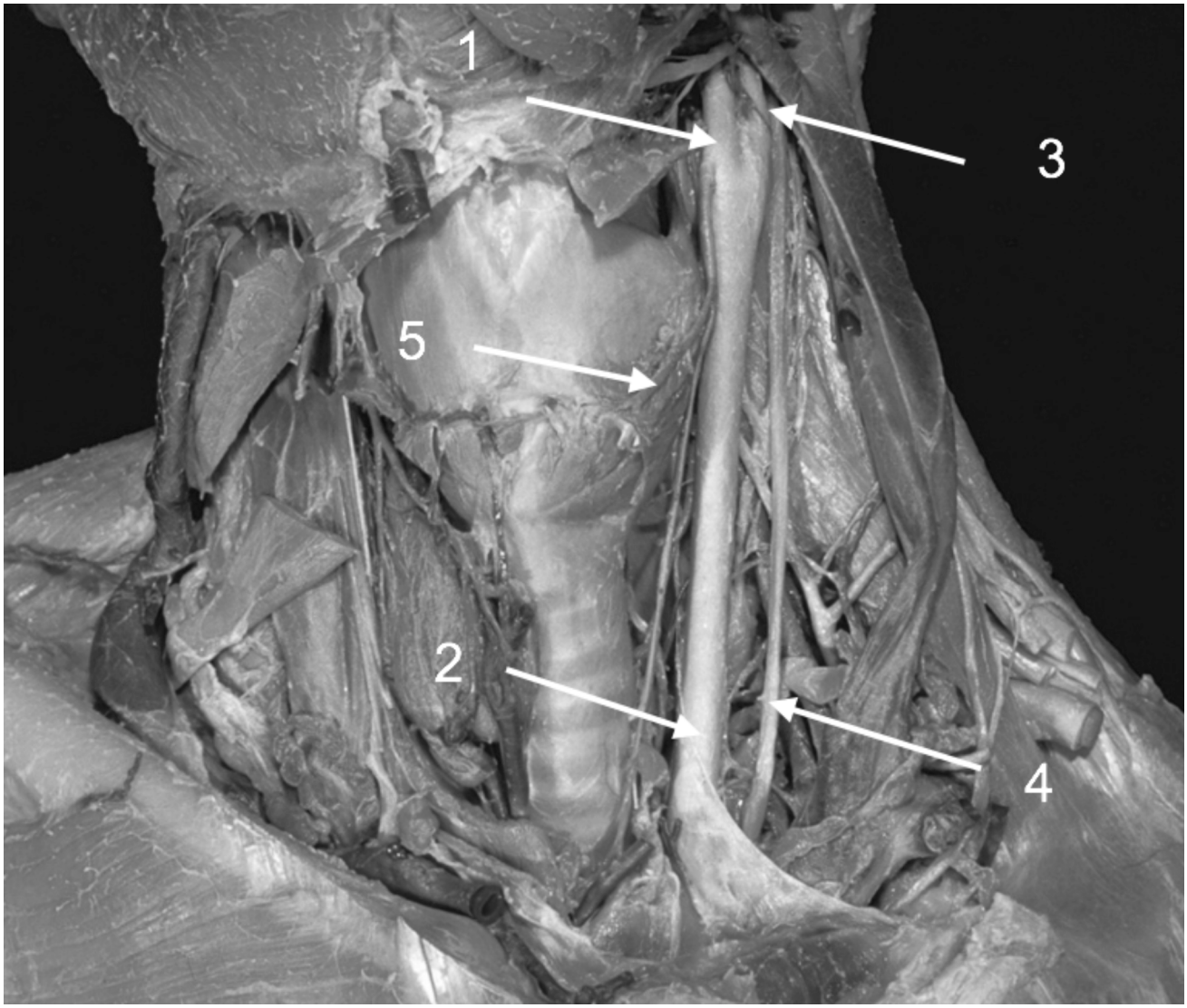

Supplemental material 2. Anatomical view of carotid artery (Q1-Q5) from David Lee Basset stereoscopic Atlas. Creative Commons Attribution-Noncommercial-Share Alike 3.0 United States License.

Pre- and post-course testing

This pedagogical approach aims to help students achieve the acquisition of anatomical knowledge and understanding of vascular anatomy and its surrounding structures. The quiz consisted of several multiple-choice questions (MCQs). The post-test in this study took place one month after the participants studied the material using the video or the book. This timing was chosen to evaluate the long-term retention of knowledge gained through the different learning methods. According to the pedagogical committee, three key skills had to be evaluated: fundamental knowledge, structural relationships in space, and clinical and surgical relevance (Table 2). The same quiz on the above topics was given to both groups. For each group, an average score out of 100 was calculated for each question, as well as the percentage of correct answers.

Several precautions were taken to minimize possible biases in the analysis: (A) all data were collected using designated serial numbering without any identifying information; (B) all exams were analysed by an anatomist who was not involved in the teaching phase of the study, did not know the students and was blind to the students' designated group; (C) the resident who contributed to the design of the pedagogical videos did not participate in the delivery of the instructional sessions or the evaluation process, to prevent any potential influence on the study outcomes or the opinions of other participants. Data analysis was performed in SPSS (version 17.0). Paired t-tests were used to compare pre- and post-test perfor-

Table 2. Anatomical evaluation of thoracic brachial outlet. R/W right / wrong items.

Knowledge evaluated	Questions	Type
Descriptive anatomy	Q1 - Legend 1 = Clavicle	R/W
	Q2 - Legend 2 = Subclavian muscle	R/W
	Q3 - Legend 3 = Subclavian vein	R/W
	Q4 - Legend 4 = Axillary artery	R/W
	Q5 - Legend 5 = Brachial plexus	R/W
	Q6 - Legend 1 = Right common carotid artery	R/W
	Q7 - Legend 2 = Subclavian artery	R/W
	Q8 - Legend 3 = Pectoralis major muscle	R/W
	Q9 - The clavicle is severed.	R/W
	Q10 - The first rib is not visible on this view.	R/W
	Q11 - The cervical thoracic brachial outlet is defined by 4 successive spaces.	R/W
	Q12 - The scalene pathway is part of the cervical thoracic brachial pathway.	R/W
	Q13 - The costo-clavicular canal is part of the thoracic brachial outlet.	R/W
	Q14 - The supra pectoral tunnel is part of the thoracic brachial parade.	R/W
	Q15 - The humeral neck is part of the thoracic brachial outlet.	R/W
Anatomical relationships	Q16 - The costoclavicular canal is located between the distal part of the clavicle and the first rib.	R/W
	Q17 - The anterior and middle scalene muscles are elements of the costoclavicular canal.	R/W
	Q18 - The subclavian vein is medial to the subclavian artery.	R/W
	Q19 - The subclavian artery lies outside the C8T1 nerve roots.	R/W
	Q20 - The subclavian muscle passes in front of the lower surface of the clavicle.	R/W
Reasoning, physiopathology, clinical outcomes	Q21 - Thoracic brachial outlet syndrome is a chronic pain syndrome.	R/W
	Q22 - The thoracic outlet syndrome has a dynamic component.	R/W
	Q23 - The thoracic brachial outlet syndrome is caused by compression of the vascular and nervous structures.	R/W
	Q24 - The costo clavicular canal is part of the thoracic brachial outlet.	R/W
	Q25 - Resection of the clavicle is one of the treatments for thoracic brachial outlet syndrome.	R/W
	Q26 - Resection of the first rib is the gold standard surgical treatment for thoracic brachial outlet syndrome.	R/W
	Q27 - The section of the pectoralis minor muscle can be associated with the resection of the first rib.	R/W
	Q28 The Roos axillary approach allows for resection of the first rib.	R/W
	Q29 The Roos axillary approach passes in front of the pectoralis minor muscle.	R/W
	Q30 None of the four previous proposals is correct.	R/W

mance. Between-group performance and demographic comparisons at baseline were analysed using independent t-tests. A p-value of less than 0.05 was considered significant. The data analysis was conducted in SPSS (version 17.0). Descriptive statistics were presented in the form of frequencies and percentages.

Role of funding source

The AKIVI project was supported by University of Angers' Health Department and its 3D-lab, the Pays de la Loire Department Council and SATT oust valorisation. This funding made possible the production of the videos and the creation of the application.

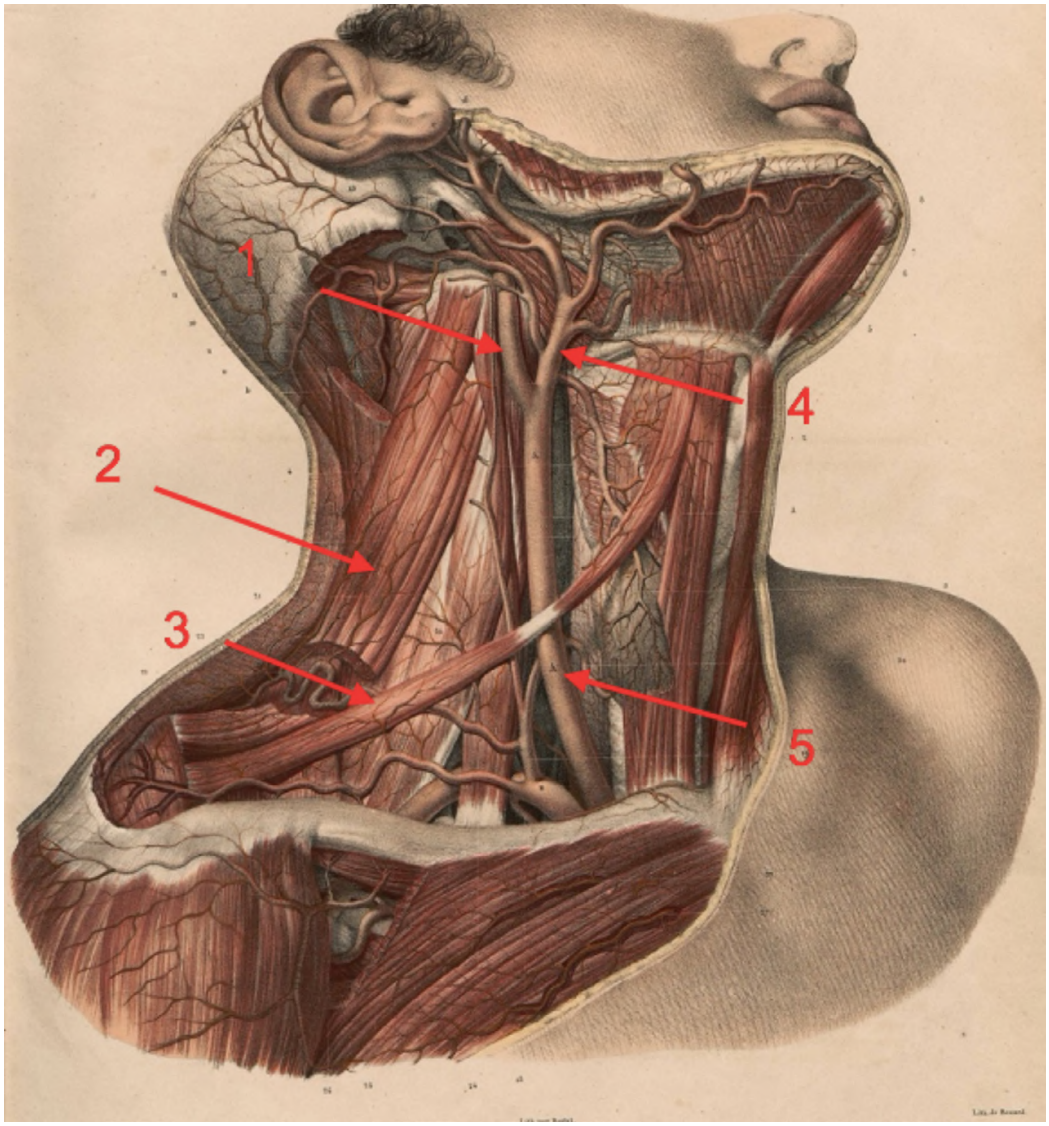

Supplemental material 3. Anatomical view of the carotid artery (Q6-Q10) Illustration for Traité complet de l'anatomie de l'homme comprenant la médecine opératoire (1831-1854) by Jean-Baptiste Marc Bourgery. Public domain.

RESULTS

Population

A total of 20 residents were enrolled in the study and successfully completed the course in the laboratory of Angers, France. All participants were surgical residents. All completed the study and followed up. The video group and books group were each composed of 10 residents who completed the first cycle of medical studies in different French universities. They were residents in different surgical specialties. Among the residents in the video group, there were 6 males and 4 females from Angers (n=3), Nantes (n=1), Marseille (n=1), Paris, (n=1), Caen (n=1), Toulouse (n=1), Amiens (n=1) and Reims (n=1). In this group, there were two vascular surgery residents (2nd and 3rd year), two visceral surgery residents (2nd and 3rd year), one maxillofacial surgery resident (1st year), one ophthalmology resident (1st year), two orthopedics surgery residents (1st and 5th year), one ENT surgery resident (4th year) and one urological surgery resident (1st year). Among the book group, there were 5 males and 5 females from Angers (n=2), Nantes (n=1), Paris (n=2), Rennes (n=1), Poitiers (n=1), Caen (n=1), Toulouse (n=1) and Bordeaux (n=1). In this group, there were two vascular surgery residents (two in 1st year), two thoracic and cardiovascular surgery residents (1st and 3rd year), two visceral surgery residents (2nd and 3rd year), one neurosurgery resident (1st year), one gynaecology-obstetrics resident (4th year), one ENT surgery resident (2nd year), and one urological surgery resident (2nd year).

Knowledge evaluated	Questions	Type
Descriptive anatomy	Q1 – Legend 1 = Celiac trunk	R/W
	Q2 – Legend 2 = Inferior vena cava	R/W
	Q3 – Legend 3 = Left Primitive Iliac Artery	R/W
	Q4 – Legend 4 = Left internal iliac artery	R/W
	Q5 – Legend 5 = Right external iliac artery	R/W
	Q6 - Legend 1 = Sub-renal aorta	R/W
	Q7 - Legend 2 = Urethra	R/W
	Q8 - Legend 3 = Iliac muscle	R/W
	Q9 - Legend 4 = Left renal artery	R/W
	Q10 Legend 5 = Inferior mesenteric artery	R/W
	Q11 - The abdominal aorta gives rise to parietal, visceral and urogenital collaterals.	R/W
	Q12 - The subrenal abdominal aorta gives rise to the lumbar arteries.	R/W
	Q13 - Each common iliac artery divides into an internal iliac artery and an external iliac artery.	R/W
	Q14 - The external iliac artery vascularises the pelvic viscera.	R/W
	Q15 - The inferior phrenic arteries are collaterals of the subrenal abdominal aorta.	R/W
Anatomical relationships	Q16 - The aorta enters the abdomen at the level of the T12 vertebra.	R/W
	Q17 - The abdominal aorta is retroperitoneal and follows the right edge of the vertebral bodies.	R/W
	Q18 - The abdominal aorta divides, at the level of the L4 vertebra, into the common iliac arteries.	R/W
	Q19 - The median sacral artery arises at the level of the subrenal abdominal aorta termination.	R/W
	Q20 - The celiac trunk arises at the anterior aspect of the abdominal aorta above the superior mesenteric artery.	R/W
	Q21 - The celiac trunk gives three branches: hepatic artery, splenic artery and left gastric artery.	R/W
	Q22 - The superior mesenteric artery arises at the posterior aspect of the abdominal aorta.	R/W
	Q23 - The inferior mesenteric artery arises from the anterior aspect of the abdominal aorta at the level of the L5 vertebra.	R/W
	Q24 - The arcade of Riolan is an anastomotic network between the superior mesenteric artery and the inferior mesenteric artery.	R/W
	Q25 - The renal arteries arise on the lateral aspect of the abdominal aorta on either side in L1.	R/W
	Q26 - They have a generally horizontal course, slightly oblique downwards and outwards.	R/W
	Q27 - The gonadal arteries arise on the anterolateral aspect of the abdominal aorta above the renal arteries.	R/W
	Q28 - The sub-renal abdominal aorta passes in front of the anterior common vertebral ligament.	R/W
	Q29 - Both the kidneys and the subrenal abdominal aorta are in a retroperitoneal position.	R/W
	Q30 - Surgery on the subrenal abdominal aorta requires opening the root of the mesentery to mobilise the intraperitoneal contents	R/W
	Q31 - The suprarenal aorta approach is more complex as it requires approaching the duodenopancreatic block via the retroperitoneal route	R/W
	Q32 - Aortic prosthesis in the management of a subrenal aneurysm can lead to phrenic artery ischaemia resulting in ventilatory failure	R/W
	Q33 - The approach to the sub-renal aorta is easier on the right side	R/W
	Q34 - Aortic prosthesis in the management of a sub-renal aneurysm can lead to ischaemia of the superior mesenteric arteries resulting in mesenteric ischaemia	R/W
Reasoning, physiopathology, clinical outcomes	Q35 - Ischaemia of the lumbar arteries can lead to necrosis of the surrounding skin	R/W
	Q36 - Ischaemia of the lumbar arteries can lead to paraplegia	R/W
	Q37 - The superior mesenteric artery passes in front of the right renal vein which explains the risk of varicocele	R/W
	Q38 - Superior mesenteric artery syndrome can result in renal failure	R/W
	Q39 - Compression of the left common iliac vein by the right common iliac artery is possible due to the anatomy of the aortic bifurcation: this is Cockett's syndrome (or May-Thurner syndrome)	R/W
	Q40 - Surgery on the aortic bifurcation may result in retrograde ejaculation due to damage to the superior hypogastric plexus	R/W
	Q41 - The left genital vein may be ligated and then cut during a retroperitoneal approach	R/W

Supplemental material 4. Anatomical evaluation of abdominal aorta. R/W: right/wrong items.

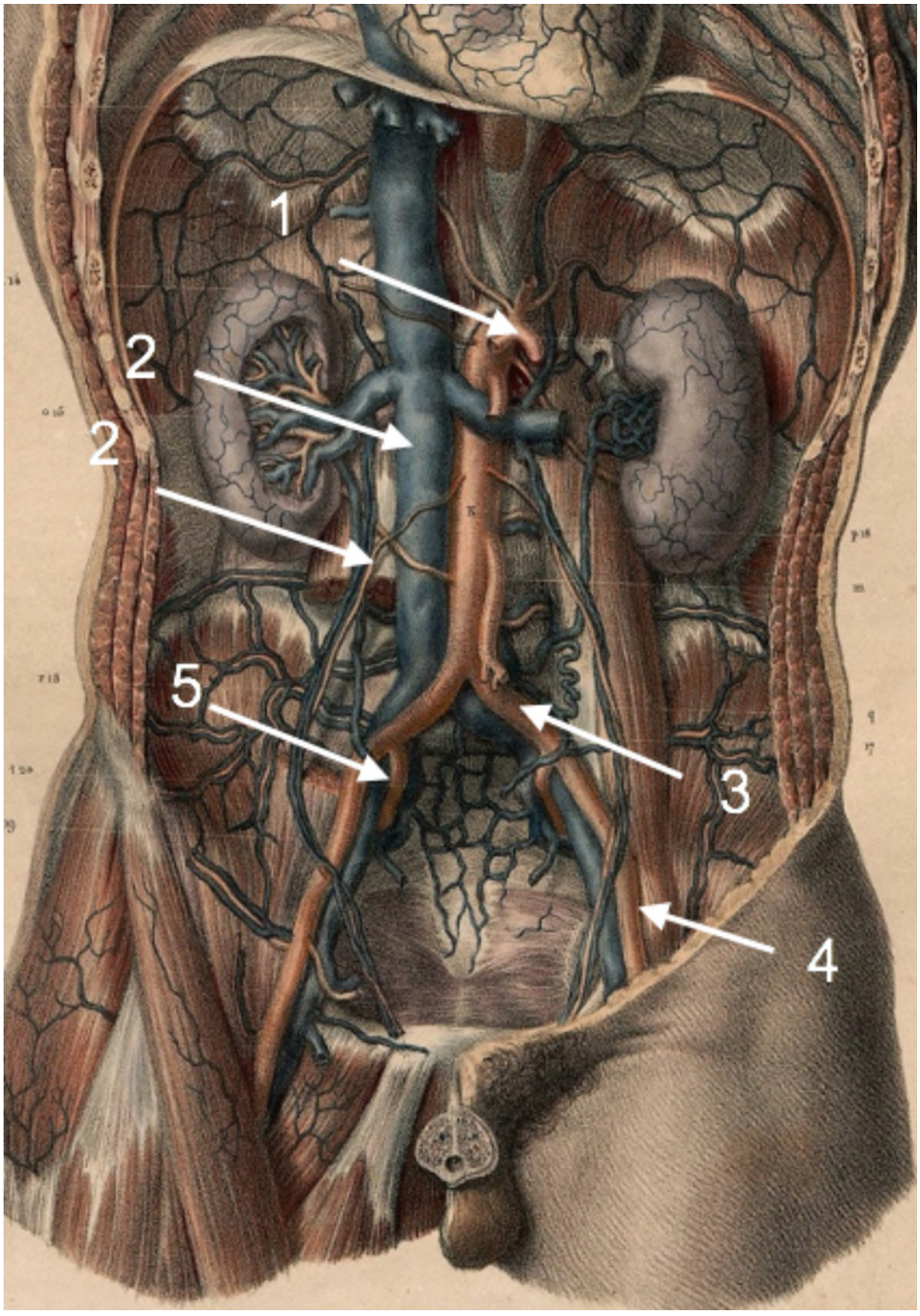

Supplemental material 5. Anatomical view of abdominal aorta (Q1-Q5). Illustration for Traité complet de l'anatomie de l'homme comprenant la médecine opératoire (1831-1854) by Jean-Baptiste Marc Bourgery. Public domain.

Pedagogical evaluation

Before taking the course, there were no statistical differences in abdominal aorta knowledge in terms of total score (78,8% vs 76,3%, p=0,162), descriptive anatomy (mean 81,3% vs 71,3%, p=0,293), anatomical relationships (mean 82,9% vs 74,3%, p=0,112), or clinical reasoning (mean 63,3% vs 61,7%, p=0,41) between the video and book group. Before taking the course, there were no statistical difference in carotid artery knowledge in terms of total score (78,6% vs 74,8%, p=0,162), anatomical relationships (mean 77,0% vs 78,0%, p=0,569), or clinical reasoning (mean 74,2% vs 70,0%, p=0,298) between the video and book group (Table 3).

After taking the course, there were statistical differences (p<0,05) between the video group and books group in terms of the total score (mean 90% vs 70,67%), descriptive anatomy (mean 90% vs 69,33%), anatomical relationships (mean 74% vs 54%), and clinical reasoning (mean 98% vs 81%) of thoracic brachial outlet (Fig. 2).

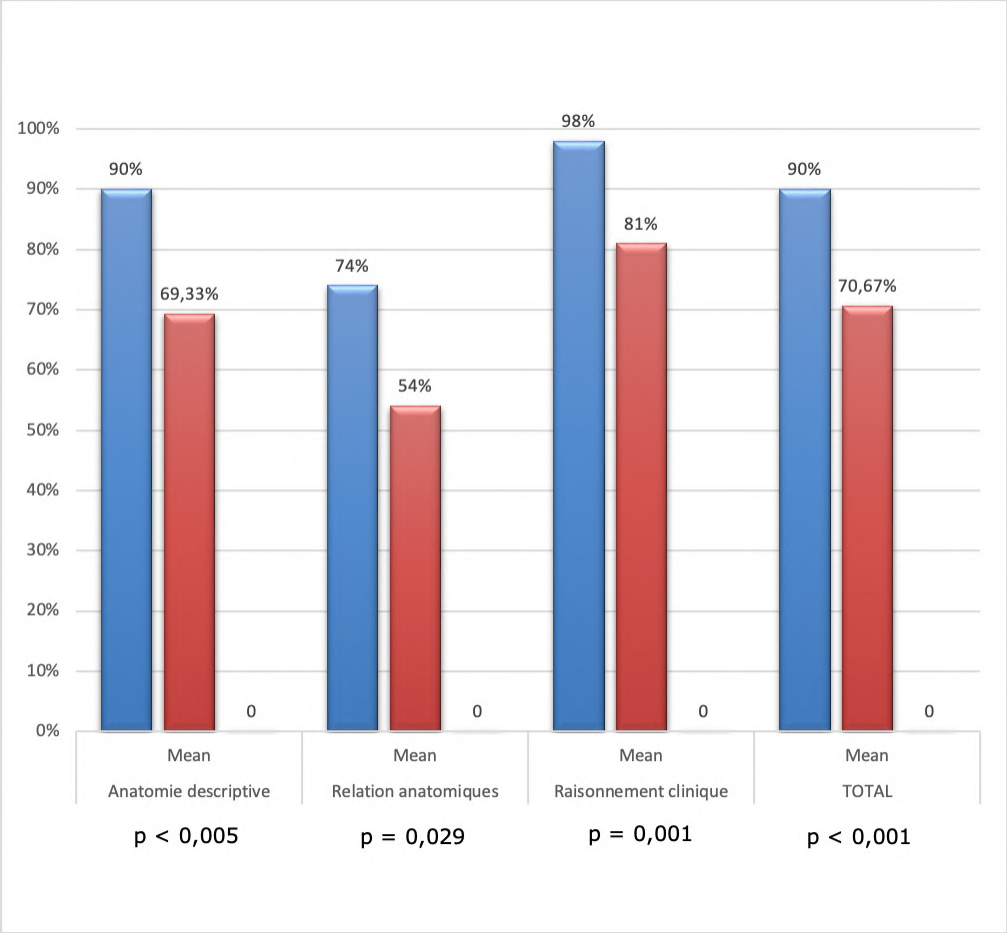

Fig. 2.- Post-test groups performances concerning Abdominal Aorta anatomy before the courses. Blue, video group; Orange, books group.

Satisfaction questionnaire (Table 1 and 4)

Regarding the residents who viewed the video of the thoracic brachial outlet and who answered the satisfaction questionnaire (n=10), results are summarized in Table 4. According to the Q1-Q2 responses, all of the residents thought that the video was an easy method to use (100%, Table 4) and close to practice. According to all residents, the possibility of reviewing the videos (100%, Q3, Table 4) and seeing dissections outside the anatomical laboratory (100%, Q4, Table 4), especially in 3-dimensional stereoscopy, was useful. Observing the relationships and depth between organs was positive (100%, Q5, Table 4). Moreover, stu-

Table 3. Group performance concerning abdominal aorta and carotid artery before instructional video or books. For each group, expression of the average score out of 100 then the average of the correct answers in percentage. This table demonstrates the group test performances before their exposure to the instructional video or books.

SUBJECT	KNOWLEDGE EVALUATED (MEAN OF GOOD RESPONSES)	PRE TEST VIDEO GROUP	PRE TEST BOOKS GROUP	P-VALUE
CAROTID ARTERY SUPPLEMENTAL MATERIAL 1-3	**Descriptive anatomy (Q1-Q10)**	**87,0%**	**74,0%**	**p = 0,028**
	Anatomical relationships(Q11-Q30)	**77,0%**	**78,0%**	**p = 0,569**
	Reasoning, physiopathology, clinical outcomes (Q31-Q42)	**74,2%**	**70,0%**	**p = 0,298**
	TOTAL	**78,8%**	**74,8%**	**p = 0,162**
ABDOMINAL AORTA SUPPLEMENTAL MATERIAL 4-6	**Descriptive anatomy (Q1-Q15)**	**81,3%**	**71,3%**	**p = 0,293**
	Anatomical relationships(Q16-Q29)	**82,9%**	**74,3%**	**p = 0,112**
	Reasoning, physiopathology, clinical outcomes (Q30-Q41)	**63,3%**	**61,7%**	**p = 0,412**
	TOTAL	**78,8%**	**76,3%**	**p = 0,162**

Table 4. Evaluation of the 3D stereoscopic video by the residents (n=10).

	Not agree at all	Rather disagree	Do not know	Agree	Totally agree	Positive reviews
Q1	0%	0%	0%	0%	100%	100%
Q2	0%	0%	0%	50%	50%	100%
Q3	0%	0%	0%	0%	100%	100%
Q4	0%	0%	0%	0%	100%	100%
Q5	0%	0%	0%	0%	100%	100%
Q6	0%	0%	0%	30%	70%	100%
Q7	0%	0%	0%	40%	100%	100%
Q8	0%	0%	0%	60%	40%	100%
Q9	10%	30%	10%	50%	0%	50%

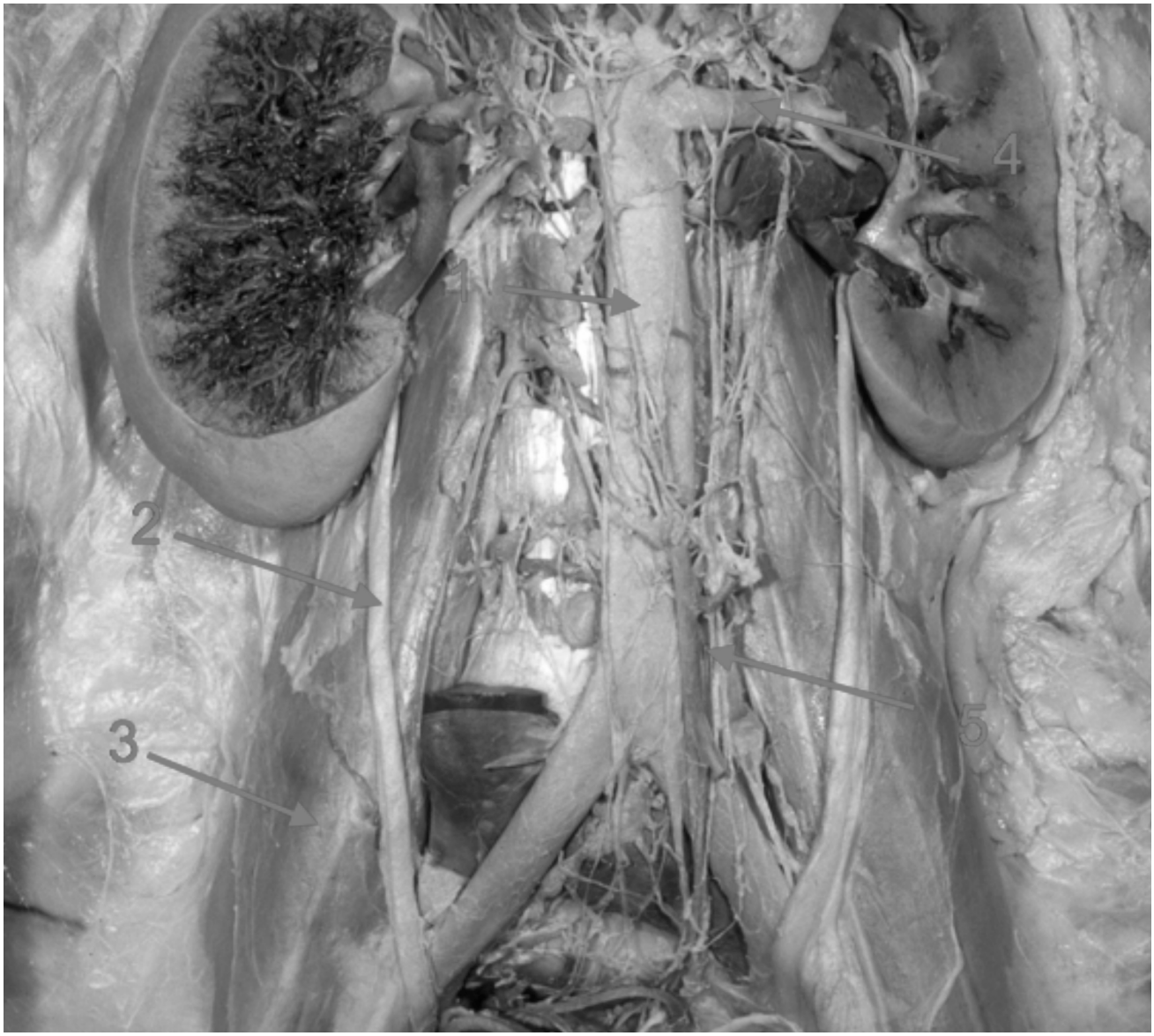

Supplemental material 6. Anatomical view of abdominal aorta (Q6-Q10) from David Lee Basset stereoscopic Atlas. Creative Commons Attribution-Noncommercial-Share Alike 3.0 United States License.

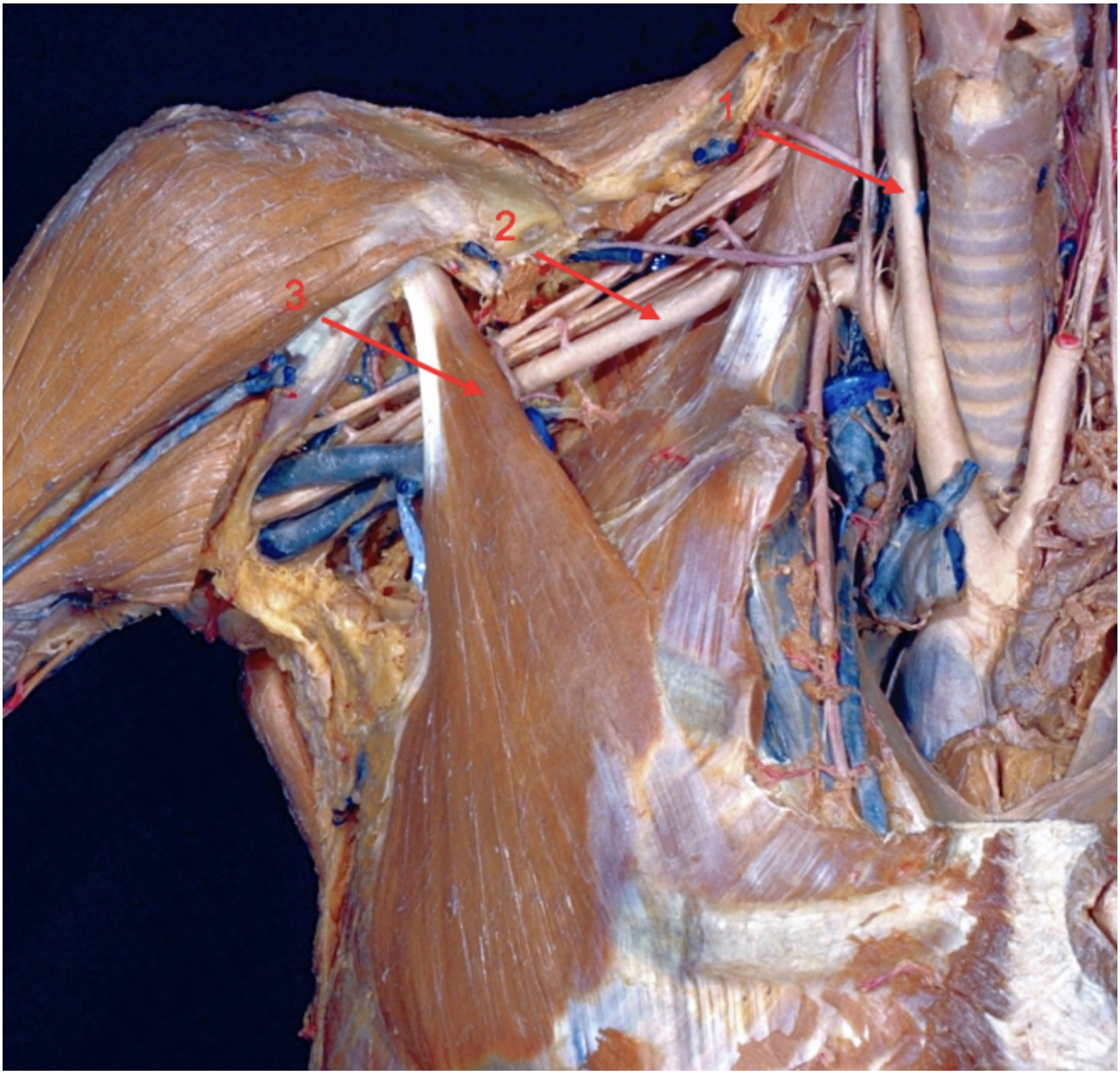

Supplemental material 7. Anatomical view of thoracic brachial outlet with section of the clavicle (Q6-Q10) from David Lee Basset stereoscopic Atlas. Creative Commons Attribution-Noncommercial-Share Alike 3.0 United States License.

dents enjoyed the ability to watch the surgery with commentary from the surgeon's point of view (100%, Q6, Table 4). Students did not give negative feedback after watching this tutorial course.

All the students thought that providing digital certified course using currently available devices (smartphone, computer and virtual reality glasses) seem indispensable to their anatomical training course (100%, Q7, Table 4). They thought they learned more with the help of the 3D video than during previous practical dissection work (100%, Q8, Table 4). However, almost half of the residents thought that this kind of video could not replace cadaver dissection (40%, Q9, Table 4).

DISCUSSION

We have shown that residents are in favour of a virtual clinical-based anatomical teaching program and that they would find it useful.

In our study, before the course (video or books) there were no statistical differences ($p>0,05$) between the groups performances in basic vascular anatomy. It is noteworthy that in the video group they had better performance in the pretest in total score knowledge and clinical reasoning (although it was not significant). After watching the tutorial, we have seen that the video group scored higher than conventionally taught residents in descrip-

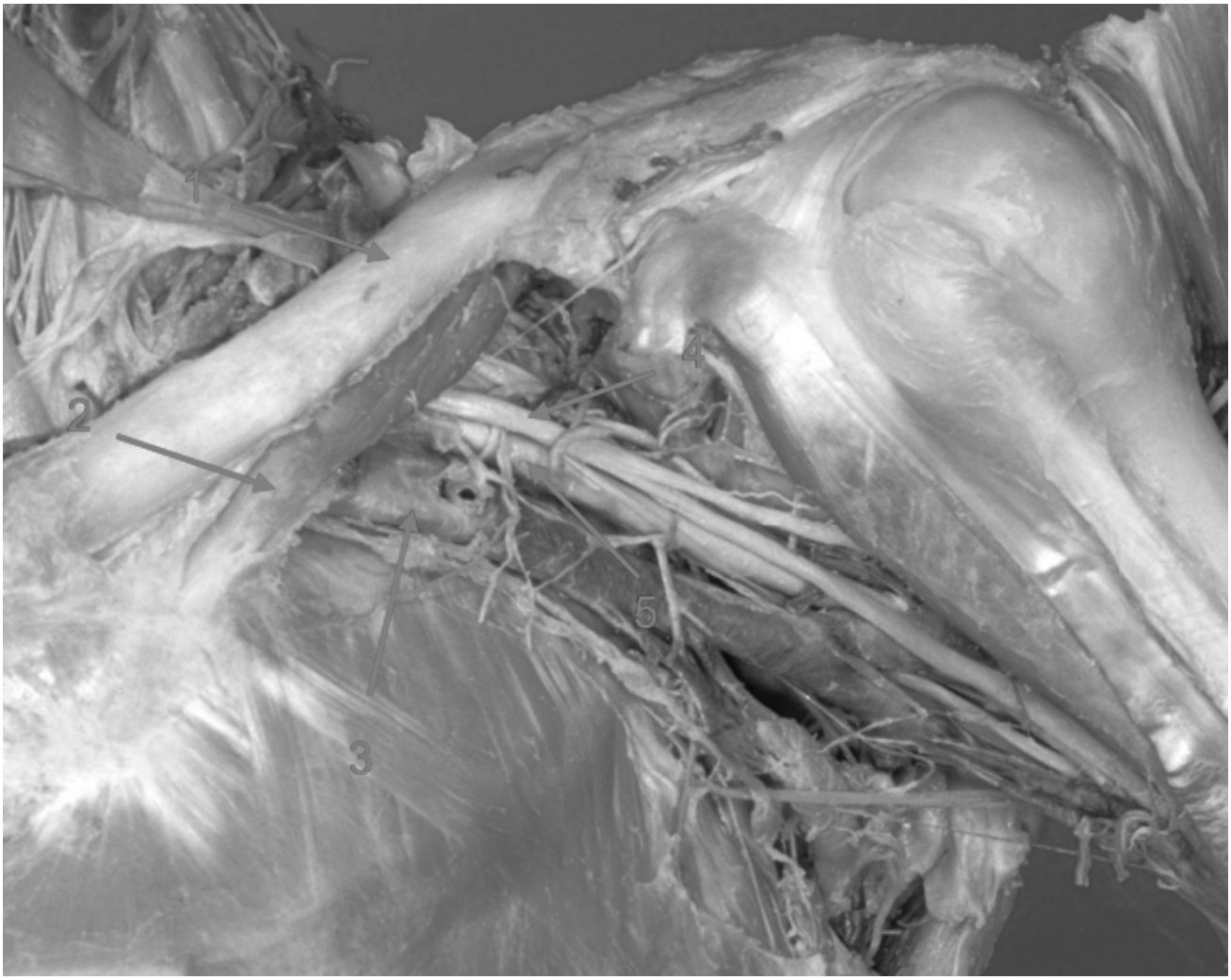

Supplemental material 8. Anatomical view of thoracic brachial outlet with section of the pectoralis minor muscle (Q1-Q5) from David Lee Basset stereoscopic Atlas. Creative Commons Attribution-Noncommercial-Share Alike 3.0 United States License.

tive anatomy, anatomical relationships and even clinical inference. These results are similar to another study conducted on a different population (Deng et al., 2018)**.** Understanding anatomy means to be able to master visual-spatial skills. However, these skills are not necessarily mastered or understood by the students' pre-specialisation, especially for specific topics such as the thoracic brachial outlet that include three anatomical regions (interscalenic triangle, costoclavicular space, pectoralis minor space) (Connolly et al., 2021; Illig et al., 2016; Jones et al., 2019; Masson, 2021), to which we can add the humeral block (Brunet, 1999).

Over the years the anatomical and surgical knowledge of the thoracic outlet has evolved. Therefore, it is necessary to provide an updated anatomical and surgical description of each area. As an example, we will discuss thoracic outlet syndrome (TOS). TOS is a disease that requires a good anatomical knowledge to understand its diagnosis and its surgical treatment. This syndrome is a good example of the implication of anatomical knowledge in relation to surgical technique.

In the clinical-based anatomical videos, the addition of a surgical section showing the view of the main surgeon during the operation allowed for a better understanding of the surgical relevance of such anatomy. Our results showed that the instructional video with stereoscopic 3D views is an effective tool for learning surgical anatomy and the steps of a surgical procedure. Although the acquisition of theoretical knowledge is essential, the mastery of surgical procedures is the cornerstone of clinical expertise (Alameddine et al., 2018). The teaching of surgical skills is one of the most important and exhilarating tasks for a university surgeon (Norman, 1985). All teaching

programs are aiming at professional skills acquisition, which is the "individual's capacity to effectively resolve various problems met in his domain of practice" (Jean et al., 1993). Most of this surgical learning is done in the operative room on real surgeries during residency. It follows 3 stages: demonstration, repeated practice, and immediate feedback on the procedure (Reznick, 1993). The first stage (demonstration) is the main one and is progressively put aside in favour of the next ones (practice and feedback). This kind of teaching is obviously dependant on day-to-day mentoring. Students need to be taught by their mentors in order to develop and acquire the technical skills for surgical procedures. Furthermore, as the surgical disciplines tend to be over specialized and with numerous new technics and instruments that are complementary or alternative to conventional procedures, these multiply the ways of teaching surgery. This progressive direction towards poles of excellence or even hyper-specialization is a trend that is widespread among institutions. The specific care needs of local populations, and the frequent medical under-staffing of university teams accentuate the phenomenon.

As 50% of the residents argue, the training program using only educational videos with a 3D method cannot obviously replace the cadaver dissection course. As described previously (Bernard et al., 2020a,b), surgical anatomy training deserves further exploration of the role of synergistic multimodal teaching strategies, such as the combination of 3D anaglyphic stereoscopy with virtual reality simulations, augmented reality teaching and 3D printing. In our study, students supported the development of stereoscopic teaching as a complementary resource. Indeed, their enthusiasm for the 3D method was mitigated by the fact that they found that this approach did not exclude the traditional pedagogical method. These findings were in accordance with previous studies, where new digital tools and integrative teaching methods have been promoted to complement anatomical education and the lecture experience (Hattie, 2012; Louw et al., 2009). Modern digitalized methods of teaching anatomy are undoubtedly useful (Louw et al., 2009; Turney, 2007). However, body dissections can still benefit significantly the new medical students, and these procedures should be maintained as part of surgical training (Shiozawa et al., 2017). 3D-stereoscopic-based learning, and new techniques such as virtual reality and 3D printing can be used to enhance and support anatomical teaching and learning in medical education (Vaccarezza and Papa, 2015). According to Papa and Vaccarezza's review (Papa and Vaccarezza, 2013), we are confident that gross anatomy through dissection and mental visualization cannot be undermined in a modern medical curriculum, since it gives a 3D experience that cannot yet be reproduced by the most advanced digital anatomy programs available.

All the participants in the study had previously completed cadaver dissection over a period of two weeks. Cadaver dissections and virtual visualizations each have distinct advantages in anatomical education. Cadaver dissections offer unparalleled realism and tactile feedback, crucial for understanding human tissue characteristics, but require a specialized lab and come with higher costs (Bernard et al., 2019; Cobolet et al., 2014). Virtual tools, while lacking in tactile feedback, provide accessibility, convenience, and customization, allowing for repeated use and updates to illustrate various anatomical variations. They are cost-effective in the long run despite high initial setup costs, and remove ethical concerns associated with cadaver use. However, they may have a learning curve and often lack the detail and accuracy found in cadaver dissections (Bernard et al., 2019; Cobolet et al., 2014). Ultimately, these methods are complementary, with cadaver dissection providing depth and realism, and virtual visualization offering innovation and practicality in anatomical learning.

In our study, we evaluated the contribution of an educational video on an uncommon surgical approach (axillary removal of the first rib) performed in a tertiary centre. This surgery requires an excellent anatomical knowledge. The contribution of educational videos including 3D stereoscopic views at the beginning of the residency could help beginning residents to understand this surgical procedure. It could also allow residents who are not part of an expert centre to access training on specific surgical techniques. Scientific societies

work hard to digitalize and promote such teaching. Vascular surgery training in France is delivered by the French College of Vascular Surgery on a national basis. During their four years of residency, vascular surgery residents must follow a national digital teaching programme. The SIDES NG platform is the result of work carried out in collaboration with all the national stakeholders concerned by the 3rd cycle of medical studies. This platform is supported by all French medical universities. This represents more than 40,000 residents, 44 postgraduate diplomas and 34 faculties of medicine (Vaccarezza and Papa, 2015). The postgraduate diploma in vascular surgery includes distance learning courses taught by different surgeon-teachers of the specialty in France. Slide shows are accessible to the residents and are divided into 3 parts (base phase, deepening phase and consolidation phase) in line with the new reform of the 3rd cycle of medical studies. The viewing of these videos could be part of the validation of the different phases of the postgraduate diploma in vascular surgery and amounts to several hours of viewing. Currently, the foundation phase includes a chapter on anatomy and surgical approaches in vascular surgery, and it should be noted that the anatomy of the thoracic brachial outlet and surgery for resection of the first rib are not included in this teaching. Moreover, it does not include 3D stereoscopic video or VR courses. In view of this new digital curriculum, the addition of educational videos of surgical anatomy could be a complement to the digital training of vascular surgery residents.

Limitations

Our study has several limitations. Our sample size was small, despite the recruitment of residents from several hospital sites and several surgical specialties. Surgical specialty is not a determining factor, as the answers to the MCQs were equivalent for both groups before viewing the video or the anatomy books. Descriptive results showed that the resident profile was heterogeneous in terms of surgical specialty, age, vascular surgery experience and university origin. Whatever the student profile, all students assume that a complementary anatomo-surgical program is needed. We can add to the limitations the fact that the students in the 3D group were probably more enthusiastic and motivated, leading to better results. Additional study time due to enthusiasm is a valid consideration; however, the study's design aimed to minimize its impact. Future research could track actual study time to further address this variable. Furthermore, the absence of a satisfaction survey for the book group precludes a comprehensive comparative analysis of students' satisfaction with the learning methods, which may have provided additional insights into the educational impact. The results of these studies should be confirmed by larger studies. Additionally, the timing of our evaluation poses a limitation: the long-term knowledge assessment was conducted only one-month post-intervention, which may not sufficiently capture the true extent of knowledge retention over a longer period. It is necessary to evaluate the impact of this teaching method on the students' long-term knowledge with assessments at multiple intervals post-intervention.

CONCLUSION

The teaching of vascular anatomy and surgical approaches in postgraduate vascular surgery studies is essential. The development of educational videos using 3D stereoscopy in particular could complement teaching in this field. This digital clinical-based method of anatomical teaching is particularly suited as a complement to traditional teaching methods.

ACKNOWLEDGEMENTS

This study was supported by the 3D-lab of the University of Angers, AKIVI and SATT Ouest Valorisation.

REFERENCES

AKIVI. URL: https://akivi.fr/ (accessed November 2022).

ALAMEDDINE MB, ENGLESBE MJ, WAITS SA (2018) A Video-based coaching intervention to improve surgical skill in fourth-year medical students. *J Surg Educ*, 75: 1475-1479.

ATLAS D'ANATOMIE HUMAINE. URL: https://www.elsevier-masson.fr/atlas-danatomie-humaine-9782294756290.html [accessed 11 August 2021].

BAUER A (2016) Modélisation anatomique utilisateur-spécifique et animation temps-réel : application à l'apprentissage de l'anatomie. *Université Grenoble Alpes (ComUE)*. These de doctorat.

BERNARD F, LEMÉE J-M, TER MINASSIAN A, MENEI P (2018a) Right hemisphere cognitive functions: from clinical and anatomic bases to brain mapping

during awake craniotomy Part I: Clinical and functional anatomy. *World Neurosurg*, 118: 348-359.

BERNARD F, TROUDE L, LACCOURREYE L, ROCHE P-H, FOURNIER H-D (2018b) *Operative Neurosurgery* (Hagerstown, Md.).

BERNARD F, GALLET C, FOURNIER H-D, LACCOUREYE L, ROCHE P-H, TROUDE L (2019) Toward the development of 3-dimensional virtual reality video tutorials in the French neurosurgical residency program. Example of the combined petrosal approach in the French College of Neurosurgery. *Neurochirurgie*, 65: 152-157.

BERNARD F, LEMEE J-M, MAZERAND E, LEIBER L-M, MENEI P, TER MINASSIAN A (2020a) The ventral attention network: the mirror of the language network in the right brain hemisphere. *J Anat*, 237: 632-642.

BERNARD F, RICHARD P, KAHN A, FOURNIER H-D (2020b) Does 3D stereoscopy support anatomical education? *Surg Radiol Anat*, 42(7):843-852.

BERNARD F, HAEMMERLI J, ZEGAREK G, KISS-BODOLAY D, SCHALLER K, BIJLENGA P (2021) Augmented reality-assisted roadmaps during periventricular brain surgery. *Neurosurg Focus*, 51: E4.

BERNEY S, BÉTRANCOURT M, MOLINARI G, HOYEK N (2015) How spatial abilities and dynamic visualizations interplay when learning functional anatomy with 3D anatomical models. *Anat Sci Educ*, 8: 452-462.

BOGOMOLOVA K, HAM IJM VAN DER, DANKBAAR MEW, BROEK WW VAN DEN, HOVIUS SER, HAGE JA VAN DER, HIERCK BP (2020) The effect of stereoscopic augmented reality visualization on learning anatomy and the modifying effect of visual-spatial abilities: a double-center randomized controlled trial. *Anat Sci Educ*, 13: 558-567.

BRUNET C (1999) Anatomie de la traversée cervico-thoraco-brachiale. *Rev Médecine Interne*, 20: 453s-463s.

CHAIKOF EL, CAMBRIA RP (2014) Atlas of vascular surgery and endovascular therapy. E-Book: Anatomy and Technique. *Elsevier Health Science*s, p 859.

COBOLET G, GARRISON D, VONS J, VELUT S, NUTTON V, WILLIAMS DJ (2014) Andreas Vesalius--the work. *Vesalius Acta Int Hist Med*, 20: 19-24.

CONNOLLY MR, AUCHINCLOSS HG (2021) Anatomy and embryology of the thoracic outlet. *Thorac Surg Clin*, 31: 1-10.

DENG X, ZHOU G, XIAO B, ZHAO Z, HE Y, CHEN C (2018) Effectiveness evaluation of digital virtual simulation application in teaching of gross anatomy. *Ann Anat*, 18: 276-282.

FUNG W, LO W, LIU Y, XI N (2005) A case study of 3D stereoscopic vs. 2D monoscopic tele-reality in real-time dexterous teleoperation. 2005 IEEE/RSJ International Conference on Intelligent Robots and Systems. IEEE. pp 181-186.

GRAY'S ATLAS D'ANATOMIE HUMAINE. URL: https://www.elsevier-masson.fr/grays-atlas-danatomie-humaine-9782294747809.html (accessed 11 August 2021).

HATTIE J (2012) Visible Learning for Teachers: Maximizing Impact on Learning. Routledge.

ILLIG KA, DONAHUE D, DUNCAN A, FREISCHLAG J, GELABERT H, JOHANSEN K, JORDAN S, SANDERS R, THOMPSON R (2016) Reporting standards of the Society for Vascular Surgery for thoracic outlet syndrome. *J Vasc Surg*, 64: e23-35.

JEAN P, DELORME P, DES MARCHAIS JE (1993) Apprendre à enseigner les sciences de la santé: Guide de formation pratique: Cahier 1 [-Cahier 5]. *Faculté de médecine des universités de Montréal et de Sherbrooke.*

JONES MR, PRABHAKAR A, VISWANATH O, URITS I, GREEN JB, KENDRICK JB, BRUNK AJ, ENG MR, ORHURHU V, CORNETT EM, KAYE AD (2019) Thoracic outlet syndrome: a comprehensive review of pathophysiology, diagnosis, and treatment. *Pain Ther*, 8: 5-18.

KUHN JE, LEBUS V GF, BIBLE JE (2015) Thoracic outlet syndrome. *J Am Acad Orthop Surg*, 23: 222-232.

LEUNG BC, WILLIAMS M, HORTON C, COSKER TD (2020) Modernising anatomy teaching: which resources do students rely on? *J Med Educ Curric Dev*, 7: 2382120520955156.

LOUW G, EIZENBERG N, CARMICHAEL SW (2009) The place of anatomy in medical education: AMEE Guide no 41. *Med Teach*, 31: 373-386.

MASSON E (2021) Chirurgie des syndromes de compression du défilé thoracobrachial. *EM-Consulte*. URL: https://www.em-consulte.com/article/778779/chirurgie-des-syndromes-de-compression-du-defile-t (accessed 11 August 2021).

NORMAN GR (1985) Defining competence: a methodological review. *Assess Clin Competence*, NY Springer, pp 15-35.

PAPA V, VACCAREZZA M (2013) Teaching anatomy in the XXI century: new aspects and pitfalls. *Sci World J*, 2013: 310348.

REZNICK RK (1993) Teaching and testing technical skills. *Am J Surg*, 165: 358-361.

SATAVA RM (1995) Virtual reality, telesurgery, and the new world order of medicine. *J Image Guid Surg*, 1: 12-16.

SHIOZAWA T, BUTZ B, HERLAN S, KRAMER A, HIRT B (2017) Interactive anatomical and surgical live stream lectures improve students' academic performance in applied clinical anatomy. *Anat Sci Educ*, 10: 46-52.

THE SURGICAL CLERKSHIP: CHARACTERISTICS OF THE EFFECTIVE TEACHER - Sloan - (1996) - Medical Education - *Wiley Online Library*. URL: https://onlinelibrary.wiley.com/doi/abs/10.1111/j.1365-2923.1996.tb00712.x (accessed 5 July 2018).

TURNEY B (2007) Anatomy in a modern medical curriculum. *Ann R Coll Surg Engl*, 89: 104-107.

UNESS formation - SIDES NG | UNESS. URL: https://www.uness.fr/nos-services/ecosysteme-uness/nos-outils/uness-formation-sides-ng (accessed 11 August 2021).

VACCAREZZA M, PAPA V (2015) 3D printing: a valuable resource in human anatomy education. *Anat Sci Int*, 90: 64-65.

SCOTT DJ, CENDAN JC, PUGH CM, MINTER RM, DUNNINGTON GL, KOZAR RA (2008) The changing face of surgical education: simulation as the new paradigm. *J Surg Res*, 147: 189-193.

GIMM O, BARCZYŃSKI M, MIHAI R, RAFFAELLI M (2019) Training in endocrine surgery. *Langenbecks Arch Surg*, 404(8): 929-944.

SOSA JA, WANG TS, YEO HL, MEHTA PJ, BOUDOURAKIS L, UDELSMAN R, ROMAN SA (2007) The maturation of a specialty: workforce projections for endocrine surgery. *Surgery*, 142: 876-883.

SOLORZANO CC, SOSA JA, LECHNER SC, LEW JI, ROMAN SA (2010) Endocrine surgery: where are we today? A national survey of young endocrine surgeons. *Surgery*, 147(4): 536-541.

MIHAI R, DONATINI G, VIDAL O, BRUNAUD L (2019) Volume-outcome correlation in adrenal surgery-an ESES consensus statement. *Langenbecks Arch Surg*, 404: 795-806.

PALAZZO F, DICKINSON A, PHILLIPS B, SAHDEV A, BLISS R, RASHEED A, KRUKOWSKI Z, NEWELL-PRICE J (2016) Adrenal surgery in England: better outcomes in high-volume practices. *Clin Endocrinol (Oxf)*, 85(1): 17-20.

The effect of ethanolic extract of Moringa oleifera leaves on sperm parameters in 4G-cellphone-EMR exposed rats

Sudha Ramalingam, Deepa Somanath

Department of Anatomy, Sri Manakula Vinayagar Medical College and Hospital, Puducherry- 605 107, India

SUMMARY

Cell phone use and infertility are topics of scientific investigation. 2G, 3G and 4G cell phone radiation causes negative effects on spermatogenesis. The aim of this study is to assess the protective efficiency of Moringa oleifera leaves (MOL) on the sperm parameters of Wistar rats against electromagnetic radiation (EMR) emitted from a 4G mobile phone. Male Wistar rats were divided into five groups. Control group (n=3) without mobile phone; Sham group (n=3) with mobile phone in switched-off mode; MOL-2 group (n=6) obtained orally 200 mg ethanol extract of MOL/kg BW/two months; R2 group (n=6) subjected to 4G-EMR for 96 minutes/day/two months; R2+MOL group (n=6) treated with MOL extract while exposed to EMR for two months. After the experimental period, rats were sacrificed to get epididymises. The epididymal fluid was collected to evaluate count, viability, motility and morphology of sperms. The 4G-EMR induced a significant reduction in the count and tail defects of sperms ($P<0.05$) in R2 rats as compared to control, sham and MOL-2 groups. Nevertheless, *MOL* extract significantly inhibited the EMR-caused fall of those variables in R2+MOL group. The R2 group had significantly ($P<0.0001$) lower and higher values concerning the sperm's progressive motility and non-motility rates, the percentages of alive and dead sperms than those in the control, sham, and MOL-2 groups, but the *MOL* extract restored the parameters in R2+MOL as compared to R2 group. The oral administration of 200 mg of ethanolic extract of Moringa leaves protected the sperm parameters of Wistar rats to near normal level from harmful effects of 4G-cell phone-EMR.

Key words: Cell phone – Moringa leaves – Testis – Oxidative stress – Sperm

INTRODUCTION

Infertility is defined as failure to get pregnant after a year of regular, unrestricted sexual copulation, which is a widespread problem with human reproduction ranging from 2.5 to 15 %. It significantly affected 27.5 million of Indian couples, and 40–50% of infertility in those couples is attributable to the male spouse (Agarwal and Durairajanayagam, 2015; Toragall et al., 2019). Male infertility is associated with the use of tobacco, alcohol,

Corresponding author:
Deepa Somanath. Department of Anatomy, Sri Manakula Vinayagar Medical College and Hospital, Puducherry- 605 107, India. Phone:0413-260400. E-mail: deepa.somanath@gmail.com - Orcid: 0000-0002-4732-5406

Submitted: January 10, 2024. **Accepted:** January 21, 2024

https://doi.org/10.52083/YHZW2649

pesticides, heavy metals, and radiation, in addition to a few clinical disorders and genetic factors (Oliva et al., 2008).

Smartphones utilize high frequency (850 MHz-2.4 GHz) and emit non-ionizing radiation called radio-frequency electromagnetic radiation (RF-EMR) during its working mode (Agarwal et al., 2008; Kim et al., 2007; Oh et al., 2018). Few human researches has investigated the relationship between cell phone exposure and poor semen quality, which may lower sperm count, motility, viability and normal morphology (Agarwal et al., 2008; Erogul et al., 2006). The rate at which RF-EMR energy is absorbed by human tissues is known as the specific absorption rate (SAR). The amount of SAR absorbed depends on the exposure's frequency, intensity, polarisation, and duration. When conversing on the phone or keeping the phone close to the head or in a pocket of clothing, a greater radiation absorption rate may be seen (Kesari et al., 2018). Health risks by RF-EMR might arise from thermal, non-thermal, or a mixture of both processes (Meo et al., 2011). It may affect gene responsiveness, causes DNA damage or inhibit its repair, and causes oxidative stress (OS) in a non-thermal manner (Belpomme et al., 2018). OS is a condition caused by an imbalance between oxidants and antioxidants, which results in an excessive accumulation of oxidants relative to antioxidants. The relationship between RF-EMR exposure and harmful biological effects is due to the production of reactive oxygen species (ROS) as a result of elevated OS, which undermines the body's natural defences (Avci et al., 2012). Compounds known as bio-antioxidants eliminate, scavenge and resist the formation of ROS or their activity. Among the well-known biological antioxidants, super oxide dismutase (SOD) and its two isozymes, glutathione reductase (GR) and catalase, play a significant role (Turk et al., 2008). The protective properties of plant material including antioxidant chemicals against cell-phone-related RF-EMR tissue damage have been well-documented by academics (Avci et al., 2012; Khaki, 2011; Mailankot et al., 2009). The leaves of the Moringa oleifera (MOL) (drumstick tree), which is an Indian staple food, is a good source of vitamins, minerals, and amino acids. There is literature available regarding the anti-diabetic, anti-hypertensive, anti-inflammatory, antiepileptic and antitumor properties of MOL. A variety of anti-oxidants are identified in MOL such as kaempferol, quercetin, myricetin, vanillin, gallic acid, ellagic acid, ferulic acid, and flavonoids (Stohs and Hartman, 2015). There is a scarcity in the literature investigating MOL as a protector of sperms against the hazardous effects of RF-EMR arising from 4G-cell phone. Hence, this experiment was conducted to determine the possible radio-protective efficacy of ethanolic extract of MOL on sperm parameters in Wistar rats during RF-EMR exposure from 4G-cell phone for duration of two months.

MATERIALS AND METHODS

Animals

Four-week-old male Wistar rats, weighing approximately 150-180 gm, were used in this study. They were housed in Plexiglas cages with a commercially available balanced diet and tap water ad libitum. They were subjected to light and dark periods of 12 h/12 h and a temperature of 22 to 24°C.

Ethical clearance

The animal experimentation procedures listed in this study were done according to the internationally accepted guidelines for the Care and Use of Laboratory Animals and approved by the Institutional Animal Ethics Committee (Approval letter No. IAEC/2015/02).

Animal grouping

After a week of acclimatization, rats were randomly divided into five groups, and they were maintained in separate rooms without any other external EMR-sources.

Control group (n=3): No cell phone radiation.

Sham group (n=3): Exposed to the cell phone in switch off mode.

MOL-2 group (n=6): Received orally 200 mg of ethanolic extract of *MOL*/kg body weight/day for two months.

R2 group (n=6): Exposed to EMR for 96 minutes/day for two months (4 minutes/every half an hour from 8 AM to 8 PM).

R2+MOL (n=6): Exposed to EMR for 96 minutes/day (4 minutes/every half an hour from 8 AM to 8 PM) and concurrently treated orally with 200 mg of ethanolic extract of *MOL*/kg body weight/day for two months.

Cell phone-EMR System for exposure

A typical commercial brand of Android smartphone with a peak power density of 2W/kg and a whole-body SAR value of 1.6W/kg was employed in this study (as stated by the manufacturer). The Cornet Electrosmog RF meter was used to calculate the average power density of the phones, which was 187.9 mW/m^2, based on the electromagnetic field values of the rat cage's interior. The smartphone was suspended from the rat cage's ceiling to reach the center of the cage while ensuring the free movement of the animals (Narayanan et al., 2009).

MOL collection and preparation of the extract

M. Oleifera leaves that had been verified by a Botanist were collected from a village in Tamil Nadu, India. The leaves were washed with water and air-dried at 44°C for four hours, and then powdered in an electric mixer grinder. The powdered leaves were macerated with 70% ethanol at a ratio of 1:40, w/v, for 72 hours at room temperature to prepare the extract. The extract was filtered using No. 1 Whatman filter paper, and any leftover material was extracted again using the same procedure and solvent until the entire amount of marc was used completely (Vongsak et al., 2013). The resulting crude extract was stored at -4°C for later usage after the solvent was removed using a rotary evaporator.

Collection of semen and sperm evaluation

An intraperitoneal injection of 45 mg/kg of ketamine hydrochloride was given 24 hours after the completion of the experiment to anesthetize the rats, accompanied by sacrifice. Epididymises were obtained by trans-abdominal incision and minced to extract the epididymal fluid to evaluate count, viability, motility and morphology of sperms.

Epididymal fluid was collected from both cauda epididymides, which were cleared from other soft tissues and cut into pieces in a Petri dish containing one ml of physiological saline (0.9% w/v NaCl) and allowed to stay for 15 minutes at room temperature to release all sperms into the saline to make semen sample (Aksu et al., 2015).

Sperm motility

A small drop of semen sample was poured into two droplets of Tris buffer solution which was kept on the slide and mixed on the pre-heated stage of the light microscope. To evaluate the percentage of sperm motility, three random fields were chosen under 400x and the mean of three successive fields was considered as the final score (Sonmez et al., 2005). The percentages of progressively motile (sperms moving faster from one place to another), sluggishly motile (moving sperms at the same place) and non-motile (sperms with the absence of movement) spermatozoa were determined (Luthfi, 2015).

Sperm count

Sperm count was determined with a hemocytometer (Bahmanzadeh et al., 2008).

Abnormalities of spermatozoa

The semen-smeared slides were stained with eosin-nigrosin and studied under a light microscope at a magnification of 400-1000x. 400 spermatozoa were assessed on each slide and abnormalities of spermatozoa were categorized into head, neck and tail defects and given in percentage (%) (Kesari and Behari, 2012).

Alive and dead spermatozoa

Previously stained slides intended for the evaluation of abnormal spermatozoa were used to determine the percentage of live and dead sperm. The slides were examined under a light microscope at 400x magnification and 200 spermatozoa were counted from each sample. They were listed as alive (unstained head) and dead (stained head) as per the eosin staining state of the sperm head (Aksu et al., 2015).

Statistical analysis

Differences between obtained values were compared by one-way analysis of variance (ANOVA),

followed by a post hoc test (Tanhane/LSD). Kruskal Wallis test was applied for the continuous type of data, but not following normal distribution and Mann Whitney U test was used to identify the difference between the groups using JASP statistical software (University of Amsterdam, Netherland). Values were represented as mean±SE and they were considered to be statistically significant at $P < 0.05$.

RESULTS

Epididymal sperm count

Short-term 4G-EMR induced a significant reduction in the sperm count in R2 rats as compared to control, sham and MOL-2 groups. Nevertheless, *MOL* extract inhibited the EMR-caused fall of sperm density in R2+MOL but not to the level seen in control, sham and MOL-2 groups (Fig. 1).

Motility pattern of sperm

The R2 group had significantly ($P<0.0001$) lower and higher values concerning the sperm progressive motility and non-motility rates than those in the control, sham, and MOL-2 groups. The *MOL* extract effectively restored these parameters from radiation in R2+MOL, when compared to R2 group. About the percentage of sluggish sperm motility, no significant differences were seen between groups (Fig. 2).

Sperm viability

The percentages of alive and dead sperms in the R2 group were significantly lower ($P<0.05$) and higher than in control, sham, and MOL-2 groups respectively. In comparison with the R2 group, these parameters were kept at a normal level in R2+MOL but the rate of dead sperms was significantly lower than control and sham groups (Fig. 3).

Sperm morphology

Cell phone-EMR caused significantly more sperm head defects in R2 group as compared to the MOL-2 group only. But no statistically signifi-

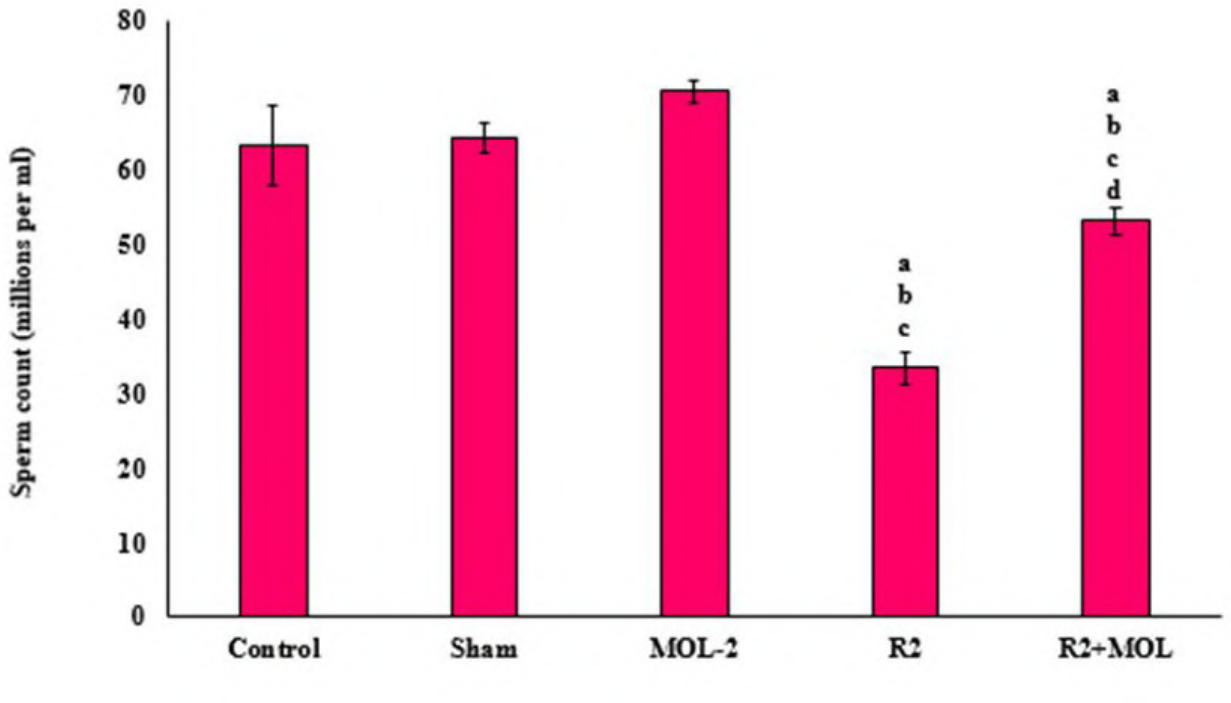

Fig. 1.- Effect of ethanolic extract of MOL on epididymal sperm count in the 4G-mobile phone-induced-EMR exposed rats. Control group-not exposed to 4G-cell phone for two-months, sham group-exposed to 4G-cell phone in switch off mode for two-months (n=3), MOL-2 group-not irradiated and treated with ethanolic extract of MOL 200 mg/kg for two-months (n=6), R2 group-exposed to 4G-EMR for two-months (n=6) and R2+MOL group-treated with ethanolic extract of MOL 200 mg/kg during 4G-EMR exposure for two-months (n=6). Values are expressed as mean ± SE in each group. P values are by one-way ANOVA with LSD/Tanhane test. Different superscript letters show significant differences between groups ($P<0.05$). a- different from the control group; b- different from the sham group; c- different from the MOL-2 group; d- different from the R2 group.

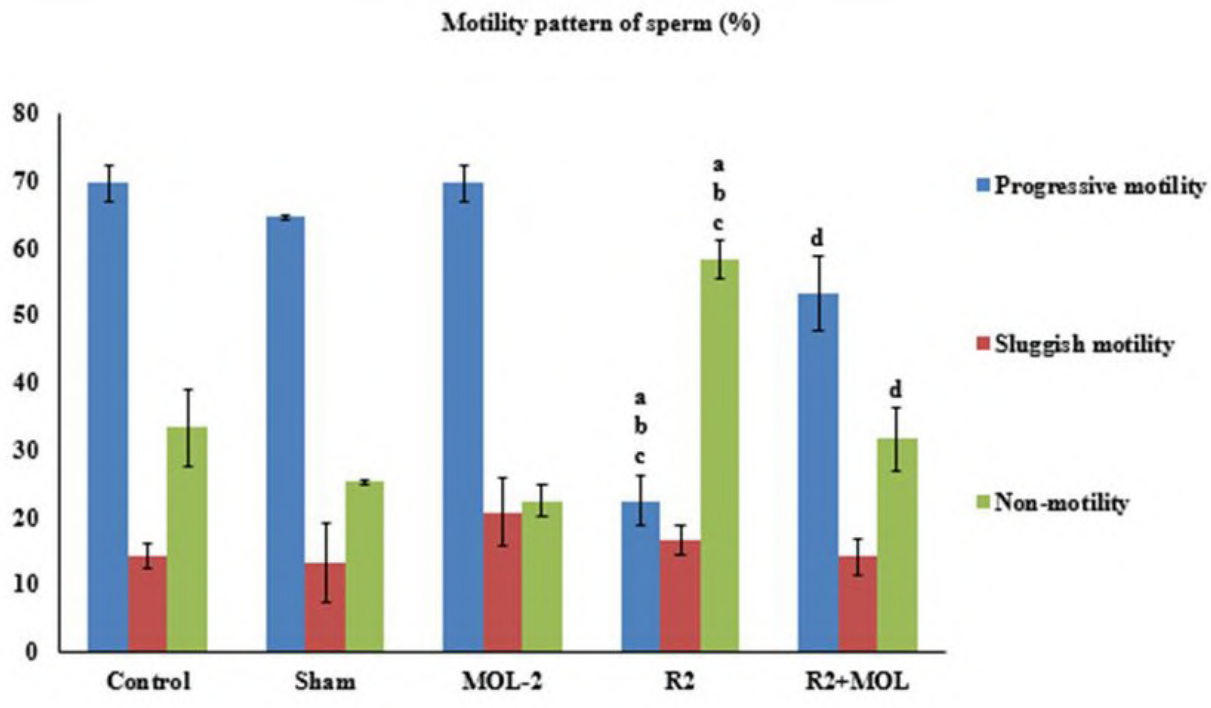

Fig. 2.- Effect of ethanolic extract of MOL on sperm motility pattern in the 4G-mobile phone-induced-EMR exposed rats. Control group-not exposed to 4G-cell phone for two-months, sham group-exposed to 4G-cell phone in switch off mode for two-months (n=3), MOL-2 group-not irradiated and treated with ethanolic extract of MOL 200 mg/kg for two-months (n=6), R2 group-exposed to 4G-EMR for two-months (n=6) and R2+MOL group-treated with ethanolic extract of MOL 200 mg/kg during 4G-EMR exposure for two-months (n=6). Values are expressed as mean ± SE in each group. P values are by one-way ANOVA with LSD/Tanhane test. Different superscript letters show significant differences between groups (P<0.05). a- different from the control group; b- different from the sham group; c- different from the MOL-2 group; d- different from the R2 group.

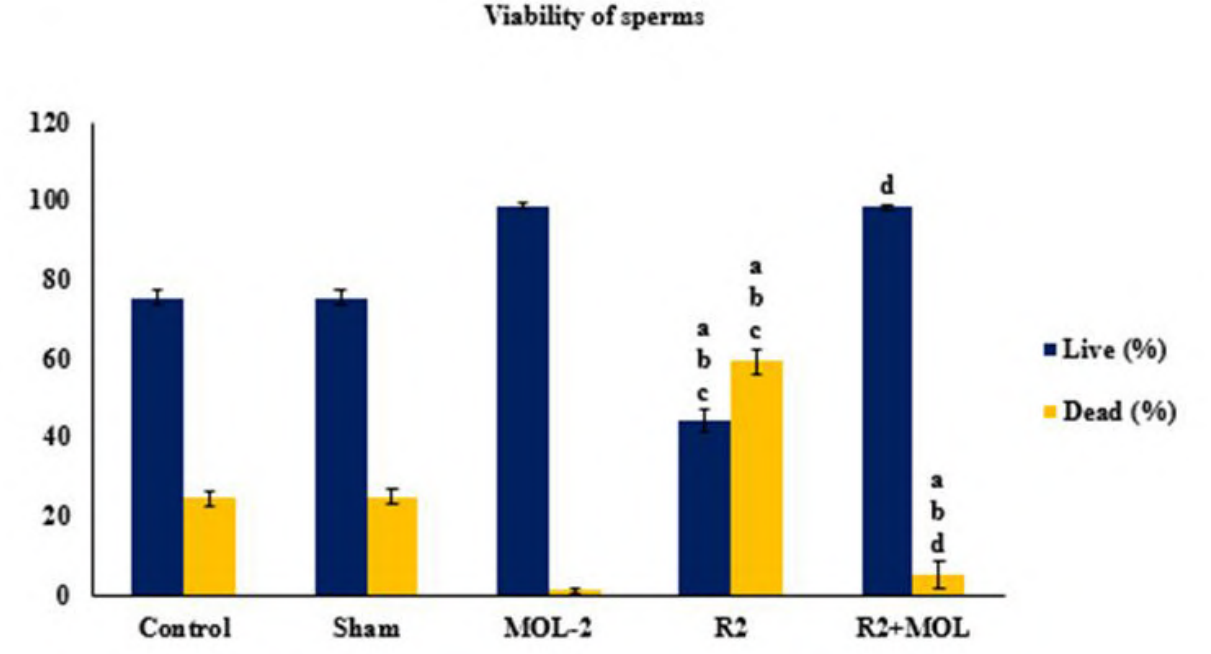

Fig. 2.- Effect of ethanolic extract of MOL on sperm motility pattern in the 4G-mobile phone-induced-EMR exposed rats. Control group-not exposed to 4G-cell phone for two-months, sham group-exposed to 4G-cell phone in switch off mode for two-months (n=3), MOL-2 group-not irradiated and treated with ethanolic extract of MOL 200 mg/kg for two-months (n=6), R2 group-exposed to 4G-EMR for two-months (n=6) and R2+MOL group-treated with ethanolic extract of MOL 200 mg/kg during 4G-EMR exposure for two-months (n=6). Values are expressed as mean ± SE in each group. P values are by one-way ANOVA with LSD/Tanhane test. Different superscript letters show significant differences between groups (P<0.05). a- different from the control group; b- different from the sham group; c- different from the MOL-2 group; d- different from the R2 group.

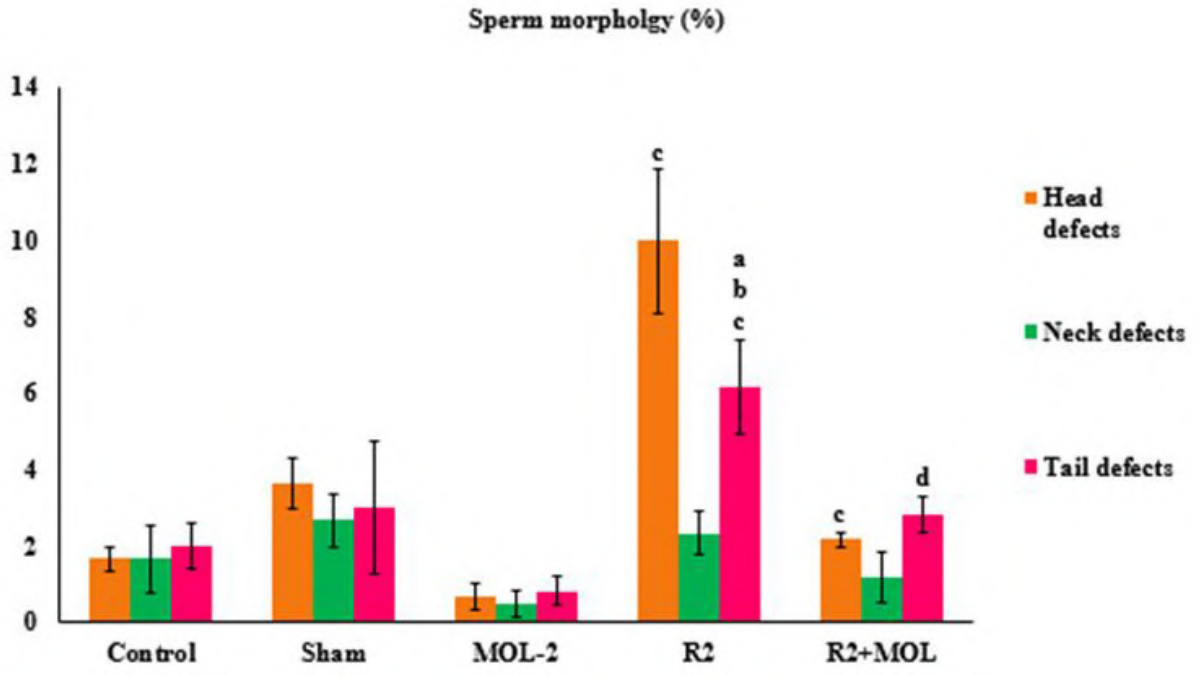

Fig. 4.- Effect of ethanolic extract of MOL on sperm morphology in the 4G-mobile phone-induced-EMR exposed rats. Control group-not exposed to 4G-cell phone for two-months, sham group-exposed to 4G-cell phone in switch off mode for two-months (n=3), MOL-2 group-not irradiated and treated with ethanolic extract of MOL 200 mg/kg for two-months (n=6), R2 group-exposed to 4G-EMR for two-months (n=6) and R2+MOL group-treated with ethanolic extract of MOL 200 mg/kg during 4G-EMR exposure for two-months (n=6). Values are expressed as mean ± SE in each group. P values are by one-way ANOVA with LSD/Tanhane test. Different superscript letters show significant differences between groups ($P<0.05$). a- different from the control group; b- different from the sham group; c- different from the MOL-1 group; d- different from the R2 group.

cant change was observed in the sperm neck defects among the groups. High-frequency radiation significantly elevated the percentage of sperm tail defects in R2 group as compared to the control, sham and MOL-2 groups. The simultaneous treatment with MOL significantly protected the sperms from such defects in R2+MOL group from radiation as compared to the R2 group (Fig. 4).

DISCUSSION

Depending on the power density of the EMR apparatus and the distance from the apparatus, electromagnetic waves can pass through the tissues and promote the synthesis of ROS either directly or indirectly (Kesari et al., 2018). The metabolic cycle of all living cells including spermatozoa produce ROS normally. However, when it builds up too much, the body's own antioxidants help the cell to defend itself (Turk et al., 2008). The OS may be activated by such enhanced ROS production, which could affect the functioning of sperm (Kesari et al., 2018). In this study, the 4G-cell-phone-EMR significantly decreased the sperm count, progressive motility and viability rates but increased the sperm head and neck defects in the radiation group. On the other hand, the ethanolic extract of MOL nearly normalized all the affected values.

Intracellular molecules, notably polyunsaturated fatty acids and transmembrane proteins, are the main targets of ROS. In order to oxidize these molecules with the byproducts of peroxides, lipid aldehydes and alcohol, ROS combines spontaneously with them. Increased permeability results from this, and encourages the oxidative destruction of unsaturated fatty acids in cell membranes (Turk et al., 2008). This disruption can lead to axonemal damage and decreased sperm viability, which may be the cause of the increased sperm mortality rate and decreased sperm count in the R2 group of this study (Turk et al., 2008; Kesari and Behari, 2012). Further, Gautam et al. (2019) concluded that 3G cell phone radiation on male Wistar rats' testes could provoke the development of free radicals causing reduction in sperm count, changes in sperm membrane integrity.

The results of this study are supported by Salama et al. (2010) showed that 12 week-exposure to the GSM handset can result in a significantly low sperm count at the 8th week and more declined sperm motility after 10 weeks in the phone group. Similarly, Abd El Rahman et al. (2014) documented 950 MHz for 2 months could provoke oxidative stress with a significant increase in the level of TBARS, advanced oxidation protein products and carbon monoxide associated with a significant decrease in activities of antioxidant enzymes and GSH content. He added that OS will be accompanied by reproductive hormonal disturbances.

Few studies documented that mobile phone duration for a longer period did not lead to male infertility. Lee et al. (2010) concluded that rats treated with RF-EMR of 848.5 MHz with 2.0 W/kg SAR value for the period of 45 minutes twice a day with the interval of 15 minutes for 12 weeks could not produce harmful effects on male infertility, because EMR did not alter the sperm counts, the testicular and epididymal concentration of MDA. He also reported that CDMA (SAR-2.0 W/kg) and WCDMA (SAR-2.0 W/kg) RF signals failed to produce changes in similar parameters (Lee et al., 2012). Similarly, Ribeiro et al. (2007) argued that rats exposed to RF-EMR emitted by a cellular phone using GSM at the frequency rate of 1835–1850 MHZ for 1 h/d for 11 weeks did not show alteration in testicular and epididymal weight and sperm count. The negative changes in the variables of the present study can be due to the high-frequency induced-EMR and longer duration of exposure/day.

The leaves of drumstick tree are an abundant source of natural antioxidants, as they contain polyphenols and flavonoids that safeguard organisms and cells from oxidative DNA damage involved in aging, cancer and degenerative diseases (Nayak et al., 2016). In this research, the ethanolic extract of MOL recovered all parameters to a near-normal level in R2+MOL (as in the control group). The group with only MOL intervention showed significantly enhanced and decreased viability and abnormal morphology of sperms respectively as compared to the control and sham groups; created negligible discrepancies in the remaining sperm variables.

The antioxidant potential of MOL-Phyto molecules was shown from OH-mediated oxidative damage in human serum albumin protein. It is claimed that phytomolecules of MOL like phenols and flavonoids may hunt free radicals or chelate transitional metal ions resulting in inhibition of Fenton-like reaction or transformation of radical to non-radical (Singh et al., 2009). The results of the present experiments in irradiated animals administered with MOL are in agreement with Nayak et al. (2015), who indicated that previous administration of MOL ethanolic extract could restore the depletion of male gonadal function to normal levels in the case of cyclophosphamide chemotherapy. He continued that perhaps the MOL-phytochemicals and secondary metabolites possess a marked ability to scavenge free radicals. Similar patterns have been shown by Zahran et al. (2015), who conclude that simultaneous administration of MOL extract performed a preventative role against testicular harm caused by Equigan. It can significantly increase the sperm count, germ cell count, testicular superoxide dismutase and total protein in the crypt orchid rats (Afolabi et al., 2013). Bin-Meferij and El-Kott (2015) provided evidence that 900 MHz-EMR treatment can cause microscopic testicular abnormalities with deteriorated spermatozoa in animals, and these effects can be reversed by administering 200 mg/kg of MOL aqueous extract concurrently with EMR; these findings are consistent with the findings of the current investigation.

In conclusion, in this study, short-term exposure to 4G-mobile phone radiation caused a significant change in the sperm count and other sperm parameters. The ethanolic extract of MOL could save the variables from the harmful effects of 4G-EMR. Such protective ability of MOL could be due to antioxidant activity of its phytochemicals.

ACKNOWLEDGEMENTS

The authors like to thank the management of Sri Manakula Vinayagar Medical College and Hospital for its support to complete the study.

Authors' contributions

All the authors contributed significantly to the intellectual content, collection and analysis of data and the reviewing of final version of the work.

REFERENCES

ABD EL RAHMAN NA, ABD EL HADY AM, ELTAHAWY NA (2014) Silymarin and vitamin E modulate 950MHz electromagnetic field-induced oxidative stress and hormonal changes in male albino rats. *J Amer Sci*, 10(9): 170-176.

AFOLABI AO, ADEROJU HA, ALAGBONSI IA (2013) Effects of methanolic extract of Moringa Oleifera leave on semen and biochemical parameters in cryptorchid rats. *Afr J Tradit Complement Altern Med*, 10(5): 230-235.

AGARWAL A, DEEPINDER F, SHARMA R, RANGA G, LI J (2008) Effect of cell phone usage on semen analysis in men attending infertility clinic: an observational study. *Fertil Steril*, 89(1): 124-128.

AGARWAL A, DURAIRAJANAYAGAM D (2015) Are men talking their reproductive health away? *Asian J Androl*, 17(3): 433-434.

AKSU EH, AKMAN O, ÖZKARACA M, ÖMÜR A, UÇAR Ö (2015) Effect of Maclura Pomifera extract on cisplatin-induced damages in reproductive system of male rats. *Kafkas Univ Vet Fak Derg*, 21(3): 397-403.

AVCI B, AKAR A, BILGICI B, TUNÇEL Ö (2012) Oxidative stress induced by 1.8 GHz radio frequency electromagnetic radiation and effects of garlic extract in rats. *Int J Radiat Biol*, 88(11): 799-805.

BAHMANZADEH M, ABOLHASANI F, AMIDI F, EJTEMAEIMEHR S, SALEHNIA M, ABASI M (2008) The effects of nitric oxide synthase inhibitor (L-NAME) on epididymal sperm count, motility, and morphology in varicocelized rat. *DARU J Pharm Sci*, 16(1): 23-28.

BELPOMME D, HARDELL L, BELYAEV I, BURGIO E AND CARPENTER D (2018) Thermal and non-thermal health effects of low intensity non-ionizing radiation: An international perspective. *Environ Pollut*, 242(Pt A): 643-658.

BIN-MEFERIJ MM, EL-KOTT AF (2015) The radioprotective effects of Moringa oleifera against mobile phone electromagnetic radiation-induced infertility in rats. *Int J Clin Exp Med*, 8(8): 12487-12497.

EROGUL O, OZTAS E, YILDIRIM I, KIR T, AYDUR E, KOMESLI G, IRKILATA HC, IRMAK MK, PEKER AF (2006) Effects of electromagnetic radiation from a cellular phone on human sperm motility: an in vitro study. *Arch Med Res*, 37(7): 840-843.

GAUTAM R, SINGH K, NIRALA J, MURMU N, MEENA R, RAJAMANI P (2019) Oxidative stress-mediated alterations on sperm parameters in male Wistar rats exposed to 3G mobile phone radiation. *Andrologia*, 51(3): e13201.

KESARI KK, BEHARI J (2012) Evidence for mobile phone radiation exposure effects on reproductive pattern of male rats: role of ROS. *Electromagn Biol Med*, 31(3): 213-222.

KESARI K, AGARWAL A, HENKEL R (2018) Radiations and male fertility. *Reprod Biol Endocrinol*, 16(1): 118.

KHAKI A (2011) Effect of Ocimum basilicum on apoptosis in testis of rats after exposure to electromagnetic field. *Afr J Pharm Pharmacol*, 5(12): 1534-1537.

KIM JY, KIM HT, MOON KH, SHIN HJ (2007) Long-term exposure of rats to a 2.45 GHz electromagnetic field: effects on reproductive function. *Korean J Urol*, 48: 1308-1314.

LEE HJ, PACK JK, KIM TH, KIM N, CHOI SY, LEE JS, KIM SH, LEE YS (2010) The lack of histological changes of CDMA cellular phone-based radio frequency on rat testis. *Bioelectromagnetics*, 31(7): 528-534.

LEE HJ, JIN YB, KIM TH, PACK JK, KIM N, CHOI HD, LEE JS, LEE YS (2012) The effects of simultaneous combined exposure to CDMA and WCDMA electromagnetic fields on rat testicular function. *Bioelectromagnetics*, 33(4): 356-364.

LUTHFI MJ (2015) A simple and practical method for rat epididymal sperm count (Rattus norvegicus). *Biol Med Natural Product Chem*, 4(1): 1-3.

MAILANKOT M, KUNNATH AP, JAYALEKSHMI H, KODURU B, VALSALAN R (2009) Radio frequency electromagnetic radiation (RF-EMR) from GSM (0.9/1.8GHz) mobile phones induces oxidative stress and reduces sperm motility in rats. *Clinics* (Sao Paulo), 64(6): 561-565.

MEO SA, ARIF M, RASHIED S, HUSAIN S, KHAN MM, VOHRA MS, USMANI AM, IMRAN MB, AL-DREES AM (2011) Hypospermatogenesis and spermatozoa maturation arrest in rats induced by mobile phone radiation. *J Coll Physicians Surg Pak*, 21(5): 262-265.

NARAYANAN S, KUMAR R, POTU B, NAYAK S, MAILANKOT M (2009) Spatial memory perfomance of Wistar rats exposed to mobile phone. *Clinics*, 64(3): 231-234.

NAYAK G, VADINKAR A, NAIR S, KALTHUR SG, D'SOUZA AS, SHETTY PK (2015) Sperm abnormalities induced by pre-pubertal exposure to cyclophosphamide are effectively mitigated by Moringa oleifera leaf extract. *Andrologia*, 48(2): 125-136.

NAYAK G, VADINKAR A, NAIR S, KALTHUR SG, D'SOUZA AS, SHETTY PK, KALTHUR G, ADIGA SK (2016) Sperm abnormalities induced by pre-pubertal exposure to cyclophosphamide are effectively mitigated by Moringa oleifera leaf extract. *Andrologia*, 48(2): 125-136.

OH J, BYUN S, LEE S, CHOE G, HONG S (2018) Effect of electromagnetic waves from mobile phones on spermatogenesis in the era of 4G-LTE. *Biomed Res Int*, 2018: 1801798.

OLIVA A, SPIRA A, MULTIGNER L (2001) Contribution of environmental factors to the risk of male infertility. *Hum Reprod*, 16(8): 1768-1776.

RIBEIRO EP, RHODEN EL, HORN MM, RHODEN C, LIMA LP, TONIOLO L (2007) Effects of subchronic exposure to radio frequency from a conventional cellular telephone on testicular function in adult rats. *J Urol*, 177(1): 395-399.

SALAMA N, KISHIMOTO T, KANAYAMA HO, KAGAWA S (2010) Effects of exposure to a mobile phone on sexual behavior in adult male rabbit: an observational study. *Int J Impot Res*, 22: 127-133.

SINGH BN, SINGH BR, SINGH RL, PRAKASH D, DHAKAREY R, UPADHYAY G, SINGH HB (2009) Oxidative DNA damage protective activity, antioxidant and anti-quorum sensing potentials of Moringa oleifera. *Food Chem Toxicol*, 47(6): 1109-1116.

SÖNMEZ M, TÜRK G, YÜCE A (2005) The effect of ascorbic acid supplementation on sperm quality, lipid peroxidation and testosterone levels of male Wistar rats. *Theriogenology*, 63(7): 2063-2072.

STOHS SJ, HARTMAN MJ (2015) Review of the safety and efficacy of Moringa oleifera. *Phytother Res*, 29(6): 796-804.

TORAGALL M, SATAPATHY S, KADADEVARU G, HIREMATH M (2019). Association of demographic and lifestyle factors with semen quality of men with fertility problems attending infertility center in North Karnataka. *Indian J Med Spec*, 10(2): 79.

TÜRK G, SÖNMEZ M, AYDIN M, YÜCE A, GÜR S, YÜKSEL M, AKSU EH, AKSOY H (2008) Effects of pomegranate juice consumption on sperm quality, spermatogenic cell density, antioxidant activity and testosterone level in male rats. *Clin Nutr*, 27(2): 289-296.

VONGSAK B, SITHISARN P, MANGMOOL S, THONGPRADITCHOTE S, WONGKRAJANG Y, GRITSANAPAN W (2013) Maximizing total phenolics, total flavonoids contents and antioxidant activity of Moringa oleifera leaf extract by the appropriate extraction method. *Ind Crops Prod*, 44: 566-571.

ZAHRAN F, TOUSSON E, SHALAPY M (2015) Ameliorating effect of Ginkgo biloba and Moringa oleifera against Equigan induced testicular toxicity and oxidative stress in male rat. *Am J Biol Chem*, 3(2): 39-44.

The anatomical descriptive pattern of the greater occipital nerve in identified Brazilian cadavers and its clinical implications for scalp anesthesia and migraine treatment

Rubens M.M. da Silva[1], Amanda A.R. Massoni[1], Giuliano R. Gonçalves[2], Igor E.U. Ordenes[2], Leandro H. Grecco[2], Diogo C. Maldonado[1]

[1] *Department of Morphology and Genetics, Federal University of São Paulo, São Paulo, Brazil*

[2] *Department of Anatomy - Universidade São Leopoldo Mandic, Campinas, Brazil*

SUMMARY

Among the measures instituted for the treatment of migraine, the greater occipital nerve (GON) block is described as being an effective, safe, easy to perform and useful technique for the treatment of this condition. However, the measures used to block the GON vary, and there is a lack of information data about the Brazilian population. Therefore, a morphometric study was carried out on 22 identified cadavers, in which the distances were measured on both sides of the following anatomical points: EOP, MP, and GON with anatomical references of the nuchal ligament, Trapezius muscle aponeurosis and MSEC perforation. ANOVA was used for statistical analysis, with Tukey post-hoc and Eta Square (η2) for effect size. Significance was adopted when $p \leq 0.05$. The ANOVA found a significant effect of ethnicity regarding the distances in the GON measurements of the EOP on the line between the EOP and MP – Left antimere; subsequent univariate analysis showed differences between white and oriental ethnicity (pTukey= 0.02); horizontal distance of the GON about the nuchal line – Right antimere; Subsequent univariate analysis showed differences between white and brown ethnicities (pTukey= 0.02); horizontal distance of the GON about the nuchal line – Left antimere. Subsequent univariate analyses showed differences between white and brown ethnicities (pTukey= 0.02). There are morphometric differences in some anatomical points used to block the GON when comparing the two antimeres, as well as in white, brown, and oriental ethnicities.

Keywords: Migraine - Scalp anesthesia - Greater occipital nerve

ABBREVIATIONS

EOP: External occipital protuberance

GON: Greater Occipital Nerve

MD: Midline

MP: Mastoid process

MSEC: Musculus Semispinalis capitis

Corresponding author:
Diogo Corrêa Maldonado. Department of Morphology and Genetics, Federal University of São Paulo, São Paulo, Brazil. Phone: +55 (11) 986060437. E-mail: maldonado@unifesp.br

Submitted: December 22, 2024. **Accepted:** January 24, 2024

https://doi.org/10.52083/CDAR8373

INTRODUCTION

The International Classification of Headache Disorders, third edition (ICHD-3; beta version) in 2013 described migraine as a common and disabling type of primary headache. Among the measures instituted for the treatment of migraine, the block of the greater occipital nerve (GON) is described as being an effective, safe, easy to perform, and useful technique for the treatment of this condition (Castillo-Álvarez et al., 2023; Chowdhury et al., 2021). The GON originates from fibers of the dorsal primary branch of the second cervical nerve and, to a lesser extent, from fibers of the third cervical nerve. The GON provides cutaneous innervation to most of the posterior scalp (Shin et al., 2018). Along its path, it is closely related to the rectus capitis posterior major and semispinatus capitis muscles. It becomes superficial at the level of the superior nuchal line medially to the occipital artery and follows together (Kwon et al., 2018), piercing the aponeurosis of the trapezius muscle to then emerge on the scalp (Choi and Jeon, 2016). According to Santos et al. (2017) and Stern et al. (2022), the location of the GON is based on drawing an imaginary line between the occipital protuberance and the mastoid process, locating the exit of the nerve at the point that joins the medial third of this line with the two most lateral thirds (Fig. 1).

Uyar Türkyilmaz et al. (2018) described in their study that the treatment of occipital neuralgia with GON block appears to be a minimally invasive, easy, and effective method. In their research, bilateral blockade of the GON was performed using a method based on anatomical landmarks, in which the GON is located approximately two-thirds of the way along a line drawn from the center of the mastoid process to the external occipital protuberance.

However, this method is challenging to obtain significant results due to the variations in distances and perforations that the GON may have during its anatomical course (Tubbs et al., 2014).

The external occipital protuberance (EOP), mastoid process (MP), and midline (ML) corresponding to the nuchal ligament are important topographic references for analgesia (Choi and Jeon, 2016; Simon et al., 2023). Natsis et al. (2006) emphasized in their work that simple palpation of the occipital region as a method to anesthetize the GON is an inadequate way, as in their results important variations of the peripheral path of the GON were identi-

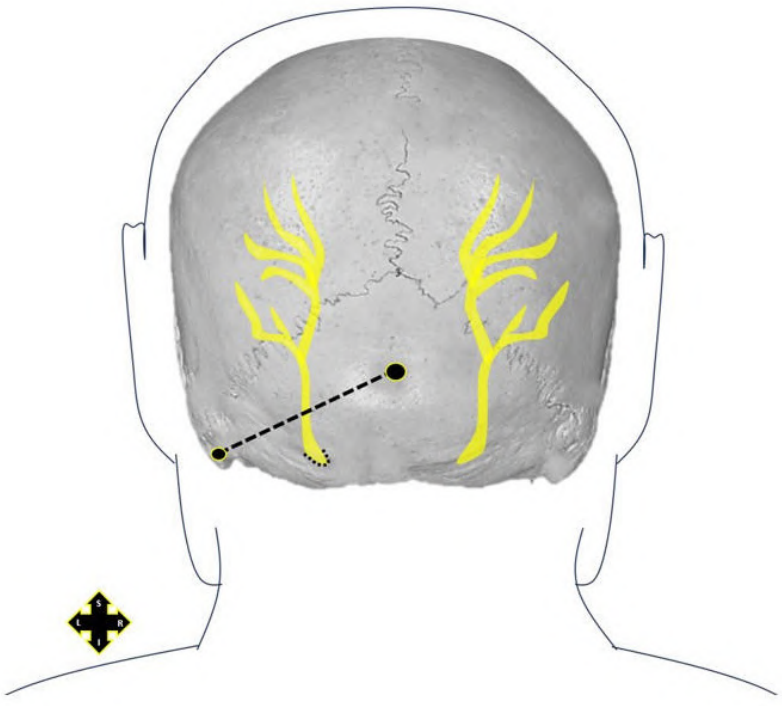

Fig. 1.- Representation of the EOP and MP anatomical points as well as the usual location of GON emergence in the subcutaneous tissue, according to Santos et al. (2017) and Stern et el. (2022).

fied, including significant changes on the right and left sides of the neck of the same cadaver.

Therefore, the use of accurate anatomical parameters proves to be essential in the treatment of migraines, as well as in scalp anesthesia. In this sense, in a scenario in which we have a lack of studies that analyzed identified Brazilian cadavers, this work seeks to analyze the path of the GON in different sexes and ethnicities to find possible correlations as well as anatomical variations and morphological disparities in the two antimeres, thus promoting a standard to be followed by clinicians working in the areas of anesthesiology and neurology.

MATERIALS AND METHODS

A morphometric study was carried out on 22 identified corpses, 13 of which were female, 9 were male, 17 were white, 3 were mixed-race, one was black and one was Asian, with no history of trauma in the region studied. All cadavers were donated for study and scientific research to the descriptive and topographic human anatomy laboratory at the Federal University of São Paulo (Brazil), the ages ranging between 39 and 88 years with an average of 69 years. The study was submitted to the ethics and research committee of the Federal University of São Paulo, Brazil, and had its opinion approved under no. 6,062,607. The distances on both sides of the neck of the following anatomical points were measured using a Mitutoyo® 150 mm Digital Caliper – 150 mm capacity, 0.01 mm resolution, accuracy +/- 0.03 mm: EOP, MP and GON with ML anatomical references, point of perforation of the GON in the aponeurosis of the Trapezius muscle and point of perforation of the GON in the semispinalis capitis muscle (MSEC) (Fig. 2). Two main groups of measurements were carried out on both sides, right and left. In the first, the horizontal distance between the GON, at the point where it pierces the MSEC, and the LM was measured, taking the nuchal ligament as a reference. The vertical distance, parallel to the nuchal ligament, between the GON, at the point where it pierces the MSEC, and the EOP was also measured. In the second group, a line was drawn between the EOP and the MP, and the distance from the GON at the point where it pierces the trapezius aponeurosis in relation to the EOP was obtained. Data were tabulated for descriptive and statistical analyses using Jamovi software (version 2.3). The descriptive data for the categorical variables, age group, race, and gender, were described with frequency (%). Data on continuous variables of measured distances were described with mean ± standard deviation. The age variable was categorized into 'elderly and non- elderly', according to the IBGE age classification – the Brazilian Institute of Geography and Statistics (2023), with ≤ 59 years old being considered 'non-elderly' and ≥ 60 years old 'elderly'. A one-way ANOVA was used to ver-

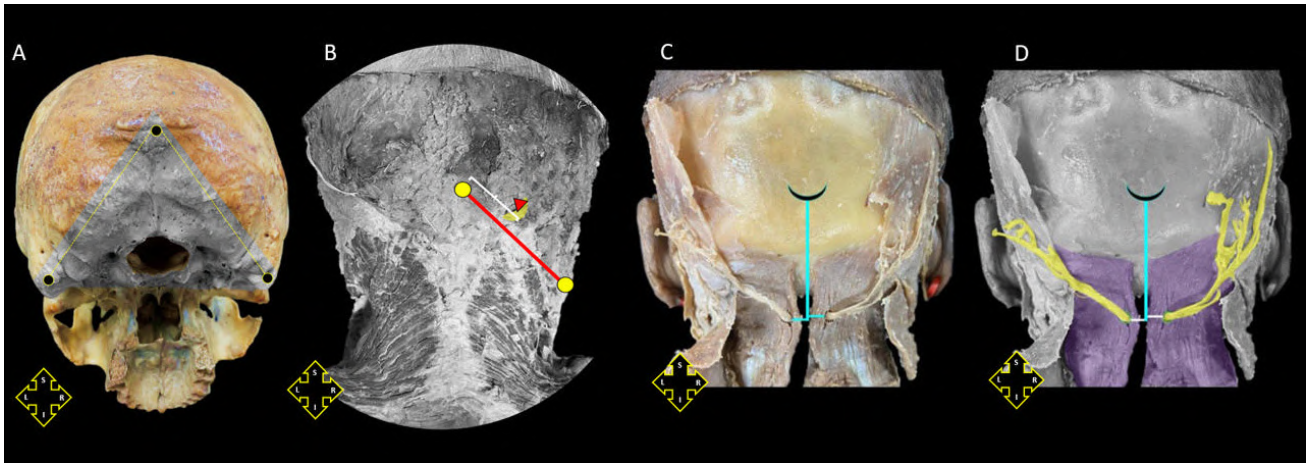

Fig. 2.- Suboccipital region in dissected planes demonstrating the anatomical reference points for analyzing the appearance of the greater occipital nerve. **A**: in skull posterior view, external occipital protuberance in the upper marking and bilateral mastoid process in the lower markings. **B**: dissection at the superficial muscular level demonstrating the identification and measurement of the appearance of the greater occipital nerve. **C-D**: bilateral measurement between the appearances of the greater occipital nerves with standardization to the midline and external occipital.

ify the effect of gender, ethnicity and age groups on the distance measurements taken as a basis in relation to the position of the GON. The Shapiro-Wilk and Levene tests were applied to test the requirements for normality and homogeneity respectively. The data presented normality and homogeneity, so no correction was necessary. Univariate 2 to 2 comparisons were made using Tukey's post-hoc; and to report the magnitude of differences, the Cohen's d effect size measure was used for post hoc and Eta Square (η2) for ANOVA. Significance levels were accepted when $p \leq 0.05$.

RESULTS

Table 1 presents the descriptive data of the categorical variables: gender, age group and ethnicity. The values of the distances measured in relation to the anatomical points are described in Table 2, with mean ± standard deviation and minimum and maximum values.

Table 1. Sample description.

Sex	Age Group	Ethnicity	Counts	% of Total
Male	Non-elderly	White	3	13.6 %
		Asian	0	0.0 %
		Black	1	4.5 %
		Brown	1	4.5 %
	Elderly	White	2	9.1 %
		Asian	0	0.0 %
		Black	0	0.0 %
		Brown	2	9.1 %
Female	Non-elderly	White	0	0.0 %
		Asian	0	0.0 %
		Black	0	0.0 %
		Brown	0	0.0 %
	Elderly	White	12	54.5 %
		Asian	1	4.5 %
		Black	0	0.0 %
		Brown	0	0.0 %

Table 3. ANOVA distance and ethnicity.

Distance GON (EOP) line EOP MP - Left			
	F	p	η^2
Ethnicity	4.92	0.01*	0.451
Horizontal distance GON in relation ML - Left			
	F	p	η^2
Ethnicity	3.01	0.05*	0.334
Horizontal distance GON in relation ML - Right			
	F	p	η^2
Ethnicity	4.16	0.02*	0.409

*significant differences between ethnicity in relation to the distances of anatomical points

The main results of the analysis of variance (ANOVA) are described in Table 3. ANOVA found a significant difference in the categories of the ethnicity variable depending on the distances in the GON measurements from the EOP and the line between the EOP and MP – Left antimere F= (3.18) 4.92, p= 0.01, η^2p= 0.45, subsequent univariate analysis showed differences between white and brown ethnicities (pTukey =0.02); Horizontal Distance of the GON in relation to the ML – Right antimere F= (3.18) 4.16, p= 0.02, η^2p= 0.40, subsequent univariate analysis showed differences between white and oriental ethnicity (pTukey = 0.02); Horizontal Distance of the GON in relation to the ML – Left antimere F= (3.18) 3.01, p=0.05, η^2p= 0.33, subsequent univariate samples showed differences between white and brown ethnicities (pTukey =0.02). Two anatomical variations were found during the study: in one of the cases, the GON passed medially to the MSEC, without perforating it, and in the other case there was a double perforation of the MSEC (Fig. 4).

Figure 3 presents the confidence intervals of the univariate analysis showing the statistically significant differences between the groups. There are morphometric differences in some anatomical points used to block the GON when comparing the two antimeres, as well as in white, brown and oriental ethnicities.

Table 2. Distances from anatomical points.

	N	Mean	SD	Minimum	Maximum
Distance between the EOP and MP	22	98.8	8.91	74.00	115.4
Distance of the GON from the EOP on the line between EOP and MP - right	22	35.2	7.62	19.58	49.9
Distance from the GON to the EOP on the line between EOP and MP - left	22	34.7	10.56	17.02	61.5
Vertical distance of the GON from the EOP (in relation to the ML) - right	22	36.2	12.21	15.72	55.1
Vertical distance of the GON from the EOP (in relation to the ML) - left	22	35.8	10.50	16.40	55.1
Horizontal distance of the GON in relation to ML - right	22	14.9	4.65	7.81	26.1
Horizontal distance of the GON in relation to ML - left	22	15.0	5.71	3.76	26.1

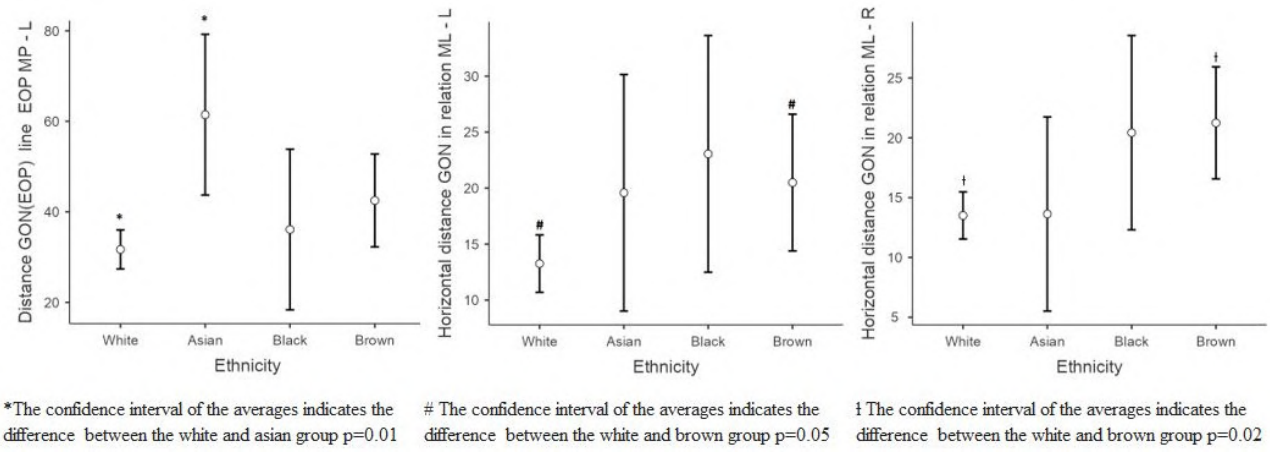

Fig. 3.- Confidence intervals of univariate analysis – Ethnicity.

Fig. 4.- Suboccipital regions in dissected planes demonstrating the anatomical variations of the appearance of the greater occipital nerve. A: anatomical variation in which the nerve passes medial to the MSEC without piercing. B: anatomical variation with double perforation of the m. semispinalis capitis (plane of the MSEC). C: anatomical variation with double perforation of the MSEC (plane of the suboccipital triangle – point where the nerve passes below the inferior oblique capital muscle).

DISCUSSION

This study aimed to analyze the morphological distribution of GON in the most superficial plane in the necks of identified Brazilian cadavers. In addition to this, statistical analysis was carried out to verify possible associations between the ethnicities, sex, and antimeres studied to generate a descriptive, pattern-safe anatomical approach to GON.

According to Stern et al. (2022) and Pingree et al. (2017), there are several techniques for blocking the GON, generally with the patient sitting and facing away from the doctor. The block can occur based on distances of 1.5 to 2 cm lateral and 2 to 3 cm inferior to the occipital protuberance, At a deeper level, the block can be performed at the C2 level, by ultrasonographic localization of the GON nerve over the inferior oblique muscle of the head. In both cases, it must be remembered that the occipital artery runs laterally to the GON. Therefore, it is advisable to perform aspiration before infusing the medication to avoid perfusing the anesthetic into the bloodstream.

Regarding the distances between GON and EOP, Guvençer et al. (2011) found a distance between the GON at the point where it pierces the semispinalis capitis in relation to the EOP of 53.6 ± 5.0 mm on the right and 53.3 ± 6.1 mm on the left, without differentiation between sexes. Mosser et al. (2002), in turn, described a distance of 29.1 ± 7.8 mm on the right and 28.7 ± 6.6 mm on the left, without also differentiating genders. In our findings, on the other hand, we found, on the right, a distance of 40.7 ± 8.37 in females and 47.6 ± 13.26 in males and, on the left, 39.6 ± 9.91 in females and 43.1 ± 5.45 in males. Therefore, there are significant differences in the distances of our sample, derived from Brazilian cadavers, in relation to those measured in cadavers of other nationalities in the aforementioned studies. It is worth mentioning that the point at which the nerve is measured finds its importance in the fact that the GON trunk anesthesia is performed in this location.

Huanmanop et al. (2021) reported that the number of specimens and ethnicity can influence the

prevalence of different routes of the GON throughout its course. These data are in line with ours, as we noticed significant differences in the emergence pattern, and distances from pre-defined anatomical points for measurements, especially between white, brown, and Asian ethnicities, as there was a significant effect of ethnicity in terms of distances in measurements of the GON of the EOP and the line between the EOP and MP in the left antimere.

When we took the inter mastoid line as a reference, our data revealed that in none of the cases did the GON perforate the most superficial plane of the neck, below it, this finding is in line with the work of Loukas et al. (2006). The perforation point in the subcutaneous region, taking the aponeurosis of the trapezius muscle as a reference, was 44% (44.36 ± 4.52%) of the distance along the MD of the ipsilateral MP with an average vertical distance of about 18 mm (17.97 ± ± 5.80 mm) (Fig. 2B). No statistically significant difference was found between sexes and sides.

Furthermore, it was demonstrated that the GON perforated the MSEC in 98%, a result similar to that of Huanmanop et al. (2021), where it was reported that this perforation occurred in 95% of cases.

Finally, it should be mentioned that, in relation to the anatomical variations found in our work (Fig. 4), the non-perforation of the MSEC by the GON was also described by Bovin et al. (1990), in a case in which the GON evaded the muscle bilaterally and in two others where penetration was present on one side and absent on the other. In the work of Huanmanop et al. (2020), in 33% of cases, the GON ran between the most medial fibers of the MSEC and the nuchal ligament, and, finally, in the work of Ducic et al. (2009), in 1.5% of cases, the GON ran medially to the MSEC.

The present study has some limitations. The first is that the measurements were carried out by a single researcher. We suggest that researchers who may want to repeat our method use two researchers to carry out the measurements. Secondly, 22 samples could be included in the study, because it was carried out with donated and identified cadavers. In this sense, we did not have homogeneity between the samples, especially in the ethnicities that were compared. We encourage that, in another opportunity, anatomists can repeat our method with equality between sexes and compared ethnicities.

Finally, we know that cadaveric tissues are essential for the evolution of research into human tissues, as well as for human anatomy teachers around the world. We agree in all aspects with the manuscript by Iwanaga et al. (2020): “The results of this research can potentially increase humanity’s overall knowledge, which can then improve patient care. Therefore, these donors and their families deserve our utmost gratitude” .

Knowledge of the distribution of the GON and its trajectory, as well as its anatomical variations, is of great clinical importance, since the definition of accurate anatomical parameters for carrying out procedures involving the GON is essential. We observed that there is homogeneity in the distribution of GON, with no significant differences in sex and laterality. Differences in the perforation patterns and path of the GON were observed in studies carried out in Asia, Central America, and Europe. In this sense, we need more studies in the Latin American continent to define whether the anatomical points commonly used in other continents can be reproduced with security in the Brazilian population.

REFERENCES

BALLESTEROS-DEL RIO B, ARES-LUQUE A, TEJADA-GARCIA J, MUELA-MOLINERO A (2003) Occipital (Arnold) neuralgia secondary to greater occipital nerve schwannoma. *Headache*, 43(7): 804-807.

BIGAL ME, LIPTON RB (2009) The epidemiology, burden, and comorbidities of migraine. *Neurol Clin*, 27: 321-334.

BRESLAU N, SCHULTZ L, LIPTON R, PETERSON E, WELCH KM (2012) Migraine headaches and suicide attempt. *Headache*, 52: 723-731.

BUSE D, MANACK A, SERRANO D, REED M, VARON S, TURKEL C, LIPTON R (2012) Headache impact of chronic and episodic migraine: results from the American Migraine Prevalence and Prevention study. *Headache*, 52: 3-17.

CASTILLO-ÁLVAREZ F, BÁRCENA IH, MARZO-SOLA MEM (2023) Greater occipital nerve block in the treatment of headaches. Review of evidence. *Med Clin (Barc)*, 161(3): 113-118.

CESMEBASI A, LOUKAS M, HOGAN E, KRALOVIC S, TUBBS RS, COHEN-GADOL AA (2015) The Chiari malformations: a review with emphasis on anatomical traits. *Clin Anat*, 28(2): 184-194.

CHOI I, JEON SR (2016) Neuralgias of the head: occipital neuralgia. *J Korean Med Sci*, 31(4): 479-488.

CHOWDHURY D, DATTA D, MUNDRA A (2021) Role of greater occipital nerve block in headache disorders: a narrative review. *Neurology India*, 69: 228-259.

DUCIC I, HARTMANN EC, LARSON EE (2009) Indications and outcomes for surgical treatment of patients with chronic migraine headaches caused by occipital neuralgia. *Plast Reconstr Surg*, 123(5): 1453-1461.

DUCIC I, MORIARTY M, AL-ATTAR A (2009) Anatomical variations of the occipital nerves: implications for the treatment of chronic headaches. *Plast Reconstr Surg*, 123: 859-863.

GÜVENÇER M, AKYER P, SAYHAN S, TETIK S (2011) The importance of the greater occipital nerve in the occipital and the suboccipital region for nerve blockade and surgical approaches – an anatomic study on cadavers. *Clin Neurol Neurosurg*, 113: 289-294.

HECHT JS (2004) Occipital nerve blocks in postconcussive headaches: a retrospective review and report of ten patients. *J Head Trauma Rehabil*, 19(1): 58-71.

HEADACHE CLASSIFICATION COMMITTEE OF THE INTERNATIONAL HEADACHE SOCIETY (IHS) (2018) The International Classification of Headache Disorders. 3rd ed. *Cephalalgia*, 38(1): 1-211.

HUANMANOP T, ISSARA I, AGTHONG S, CHENTANEZ V (2021) Evaluations of the greater occipital nerve location regarding its relation to intermastoid and external occipital protuberance to mastoid process lines. *Folia Morphol*, 80(3): 533-541.

IWANAGA J, SINGH V, OHTSUKA A, HWANG Y, KIM HJ, MORYŚ J, RAVI KS, RIBATTI D, TRAINOR PA, SAÑUDO JR, APAYDIN N, ŞENGÜL G, ALBERTINE KH, WALOCHA JA, LOUKAS M, DUPARC F, PAULSEN F, DEL SOL M, ADDS P, HEGAZY A, TUBBS RS (2020) Acknowledging the use of human cadaveric tissues in research papers: Recommendations from anatomical journal editors. *Clin Anat*, 34(1): 2-4.

JANIS JE, HATEF DA, REECE EM, MCCLUSKEY PD, SCHAUB TA, GUYURON B (2010) Compressão neurovascular do nervo occipital maior: implicações para enxaquecas. *Plast Reconstr Surg*, 126(6): 1996-2001.

KEMP WJ, TUBBS RS, COHEN-GADOL AA (2011) The innervation of the scalp: A comprehensive review including anatomy, pathology, and neurosurgical correlates. *Surg Neurol Int*, 2: 178.

KWON HJ, KIM HS, KANG HJ, WON JY, YANG HM, CHOI Y (2018) Anatomical analysis of the distribution patterns of occipital cutaneous nerves and the clinical implications for pain management. *J Pain Res*, 11: 2023-2031.

LOUKAS M, EL-SEDFY A, TUBBS RS, LOUIS RG JR, WARTMANN CHT, CURRY B, JORDAN R (2006) Identification of greater occipital nerve landmarks for the treatment of occipital neuralgia. *Folia Morphol (Warsz)*, 65(4): 337-342.

MEGAN Y, WANG SM (2022) Anatomy Head and Neck, Occipital Nerves. *StatPearls Publishing [Internet]*.

MOSSER SW, GUYURON B, JANIS JE, ROHRICH RJ (2004) The anatomy of the greater occipital nerve: implications for the etiology of migraine headaches. *Plastic Reconst Surg*, 113(2): 696-697.

MUELLER O, HAGEL V, WREDE K, SCHLAMANN M, HOHN HP, SURE U, GAUL C (2013) Stimulation of the greater occipital nerve: anatomical considerations and clinical implications. *Pain Physician*, 16(3): E181-189.

NATSIS K, BARALIAKOS X, APPELL HJ, TSIKARAS P, GIGIS I, KOEBKE J (2006) The course of the greater occipital nerve in the suboccipital region: A proposal for setting landmarks for local anesthesia in patients with occipital neuralgia. *Clin Anat*, 19(4): 332-336.

PERELSON HN (1947) Occipital nerve tenderness: a sign of headache. *South Med J*, 40(8): 653-656.

PINGREE MJ, SOLE JS, O'BRIEN TG, ELDRIGE JS, MOESCHLER SM (2017) Clinical efficacy of an ultrasound-guided greater occipital nerve block at the level of C2. *Reg Anesth Pain Med*, 42: 99-104.

SANTOS LASAOSA S, CUADRADO PÉREZ ML, GUERRERO PERAL AL, HUERTA VILLANUEVA M, PORTA-ETESSAM J, POZO-ROSICH P, PAREJA JA (2017) Consensus recommendations for anaesthetic peripheral nerve block. *Neurologia*, 32: 316-330.

SIMON SK, ROUT S, LIONEL KR, JOEL JJ, DANIEL P (2023) Anatomical considerations of cutaneous nerves of scalp for an effective anesthetic blockade for procedures on the scalp. *J Neurosci Rural Pract*, 14(1): 62-69.

SHIMIZU S, OKA H, OSAWA S, FUKUSHIMA Y, UTSUKI S, TANAKA R, FUJII K (2007) Can proximity of the occipital artery to the greater occipital nerve act as a cause of idiopathic greater occipital neuralgia? An anatomical and histological evaluation of the artery-nerve relationship. *Plast Reconstr Surg*, 119(7): 2029-2034.

SLAVIN KV, NERSESYAN H, WESS C (2006) Peripheral neurostimulation for treatment of intractable occipital neuralgia. *Neurosurgery*, 58(1): 112-119.

SHIN KJ, KIM HS, JEHOON O, KWON HJ, YANG HM (2018) Anatomical consideration of the occipital cutaneous nerves and artery for the safe treatment of occipital neuralgia. *Clin Anat*, 31(7): 1058-1064.

STERN JI, CHIANG C, KISSOON NR, ROBERTSON CE (2022) Narrative review of peripheral nerve blocks for the management of headache. *Headache J Head Face Pain*, 62: 1077-1092.

THIEL W (2004) Atlas Fotográfico Colorido de Anatomia Humana: Cabeça e Pescoço. Revinter, Rio de Janeiro, p 372.

TUBBS RS, SALTER EG, WELLONS JC, BLOUNT JP, OAKES WJ (2007) Landmarks for the identification of the cutaneous nerves of the occiput and nuchal regions. *Clin Anat*, 20(3): 235-238.

TUBBS RS, WATANABE K, LOUKAS M, COHENGADOL AA (2014) The intramuscular course of the greater occipital nerve: novel findings with potential implications for operative interventions and occipital neuralgia. *Surg Neurol Int*, 5: 155.

UYAR TÜRKYILMAZ E, CAMGÖZ ERYILMAZ N, AYDIN GÜZEY N, MORALOĞLU Ö (2016) Bilateral greater occipital nerve block for treatment of post-dural puncture headache after caesarean operations. *Braz J Anesthesiol*, 66(5): 445-450.

WON HJ, JI HJ, SONG JK, KIM YD, WON HS (2018) Topographical study of the trapezius muscle, greater occipital nerve, and occipital artery for facilitating blockade of the greater occipital nerve. *PLoS One*, 13(8): e0202448.

Sensory nerve formations in the myodural bridge complex of adult humans

Ruth Esteban-Marín[1,2], Yolanda García-Mesa[2], Patricia Cuendias[2], Olivia García-Suárez[2], María A. Franco-Sierra[3], Pablo Herrero[3], Yolanda Marcén-Román[1], José A. Vega[2,4]

[1] Department of Human Anatomy and Histology, Faculty of Medicine, University of Zaragoza, IIS Aragón, Spain

[2] Department of Morphology and Cell Biology, SINPOS Group, Faculty of Medicine, University of Oviedo, Spain

[3] Department of Physiatry and Nursing, Faculty of Health Sciences, University of Zaragoza, IIS Aragón, Spain

[4] Faculty of Health Sciences, Autonomous University of Chile, Providencia - Santiago, Chile

SUMMARY

The myodural bridge complex (MDBC) consists of connective tissue bands connecting the spinal dura mater to the suboccipital muscles passing throughout the posterior atlanto-occipital and atlanto-axial spaces. It is a universal evolutionarily conserved anatomical structure present in most vertebrate species including humans. Its physiology is unknown, but it is thought that it may be related to cerebrospinal fluid circulation. On the other hand, there is no information about the possible innervation of MDBC in humans. In the present study, immunohistochemistry (S100 protein and neurofilament proteins) was used to study the innervation of MDBC in five specimens of adult human cadavers. In all cases, nerve profiles were observed forming isolated nerve fibers or small nerve bundles, sometimes associated with blood vessels. In one case (1/5), at the level of the junction of the MDBC with the *posterior rectus capitis minor* muscle, complex capsulated formations containing a variable number of sensory nerve formations were found. We consider that such formations may be related to the proprioceptor system of the suboccipital muscles, but further studies are needed to determine their frequency, density and possible function.

Key words: Myodural bridge complex – Innervation – Sensory nerve formations – Human

INTRODUCTION

In 1995, Hack et al. described in human a dense bilateral band of connective tissue that connects the spinal dura mater to the suboccipital musculature (primarily the *rectus capitis posterior minor* muscle, but also the *rectus capitis posterior major* and *obliquus capitis inferior* muscles) and the *ligamentum nuchae* (LN), passing throughout the posterior atlanto-occipital and atlanto-axial membranes (see Humphreys et al., 2003). All together these structures are currently known as myodural bridge complex (MDBC) (Kahkeshani and Ward, 2012; Scali et al., 2011, 2015, 2022; Pontell et al., 2013; Zheng et al., 2020), regarded as an universal evolutionarily conserved anatomical structure present in different vertebrate species (Zheng et

Corresponding author:
Ruth Esteban-Marín. Facultad de Medicina (Edificio A), Departamento de Anatomía e Histología Humanas, Universidad de Zaragoza, C/ Domingo Miral s/n, 50009 Zaragoza, Spain. Phone: +34678526990. E-mail: ruthesteban@unizar.es

Submitted: January 10, 2024. **Accepted:** January 31, 2024

https://doi.org/10.52083/VTPE2412

al., 2017) including horses (McElroy et al., 2019), rats (Lai et al., 2021; Song et al., 2023), marine mammals (Liu et al., 2017, 2018; Zhang et al., 2021), reptilians (Zhang et al., 2016; Huangfu et al., 2019; Grondel et al., 2022), and birds (Okoye et al., 2018; Dou et al., 2019; Chen et al., 2021).

After the description of Hack et al. (1995), numerous studies have been conducted in humans to establish in detail the anatomy of MDBC (see Scali et al., 2015). Using imaging techniques, Humphreys et al. (2003) compared magnetic resonance with anatomical dissection images and reported that MDBC appeared as a small low signal intensity band on T_1-weighted images. Later, Scali et al. (2013b) examined the anatomy of the posterior atlanto- axial space using T_2-weighted MR imaging and identified MDBC as oblique hypointense fibers (see for a review Sun et al., 2020). Structurally, MDBC consists of connective tissue containing vessels and very scarce nerves (Pontell et al., 2013; Scali et al., 2013a).

Functionally, MDBC is theorized to stabilize the dura mater during the extension of the head and neck, thus serving as dural tension monitors, preventing compression of the dura mater during motion of the spinal column and infolding of the dura mater and disruption of the flow of cerebrospinal fluid (Hallgren et al., 1997; Pontell et al., 2013; Enix et al., 2014; Chen et al., 2015; Sillevis and Hogg, 2020).

In this study, it is hypothesized that, in addition, MDBC are sources of proprioceptive inputs that regulate the contraction of the suboccipital muscles. These muscles are involved in head movements, but they also play important roles as joint stabilizers of the upper cervical spine or postural controllers (Hallgren et al., 2014a, b, 2017). Here, we have studied the presence of sensory nerve formations in MDBC using immunohistochemistry techniques. The purpose of the study is to contribute to the knowledge of the possible functions of MDBC in humans, and to demonstrate that they are sensory-innervated structures able to transmit stimuli, via afferent pathways, to the central nervous system related to the control of head stability.

MATERIAL AND METHODS

Tissues

Five formalin-fixed hemi-heads, corresponding to 5 different subjects, 3 males and 2 females, were obtained at the Área de Anatomía y Embriología Humana de la Universidad de Oviedo, Spain. These materials were obtained in accordance with Spanish legislation (RD 1301/2006; Law 14/2007; RD 1716/2011; Order ECC/1404/2013). Thereafter, MDBC were identified (mobilizing the cephalo-cervical junctions and observing the tension of the connective bands arranged between the dura mater, the atlanto-occipital membrane, or the suboccipital muscles) and dissected (Fig. 1). The pieces were washed in tap water for 24 hours, then processed for routinely paraffin embedding. The pieces were cut into10 µm sections, mounted on gelatin-coated microscope slides and processed for indirect immunohistochemistry using the peroxidase-antiperixidase method. To ascertain structural details, some sections were stained with hematoxylin & eosine.

Immunohistochemistry

Deparaffinized and rehydrated sections were processed for immunohistochemical detection of S100 protein (S100P) to label Schwann cells and terminal glial cells in sensory nerve formations and neurofilament proteins (NFP) which selectively label the axons (see Vega et al., 2009; Cobo et al., 2021). The EnVision antibody complex detection kit (Dako, Glostrup, Denmark) was used following the manufacturer's instructions. Briefly, the endogenous peroxidase activity was inhibited (3% H_2O_2 for 15 minutes) and non-specific binding was blocked (10% bovine serum albumin for 20 minutes). The sections were then incubated overnight at 4°C with primary antibodies against S100P (Dako; polyclonal raised in rabbit used diluted 1:5000) and against NFP (Dako; clone 2F11, monoclonal antibody raised in mouse, used diluted 1:100). After incubation with the primary antibodies, sections were washed in tris-phosphate buffered saline (PBS-T) for 15 minutes and incubated at room temperature with the corresponding peroxidase-conjugated secondary antibody for 90 minutes (Dako EnVision labeled

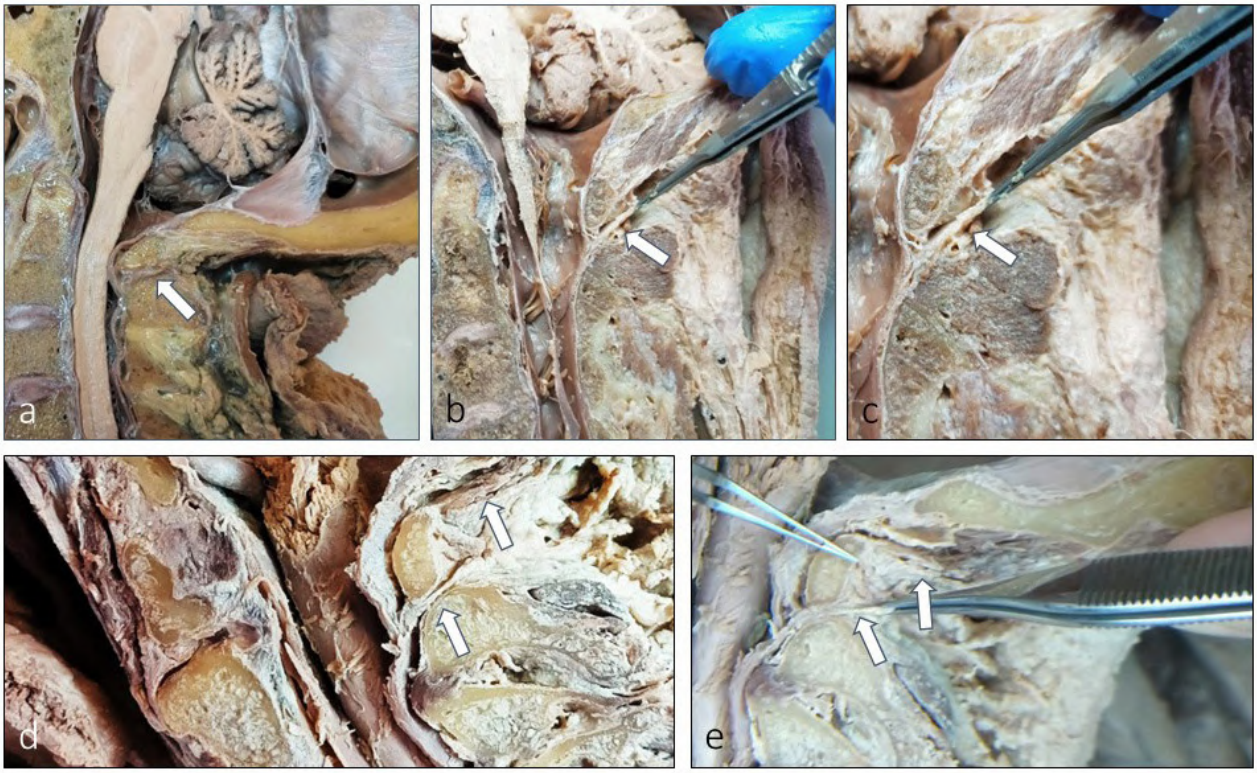

Fig. 1.- Myodural bridge complexes (arrows) in all five specimens examined (**a-e**).

polymer-HRP anti-rabbit IgG or anti-mouse IgG). After washing in PBS-T, the immunoreaction was revealed with a solution of 3-3' diaminobenzidine (Leica BondTM Polymer Refine Detection Kit, Leica BiosystemsTM). The sections were contrasted with hematoxylin, washed in water, dehydrated with alcohols of increasing concentration, diaphanized in xylol and mounted with Entellan®. Processed slides were reviewed and photographed on a Nikon Eclipse® 80i light microscope coupled to a Nokia® DS-5M camera. For control purposes, some sections were processed in the same way described above but using mouse or rabbit serum instead of the primary antibody, or omitting incubation with secondary antibodies, to obtain a negative immunoreaction (not shown). On the other hand, nerve trunks and fibers from the same sections served as positive internal controls for the antigens investigated (Vega et al., 2009).

RESULTS

MDBC in adult humans consist of bands of connective tissue, between 1 and 3, extending from the upper segment of the spinal dura mater and the suboccipital muscles. The fibrous bands follow an oblique direction, and between the fibrillary fascicles there are blood vessels and nerves of different calibers. Nerve profiles are isolated nerve fibers or small nerve bundles, and the innervation density of MDBC can be regarded as low; on the other hand, within the thickness of the MDBC no differentiated structures identifiable as sensory nerve formations have been found.

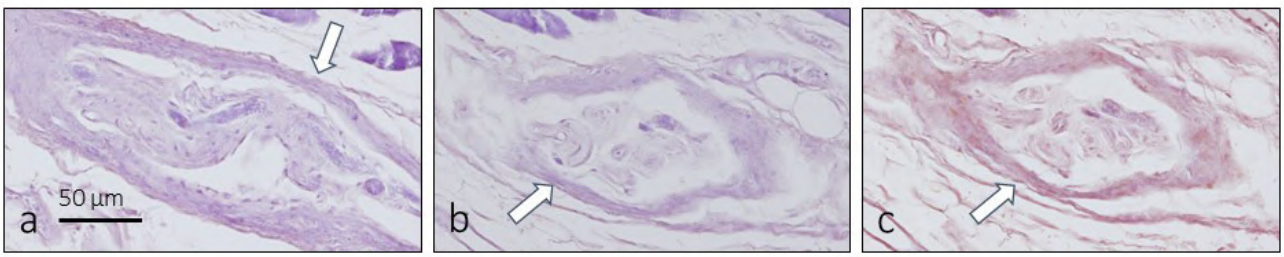

Fig. 2.- Ovoidal structures (arrows) localized in the junction of one myodural bridge complexes with the *rectus capitis posterior minor* muscle. Scale bar = 50 µm.

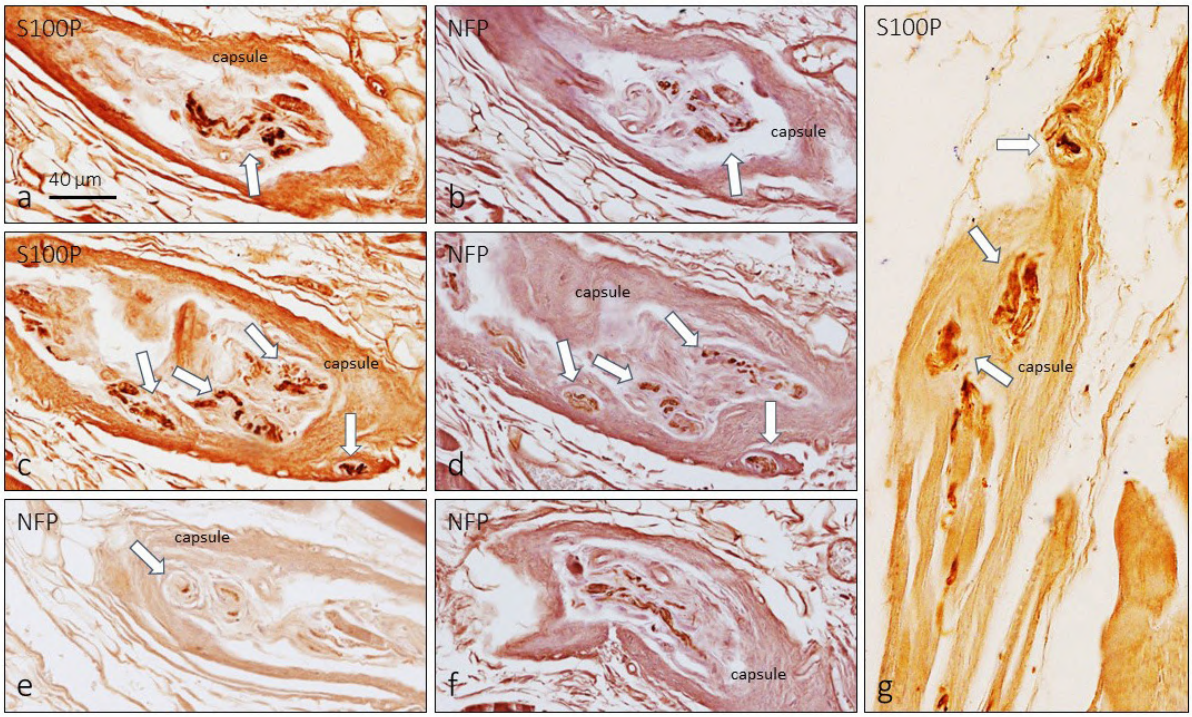

Fig. 3.- Serial sections (**a** and **b**; **c** and **d**) of the ovoidal structures localized in the junction of one myodural bridge complexes with the *rectus capitis posterior minor* muscle immunostained for the detection of S100P (**g**) and NFP (**e, f**). These formations contain sensory nerve formations and isolated nerve fibers. Scale bar = 40 µm.

However, in one case (1/5), at the junction level of one band of connective tissue of the upper MDBC with the *rectus capitis posterior minor* muscle three ellipsoid formations with a well- developed capsule were observed (Fig. 2). The immunohistochemical study revealed that these structures contain clusters of nerve structures, variably arranged and grouped in a common capsule, which were identified as sensory nerve formations. They consist of NFP positive axons and Schwann-related or terminal glial cells (Fig. 3). These sensory nerve formations are immersed in an amorphous connective tissue, and in no case muscle fibers were found inside; therefore, it must be ruled out that they are muscle spindles.

DISCUSSION

Over the past years, the suboccipital region has received an increasing attention, since research has revealed multiple soft-tissue connections extending from the suboccipital structures to the cervical dura mater through the posterior intervertebral spaces; these formations were called MDBC (Kahkeshani and Ward, 2011; Scali et al., 2011, 2015; Pontell et al., 2013; Zheng et al., 2020). Different studies have concluded that MDBC serve as monitors of dural tension (Hallgren et al., 1997; Pontell et al., 2013; Enix et al., 2014; Scali et al., 2013a, b; Chen et al., 2015; Sillevis and Hogg, 2020). Here, we hypothesized that MDBC are sources of proprioceptive inputs, and thus are involved in the regulation of cervical spine positioning and movements, which in turn inform the central nervous system about the tension of the spinal dura mater. To perform this function, MDBC must have a nervous system that, as far as we know, has never been investigated. Only Scali et al. (2013a) have reported the occurrence of nerves in 1/11 human specimen examined. Our findings about the presence of isolated nerve fibers and small nerves bundles in MDBC are in good agreement with those authors.

The most striking finding of the present research was the discovery of sensory nerve formations in one specimen of our small series (1/5). These structures are formed by a well- developed capsule containing an amorphous tissue and, inside, groups of independent sensory nerve formations, of variable morphology. These nerve formations cannot be classified within the typical nerve formations (see Cobo et al., 2021; Martín-Aguacil et al., 2022) but, presumably, they represent propi-

oceptor organs, different from muscle spindles or tendon organs. Given the unexpectedness of the findings and the small sample analyzed, further studies are needed to deepen the study of the innervation of MDBC and to draw definitive conclusions regarding its function.

REFERENCES

CHEN R, SHI B, ZHENG X, ZHOU Z, JIN A, DING Z, LV H, ZHANG H (2015) Anatomic study and clinical significance of the dorsal meningovertebral ligaments of the thoracic dura mater. *Spine*, 40: 692-698.

CHEN C, YU SB, CHI YY, TAN GY, YAN BC, ZHENG N, SUI HJ (2021) Existence and features of the myodural bridge in *Gentoo penguins*: A morphological study. *PLoS One*, 16: e0244774.

COBO R, GARCÍA-PIQUERAS J, COBO J, VEGA JA (2021) The Human cutaneous sensory corpuscles: an update. *J Clin Med*, 10: 227.

DOU YR, ZHENG N, GONG J, TANG W, CHUKWUEMEKA SAMUEL OKOYE, ZHANG Y, PI SY, QU LC, YU SB, SUI HJ (2019) Existence and features of the myodural bridge in *Gallus domesticus*: indication of its important physiological function. *Anat Sci Int*, 94: 184-191.

ENIX DE, SCALI F, PONTELL ME (2014) The cervical myodural bridge, a review of literature and clinical implications. *J Can Chiropr Assoc*, 58: 184-192.

GRONDEL B, CRAMBERG M, GREER S, YOUNG BA (2022) The morphology of the suboccipital region in snakes, and the anatomical and functional diversity of the myodural bridge. *J Morphol*, 283: 123-133.

HACK GD, KORITZER RT, ROBINSON WL, HALLGREN RC, GREENMAN PE (1995) Anatomic relation between the rectus capitis posterior minor and the dura mater. *Spine*, 20: 2484-2486.

HALLGREN RC, HACK GD, LIPTON JA (1997) Clinical implications of a cervical myodural bridge. *AAO J*, 7: 30-34.

HALLGREN RC, PIERCE SJ, PROKOP LL, ROWAN JJ, LEE AS (2014a) Electromyographic activity of rectus capitis posterior minor muscles associated with voluntary retraction of the head. *Spine J*, 14: 104-112.

HALLGREN RC, ROWAN JJ, BAI P, PIERCE SJ, SHAFER-CRANE GA, PROKOP LL (2014b) Activation of rectus capitis posterior major muscles during voluntary retraction of the head in asymptomatic subjects. *J Manip Physio. Ther*, 37: 433-440.

HALLGREN RC, PIERCE SJ, SHARMA DB, ROWAN JJ (2017) Forward head posture and activation of rectus capitis posterior muscles. *J Am Osteopath Assoc*, 117: 24-31.

HUANGFU Z, ZHANG X, SUI J Y, ZHAO QQ, YUAN XY, LI C, DOU YR, TANG W, DU ML, ZHENG N, CHI YY, YU SB, SUI HJ (2019) Existence of myodural bridge in the *Trachemys scripta elegans:* indication of its important physiological function. *Int J Morphol*, 37: 1353-1360.

HUMPHREYS BK, KENIN S, HUBBARD BB, CRAMER GD (2003) Investigation of connective tissue attachments to the cervical spinal dura mater. *Clin Anat*, 16: 152-159.

LAI HX, ZHANG JF, SONG TW, LIU B, TANG W, SUN SZ, QIN T, YUN ZF, ZHU SJ, YU SB, SUI HJ (2021) Development of myodural bridge located within the atlanto-occipital interspace of rats. *Anat Rec (Hoboken)*, 304: 1541-1550.

LIU P, LI C, ZHENG N, XU Q, YU SB, SUI HJ (2017) The myodural bridge existing in the *Nephocaena phocaenoides. PLoS One*, 12: e0173630.

LIU P, LI C, ZHENG N, YUAN XY, ZHOU Y, CHUN P, CHI Y, GILMORE C, YU S, SUI H (2018) The myodural bridges' existence in the sperm whale. *PLoS One*, 13: e0200260.

KAHKESHANI K, WARD PJ (2012) Connection between the spinal dura mater and the suboccipital musculature: evidence for the myodural bridge and a route for its dissection - A review. *Clin Anat*, 25: 415-422.

MARTÍN-ALGUACIL N, DE GASPAR I, SCHOBER JM, PFAFF DW, VEGA JA (2022) Somatosensation. In: Pfaff DW, Volkow ND, Rubenstein JL (eds.). *Neuroscience in the 21st Century*. Springer, Cham., New York.

MCELROY A, RASHMIR A, MANFREDI J, SLEDGE D, CARR E, STOPA E, KLINGE P (2019) Evaluation of the structure of myodural bridges in an equine model of Ehlers-Danlos syndromes. *Sci Rep*, 9: 9978.

OKOYE CS, ZHENG N, YU SB, SUI HJ (2018) The myodural bridge in the common rock pigeon (*Columbia livia*): Morphology and possible physiological implications. *J Morphol*, 279: 1524-1531.

PONTELL ME, SCALI F, MARSHALL E, ENIX D (2013) The obliquus capitis inferior myodural bridge. *Clin Anat*, 26: 450-454.

SCALI F, MARSILI ES, PONTELL ME (2011) Anatomical connection between the rectus capitis posterior major and the dura mater. *Spine*, 36: E1612-E1614.

SCALI DC, PONTELL ME, ENIX DE, MARSHALL E (2013a) Histological analysis of the rectus capitis posterior major's myodural bridge. *Spine J*, 13: 558-563.

SCALI F, PONTELL ME, WELK AB, MALMSTROM TK, MARSHALL E, KETTNER NW (2013b) Magnetic resonance imaging investigation of the atlanto-axial interspace. *Clin Anat*, 26: 444-449.

SCALI F, PONTELL ME, NASH LG, ENIX DE (2015) Investigation of meningomyovertebral structures within the upper cervical epidural space: a sheet plastination study with clinical implications. *Spine J*, 15: 2417-24.

SCALI F, OHNO A, ENIX D, HASSAN S (2022) The posterior atlantooccipital membrane: the anchor for the myodural bridge and meningovertebral structures. *Cureus*, 14: e25484.

SILLEVIS R, HOGG R (2020) Anatomy and clinical relevance of sub occipital soft tissue connections with the dura mater in the upper cervical spine. *PeerJ*, 8: e9716.

SONG X, GONG J, YU SB, YANG H, SONG Y, ZHANG XH, ZHANG J, HACK GD, LI TL, CHI YY, ZHENG N, SUI HJ (2023) The relationship between compensatory hyperplasia of the myodural bridge complex and reduced compliance of the various structures within the cranio-cervical junction. *Anat Rec (Hoboken)*, 306: 401-408.

SUN MY, SUI HJ, ETEER K, YU SB, HU JN (2020) Utilization of MR imaging in myodural bridge complex with relevant muscles: current status and future perspectives. *J Musculoskelet Neuronal Interact*, 20: 382-389.

VEGA JA, GARCÍA-SUÁREZ O, MONTAÑO JA, PARDO B, COBO JM (2009) The Meissner and Pacinian sensory corpuscles revisited new data from the last decade. *Microsc Res Tech*, 72: 299-309.

ZHANG JH, TANG W, ZHANG ZX, LUAN BY, YU SB, SUI HJ (2016) Connection of the posterior occipital muscle and dura mater of the siamese crocodile. *Anat Rec (Hoboken)*, 299: 1402-1408.

ZHANG ZX, GONG J, YU SB, LI C, SUN JX, DING SW, MA GJ, SUN SZ, ZHOU L, HACK GD, ZHENG N, SUI HJ (2021) A specialized myodural bridge named occipital- dural muscle in the narrow-ridged finless porpoise (*Neophocaena asiaeorientalis*). *Sci Rep*, 11: 15485.

ZHENG N, YUAN XY, CHI YY, LIU P, WANG B, SUI JY, HAN SH, YU SB, SUI HJ (2017) The universal existence of myodural bridge in mammals: an indication of a necessary function. *Sci Rep*, 7: 8248.

ZHENG N, CHUNG BS, LI YL, LIU TY, ZHANG LX, GE YY, WANG NX, ZHANG ZH, CAI L, CHI YY, ZHANG JF, SAMUEL OC, YU SB, SUI HJ (2020) The myodural bridge complex defined as a new functional structure. *Surg Radiol Anat*, 42: 143-153.

Effects of *chlorophytum borivilianum* extract against high-fat diet-induced obesity in male Wistar albino rats

B. Ashwinidevi, Dr. S. Kavitha

Department of Anatomy, Kirupanandha varier Medical College and Hospital, Vinayaka Mission Research Foundation [DU], Salem - 636308, Tamilnadu, India

SUMMARY

The effect of Chlorophytum borivilianum extract against high-fat-diet-induced obesity is unknown. Therefore, this study investigates activity of 250 & 500 mg/kg/day of Chlorophytum borivilianum extract in male Wistar Albino rats, on parameters like weight gain, Follicle Stimulating Hormone, Luteinizing hormone, and Testosterone. The objective is to determine the effects of Chlorophytum Borivilianum extract against high-fat-diet-induced obesity in male Wistar Albino rats. It is an interventional, comparative, animal study of 60 days, conducted at KMCH College of Pharmacy, Coimbatore. 20 male Wistar Albino rats were randomly divided into 5 experimental groups with 6 rats per group. At the end of experimental period, all rats were fasted overnight, weighted, and sacrificed within 24 hours by the mode of decapitation, and the blood was collected. Later, the organs were dissected out and fixed with formalin. The post-fixed tissue, slides were stained. Ethics committee approval was obtained initially. Statistical analysis was done by SPSS software.

The Obese group showed an increase in body weight due to high-fat diet administration, whereas the Treatment group receiving Chlorophytum borivilianum extract showed reduction in body fat and improvement in the semen analysis when compared to control group. When treated with Chlorophytum borivilianum, body weight as well as sperm function of the animals were significantly improved mediated through enhanced spermatogenesis, steroid genesis, and antioxidant mechanisms with histological studies. Thus, findings reinforce the advice recommending consumption of Chlorophytum borivilianum extract to modulate obesity and sperm morphology.

Key words: Chlorophytum borivilianum – Wistar albino rats – Obesity – Sperm morphology

INTRODUCTION

In the present times, obesity and infertility are one of the gravest social complications. Obesity is a condition in which excessive fat accumulation triggers a disproportion in energy intake and

Corresponding author:
B. Ashwinidevi, Research Scholar, Department of Anatomy, Kirupanandha varier Medical College and Hospital, Vinayaka Mission Research Foundation [DU], Salem - 636308, Tamilnadu, India. Mobile: +91-9489780475. E-mail: bashwinidevi2@gmail.com

Submitted: January 16, 2024. **Accepted:** January 31, 2024

https://doi.org/10.52083/GEFT3895

expenditure due to alteration in healthy dietary habits (Williams et al., 2015). Less physical activity also causes various disorders like infertility, Diabetes mellitus, hypertension, and cardiovascular problems. Infertility can also be caused by several factors such as genetic, environmental, bad habits like smoking, sedentary lifestyle leading to body hormonal and sexual disorders (Christensen, 1975).

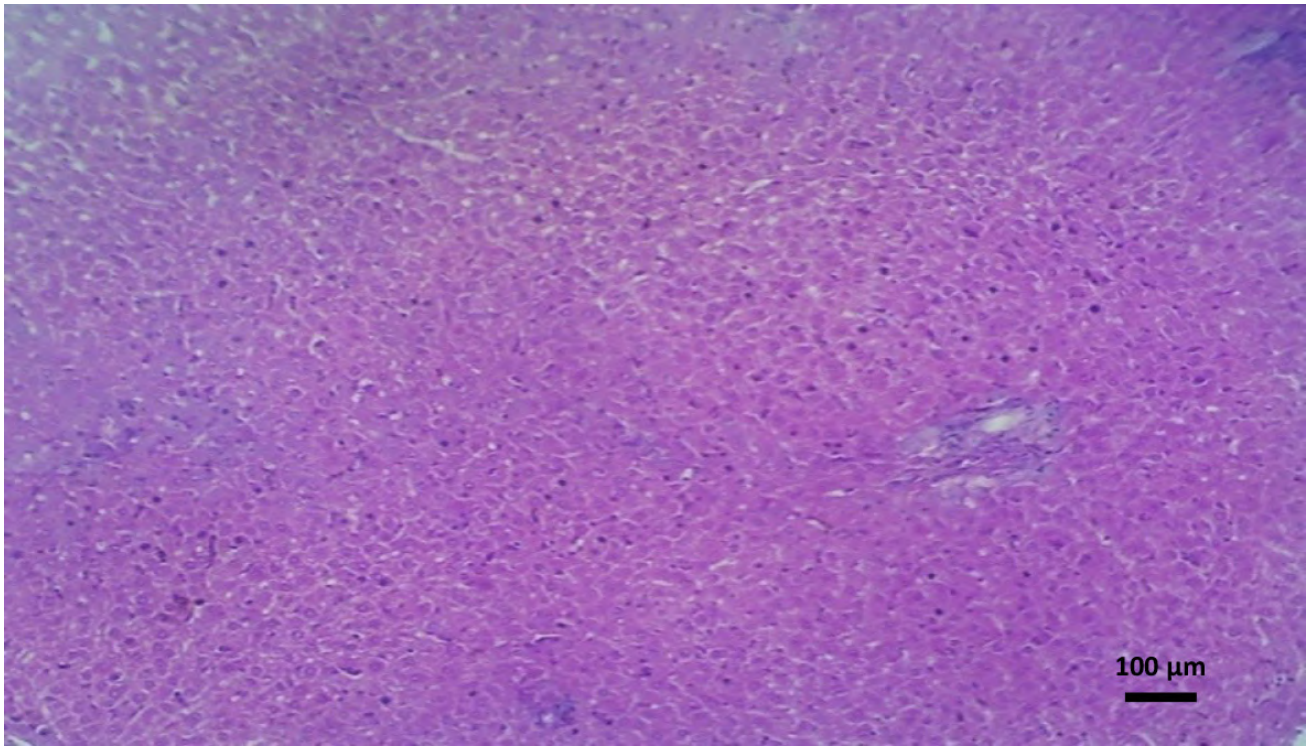

Fig. 1.- Control group – shows normal architecture of liver, hepatocytes.

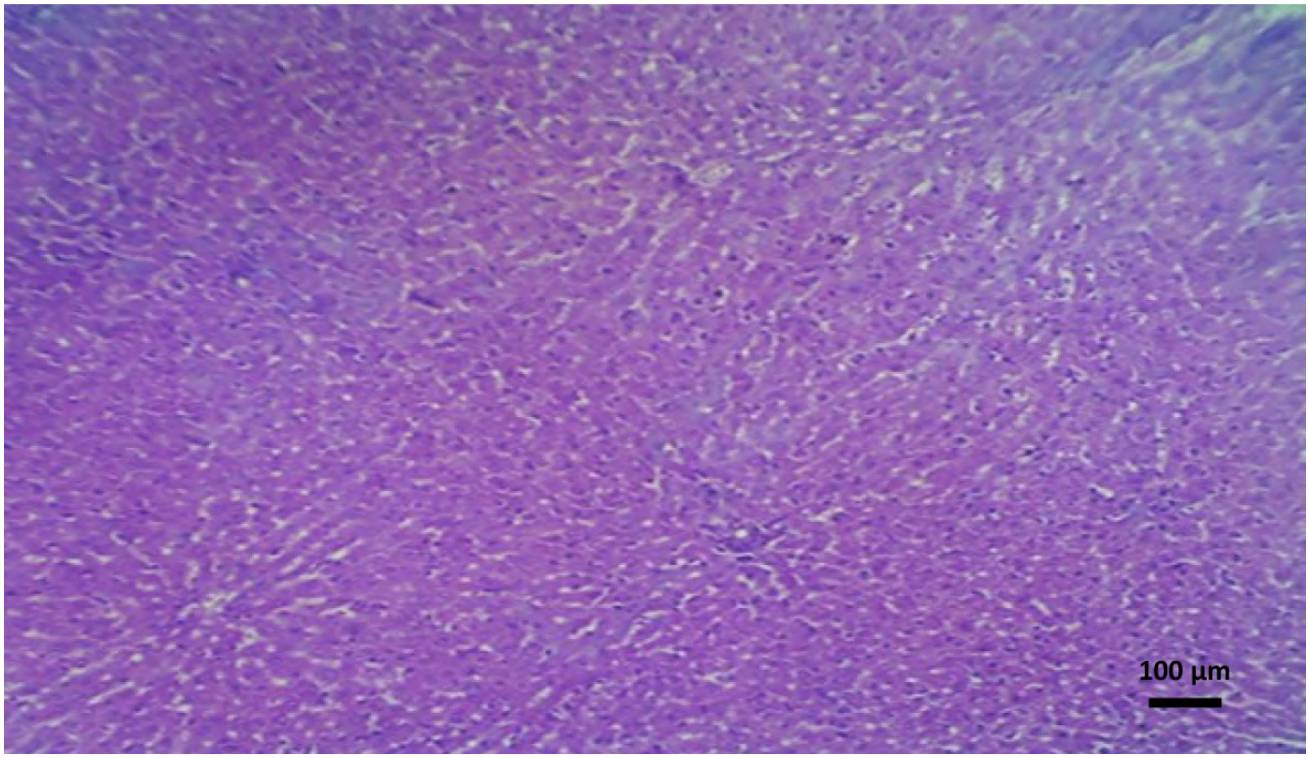

Fig. 2.- High-fat diet induce group – shows mild interface hepatitis with sinusoidal dilatation.

Currently, no pharmacological treatments provide sustained weight loss without adverse effects. A variety of plant and their byproducts (extracts) are helpful to induce body weight reduction and also prevent diet-related obesity and infertility (Lohiya et al., 1994; Raji and Bolarinwa, 1997). However, a previous study has reported that regular intake of antioxidants and vitamins such as vitamins A, B, C, and E improves testicular blood barrier stability, and protects sperm DNA damage from endogenous oxidative stress resulting from the activities of highly reactive free radicals generated within the body (Raji et al., 2003).

The literature revealed that traditional medicine helps to nourish and stimulates the sexual tissues and ameliorates male reproductive health issues by various plant herb extracts such as Panax spp. (ginseng), Moringa oleifera and Lepidium meyenii (Maca), which are reputed for their supposed aphrodisiac- and spermatogenesis-enhancing effects (Chauhan et al., 2014).

Chlorophytum borivilianum belongs to the family 'Liliaceae' and the genus 'Chlorophytum'. It has various properties like antitussive activity, osteopenia, anti-diabetic activity, immune-modulatory activity, antioxidant activity, anti-stress property, anti-ulcer activity, anthelmintic activity, etc. (Sharma and Chandrul, 2017).

Recently, anti-obesity and antioxidant properties of the plant Chlorophytum borivilianum have been explored; and their relationship to the improvement of infertility has to be explored (Kenyale et al., 2008). The present study is conducted with the intent to investigate the effects of Chlorophytum Borivilianum extract against high-fat-diet-induced obesity in male Wistar Albino rats for the parameters, body weight management and sperm morphology.

MATERIALS AND METHODS

Study design and population

It is an interventional, comparative animal study of 60 days, conducted at KMCH College of Pharmacy, Coimbatore. In the present study, a total of 20 male Winstar Albino rats were taken.

The study was conducted in accordance with the recommendations from the declaration of the institutional animal ethical committee no. KMCRET/RERc/Ph.D/28/2021 under proper care and use of animals.

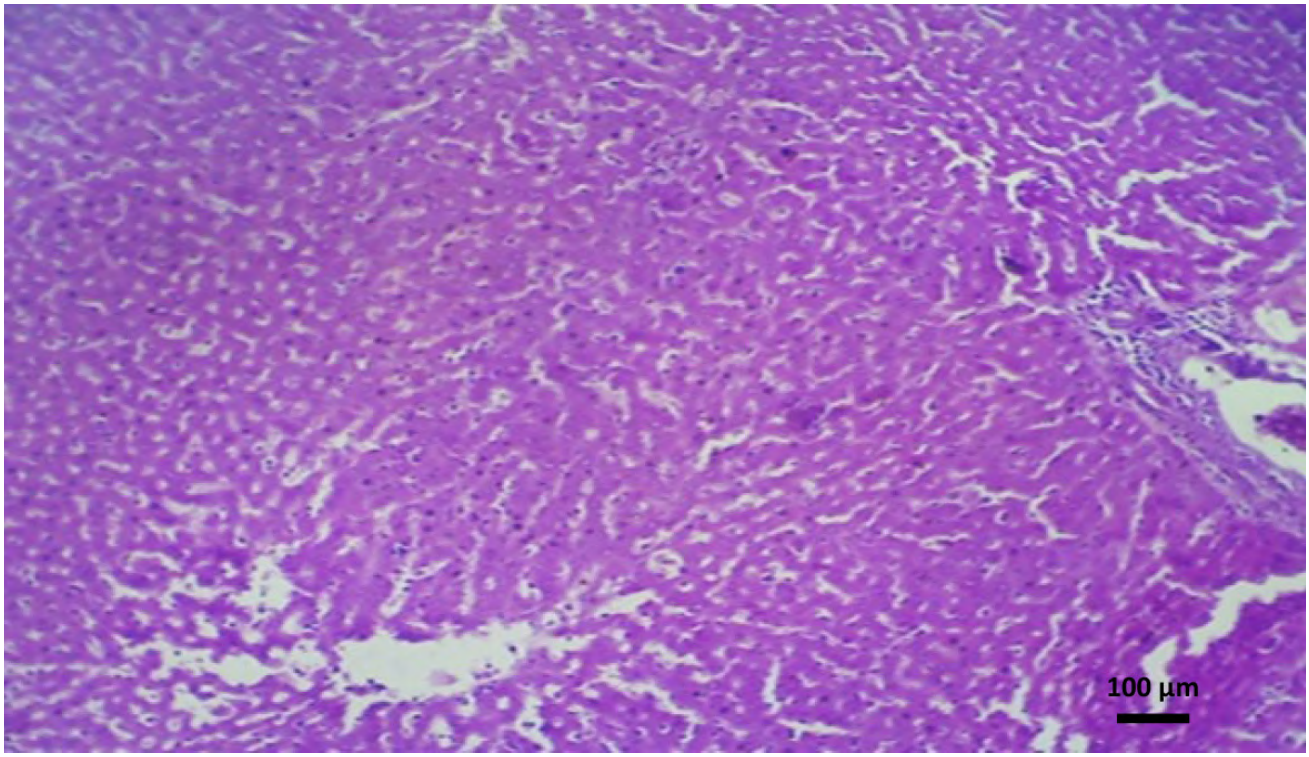

Fig. 3.- High fat + Sildenafil citrate treated group shows mild sinusoidal dilatation.

Group allocation

The animals were randomly assigned into five experimental groups with four rats per group:

- Group 1: Control/Normal group (n=4), healthy male Winstar Albino rats.
- Group 2: High-fat diet (HF) group (n=4), animals receiving high fat diet.
- Group 3: High-Fat diet (HF) + Sildenafil citrate (SC), animals receiving standard drug, Sildenafil citrate (5mg/kg) for 28 days (n=4).
- Group 4: High-Fat diet (HF) + Chlorophytum borivilianum (CB), receiving low dose of CB (250mg/kg/day) for 28 days (n=4).
- Group 5: High-Fat diet (HF) + Chlorophytum borivilianum (CB), receiving high dose of CB (500 mg/kg/day) for 28 days (n=4).

At the end of the experimental period, all rats were fasted overnight, weighed, and sacrificed within 24 hours by the mode of decapitation, and the blood was collected through the retro-orbital puncture.

Plant material

Dried roots of Chlorophytum borivilianum were procured from the Ayurvedic store online. The dried roots were cut into small pieces and then shaded and ground into fine powder. The root powder (1000 g) of the powdered sample was exhaustively extracted with ethanol. The solvent was then distilled off, to give the solid extract, which was stored at 4°C. The solid extract was then dissolved in normal saline and used for study purposes.

Animal Model

Male Wistar Albino rats (250-440 g) obtained from the KMCH College of Pharmacy, Coimbatore, were used for the study. The rats were housed in wire mesh cages under standard temperatures of 25-29 °C, 12h light, and 12h darkness cycles. Animals were fed with a pelleted standard rat diet with proper water ad libitum.

Histopathology studies

The organs were dissected out and fixed with formalin. The post-fixed tissue was embedded with a serial section by using a rotary microtome

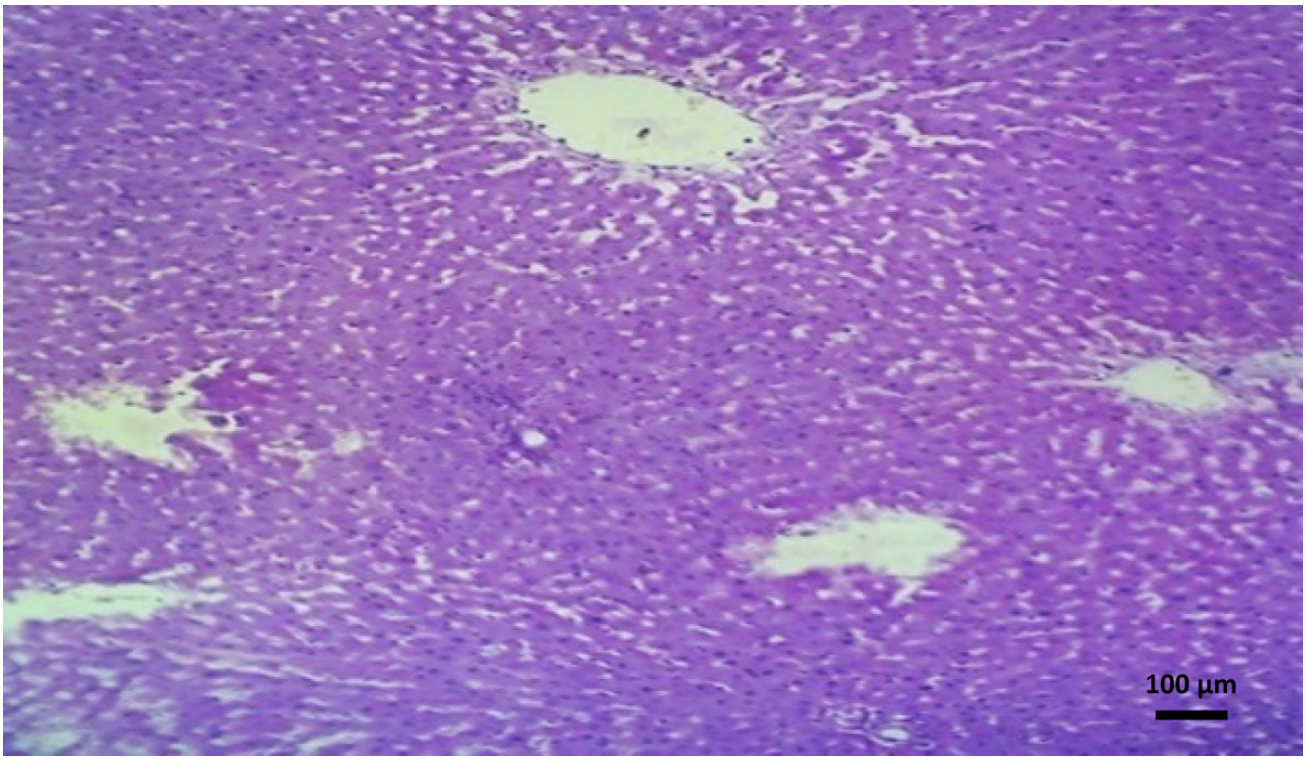

Fig. 4.- High-Fat diet (HF) + Chlorophytum borivilianum (CB) low dose treated group shows mild dilatation hepatocytes look normal architecture.

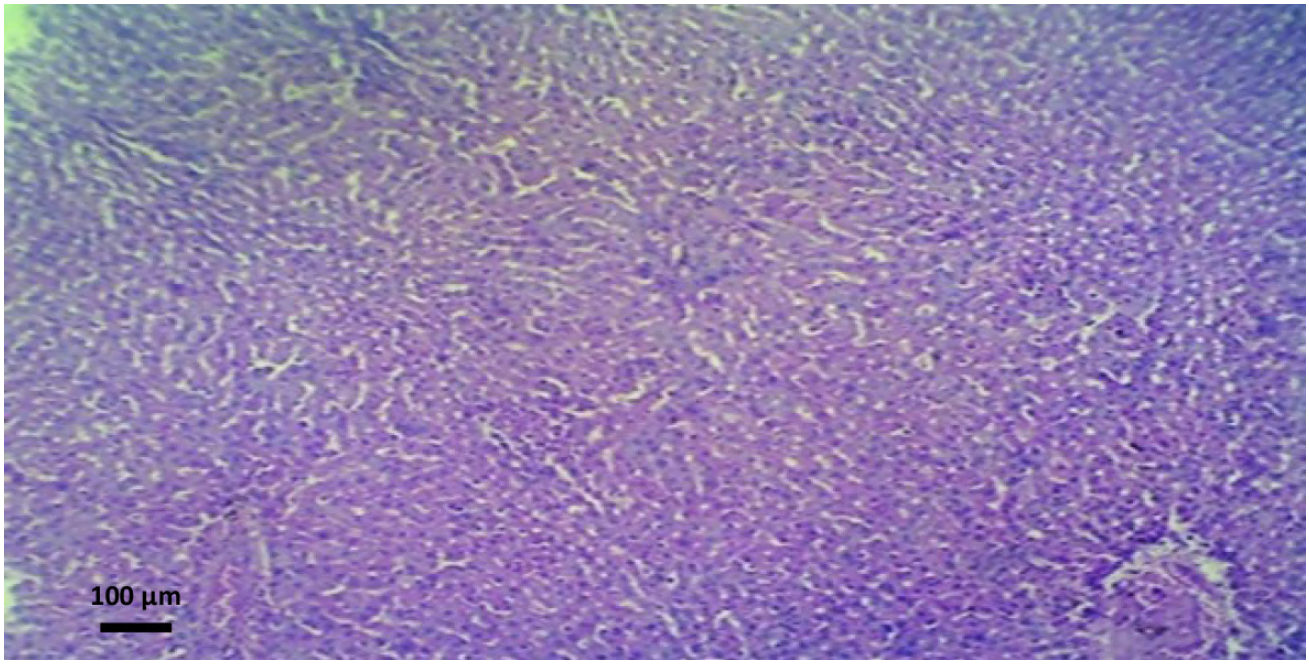

Fig. 5.- (High-Fat diet (HF) + Chlorophytum borivilianum (CB) high dose treated group shows very minimal dilatation of sinusoidal space and restores the hepatocytes.

at 5 microns. The slides were stained with Haematoxylin and Eosin.

Weight Measurement

Animal Body Weight: Rat body weights were measured by using a digital Mettler weighing balance, and values obtained were recorded a day before the commencement of the experiment, and also during the treatment period, as well as at the last day of the experiment.

Organ weights: At the end of the experiment period, each animal was sacrificed, at weekly intervals of two, four, or twelve weeks respectively. Various parts of body organ tissues were removed, and weight was calculated and recorded.

Analysing Sperm motility, viability, counts, and morphology

After carefully separating the epididymis from the testes, the epididymis was minced in 0.1M phosphate buffer solution (1 mL). For obtaining the epididymal fluid, the minced tissues were swirled gently in the buffer solution for the proper diffusion of sperm cells. Sperm cell motility analysis, 10 µL of the epididymal fluid was charged into a Neubauer chamber and the total number of sperms was estimated. The number of sperms per cauda epididymis was calculated as follows:

{Mean count x 50} ÷ {0.01 x 0.01}

Biochemical analysis

From each experimental animal, blood was obtained by a retro-orbital puncture after anaesthetization. Each blood sample was rotated at 2500 rpm for 10 minutes in a centrifuge at 10-25 °C. Serum samples were assayed for testosterone using the enzyme-linked immunoassay (EIA) technique.

Statistical analysis

The statistical analysis was done by using SPSS software (21.0 version), the data is stated as Mean±SD in tabulated form. For data comparison, One way ANOVA, followed by Dunnett comparison, was performed. In all the cases p value ≤0.001* is considered statistically significant.

Ethical approval

The ethical committee letter was obtained before the initiation of the study, (KMCRET/RERc/Ph.D/28/2021).

RESULTS

In the Table showing body weight variations, where changes in control group rats and rats treated with ethanolic extracts of Chlorophytum borivilianum were noted, it was observed that, the Chlorophytum borivilianum extract did not show any significant effect on the body weights of rats treated for 1st week (Group-1 (Control)- 122±1.23, Group-2 (HF group)- 125±1.42, Group-3 (HF + SC group)- 119±1.67, Group-4 (HF + CB group, Low dose)- 126±1.74 & Group-5 (HF + CB group, High dose)- 124±1.33) and 3rd week (Group-1 (Control)- 150±2.09, Group-2 (HF group)- 174±2.24, Group-3 (HF + SC group)- 170±2.84, Group-4 (HF + CB group, Low dose)- 174±3.11 & Group-5 (HF + CB group, High dose)- 175±2.29), respectively.

The body weight has decreased significantly in the groups treated for 4th and 6th weeks with Chlorophytum borivilianum extract (low and high doses) when compared to other groups. (Group-1 (Control)- 172±2.12, Group-2 (HF group)- 242±7.70, Group-3 (HF + SC group)- 207±5.79, Group-4 (HF + CB group, Low dose)- 212±11.03* & Group-5 (HF + CB group, High dose)- 208±8.47*).

However, normal body and organ weights were restored in rats, which were allowed for a recovery period of 6 weeks (Table 1).

In the table of reproductive organ weight, where, the effect of repeated daily oral treatments with 250-500mg/kg/day of CB ethanolic extract on the average testicular weight (TW), caudal epididymis, seminal vesicle and prostate gland of treated rats were done, it was observed that there was a significant increase in weight of reproductive organs, Testis (Group-1 (Control)- 2.75±0.07, Group-2 (HF group)- 2.27±0.08, Group-3 (HF + SC group)- 3.05±0.04, Group-4 (HF + CB group, Low dose)- 2.27±0.05 & Group-5 (HF + CB group, High dose)- 2.48±0.10*) and Seminal vesical (Group-1 (Control)- 0.88±0.04, Group-2 (HF group)- 0.83±0.03, Group-3 (HF + SC group)- 0.76±0.03, Group-4 (HF + CB group, Low dose)- 0.88±0.02 & Group-5 (HF + CB group, High dose)- 0.96±0.02*) when treated with Chlorophytum borivilianum extract (high dose).

Whereas the weight of other reproductive organs namely, Caudal epididymis and Prostate gland were not increased much and were found to be similar to the Standard drug weight (Sildenafil citrate (SC)) (Table 2).

In the table of biochemical assay, it can be clearly noticed that repeated treatments with Chlorophytum borivilianum extract (high dose) resulted in significant dose related increase in the circulating serum Follicle-stimulating hormone (FSH), (Group-1 (Control)- 0.34±0.01, Group-2 (HF group)- 0.27±0.04, Group-3 (HF + SC group)- 0.29±0.04, Group-4 (HF + CB group, Low dose)- 0.27±0.07 & Group-5 (HF + CB group, High dose)- 0.36±0.03*), increase in the circulating serum Luteinizing hormone (LH), (Group-1 (Control)- 0.11±0.32, Group-2 (HF group)- 0.14±0.01, Group-3 (HF + SC group)- 0.11±0.12, Group-4 (HF + CB group, Low dose)- 0.12±0.17 & Group-5 (HF + CB group, High dose)- 0.27±0.02*), as well as increase in the Testosterone levels, (Group-1 (Control)- 0.31±5.71, Group-2 (HF group)- 64.1±4.73, Group-3 (HF + SC group)- 85.4±8.17, Group-4 (HF + CB group, Low dose)- 102.0±4.23 & Group-5 (HF + CB group, High dose)- 207±9.18*), when compared to Group- 1 (control group) (Table 3).

In the table of sperm cell characteristics, in the group treated with Chlorophytum borivilianum extract (low and high dose), there was an increase

Table 1. Body weight. Changes in control group rats and rats treated with ethanolic extracts of Chlorophytum borivilianum. All values are expressed in grams as mean ± SD.

Visiting days/weeks	**Group-1** (Control)	**Group-2** (HF group)	**Group-3** (HF + SC group)	**Group-4** (HF + CB group, Low dose- 250 mg/kg/day)	**Group-5** (HF + CB group, High dose- 500 mg/kg/day)
1st day (1st week)	122±1.23	125±1.42	119±1.67	126±1.74	124±1.33
21st day (3rd week)	150±2.09	174±2.24	170±2.84	174±3.11	175±2.29
42nd day (4th to 6th week)	172±2.12	242±7.70	207±5.79	212±11.03*	208±8.47*

HF- High fat, SC- Sildenafil citrate, CB- Chlorophytum borivilianum. p≤0.001* considered as statistically significant and is represented as *

Table 2. Reproductive organ weight. Effect of repeated daily oral treatments with 250-500mg/kg/day of CB ethanolic extract on the average testicular weight (TW), caudal epididymis, seminal vesicle and prostate gland of treated rats. All values are expressed in grams as mean ± SD.

Organs estimated for weight	**Group-1** (Control)	**Group-2** (HF group)	**Group-3** (HF + SC group)	**Group-4** (HF + CB group, Low dose- 250 mg/kg/day)	**Group-5** (HF + CB group, High dose- 500 mg/kg/day)
Testis	2.75±0.07	2.27±0.08	3.05±0.04	2.27±0.05	2.48±0.10*
Caudal epididymis	0.19±0.18	0.16±0.18	0.11±0.13	0.19±0.17	0.11±0.14
Seminal vesicle	0.88±0.04	0.83±0.03	0.76±0.03	0.88±0.02	0.96±0.02*
Prostate gland	1.04±0.04	1.24±0.30	1.04±0.11	0.94±0.08	1.02±0.09

HF- High fat, SC- Sildenafil citrate, CB- Chlorophytum borivilianum. p≤0.001* considered as statistically significant and is represented as *

Table 3. Biochemical assay. To estimate the serum biochemical analysis between the control and treatment groups. All values are expressed as mean ± SD.

Parameters	**Group-1** (Control)	**Group-2** (HF group)	**Group-3** (HF + SC group)	**Group-4** (HF + CB group, Low dose- 250 mg/kg/day)	**Group-5** (HF + CB group, High dose- 500 mg/kg/day)
Follicle-stimulating hormone (FSH) (mIU/mL)	0.34±0.01	0.27±0.04	0.29±0.04	0.27±0.07	0.36±0.03*
Luteinizing hormone (LH) (IU/L)	0.11±0.32	0.14±0.01	0.11±0.12	0.12±0.17	0.27±0.02*
Testosterone (ng/dL)	0.31±5.71	64.1±4.73	85.4±8.17	102.0±4.23	207±9.18*

HF- High fat, SC- Sildenafil citrate, CB- Chlorophytum borivilianum. p≤0.001* considered as statistically significant and is represented as *

in the sperm count, (Group-1 (Control)- 77.4±0.39, Group-2 (HF group)- 41.6±0.68, Group-3 (HF + SC group)- 68.5±2.56, Group-4 (HF + CB group, Low dose)- 68.2±1.49 & Group-5 (HF + CB group, High dose)- 71.4±1.06*), increase in the motility (Group-1 (Control)- 80.3±0.65, Group-2 (HF group)- 61.9±1.19, Group-3 (HF + SC group)- 72.2±2.12, Group-4 (HF + CB group, Low dose)- 69.4±2.56 & Group-5 (HF + CB group, High dose)- 80.7±1.05*), and also increase in the viability percentages, (Group-1 (Control)- 85.5±0.55, Group-2 (HF group)- 61.8±4.64, Group-3 (HF + SC group)- 82.4±3.56, Group-4 (HF + CB group, Low dose)- 73.4±0.84 & Group-5 (HF + CB group, High dose)- 89.8±0.27*), when compared to Group-2 (HF group) and Group-3 (HF + SC group) significantly.

Table 4. Sperm Cell characteristics. Effects of CB extracts on sperm characteristics in rats treated for 2 weeks and their recovery groups. Estimating, Motility (%), Viability (%), Sperm Counts (million/ml) and abnormality. All values are expressed as mean ± SD.

Study groups	**Sperm Count (x106/ mL)**	**Motility (%)**	**Viability (%)**	**Abnormalities (%)**
Group-1 (Control)	77.4±0.39	80.3±0.65	85.5±0.55	21±0.57
Group-2 (HF group)	41.6±0.68	61.9±1.19	61.8±4.64	38.5±0.45
Group-3 (HF + SC group)	68.5±2.56	72.2±2.12	82.4±3.56	27±1.57*
Group-4 (HF + CB group, Low dose- 250 mg/kg/day)	68.2±1.49	69.4±2.56	73.4±0.84	30.5±0.60
Group-5 (HF + CB group, High dose- 500 mg/kg/day)	71.4±1.06*	80.7±1.05*	89.8±0.27*	17.7±2.64*

HF- High fat, SC- Sildenafil citrate, CB- Chlorophytum borivilianum. p≤0.001* considered as statistically significant and is represented as *

Table 5. Biochemical assay. Estimation of Testicular SOD, Catalase, LPO and Glutathione levels activities. All values are expressed in grams as mean ± SD.

Parameters	**Group-1** (Control)	**Group-2** (HF group)	**Group-3** (HF + SC group)	**Group-4** (HF + CB group, Low dose- 250 mg/kg/day)	**Group-5** (HF + CB group, High dose- 500 mg/kg/day)
SOD (unit/min/mg protein)	0.14±0.01	0.12±0.011	0.18±0.04	0.16±0.36	0.20±0.22*
CATALASE (µmole of H_2O_2 consumed/min/mg protein)	0.33±0.01	0.89±0.80	0.36±0.85	0.138±0.36	0.143±0.29*
GPX (µmole of glutathione oxidized/min/mg protein)	0.39±0.06	0.22±0.23	0.75±0.49	0.21±0.07	0.13±0.91*
GSH (µmol/mg of protein)	0.18±0.52	0.32±0.63	0.12±0.21	0.11±0.15	0.10±0.13*
LPO (µmol/mg (of MDA nmol/gm)	0.76±0.01	0.51±0.61	0.76±0.14	0.73±0.02	0.95±0.58*

HF- High fat, SC- Sildenafil citrate, CB- Chlorophytum borivilianum. p≤0.001* considered as statistically significant and is represented as *

The abnormalities in the sperm cell characteristics were minimal in the group treated with Chlorophytum borivilianum extract (high dose). (Group-1 (Control)- 21±0.57, Group-2 (HF group)- 38.5±0.45, Group-3 (HF + SC group)- 27±1.57*, Group-4 (HF + CB group, Low dose)- 30.5±0.60 & Group-5 (HF + CB group, High dose)- 17.7±2.64*) (Table 4).

In the table of biochemical assay, where the estimation of testicular-reduced glutathione levels of SOD and catalase activities were done along with, GPX, GSH and LPO.

In the testicular tissue SOD, (Group-1 (Control)- 0.14±0.01, Group-2 (HF group)- 0.12±0.011, Group-3 (HF + SC group)- 0.18±0.04, Group-4 (HF + CB group, Low dose)- 0.16±0.36 & Group-5 (HF + CB group, High dose)- 0.20±0.22*), CAT (Group-1 (Control)- 0.33±0.01, Group-2 (HF group)- 0.89±0.80, Group-3 (HF + SC group)- 0.36±0.85, Group-4 (HF + CB group, Low dose)- 0.138±0.36 & Group-5 (HF + CB group, High dose)- 0.143±0.29*), and LPO activities (Group-1 (Control)- 0.76±0.01, Group-2 (HF group)- 0.51±0.61, Group-3 (HF + SC group)- 0.76±0.14, Group-4 (HF + CB group, Low dose)- 0.73±0.02 & Group-5 (HF + CB group, High dose)- 0.95±0.58*) were significantly increased, when treated with Chlorophytum borivilianum extract (high dose).

In the testicular tissue GPX, (Group-1 (Control)- 0.39±0.06, Group-2 (HF group)- 0.22±0.23, Group-3 (HF + SC group)- 0.75±0.49, Group-4 (HF + CB group, Low dose)- 0.21±0.07 & Group-5 (HF + CB group, High dose)- 0.13±0.91*), GSH (Group-1 (Control)- 0.18±0.52, Group-2 (HF group)- 0.32±0.63, Group-3 (HF + SC group)- 0.12±0.21, Group-4 (HF + CB group, Low dose)- 0.11±0.15 & Group-5 (HF + CB group, High dose)- 0.95±0.58*), activities were not increased (Table 5).

Figs 1-5 show a photomicrographic view of liver sections with H&E staining (100X) after 60 days treatment. HIGH FAT DIET induced tissues show histopathological alteration with the deposition of fats and interface hepatitis. Chlorophytum borivilianum (CB) High dose group) treated rats shows improvement in histopathology of the liver.

DISCUSSION

Obesity is recognized as a metabolic disease, with chronic effects probably due to various environmental as well as hereditary factors. In the recent years, obesity in human population caused innumerable health hazards, fertility being of one them (Hammoud et al., 2012). Further studies have specified that a high fat percentage (high BMI) is also related with significant reduction in

sperm concentrations (Chavarro et al., 2010). Chlorophytum borivilianum (Safed Musli) is a highly valued Indian medicinal plant. This plant has been shown to possess anti-obesity, anti-cancer, antimicrobial, antifungal, antiulcer, anti-pyretic, antiarthritic and immunomodulatory activities (Khanam et al., 2013). The present study demonstrates the effect of Chlorophytum borivilianum extract against high-fat-diet-induced obesity in male Wistar Albino rats.

It was observed that that the body weight of the experimental animals on high-fat diet has been decreased when treated with low (250 mg/kg/day) and high doses (500 mg/kg/day) of Chlorophytum borivilianum extract, in the 4th and 6th weeks of the study. The significant weight reduction supports the fact that Chlorophytum borivilianum extract, when given to obese rats on high-fat diet, is helpful in reducing the body fat level leading towards normal body fat percentage (Giribabu et al., 2014).

In our study of the effect of repeated daily oral treatments with 250-500 mg/kg/day of Chlorophytum borivilianum extract on reproductive organ weight, it was observed that there was a significant increase in weight of reproductive organs (Testis and Seminal vesical) when treated with Chlorophytum borivilianum extract (high dose-500 mg/kg/day) (Thakur and Dixit, 2006).

When the biochemical assay was conducted to estimate the serum biochemical analysis on experimental animals having repeated treatments with Chlorophytum borivilianum extract (high dose-500 mg/kg/day), it resulted in significant dose-related increase in the circulating serum Follicle-stimulating hormone (FSH), Luteinizing hormone (LH) as well as increase in the Testosterone levels (Kenjale et al., 2008).

The sperm cell characteristics were studied extensively with Chlorophytum borivilianum extract. It was demonstrated that low (250 mg/kg/day) and high doses (500 mg/kg/day) of Chlorophytum borivilianum extract significantly increased sperm count, motility and viability (Das et al., 2016). The abnormalities in the sperm cell characteristics were also found to be minimal with Chlorophytum borivilianum extract (Jia et al., 2018).

The estimation of Testicular SOD, Catalase, LPO and Glutathione Levels activities were carried out, resulting in increase in SOD, CAT and LPO levels (Vyas et al., 2022) and decrease in Glutathione levels (Pasqualotto et al., 2008; Liu et al., 2014) when treated with Chlorophytum borivilianum extract.

CONCLUSION

Chlorophytum borivilianum extract (Low dose-250 mg/kg/day and High dose- 500 mg/kg/day) given to male Winstar Albino rats on high-fat diet for 60 days significantly improved sperm function like sperm motility, count, viability, and morphology, mediated via increased spermatogenesis, steroidogenesis, and biochemical and antioxidant mechanisms. This present study obtained results reinforce the advice recommending consumption of this plant product to modulate obesity and sperm morphology.

ACKNOWLEDGEMENTS

I sincerely thank the Dean of Kirupanandha varier Medical College and Hospital, and my guide Dr. S. Kavitha, Associate Professor, Department of Anatomy, Vinayaka Mission Research Foundation [DU] and Kirupanandha varier Medical College and Hospital, for guiding me to carry my research work, and I also thank G. Ariharasiva kumar, Professor & HOD, Department of Pharmacology, Kmch College of Pharmacy, Coimbatore, for providing us with the platform, infrastructure, and encouragement for research activities. I am also thankful to our friends and co-faculties for providing immense support and guidance.

REFERENCES

CHAUHAN NS, SHARMA V, DIXIT VK, THAKUR M (2014) A review on plants used for improvement of sexual performance and virility. *Biomed Res Int*, 2014: 868062.

CHAVARRO JE, TOTH TL, WRIGHT DL, MEEKER JD, HAUSER R (2010) Body mass index in relation to semen quality, sperm DNA integrity, and serum reproductive hormone levels among men attending an infertility clinic. *Fertil Steril*, 93: 2222-2231.

CHRISTENSEN AC (1975) Leydig Cell. In: Greep PO, Astwoods EB (eds). *Handbook of Physiology*. Washington D.C., American Physiological Society.

DAS S, SINGHAL S, KUMAR N, RAO CM, SUMALATHA S, DAVE J, DAVE R, NANDAKUMAR K (2016) Standardised extract of safed musli (Chlorophytum borivilianum) increases aphrodisiac potential besides being safe in male Wistar rats. *Andrologia*, 48(10): 1236-1243.

GIRIBABU N, KUMAR KE, REKHA SS, MUNIANDY S, SALLEH N (2014) Chlorophytum borivilianum (Safed Musli) root extract prevents impairment in characteristics and elevation of oxidative stress in sperm of streptozotocin-induced adult male diabetic Wistar rats. *BMC Complement Altern Med*, 14(1): 291.

HAMMOUD AO, MEIKLE AW, REIS LO, GIBSON M, PETERSON CM, CARRELL DT (2012) Obesity and male infertility: a practical approach. *Semin Reprod Med*, 30: 486-495.

JIA YF, FENG Q, GE ZY, GUO Y, ZHOU F, ZHANG KS, WANG XW, LU WH, LIANG XW, GU YQ (2018) Obesity impairs male fertility through long-term effects on spermatogenesis. *BMC Urol*, 18(1): 42.

KENJALE R, SHAH R, SATHAYE S (2008) Effects of Chlorophytum borivilianum on sexual behaviour and sperm count in male rats. *Phytother Res*, 22(6): 796-801.

KHANAM Z, SINGH O, SINGH R, BHAT IUH (2013) Safed musli (Chlorophytum borivilianum): A review of its botany, ethnopharmacology and phytochemistry. *J Ethnopharmacol*, 150: 421-441.

LIU B, MA D, MAO PF (2014) Role of oxidative stress injury in male infertility. *Natl J Androl*, 20: 927-931.

LOHIYA NK, GOYAL RB, JAYAPRAKASH D, ANSARI AS, SHARMA S (1994) Antifertility effects of aqueous extract of Carica papaya seeds in Male rats. *Planta Med*, 60: 400-404.

PASQUALOTTO FF, SHARMA RK, PASQUALOTTO EB, AGARWAL A (2008) Poor semen quality and Ros-TAC scores in patients with idiopathic infertility. *Urol Int*, 81: 263-270.

RAJI Y, BOLARINWA AF (1997) Antifertility activity of Quassia amara in male rats – in vivo study. *Life Sci*, 61(11): 1067-1074.

RAJI Y, UDOH US, MEWOYEKA OO, ONONYE FC, BOLARINWA AF (2003) Implication of reproductive endocrine malfunction in male antifertility efficacy of Azadirachta indica extract in rats. *Afr J Med Sci*, 32: 159-165.

SHARMA P, CHANDRUL KK (2017) Chlorophytum borivilianum (Safed musli): A vital herbal drug. *Int J Pharm Med Res*, 5(1): 401-411.

THAKUR M, DIXIT VK (2006) Effect of chlorophytum borivilianum on androgenic & sexual behavior of male rats. *Indian Drugs*, 43(4): 300-306.

VYAS R, KESARI KK, SLAMA P, ROYCHOUDHURY S, SISODIA R (2022) Differential activity of antioxidants in testicular tissues following administration of chlorophytum borivilianum in gamma-irradiated swiss albino mice. *Front Pharmacol*, 12: 774444.

WILLIAMS EP, MESIDOR M, WINTERS K, DUBBERT PM, WYATT SB (2015) Overweight and obesity: prevalence, consequences, and causes of a growing public health problem. *Curr Obes Rep*, 4(3): 363-370.

Variations of the human hyoid bone and its clinical implications

L. Hernández[1,2], Sara Quiñones[2], Marko Konschake[3], Richard S. Tubbs[4-9], Lukasz Olewnik[10], Ana Slocker[1,2], José R. Sañudo[2], Eva Maranillo[2]

[1] Department of Surgery, Medical and Social Sciences, Human Anatomy and Embryology Unit, School of Medicine and health Sciences, University of Alcalá, UAH, Alcalá de Henares, Madrid, Spain

[2] Department of Anatomy and Embryology, Faculty of Medicine, Universidad Complutense de Madrid, Spain

[3] Department of Anatomy, Histology and Embryology, Institute of Clinical and Functional Anatomy, Medical University Innsbruck (MUI), Innsbruck, Austria

[4] Department of Neurosurgery, Tulane University School of Medicine, New Orleans, LA, USA

[5] Department of Neurosurgery and Ochsner Neuroscience Institute, Ochsner Health System, New Orleans, LA, USA

[6] Department of Anatomical Sciences, St. George's University, Grenada

[7] Department of Neurology, Tulane University School of Medicine, New Orleans, LA, USA

[8] Department of Structural and Cellular Biology, Tulane University School of Medicine, New Orleans, LA, USA

[9] Department of Surgery, Tulane University School of Medicine, New Orleans, LA, USA

[10] Department of Anatomical Dissection and Donation, Medical University of Lodz, Poland

SUMMARY

The aim was to determine the variations in shape of the human hyoid bone in terms of symmetry, isometry and anisomorphism. These parameters are useful for surgeons and/or forensic anthropologists. Sixty-two human hyoid bones (31 male and 31 female) belonging to the Instituto Anatómico Forense (I.A.F.) of Madrid (Spain) were dissected. The data collected were analysed using the chi-square test.

The specimens were classified into five different patterns: U-shaped (16.7%), open (47.6%), triangular (9.5%), horseshoe-shaped (7.1%) and trapezoidal (19%). Types were distinguished according to the different shapes of the two halves (isomorphic 67.7% and anisomorphic 32.3%), the length of the greater horn (isometric 37% and anisometric 63%), and the transverse distances between the horns (symmetry 24.2% and asymmetry 75.8%). A thorough understanding of these anatomical variations could be useful for clinicians and forensics in interpreting the morphology of the hyoid bone.

Key words: Neck – Larynx – Hyoid muscles – Pharyngeal arches – Hyoid bone

Shared corresponding authors:
Prof. Dr. Marko Konschake, MD. Department of Anatomy, Histology and Embryology, Institute of Clinical and Functional Anatomy, Medical University of Innsbruck (MUI), Müllerstr. 59, 6020 Innsbruck, Austria. E-mail: marko.konschake@i-med.ac.at - Orcid: 0000-0002-9706-7396
Dr Sara Quiñones, MD. Department of Anatomy and Embryology, Faculty of Medicine, Universidad Complutense de Madrid, Spain. E-mail: saraquga97@gmail.com - Orcid: 0000-0002-5099-9962

Submitted: September 26, 2023. **Accepted:** February 6, 2024

https://doi.org/10.52083/LLMG1458

INTRODUCTION

The hyoid is a U-shaped bone located in the ventral aspect of the neck around the C4 level, ranging topographically from C3 to C5/6 (Standring, 2008; Mirjalili, 2010). It is located between the root of tongue and the thyroid cartilage (Mukhopadhyay, 2010). Some classical anatomy textbooks have described the hyoid bone as symmetric, horseshoe-shaped or U-shaped (Tubbs et al., 2016). Nonetheless, a universally accepted morphological classification for this bone has proven elusive, leading to diverse categorizations in the literature consulted (Leksan et al., 2005).

Despite the absence of such a classification, some authors have attempted to classify the hyoid bone according to its shape (Koebke et al., 1979; Papadopoulos et al., 1989; Pollanen and Chiasson, 1996; Pollanen and Ubelaker, 1997), while others have used precise measurements of the different parts of the bone, with numerical values serving as the main parameter for classification (Miller et al., 1988). These differing methodologies employed reflect the ongoing quest to understand the hyoid bone's morphology.

Furthermore, the anatomical variations of this bone structure have become even more significant due to the emergence of advanced imaging technologies in recent times.

In view of the abovementioned differences in the literature, the aim of our work was to assess the variations in the shape of the hyoid, and to compare the frequencies of certain morphological characteristics in our sample with those in the literature.

MATERIALS AND METHODS

A total of 62 human hyoids from autopsied corpses belonging to the Instituto Anatómico Forense (I.A.F.) de Madrid, Spain, were dissected (31 males and 31 females, ranging from 19 to 91 years of age, mean male 63.5, mean female 72.3 years). Written informed consent was obtained by those donating their bodies to science as required by the scientific institution.

During the dissection, a midline incision was made on the neck from a median point 15 mm below the chin (*mentum*) to the incisura jugularis. The suprahyoid and infrahyoid muscles were dissected and reflected, exposing the front part of the larynx. Subsequently, the hyoid together with the larynx were excised en bloc, removing the supra- and infra-hyoid muscles, pharynx, trachea, oesophagus, and thyroid gland.

Hyoids were fixed in 10% formalin. After removal, the infrahyoid and inferior constrictor muscles, ligaments, membranes, and neurovascular structures were microdissected under a surgical Zeiss-OPM1 microscope at original magnification X4 to X6. Consecutively, the bones were cleaned, first by mechanical dissection and then by maceration for 10 days in 5% sodium hypochlorite (diluted to 50%). Finally, the hyoids were bleached by exposure to sunlight, with or without prior immersion in 110-volume hydrogen peroxide, or by 3% ammonium hydroxide.

The hyoid shapes were classified and independently verified by two experienced anatomists. The chi-square test was used for statistical analysis; $p<0.05$ was considered statistically significant.

Following the identification of patterns and statistical analysis, the results were compared with previously published studies. This led to a new classification system with special reference to clinical practice and usability.

RESULTS

The morphology of the hyoid bone could be classified into five basic patterns. We assigned different names based on the approximate appearances of the forms as drawn (Fig. 1).

Patterns of the hyoid bone

1) **U- shape:** The anterior contour of the bone is semicircular, and its diameter coincides with the distance between the greater horns. The greater horns follow a straight or oblique line in an antero-posterior direction with the form of the letter U. The U-like shape was found in 7/42 (16.7%) of our isomorphic hyoids sample (Table 1) (Figure 1A).

1) **Open:** This has common characteristics with the U-like shape, but the greater horns follow a

Fig. 1.- Basic morphological patterns based on the shape of the whole hyoid bone. This image shows 5 different patterns: **A** (U shape), **B** (Open), **C** (Triangular), **D** (Horseshoe shape) and **E** (Trapezoidal).

Table 1. Incidence of different patterns of the hyoid bones (U shape, open, triangular, horseshoe and trapezoidal) in males and females among isomorphic hyoids. Nº: number of hyoid bones.

SEX	U shape Nº %	Open Nº %	Triangular Nº %	Horseshoe Nº %	Trapezoidal Nº %
MALE	2 4,8	11 26,2	1 2,4	2 4,7	7 16,7
FEMALE	5 11,9	9 21,4	3 7,1	1 2,4	1 2,3
TOTAL	**7 16,7%**	**20 47,6%**	**4 9,5%**	**3 7,1%**	**8 19%**

medial-lateral oblique direction, diverging from each other to create an open form. The open shape was the most frequent in our isomorphic hyoids sample (20/42, 47.6%) (Table 1) (Fig. 1B).

2) **Triangular:** As its name indicates, this is triangular, its sides being the major horns and its base the largest transverse distance between them. The triangular shape was found in 4/42, 9.5% of our isomorphic hyoids sample (Table 1) (Fig. 1C).

3) **Horseshoe-shape:** The distal-posterior ends of both greater horns are closer together than in the U-shape, so the contour of the bone is more curved and closed. The horseshoe shape was less common in our isomorphic hyoids sample (3/42, 7.1%) (Table 1) (Fig. 1D).

4) **Trapezoidal:** As its name indicates, the ventral contour of the hyoid viewed from a cranio-caudal perspective resembles this sample (8/42, 19%) (Table 1) (Fig. 1E).

Types of the hyoid bone

During this classification of the hyoid, it was observed that the morphological characteristics are not always the same on both sides; the two sides of the same bone could be distinct. We have used the term "type" to refer to the following variations to clarify this new classification:

1) Types based on the different shapes or patterns of the two halves (isomorphy). This could be split into:
   a) Isomorphic, when the two halves follow the same pattern; this was the most frequent type (42/62, 67.7% of the total cases) (Table 2) (Fig. 2A).
   b) Anisomorphic, when the halves follow different patterns (20/62, 32.3%) (Table 2) (Fig. 2B).
2) Types based on the length of greater horn (isometry). The following could be distinguished:
   a) Isometric hyoid, when the tips of both greater cornua fell on the same horizontal line (23/62, 37%) (Table 3) (Fig. 2 A).

Table 2. Incidence of types based on the different shapes of the two halves, distinguishing isomorphic and anisomorphic hyoid bones.

SEX	ISOMORPHIC Nº %	ANISOMORPHIC Nº %	TOTAL N %
MALE	**23 37.1** (74,2)	**8 12,9** (25,8)	**31 50**
FEMALE	**19 30.6 (**61,3)	**12 19,4** (38,7)	**31 50**
TOTAL	**42 67,7%**	**20 32,3**	**62 100**

b) Anisometric hyoid, when the tips of both greater cornua did not coincide on the same axis; this was the most frequent type (39/62, 63% of the total cases) (Table 3) (Fig. 2 B).

3) Types based on the transverse distances between the greater horns (symmetry):

a) Symmetric, when the middles of all the transverse diameters fell on the sagittal axis (15/62, 24.2%) (Table 4) (Fig. 3A).

b) Asymmetric, when the middles of all the transverse diameters did not fall on the sagittal axis; this was the most frequent type (47/62, 75.8% of the total cases) (Table 4) (Fig. 3B).

According to this classification, the most common hyoid bone morphology in our sample was isomorphic, asymmetric, and anisometric (32.25%). Considering these three characteristics, only 14.52% of our sample were simultaneously isomorphic, iso-

Fig. 2.- Hyoid types based on the morphology of the two halves and the different lengths of the greater horn. According to the morphology of the two halves, the hyoid bone could be divided into isomorphic (**A**) and anisomorphic (**B**). Fig. 2B corresponds to a right Horseshoe shape and left U shape. According to the different lengths of the greater horn of the hyoid bone, it could be divided into isometric (**A**) and anisometric (**B**). The lines show the similar (**A**) or different lengths (**B**). Fig. 2A corresponds to the hyoid bone of the fig. 1A.

Table 3. Incidence of types based on the length of greater horn, distinguishing isometric and anisometric hyoid bones.

SEX	ISOMETRIC Nº %	ANISOMETRIC Nº %	TOTAL Nº %
MALE	**9** **14,5** (29)	**22** **35,5** (71)	**31** **50**
FEMALE	**14** **22,5** (45,2)	**17** **27,5** (54,8)	**31** **50**
TOTAL	**23** **37**	**39** **63**	**62** **100**

Table 4. Incidence of types based on the transverse distances between the greater horns, distinguishing symmetric and asymmetric hyoid bones.

SEX	SYMMETRIC Nº %	ASYMMETRIC Nº %	TOTAL Nº %
MALE	**8** **12,9** (25,8)	**23** **37,1** (74,2)	**31** **50**
FEMALE	**7** **11,3** (22,6)	**24** **38,7** (77,4)	**31** **50**
TOTAL	**15** **24,2**	**47** **75,8**	**62** **100**

Fig. 3.- Hyoid types based on the distances between the greater horns of the two halves of the hyoid bone. It could be divided into symmetric (**A**) and asymmetric (**B**). In the asymmetric hyoid (Fig. 3B) the numbers 1 and 2 represent the different transverse distances, 1 longer than 2. Fig. 3A corresponds to the hyoid bone of the fig. 1A.

metric, and symmetric. Therefore, one side of the hyoid bone differed from the other in at least one characteristic in most of our sample (85.48%).

DISCUSSION

For clarity, we have divided the discussion in the same sections as the results (patterns of the hyoid bone, and types of the hyoid bone divided into three characteristics).

Patterns of the hyoid bone

Our results are quite like those of Papadopoulos et al. in relation to the U-shape (16.7% and 18.4% respectively), but there is no coincidence in the open shape (47.6% and 26.3%, respectively), which is the most frequent pattern in our series, as in the other authors presented in Table 5 (Papadopoulos et al., 1989).

Also, the frequency of the horseshoe shape in our sample (7.1%) does not coincide with that of Papadopoulos et al. (1989) (21.1%).

The frequency of the trapezoidal shape is the same in the Stosić-Domnić et al. (1973) series (19%) and ours (19%). This morphological type has not been described by other authors in the literature consulted, apart from Stosić-Domnić et al. (1973) (Table 5).

Most of articles do not specify the type of population used in their studies, but only the country to which the study belongs. This lack of information results in a huge variability in the populations studied across the different countries, as shown in Table 5. Therefore, it is difficult to compare the results of the present studies in terms of population (Table 5) (Stosić-Domnić et al., 1973; Koebke et al., 1979; Papadopoulos et al., 1989; Pollanen and Ubelaker, 1997).

Table 5. Comparison of present work with previous studies regarding the pattern or shape of the hyoid bones.

PATTERN OR SHAPE	Stosić-Domnić et al. 1973	Koebke and Saternus, 1979	Papadopoulos et al. 1989	Pollanen and Ubelaker 1997	Present work, 2022
Population	Croatia	Germany	Greece	United States	Spain
U shape	30.5%	35%	18.4%	55%	16,7%
Open	50.5%	41%	26.3%	45%	47,6%
Triangular	---	---	5.3%.	---	9,5%
Horseshoe	---	13%	21,1%	---	7,1%
Trapezoidal	19%	---	---	---	19,0%

Types of the hyoid bone

1) Types distinguished by the shapes or patterns of the two halves (isomorphic and anisomorphic):

Our anisomorphic hyoid was found in 32.3% (12.9% in males and 19.4% in females), comparable with the D-type of Papadopoulos et al. (1989) (28.3%), or to the asymmetrical type of Koebke and Saternus (1979) (11%). Although anisomorphic hyoids are more frequent (32.3%) in our sample than in the works of Papadopoulos et al. and Koebke and Saternus, we agree with Koebke and Saternus (1979) that the combination of open shape and U-shape (defined as B and U types) was the most frequent mixed form.

2) Types based on the length of greater horn (isometry):

Morphological anisometry was not mentioned in the literature until the study by Papadopoulos et al. (1989), which showed that 59.3% of the hyoids were anisometric (26.3% male, 23% female). In our total sample, anisometry (62.9%) predominated over isometry, as Papadopoulos et al. found in 1989.

In the work of Papadopoulos et al. (1989), the χ^2 test showed no significant sex difference in anisometry (52.6% male and 47.4% female) ($P > 0.1$), the distribution being similar. In our sample, there were more anisometric (71%) than isometric (29%) hyoids in males, while the proportions were more nearly equal in females. In the total of isometric hyoids, the females had the highest frequency (60.9%). In the work of Papadopoulos et al. (1989), the percentages of anisometric hyoids were closely similar in males and females; in our study, there was a higher percentage of anisometry in males, and similar percentages of isometry and anisometry in females. However, as in Papadopoulos et al., analysis of the relevant percentage difference (Fisher's exact statistic) could not establish sexual dimorphism in relation to the morphological trait anisometry. In terms of clinical significance, our data concerning hyoid types based on the length of the greater horn (isometry or anisometry) could be related to the clicking larynx, which could be caused by an enlarged greater horn of the hyoid bone (hyoid syndrome) (Heueveling et al., 2018).

3) Types based on the transverse distances between the greater horns (symmetry):

Although in some classical treatises on Human Anatomy (Testut, 1986; Paturet, 1951; Bouchet and Cuilleret, 1979) the hyoid is described as a symmetrical bone, Papadopoulos et al. (1989) found asymmetry in 47.4% of cases (26.3% in males and 21.1% in females). In his work, the χ^2 test showed no significant sex difference in asymmetry; 52.6% of male and 42.1% of female bones were asymmetric ($P > 0.1$). However, in our study, asymmetrical hyoids predominated (75.8%: 37.1% male and 38.7% female). Asymmetry predominated both in males (74.2%) and, with a slightly higher percentage, in females (77.4%). In the asymmetrical hyoids there was no clear sex predominance (48.9% were male and the remaining 51.1% female).

According to the relevant analysis of the percentage difference, there was no dimorphism in relation to the morphological trait asymmetry.

Pollanen and Chiasson (1996) mentioned that one anatomical feature that could be relevant in assessing hyoid fractures in cases of strangulation is the asymmetry of the greater horns, since asymmetric hyoids could be more susceptible to fracture if the compressive forces are distributed preferentially over one horn. Kasprzak et al. (1993) found by interferometric analysis of the hyoid under tension that asymmetry could be important in the site of fracturing: the deformation forces inferred from this method were not uniformly distributed over the hyoid. From a clinical point of view, this hyoid asymmetry could be related to asymmetry in the functional activity of the muscles that insert into it and therefore related to activities such as articulation of sounds, swallowing or mastication (Urbanová et al., 2014; Hong et al., 2017).

Ethical approval details

The individuals had given their written informed consent for their use for scientific purpose prior to death. According to National Law, scientific institutions (in general Institutes, Departments or Divisions of Medical Universities) are entitled to receive the body after death mainly by means of a specific legacy, which is a special form of last will and testament. No bequests are accept-

ed without the donor having registered their legacy and been given appropriate information upon which to make a decision based upon written informed consent (policy of ethics); therefore, an ethics committee approval was not necessary (Konschake et al., 2014).

Author's contribution

HL, QS, KM, TRS, OL, SA, SJ, ME did substantial contributions to the conception and design of the work, the acquisition, analysis, and interpretation of data for the work; also to drafting the work and revising it critically for important intellectual content; KM and SJ did a final approval of the version to be published; also an agreement to be accountable for all aspects of the work in ensuring that questions related to the accuracy or integrity of any part of the work are appropriately investigated and resolved.

ACKNOWLEDGEMENTS

The authors sincerely thank those who donated their bodies to science so that anatomical research could be performed. Results from such research can potentially increase mankind's overall knowledge that can then improve patient care. Therefore, these donors and their families deserve our highest gratitude (Iwanaga et al., 2021).

REFERENCES

HEUVELING DA, VAN LOON MC, RINKEL R (2018) A clicking larynx: Diagnostic and therapeutic challenges. *Laryngoscope*, 128: 697-700.

HONG KH, YANG WS, PARK MJ, OH JS, HAN BH (2017) Changes in oral vowel sounds and hyoid bone movement after thyroidectomy. *Clin Exp Otorhinolaryngology*, 10(2): 168-173.

IWANAGA J, SINGH V, OHTSUKA A, HWANG Y, KIM HJ, MORYŚ J, RAVI KS, RIBATTI D, TRAINOR PA, SAÑUDO JR (2021) Acknowledging the use of human cadaveric tissues in research papers: Recommendations from anatomical journal editors. *Clin. Anat*, 34: 2-4.

KASPRZAK H, PODBIELSKA H, VONBALLY G, FECHNER G (1993) Biomechanical investigation of the hyoid bone using speckle interferometry. *Int J Legal Med*, 106: 132-134.

KOEBKE J, SATERNUS K-S (1979) Zur Morphologie des adulten menschlichen Zungenbeins. *Z Rechtsmed*, 84: 7-18.

KONSCHAKE M, BRENNER E (2014) "Mors auxilium vitae"—Causes of death of body donors in an Austrian anatomical department. *Ann Anat*, 196: 387-393.

LEKSAN I, MARCIKIC M, NIKOLIC V, RADIC R, SELTHOFER R (2005) Morphological classification and sexual dimorphism of hyoid bone: new approach. *Coll Antropol*, 29: 237-242.

MILLER KW, WALKER PL, O'HALLORAN RL (1998) Age and sex-related variation in hyoid bone morphology. *J Forensic Sci*, 43: 1138-1143.

MIRJALILI SA, HALE SJ, BUCKENHAM T, WILSON B, STRINGER MD (2012) A reappraisal of adult thoracic surface anatomy. *Clin Anat*, 25: 827-834.

MUKHOPADHYAY PP (2010) Predictors of hyoid fracture in hanging: Discriminant function analysis of morphometric variables. *Leg Med* (Tokyo), 12: 113-116.

PAPADOPOULOS N, LYKAKI-ANASTOPOULOU G, ALVANIDOU E (1989) The shape and size of the human hyoid bone and a proposal for an alternative classification. *J Anat*, 163: 249-260.

POLLANEN MS, CHIASSON DA (1996) Fracture of the hyoid bone in strangulation: comparison of fractured and unfractured hyoids from victims of strangulation. *J Forensic Sci*, 41: 110-113.

POLLANEN M, UBELAKER DH (1997) Forensic significance of the polymorphism of hyoid bone shape. *J Forensic Sci*, 42: 890-892.

STANDRING S (2008) Gray's Anatomy: the anatomical basis of clinical practice. Churchill Livingstone.

STOSIC-DOMNIC T, MRVALJEVIC D, KOCIJANCIC M (1973) Morphology, ligamental attachments and vascularization of the hyoid bone. *Stomatol Glas Srb*, 20: 203-206.

TUBBS RS, SHOJA MM, LOUKAS M (2016) Bergman's comprehensive encyclopedia of human anatomic variation. John Wiley & Sons.

URBANOVÁ P, HEJNA P, ZÁTOPKOVÁ L, SAFR M (2014) The asymmetry and modularity of the hyoid bone. *Int J Morphol*, 32(1): 251-260.

Enhanced visualization of articular cartilage chondroprogenitor-derived extracellular vesicles using cytospin centrifugation for confocal imaging

Elizabeth Vinod[1,2], Ganesh Parasuraman[2], Soosai M. Amirtham[1], Sandya Rani[2], Abel Livingston[3], Solomon Sathishkumar[1]

[1] *Department of Physiology, Christian Medical College, Vellore, India*

[2] *Centre for Stem Cell Research, (A unit of InStem, Bengaluru), Christian Medical College, Vellore, India*

[3] *Department of Orthopaedics, Christian Medical College, Vellore, India*

SUMMARY

Characterizing Extracellular Vesicles (EVs) poses a challenge due to their complex composition and small size. Efforts to visualize fluorescently labeled EVs post-isolation with confocal microscopy encounter a significant obstacle in congregating the isolates on slides. While cytospin is a well-established method for cells, its application with EVs remains unexplored. This study aimed to isolate EVs and evaluate the efficiency of cytospin preparation to enhance their visualization using confocal microscopy. Following informed consent, cartilage shavings from a non-diseased human tibiofemoral joint were digested to obtain cartilage-resident chondroprogenitors through a migratory-assay (MCP). The MCPs were characterized for MSC markers (positive: CD105, CD73, CD90; negative: HLA-DR, CD34, CD45) using FACS. The conditioned medium was utilized to isolate EVs using the cutoff filter and precipitation technique, and their confirmation for transmembrane markers CD63 and CD81 was performed via FACS. Subsequently, the isolated EVs were subjected to confocal microscopy with and without (control) cytospin preparation.

The MCPs exhibited high expression of positive and low expression of negative MSC markers. The study effectively employed cytospin centrifugation and confocal imaging to robustly identify EVs isolated from MCPs. Fluorescently labeled with CD63 and CD81 markers, the EVs isolated using cytospin centrifugation were concentrated on glass slides, and compared to control slides; the experimental setup facilitated a 100 times concentration of EVs, thereby enabling easy identification. Confocal analysis confirmed positive expressions of CD63 and CD81, aligning with FACS results. This study introduces a novel approach that enhances the visualization of MCP-derived EVs using cytospin centrifugation.

Shared corresponding authors:
Elizabeth Vinod. Department of Physiology/Centre for Stem Cell Research, Christian Medical College, Vellore, Tamil Nadu, India – 632002. Phone: +91 9677651977. E-mail: elsyclarence@cmcvellore.ac.in - ORCID: 0000-0001-7340-8320

Submitted: November 25, 2023. **Accepted:** February 7, 2024

https://doi.org/10.52083/MUNS1446

Key words: Migratory chondroprogenitors – Cytospin – Confocal – CD63 – CD81

INTRODUCTION

In the past decade, research on Extracellular Vesicles (EVs) has significantly grown, leading to the development of robust techniques for assessing their physical and functional characteristics (Vlassov et al., 2012). EVs constitute a diverse category of vesicles released by cells through various biogenesis pathways, which include exosomes, microvesicles, and apoptotic bodies (Zhang et al., 2020). Exosomes are formed as intraluminal vesicles within multivesicular bodies and are subsequently discharged upon fusion with the cell's plasma membrane, typically measuring 30 to 200 nm in size. In contrast, microvesicles tend to be larger, with dimensions ranging from approximately 150 to 1000 nm. They are generated through a 'budding' process directly from the cell's plasma membrane, encapsulating cytosolic content. The largest among these vesicles are apoptotic bodies, which develop when a cell undergoes apoptosis.

Characterizing EVs is challenging due to their intricate composition and extremely small size. Utilizing advanced techniques such as electron microscopy and atomic force microscopy aids in their visualization and analysis (Morales-Castresana et al., 2017; Salmond et al., 2021). Nevertheless, the complexity of these methods hinders their practical application, emphasizing the need for the development of straightforward protocols for EV visualization. Recent studies demonstrate the use of fluorescent detection of EVs with lipophilic dyes (e.g., C5-Maleimide-Alexa633 or PKH26) and also labeling cell membranes/surface tetraspanin proteins (e.g., CD63, CD9, CD81) using fluorophores, each having its individual advantages and disadvantages (Grange et al., 2014; Jankovicova et al., 2020). While attempts have been made to identify fluorescently labeled EVs using confocal microscopy, a significant challenge remains in identifying the location of the isolated EVs from the suspension placed for microscopic evaluation.

In recent times, there have been important advancements in treating osteoarthritis using mesenchymal stem cells and cartilage resident cells such as chondrocytes and chondroprogenitors (Pelaez et al., 2021). Nevertheless, this approach has several challenges, including donor site morbidity, immunogenic response, inconsistent regeneration after treatment, and issues in maintaining the quality of large-scale cell production. To address these limitations, scientists have explored the use of Extracellular Vesicles as alternatives for regenerating cartilage tissue, primarily through the use of exosomes, which offer advantages of increased stability and reduced susceptibility to external influences (Liu et al., 2019; Wu et al., 2022). Furthermore, research has shown that exosomes can mitigate disease progression, providing a promising avenue for osteoarthritis management (Ni et al., 2020).

Since the field is still in its early stages of development, many of these EV labeling methods need further refinement to suit each experimental situation. This study aimed to isolate EVs from migratory chondroprogenitors (MCP), a recent subset reported to exhibit superior potential for cartilage repair (Vinod et al., 2020; 2021), and to fluorescently label the EVs using well-characterized EV markers CD81 and CD63. The study incorporated cytospin, a technique that employs centrifugal force to concentrate the isolate from a dilute cell suspension onto a circular area on a slide (Koh, 2013). In this study, we demonstrate that the cytospin method can be used to concentrate EVs. Combining this technique with confocal imaging provides a simple and robust method for efficiently identifying EVs.

MATERIALS AND METHODS

Sample procurement, cellular isolation of migratory chondroprogenitors and phenotypic characterization

Following Institutional Review Board clearance, the study was conducted in accordance with the stipulated guidelines set by the Ethics Committee. Human femorotibial joint samples were procured from a non-diseased knee joint (Male, age: 65 years) of an individual who required above-knee amputation indicated for limb salvage surgery (Fig. 1).

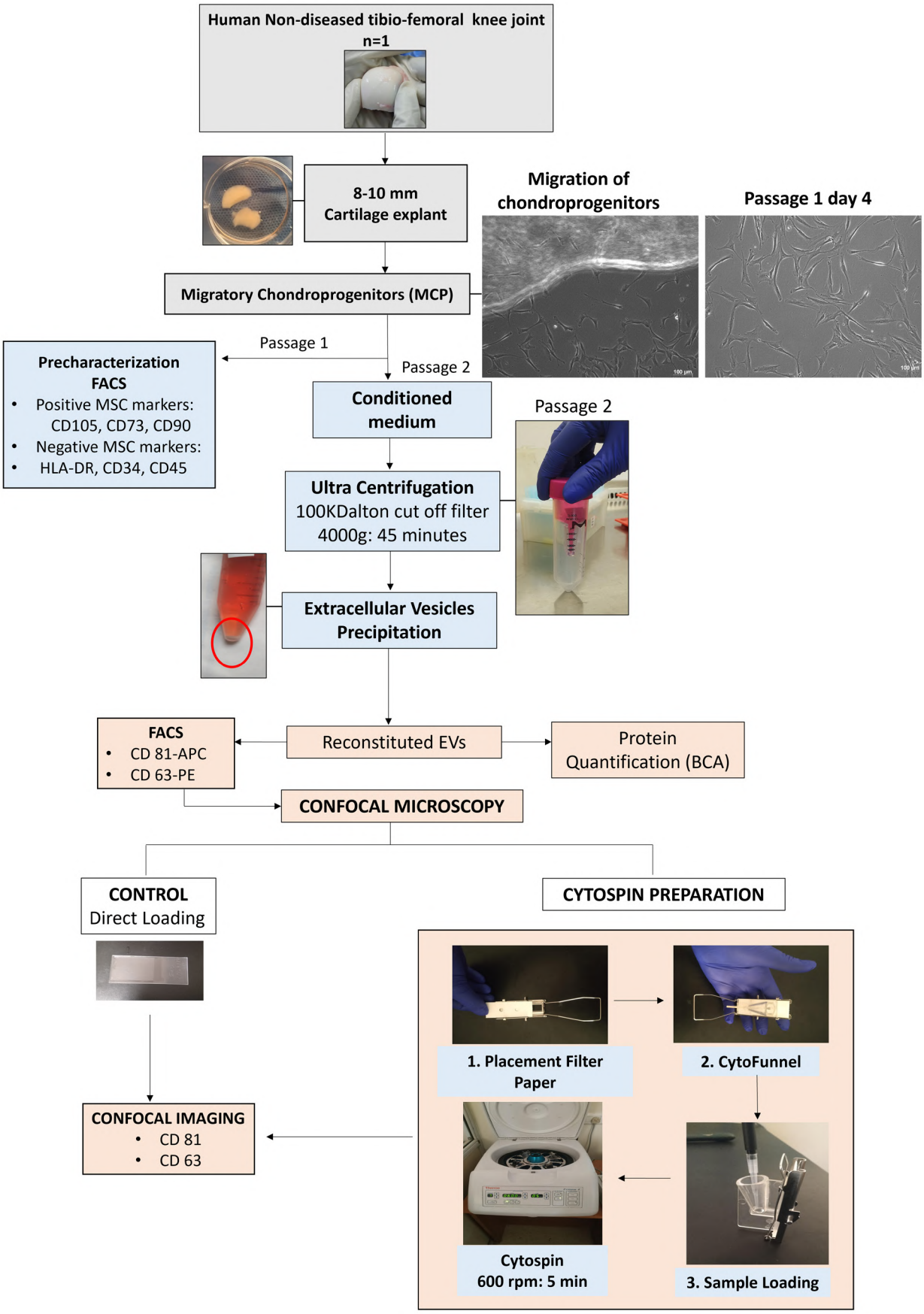

Fig. 1.- Study algorithm depicting the isolation and phenotypical characterization of human articular cartilage derived migratory chondroprogenitors. Cartilage explants (8-10 mm) obtained from a non-diseased human joint was subjected to enzymatic digestion by collagenase to loosen the matrix enabling the migration of chondroprogenitors to obtain MCPs. The MCPs were phenotypically characterized using FACS for positive and negative MSC markers. The conditioned medium obtained from the MCPs was subjected for cytospin centrifugation and precipitated to obtain EVs which were quantified, characterized for exosome markers using FACS (CD63 and CD81) and subjected for confocal microscopy with and without cytospin preparation.

Table S1. List of antibodies used in FACS (Fluorescence Activated Cell Sorting) MSC- Mesenchymal Stem Cell, CD – Cluster of differentiation, FITC – Fluorescein isothiocyanate, PE- Phycoerythrin, V 500 – Violet 500.

GROUPS	SURFACE MARKERS	FLUOROCHROME CONJUGATE	CATALOGUE NUMBER	SOURCE
Positive MSC markers	CD105: Endoglin glycoprotein	FITC	561443	BD Biosciences
	CD73: Ecto-5'-nucleotidase	PE	550257	BD Biosciences
	CD90: Thymus cell antigen 1	PE	555596	BD Biosciences
Negative MSC markers	HLA-DR: Integrin marker	V 500	561225	BD Biosciences
	CD34: Hematopoietic stem cell marker	PE	348057	BD Biosciences
	CD45: Hematopoietic stem cell marker	FITC	555482	BD Biosciences

To isolate MCPs, approximately 8-10 mm cartilage shavings were maintained in their expansion medium, composed of Dulbecco's Modified Eagle Medium containing 10% fetal bovine serum, 10mM Glutamine, and antibiotics. The isolation procedure followed the method outlined by Koelling et al. (2009). In brief, the cartilage shavings were taken and washed with phosphate-buffered solution (PBS) to remove any synovial fluid. They were then left undisturbed in their stromal medium for 48 hours. Subsequently, the explants were transferred to a 0.1% collagenase solution (Worthington) at 37°C for a 2-hour incubation, washed to eliminate any released cells, and then transferred to a culture plate containing expansion medium. The explants were observed for cell outgrowth, and the early migrated cells were harvested using 0.125% trypsin containing EDTA and further expanded to passage 2. The isolated MCPs were characterized using flow cytometric analysis (FACS) for positive MSC markers, namely CD105, CD73, CD90 and negative mesenchymal markers, HLA-DR, CD34, CD45. In brief, passage 1 MCPs at sub-confluence were trypsinized, washed, and prepared for flow cytometry analysis. Staining was carried out following the technical data sheet for each antibody. Details of the antibodies used have been listed in Table S1.

Isolation of extracellular vesicles (EVs)

At passage 2, the MCPs were seeded at a concentration of 5000 cells/cm^2 and once a confluence of 60% was achieved, the cells were washed with PBS and replaced with 8 ml/75 cm^2 of expansion medium containing exosome-depleted FBS (FBS previously centrifuged at 34,600 rpm, 17 hrs, 4°C, Beckman Coulter Optima L-100K Ultracentrifuge) and cultured for 48 hrs. The conditioned medium was collected and cleared by centrifugation at 2000 g for 20 min at 4°C. Approximately 48 ml of conditioned medium from 6 T75 flasks were collected and stored at -80°C till further use. In order to further concentrate the conditioned medium, it was filtered using 0.4 µm polyethersulfone (PES) filter and then subjected to 4000 g for 45 min at 4°C in a 100 Kdalton cutoff oak ridge centrifuge tube. The obtained yield of 1.5 ml was then processed to isolate the EVs using total exosome isolation kit via overnight precipitation method according to manufacturer's instructions (Total exosome isolation, Invitrogen, Cat No: 4478359).

In brief, for the preparation of exosomes from cell-free culture media filtrate, 0.5 volumes of the Total Exosome Isolation reagent were added. Achieving homogeneity was crucial, and this was accomplished by thorough vortexing, followed by gentle pipetting up and down. Following this, the samples underwent an overnight incubation at a temperature range of 2°C to 8°C. After the incubation period, the samples were subjected to centrifugation at 10,000 × g for one hour at 4°C. The supernatant was carefully aspirated and discarded ensuring not to disturb the pellet. The exosome containing EV pellet was resuspended in 400 µl of PBS and the protein quantified using Bicinchoninic acid (BCA) assay. Validation of EV isolation was performed by flow cytometry for CD81 and CD63.

Flow cytometry analysis of EVs and confocal microscopy

Flow cytometry analysis of EVs was performed using the Exosome – Human CD63 detection kit (ThermoFisher Scientific, Cat no: 10606D) ac-

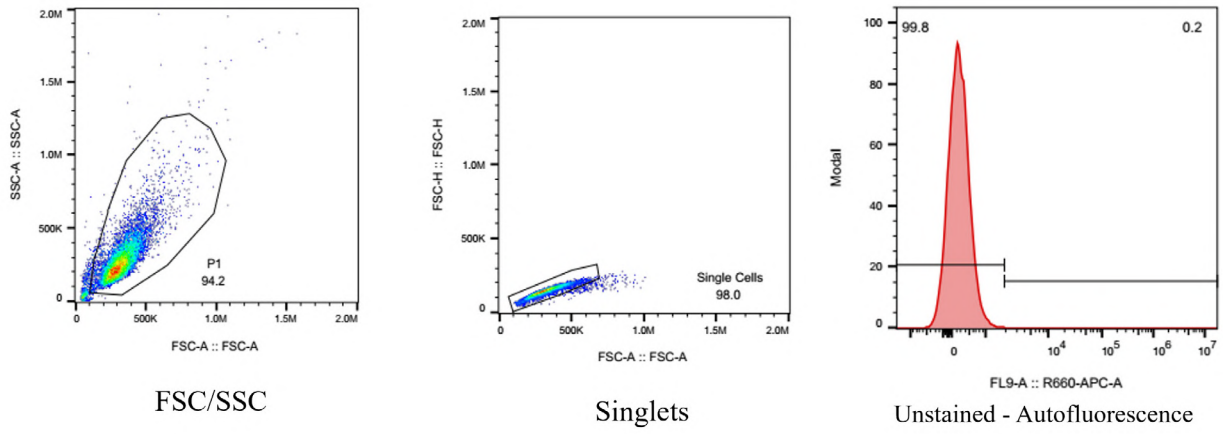

Fig. S1.- Gating strategy for flow cytometry analysis of MSCs. FSC-A/SSC-A: Forward scatter/Side scatter.

cording to the manufacturer's protocol. Briefly, the isolated EVs (diluted 1:10) were captured on Dynabeads magnetic beads with CD63 antibodies provided in the kit. The EV-magnetic bead complex was stained with APC Mouse Anti-human CD81 (Mat No: 561958) and PE Mouse Anti-human CD63 (Mat no: 561925) antibodies, and then acquired on BC CytoFLEX LX flow cytometer and CYTExpert Software Version 2.5. Flow cytometry was conducted using the Beckman Coulter CytoFLEX LX analyzer and CYTExpert Software Version 2.5. The flow cytometry data were analysed using FlowJo™ v10.8 Software (BD Life Sciences). Unstained controls were utilised for detecting background fluorescence for all the markers. Positive fluorescence was defined as any event occurring above a gate containing 99.8% of the events measured for background fluorescence in a histogram plot (Fig. S1). The flow cytometry results were analysed using FlowJo™ v10.8 Software (BD Life Sciences).

The antibody tagged EVs, following Flow cytometry, were processed for confocal microscopy using the cytospin preparation technique. First, a slide with the frosted side facing upward was inserted into the slide clip. Next, the filter card (Shandon filter cards white, Thermo Scientific, Ref: 5991022) with the absorbent surface touching the slide was inserted, ensuring that the cytofunnel matched up with the filter paper. 100 µL of the EV-containing suspension was gently pipetted into the cytofunnel. After this, the mounted holder was placed in the corresponding recess in the cytospin, ensuring it was balanced, and then centrifuged at a low speed of 600 rpm for 5 minutes (Thermo Scientific, CYTOSPIN 4 Cytocentrifuge). The filter paper was removed from the slide without smudging the preparation, followed by placing a cover slip over the concentrated area. Additionally, control slides were prepared, which included direct loading of 100 µL of the EV suspension and mounting with a cover slip (Fig. 1). Imaging for the expression of CD63 and CD81 was performed using an Olympus FV1000 laser scanning confocal microscope. After adjusting for optimal exposure, both groups were imaged using the same settings.

RESULTS

Following collagenase incubation, the cartilage explants displayed extracellular matrix loosening, and migration of the chondroprogenitors was observed as early as the day 7, resulting in a spindle-shaped morphology and subsequent fibroblastic expansion (Fig. 1). In Passage 1, there was a high expression of positive MSC markers: CD105 (100%), CD73 (99.99%), and CD90 (100%), along with low expression of negative MSC markers: HLA-DR (1.52%), CD34 (7.76%), and CD45 (2.51%) (Fig. 2). The MCPs continued to expand into Passage 2. After isolating EVs from the conditioned medium, protein quantification using BCA revealed a final concentration of 56.485 µg/µl. Analysis of the EVs for transmembrane exosomal markers, namely CD63 and CD81, showed a percentage expression of 60.64 and 79.36, respectively (Fig. 2).

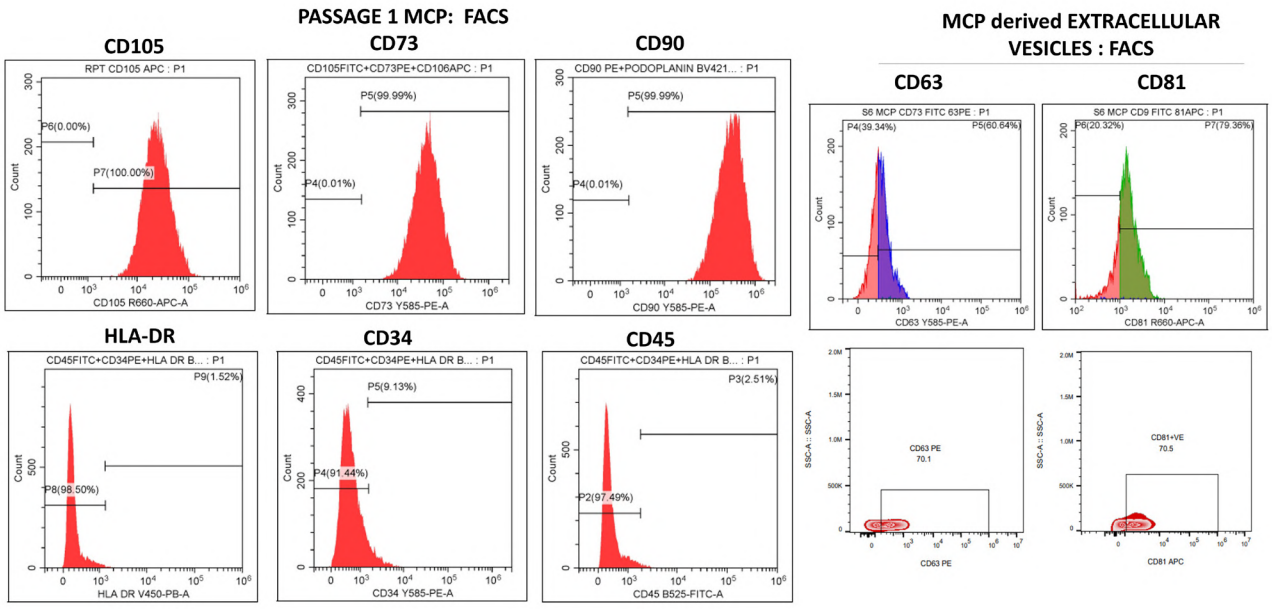

Fig. 2.- Flow cytometric analysis of the MCPs and MCP derived EVs. Graphical histogram showing the percentage of expression of positive and negative MSC and exosome markers. MCPs: migratory chondroprogenitors.

Confocal microscopy was conducted for CD63 and CD81 using 100 µl of the EV suspension (5.64 mg) per glass slide. Analysis of the slides revealed positive expressions for both CD63 and CD81, consistent with flow cytometry analysis. The cytospin technique concentrated the EVs effectively as a circular area on the slide, facilitating easy identification. It was observed that all immunocaptured beads, visible with phase contrast, exhibited positive expression for both the CD markers. In comparison to the control slides, the cytospin centrifugation allowed for a rapid and efficient 100 times concentration of the EVs, with their location easily identifiable (Fig. 3). Additionally, this method permitted the measurement and averaging of the size of the EVs.

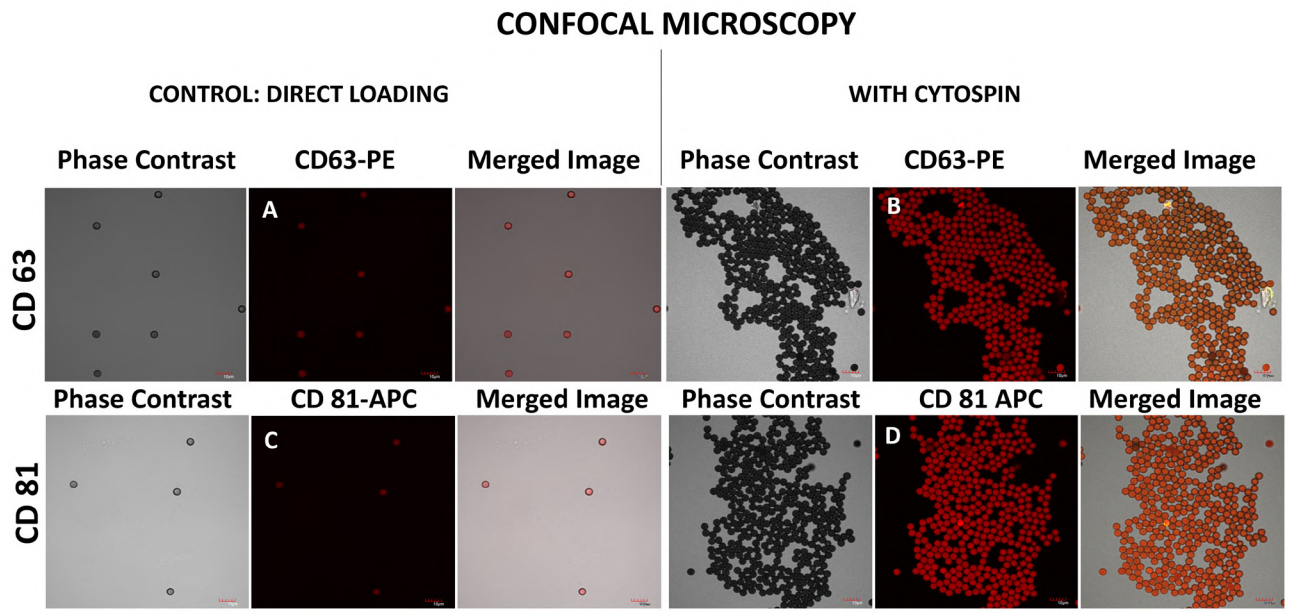

Fig. 3.- Confocal microscopy of EVs comparing the phase contrast, fluorescence and merge images for transmembrane exosome markers: CD63 and CD81 loaded on glass slides directly (controls) and following cytospin preparation.

DISCUSSION

The expanding field of EV research necessitates the development of effective techniques for their visualization, given their diverse origins and complex composition. The intricate nature of EVs, spanning exosomes, microvesicles, and apoptotic bodies, presents a challenge in identification, often necessitating advanced methods like nanotracking and electron microscopy for precise analysis (Vlassov et al., 2012; Zhang et al., 2020). However, the technical challenges associated with these techniques limit their practical application. In response to this, recent studies have explored alternative approaches, including fluorescent labelling and the utilisation of well-characterized cell-surface markers such as CD9, CD63, CD81, and Flotilin, among others (Jankovicova et al., 2020). Flow cytometry and confocal microscopy, utilizing fluorescent labelling, offer an efficient means for the easy identification of EVs, addressing practical limitations associated with traditional approaches. However, a significant limitation in visualizing EVs with confocal microscopy is the challenge of congregating the EV isolate for easier identification on the slide. While cytospin has been a well-established method for cells (Koh, 2013), its application with EVs has not been previously attempted.

In the context of cartilage repair and the emerging role of chondroprogenitors, this study aimed to enhance the visualization of EVs derived from MCPs. The utilization of cytospin centrifugation in combination with confocal imaging proved to be a straightforward and robust method for efficiently identifying EVs. The study successfully isolated EVs from MCPs, labelled them fluorescently with CD63 and CD81 markers, and employed cytospin to concentrate EVs on glass slides. The results demonstrated positive expressions for both markers, validating the effectiveness of the approach. The use of MCPs, particularly those exhibiting superior potential for cartilage repair, reflects an innovative approach in regenerative medicine. Furthermore, the concentration and sizing of EVs play pivotal roles in their characterisation. Our results indicate successful isolation of EVs from MCPs by cytospin centrifugation, supported by flow cytometry analysis and confocal microscopy. The efficiency of the cytospin method in concentrating EVs onto slides enhances their visibility, addressing a significant challenge in the field.

In conclusion, our study introduces a novel approach in order to enhance the visualization of articular cartilage chondroprogenitor-derived Extracellular Vesicles using cytospin centrifugation. This method proves to be a valuable addition for EV research, providing a simple and robust means of identifying and characterizing them.

ACKNOWLEDGEMENTS

We would like to acknowledge Mr. Abdul Muthallib, and the Centre for Stem Cell Research (A unit of inStem Bengaluru), Christian Medical College, Vellore for infrastructural support. This project was supported by Fluid Research Grant (IRB Min No: 13824), Christian Medical College, Vellore.

STATEMENT OF ETHICS

All techniques observed were, according to the institution's Review Board and Ethics Committee regulations, as per the declaration of Helsinki following the obtainment of informed written consent. This study was reviewed and approved by Institutional Review Board, Christian Medical College, Vellore, IRB Min No: 13824 dated 24.02.2021.

Author Contributions

E.V, G.P, S.M.A were involved in the study conception and design. E.V, G.P, S.M.A, A.L, S.R performed the experiments and were involved in data collection. E.V, G.P, S.M.A, A.L, S.R, S.S were involved in data analysis and interpretation. E.V provided financial support. All authors were involved in preparing the final version of the manuscript.

REFERENCES

GRANGE C, TAPPARO M, BRUNO S, CHATTERJEE D, QUESENBERRY PJ, TETTA C, CAMUSSI G (2014) Biodistribution of mesenchymal stem cell-derived extracellular vesicles in a model of acute kidney injury monitored by optical imaging. Int J Mol Med, 33(5): 1055-1063.

JANKOVIČOVÁ J, SEČOVÁ P, MICHALKOVÁ K, ANTALÍKOVÁ J (2020) Tetraspanins, more than markers of extracellular vesicles in reproduction. Int J Mol Sci, 21(20): 7568.

KOELLING S, KRUEGEL J, IRMER M, PATH JR, SADOWSKI B, MIRO X, MIOSGE N (2009) Migratory chondrogenic progenitor cells from repair tissue during the later stages of human osteoarthritis. Cell Stem Cell, 4(4): 324-335.

KOH CM (2013) Preparation of cells for microscopy using cytospin. Methods Enzymol, 533: 235-240.

LIU Y, MA Y, ZHANG J, YUAN Y, WANG J (2019) Exosomes: a novel therapeutic agent for cartilage and bone tissue regeneration. Dose Response, 17(4): 1559325819892702.

MORALES-KASTRESANA A, TELFORD B, MUSICH TA, MCKINNON K, CLAYBORNE C, BRAIG Z, ROSNER A, DEMBERG T, WATSON DC, KARPOVA TS, FREEMAN GJ, DEKRUYFF RH, PAVLAKIS GN, TERABE M, ROBERT-GUROFF M, BERZOFSKY JA, JONES JC (2017) Labeling extracellular vesicles for nanoscale flow cytometry. Sci Rep, 7(1): 1878.

NI Z, ZHOU S, LI S, KUANG L, CHEN H, LUO X, OUYANG J, HE M, DU X, CHEN L (2020) Exosomes: roles and therapeutic potential in osteoarthritis. Bone Res, 8: 25.

PELÁEZ P, DAMIÁ E, TORRES-TORRILLAS M, CHICHARRO D, CUERVO B, MIGUEL L, DEL ROMERO A, CARRILLO JM, SOPENA JJ, RUBIO M (2021) Cell and cell free therapies in osteoarthritis. Biomedicines; 9(11): 1726.

SALMOND N, KHANNA K, OWEN GR, WILLIAMS KC (2021) Nanoscale flow cytometry for immunophenotyping and quantitating extracellular vesicles in blood plasma. Nanoscale, 13: 2012-2025.

VINOD E, JOHNSON NN, KUMAR S, AMIRTHAM SM, JAMES JV, LIVINGSTON A, REBEKAH G, DANIEL AJ, RAMASAMY B, SATHISHKUMAR S (2021) Migratory chondroprogenitors retain superior intrinsic chondrogenic potential for regenerative cartilage repair as compared to human fibronectin derived chondroprogenitors. Sci Rep, 11(1): 23685.

VINOD E, PARAMESWARAN R, RAMASAMY B, KACHROO U (2020) Pondering the potential of hyaline cartilage–derived chondroprogenitors for tissue regeneration: a systematic review. Cartilage, 13(2 suppl): 34S-52S.

VLASSOV AV, MAGDALENO S, SETTERQUIST R, CONRAD R (2012) Exosomes: current knowledge of their composition, biological functions, and diagnostic and therapeutic potentials. Biochim Biophys Acta, 1820(7): 940-948.

WU Y, LI J, ZENG Y, PU W, MU X, SUN K, PENG Y, SHEN B (2022) Exosomes rewire the cartilage microenvironment in osteoarthritis: from intercellular communication to therapeutic strategies. Int J Oral Sci, 14(1): 40.

ZHANG Y, BI J, HUANG J, TANG Y, DU S, LI P (2020) Exosome: a review of its classification, isolation techniques, storage, diagnostic and targeted therapy applications. Int J Nanomedicine, 15: 6917-6934.

A detailed look in radioanatomical aspects of ligamentum arteriosum calcification in pediatric population

Huseyin Aydemir[1], Erdem Fatihoglu[1], Volkan Kizilgoz[1], Sevket Kahraman[1], Mesut F. Yazar[2], Sonay Aydin[1], Mecit Kantarci[3]

[1] Erzincan Binali Yıldırım University, Faculty of Medicine, Department of Radiology, Erzincan, Turkey

[2] Bilecik Education and Reseach Hospital, Department of Radiology, Bilecik, Turkey

[3] Atatürk University, Faculty of Medicine, Department of Radiology, Erzurum, Turkey

SUMMARY

After birth, ductus arteriosus forms ligamentum arteriosum and sometimes can be calcified. Ligamentum arteriosum calcification can be seen as subtle-punctate or coarse-linear between pulmonary artery and the aorta in the non-contrast computed tomography (CT) images, and between the pulmonary conus and the aortic knob in the chest radiography. In this study, we aim to estimate the prevalence of ligamentum arteriosum calcification on non-contrast CT and chest radiography in a pediatric population. Patients aged 0-18 years, who underwent non- contrast CT and chest radiography at Department of Radiology between March 1, 2020 and October 31, 2021 were evaluated retrospectively. It was examined whether there was ligamentum arteriosum calcification in non-contrast CT and chest radiography. If there is calcification, it was recommended as subtle-punctate or coarse-linear, and information was documented by grouping the patients' age. If ligamentum arteriosum calcification was present, it was divided morphologically into two groups (subtle-punctate and coarse-linear) and classified according to the age groups. The research population consisted of 1003 patients. Non-contrast CT revealed calcification in 25.5% of patients (n=256). 11.3% of patients had subtle-punctate calcification, and 14.3% had coarse-linear calcification. Radiography had a 1.7% (n:17) detection rate for calcification. Ligamentum arteriosum calcification is a common finding in all age groups in the pediatric population. When reporting pediatric CT studies, radiologists should be able to distinguish ligamentum arteriosum calcification from other pathological and anatomical conditions and accept it as a normal finding in order to avoid unnecessary further investigations.

Key words: Ligamentum arteriosum – Non-contrast computed tomography – Chest radiography – Calcification – Pediatric population

INTRODUCTION

The ductus arteriosus is an important structure that connects the pulmonary artery to the aorta

Shared corresponding authors:
Dr. Huseyin Aydemir. Erzincan Binali Yıldırım University, Faculty of Medicine, Department of Radiology, Erzincan, Turkey. Phone: +905443347626. E-mail: aydemir334@hotmail.com - Orcid: 0000-0002-5698-1560

Submitted: November 28, 2023. **Accepted:** February 7, 2024

https://doi.org/10.52083/MNWF9038

and plays a role in the right-to-left shunt of blood passing through the lungs during the fetal period. After birth, the ductus arteriosus closes and forms the ligamentum arteriosum. Sometimes the ligamentum arteriosum can be calcified (Currarino and Jackson Jr, 1970; Murphy, 2005; Ampanozi et al., 2010; Keet et al., 2018). On computed tomography (CT) in adults, the ligamentum arteriosum calcification can be seen subtle-punctate or coarse-linear between the proximal descending aorta and the pulmonary artery superior (Ampanozi et al., 2010). Calcification of the ligamentum arteriosum in adults is considered a benign formation and calcified in the mediastinum is different from other anatomical structures (calcified pulmonary artery seen in patients with long-standing pulmonary hypertension, aortic coarctation, ductus arteriosus aneurysm) and pathological conditions (granulomatous infections and neoplastic diseases such as neuroblastoma, teratoma, treated lymphoma). The distinction is made by the precise anatomical location of the calcification, the absence of associated soft tissue mass, and the absence of other signs of mediastinal or congenital heart disease (including indirect manifestations of patent ductus arteriosus) (Bisceglia and Donaldson, 1991; Ampanozi et al., 2010).

Although ligamentum arteriosum calcification is a well-known phenomenon among experienced pediatric radiologists, there are few publications in the medical literature to date, all of which have different findings. General radiologists may also have a greater obligation to report on routine pediatric imaging given the rising demand for pediatric imaging across the country and the dearth of specialist services for reporting. In order to avoid needless additional testing and incorrect diagnoses, the ability to recognize pathological formation and normal anatomical variation will be essential (Halliday et al., 2016).

The aim of our study is to define the frequency and types of ligamentum arteriosum calcification seen in the pediatric population. Our aims are to facilitate accurate and effective diagnosis for radiologists and to provide information about ligamentum arteriosum calcification to other physicians.

MATERIALS AND METHODS

The local institutional review board approved this study, and as a result of retrospective nature, informed consent was waived (Desicion number: E-21142744-804.99-96230).

At the Radiology Department of Erzincan Binali Yıldırım University, Mengücek Gazi Training and Research Hospital, 1028 patients, ages 0 to 18, who underwent non-contrast thorax CT and posteroanterior chest radiography, were retrospec-

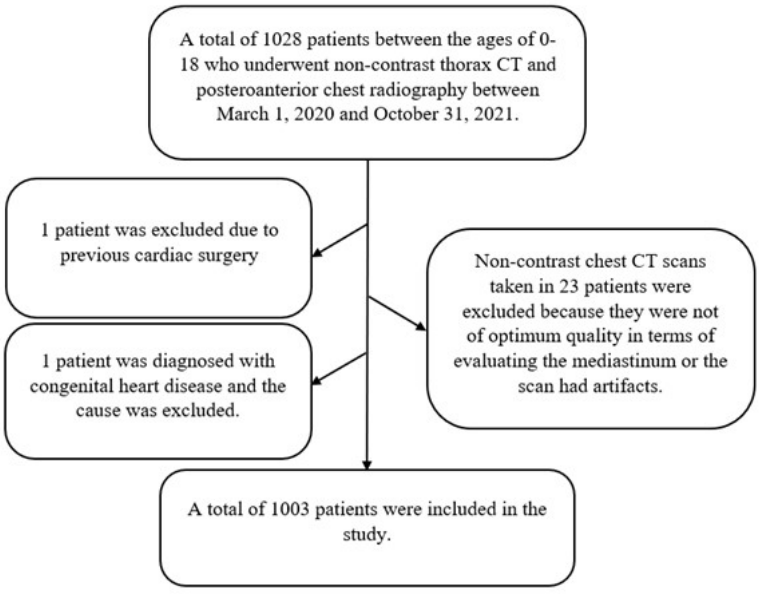

Fig. 1.- Diagram showing study population.

tively scanned between March 1, 2020, and October 31, 2021. Among these patients, one patient was excluded because of cardiac surgery, one patient was diagnosed with congenital heart disease, and 23 patients were excluded because the uncontrasted thorax CT scan was not of optimum quality in terms of evaluating the mediastinum or the examination was artifact. The study involved 1003 patients in total, with 548 males (54.6%) and 455 females (45.4%) (Fig. 1).

With no contrast, a 16-section multi-detector computed tomography machine (Siemens Somatom, Forchheim, Germany) was used to examine all of the study participants. The following technical specifications were used in the CT machine: pitch was 0.8, rotation time was 0.6 seconds, slice thickness was 1.5 mm, tube voltage was 130 kVp, automatic tube current modulation was 70 mAs.

Using the Siemens Somatom Sensation-Syngo. via software program from the PACS (Picture Archiving Communication System) archive, evaluation of images in the axial, coronal, and sagittal planes was performed. To accurately determine the location and presence of ligamentum arteriosum calcification, evaluation was performed using multiplanar reconstruction techniques on non-contrast thorax CT using both standard mediastinal/soft tissue window settings and bone window settings.

The evaluation was carried out by two radiologists with 4 years and 10 years of radiology experience, and the final decision about the presence and the form of calcification of each patient was noted by common consensus. For each patient, the presence and the form of calcification were decided by using all of axial, coronal and sagittal CT images. Presence of calcification was defined as the detection of any calcification between the superior pulmonary artery and the proximal descending aorta. The calcifications were divided into two morphological groups; while linear and amorphous shaped calcifications were called coarse- linear (Fig. 2), other calcifications were called subtle-punctate (Fig. 3).

All the data was classified according to age groups (0-18 years, 18 age groups, one group for each year of age).

In addition, posteroanterior chest radiographs of the cases were also evaluated. Evaluators reviewed chest radiographs and CT images in a double-blind manner. They did not have information about the CT images of the cases whose chest radiographs were evaluated. The presence/absence of calcification was noted by looking at the chest radiographs, and no comment was made about the morphological structure. The presence of calcification on chest radiographies was also decided with consensus.

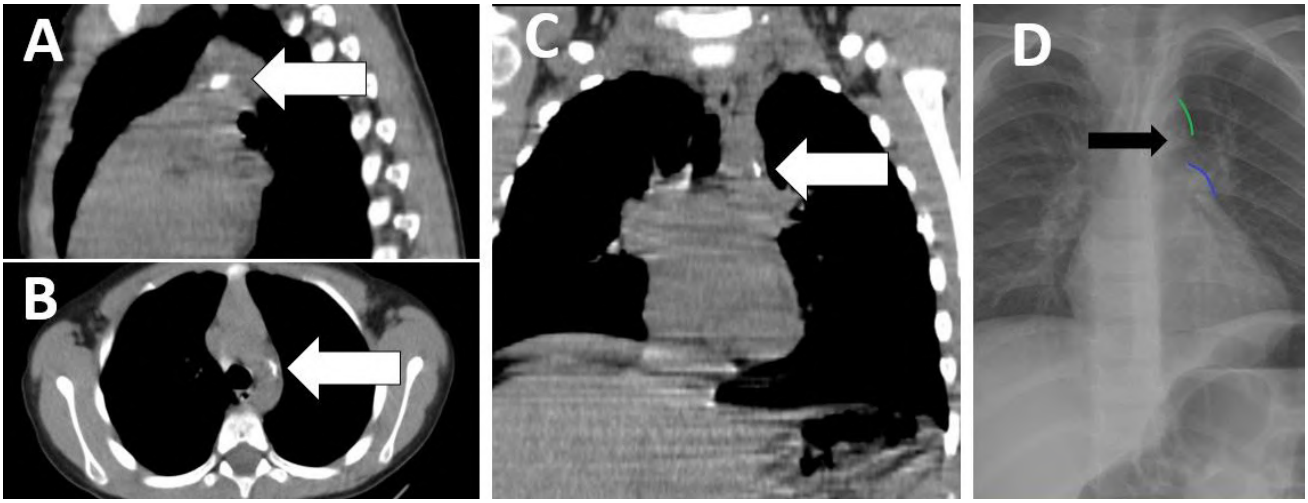

Fig. 2.- Demonstrating coarse-linear calcification of the ligamentum arteriosum on non-contrast thorax CT and chest radiography; In the sagittal (**A**), axial (**B**), and coronal (**C**) sections of the non-contrast thorax CT of a 3-year-and-11-month-old male patient, coarse-linear calcification (white arrows) is visible between the proximal descending aorta and the pulmonary artery. On the radiograph of the same patient (**D**), millimetric opacity (black arrow) is observed at the level of the 5th costochondral junction, between the aortic knob (green line) and pulmonary conus (blue line), and it corresponds to the calcification of the ligamentum arteriosum between the pulmonary artery and the aorta described in the CT images.

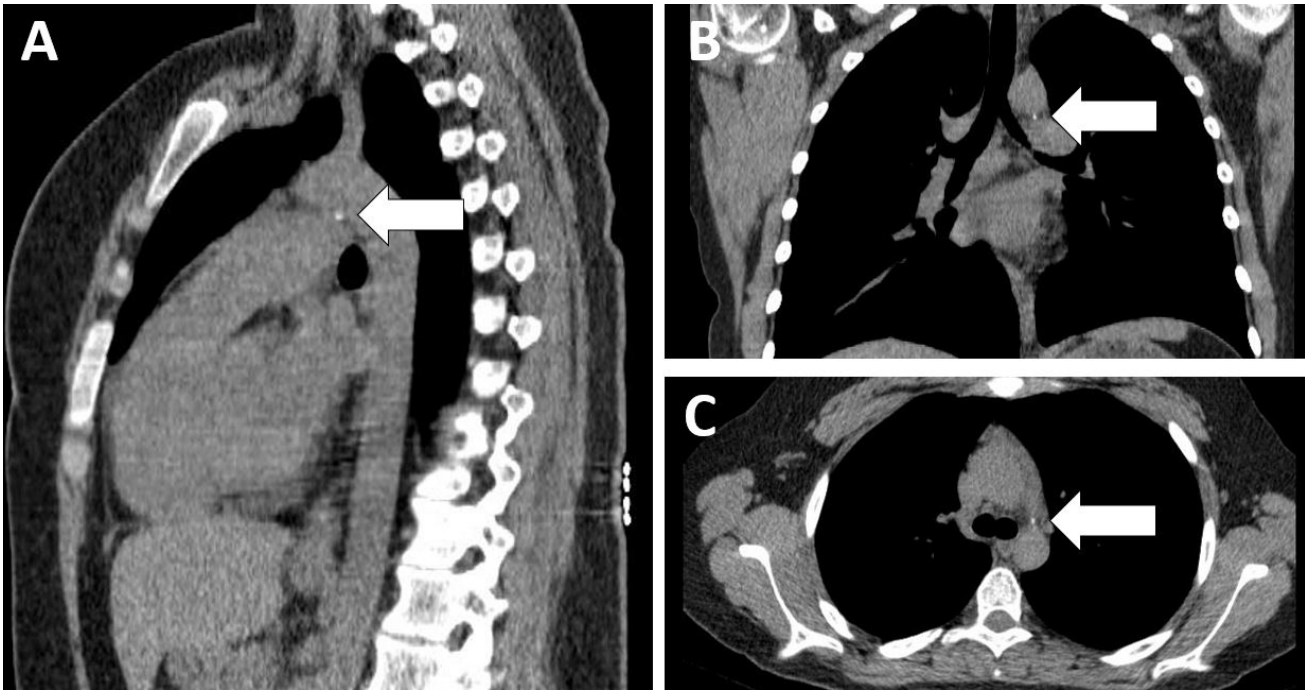

Fig. 3.- Demonstrating subtle-punctate calcification of the ligamentum arteriosum on non-contrast thorax CT; In the sagittal (**A**), coronal (**B**), and axial (**C**) sections of the unenhanced thorax CT of a 14 years and 7 months old female patient, subtle-punctate calcification (white arrows) is visible between the proximal descending aorta and the pulmonary artery.

Final data regarding the presence and morphology of calcification were determined using CT images.

Statistical analysis

Statistical analysis was performed using the IBM SPSS v20.0 (IBM Corp., Armonk, NY, USA) package program. The normal distribution of data was evaluated using the Kolmogorov-Smirnov test. Numerical with non-normal distribution were expressed as the median (min-max). The categorical variables were expressed as numbers and percentages. For comparisons between age groups, Mann-Whitney *U* test was used. Chi-square, Yates correction and Fischer tests were used to compare the rate of presence of calcification. The predictive value of age in terms of calcification presence was determined by Roc Curve analysis and Youden index method; $p < 0.05$ was regarded as statistically significant.

RESULTS

The study population consisted of 1003 patients, 548 males (54.6%) and 455 females (45.4%). The median age of the patients was 135 months (range: 3-215 months). The rate of patients with calcification on CT was 25.5% (n:256). Within these 256 patients, 113 calcifications were classified as subtle-punctate (11.3%, 113/1003); whereas 143 were coarse- linear (14.3%, 143/1003). The rate of calcification detected with chest radiography was 1.7% (17/1003). These results are shown in Table 1.

The presence of calcification did not differ significantly by gender (p=0.479). The median age was lower in those with calcifications than in those without (118 vs 139 months; p=0.013). While ligamentum arteriosum calcification is most commonly seen in the 8-to-9-age range, it was at least detected in the 0-to-1-year age range, however the rates of calcification presence did not show a statistically significant difference according to age groups (p=0.065). These results are shown in Table 2 and Fig. 4.

Calcification was also detected on chest radiography in 6.6% (17/256) of those with calcification detected on CT. In patients without calcification on CT, also no calcification was found on chest radiography. These results are shown in table 2. In those with subtle-punctate calcification on CT, no calcification was found on chest radiography. The cut-off value of age in terms of calcification presence was found to be <139 months with 61.3% sensitivity and 50.9% specificity.

Table 1. Demographic data and presence of calcification.

Variables	Population number (n=1003)
Gender	**n (%)**
Male	548(54.6)
Female	455(45.4)
Age groups (in months)	**n (%)**
0-12	10(1.0)
12-24	50(5.0)
24-36	52(5.2)
36-48	47(4.7)
48-60	37(3.7)
60-72	50(5.0)
72-84	49(4.9)
84-96	49(4.9)
96-108	36(3.6)
108-120	51(5.1)
120-132	61(6.1)
132-144	66(6.6)
144-156	54(5.4)
156-168	57(5.7)
168-180	67(6.7)
180-192	83(8,3)
192-204	101(10.1)
204-216	83(8.3)
Calcification on unenhanced CT	**n (%)**
Not present	747(74.5)
Present	256(25.5)
Subtle-Punctate	113(11.3)
Coarse-Linear	143(14.3)
Calcification on radiography	**n (%)**
Not present	986(98.3)
Present	17(1.7)

CT: Computed tomography, n: Number, %: Percentage

Table 2. Distribution of demographic and clinical departments according to the presence of calcification.

Variables	Calcification		p
	Not present n=747	Present n=256	
Gender			
Male	413(55.3)	135(52.7)	0.479
Female	334(44.7)	121(47.3)	
Age (in months)	**median (min-max)**	**median (min-max)**	
	139(3-215)	118(3-215)	0.013*
Age groups (in months)	**n**	**n**	
0-12	9	1	0.065
12-24	40	10	
24-36	36	16	
36-48	36	11	
48-60	23	14	
60-72	31	19	
72-84	33	16	
84-96	35	14	
96-108	21	15	
108-120	38	13	
120-132	43	18	
132-144	49	17	
144-156	45	9	
156-168	40	17	
168-180	57	10	
180-192	65	18	
192-204	81	20	
204-216	65	18	
Calcification on radiography	**n(%)**		
Not present	747(100.0)	239(93.4)	<0.001*
Present	-	17(6.6)	

n: Number, %: Percentages, min: Minimum, max: Maximum, *: Indicates statistical significance.

DISCUSSION

The main purpose of this study is to determine the frequency and pattern of ligamentum arteriosum calcification in the pediatric population. According to the data of our study, the frequency of ligamentum arteriosum calcification in the pediatric population was 25.5%. The presence of calcification did not differ significantly by gender. The rates of calcification presence did not show a statistically significant difference according to age groups.

Kaushik et al. (2004) suggested that the cambering of the ductus arteriosus, which is known as a normal formation by the pediatric radiologist, is actually a benign and self-limiting ductus arteriosus aneurysm, and that calcification of the ligamentum arteriosum results from the regression of the thrombus within the aneurysm; this was supported by Slovis and Berdon (2004).

The frequency of ligamentum arteriosum calcification of our population is slightly lower than

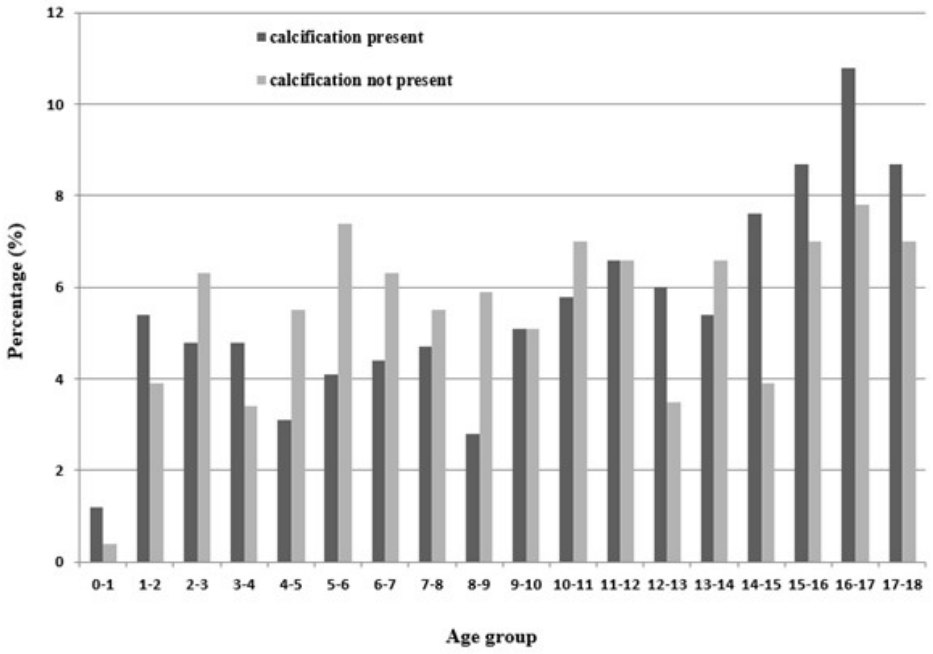

Fig. 4.- Calcification distributions in age groups.

Davendralingam et al. (2021) (Our data: %25.6 vs 30.5%). The possible reason for the mentioned difference can be explained with population characteristics: Davendralingam et al. (2021) studied with postmortem CTs in pediatric population, so that they can easily use thinner sections (0.7 mm sections), where as we used 1.5 mm sections. Thinner sections are especially useful in the detection of subtle-punctate calcifications. In addition, due to the fact that the patient group was in the postmortem period, they eliminated the respiratory and motion artifacts that may occur in CT scans and increased the sensitivity of the study. Similarly with Davendralingam et al. (2021), Proisy et al. (2015) also studied with postmortem pediatric cases, however they found a higher calcification rate (60.9%) in comparison with both the results in Davendralingam et al. (2021) and in ours. This situation can be explained by the population number . Proisy et al. (2015) had the lowest population number. When Davendralingam et al. (2021) and our study are evaluated together, it is seen that the frequency of calcification detection decreases as the population size increases.

In addition to studies conducted with postmortem cases, there are also publications involving living pediatric patients. Bisceglia and Donaldson (1991) found the rate of calcification as 13.2% in their study using 5-10 mm thick CT images, whereas Hong et al. (2012) defined this rate as 37.8% in their study performed with 3-5 mm thick CT images. Our rate falls between the rates in the mentioned publications. The differences between the mentioned publications and our results can basically be explained by population numbers. Our study constitutes the widest-ranging publication in the literature with a population of 1003 participants.

In the study of Davendralingam et al. (2021), the rate of calcification detection in pediatric radiography was 1.6%; in the study of Hong et al. (2012), this rate was 3.6%, and it was 1.7% in our study. Similar to the CT-based studies, these differences also can be attributed to the population numbers. Beluffi et al. (1998) reported a lower rate of 0.1% in their study, although they performed their study with film-screen images. Both our results and the results of the above-mentioned studies were acquired from digital radiographic images. Improvements in radiographic imaging techniques may have contributed to the better detection rate of ligamentum arteriosum calcifications.

In the study of Davendralingam et al. (2021), a higher frequency of ligamentum arteriosum calcification was observed in children younger than 8

years of age compared to those older than 12 years of age. In the study of Hong et al. (2012), ligamentum arteriosum calcification was most frequently observed between 6 and 10 years of age (48.7%), and no significant difference was found in the prevalence of ligamentum arteriosum calcification among pediatric age groups. In the study of Beluffi et al. (1998), an increase in the frequency of ligamentum arteriosum calcification was found in girls aged 4-6 years. In the studies of Proisy et al. (2015) and Bisceglia and Donaldson (1991), age classifications did not differ significantly in terms of the presence of calcification. In the study of Davendralingam et al. (2021), ligamentum arteriosum calcification was not observed in any patient over 12 years of age. However, in this study, patients over the age of 12 constituted a very small portion of the patient population (10/220). The majority of the patient population consisted of patients in the 0-to-1-year age group (118/220). It is supported that the frequency of ligamentum arteriosum calcification is lower in studies conducted in adult patients (Keys and Shapiro, 1943; Wimpfheimer et al., 1996) than in studies conducted in the pediatric population (Bisceglia and Donaldson, 1991; Beluffi et al., 1998; Hong et al., 2012; Proisy et al., 2015). Hong et al. (2012) reported in their study that the frequency of ligamentum arteriosum calcification decreased with increasing age (in people over 30 years old). In our study, the age range in which ligamentum arteriosum calcification was seen at the lowest rate (10%) was the 0-to-1-year age range with the lowest rate of the population (n:10). The calcification rate was highest (15/36; 41.7%) between the ages of 8 and 9; however, in our study, age classifications did not differ significantly in terms of the presence of calcification. The patient population of our study was more homogeneous than the patient population of Davendralingam et al. (2021). It is thought that this homogeneity increases the sensitivity of the incidence of calcification according to age in our study. As a result of the COVID-19 pandemic, more pediatric patients underwent non-contrast thoracic CT scans, and more people participated in our study. To the best of our knowledge, our study had the highest population evaluated for non-contrast thoracic CT scans in the literature (Table 3). Due to this situation, our study may have a higher sensitivity than other studies.

There was no discernible difference in the gender distribution in our study when compared to other studies. However, only in the study of Beluffi et al. (1998), there was a slight female gender predominance.

There were some limitations in our study worth mentioning. One of them is the fact that the rate of patients aged between 0 and 1 years is lower than

Table 3. Previous studies investigating ligamentum arteriosum calcification in the pediatric population.

Study	Study Group	Population	Calcification Frequency	Gender Distribution	Median Age
Bisceglia and Donaldson (1991)	Living infants and children	Unenhanced CT: 53	Unenhanced CT:7 (13.2%)	No significant difference	Unspecified
Beluffi et al. (1998)	Living infants and children	Radiography: 38.476	Radiography:32 (0.1%)	Slight female predominance	Unspecified
Hong et al. (2012)	Living infants and children	Unenhanced CT: 164 Enhanced CT: 336 Radiography: 476	Unenhanced CT: 62 (37.8%) Enhanced CT: 55 (16.3%) Radiography: 17 (3.6%)	No significant difference	6.8 years
Proisy et al. (2015)	Post mortem infants and children	Unenhanced CT: 69	Unenhanced CT: 42 (60.9%)	No significant difference	9.7 month
Davendralingam et al. (2021)	Post mortem infants and children	Unenhanced CT: 220 Radiography: 182	Unenhanced CT: 67 (30.5%) Radiography: 3 (1.6%)	No significant difference	2.3 years

CT: Computed tomography, %: Percentage

the other age groups. The possible reason is that it is difficult to obtain optimal quality of radiological examinations, especially CT, in 0-to-1-year age group due to the lack of patient orientation, and to protect these patients in infancy from radiation exposure. In our study, 1.5 mm sections were routinely used in CT scans in children, and the sensitivity of the detection of subtle-punctate calcifications decreased due to the current section thickness. Examination of thinner sections may increase the sensitivity of the detection of subtle-punctate calcifications. Due to the prevalence of pediatric patients and the fact that patient orientation declines with age, optimization of the examination also decreases. One of the limitations of our study is that the study was carried out on live patient groups, which may cause respiratory and movement artifacts.

In conclusion, ligamentum arteriosum calcification is a common finding in all age groups in the pediatric population. Non-contrast thorax CT can detect it better than chest radiography. It is most commonly observed as coarse-linear type calcification, and if calcification is present, it can be easily detected on CT. Radiologists should be able to differentiate ligamentum arteriosum calcification found in the pediatric population from other pathological and anatomical conditions when reporting pediatric CT studies in order to avoid needless additional investigations.

STATEMENTS AND DECLARATIONS

This study has been approved by the institutional ethics committee (Ethics Commitee of Clinical Researches of Erzincan Binali Yıldırım University, Protocol number: E-21142744-804.99-96230, Date: 26.07.2021). The authors of this study received no financial support for this research and publication of the article.

The datasets generated and/or analyzed during the current study are not publicly available due to the risk of breach of patient data privacy but are available from the corresponding author (without patients private data) upon reasonable request.

REFERENCES

AMPANOZI G, RUDER TD, HATCH GM, BOLLIGER S, THALI MJ (2010) Incidental findings in post- mortem CT: Calcified ligamentum arteriosum. *Legal Med*, 12: 313-315.

BELUFFI G, ROTOLI P, CALO L, TINELLI C, FIORI P (1998) Botallo's duct calcification in children: radiologic findings. *La Radiologia Medica*, 96: 204-208.

BISCEGLIA M, DONALDSON JS (1991) Calcification of the ligamentum arteriosum in children: a normal finding on CT. *Am J Roentgenol*, 156: 351-352.

CURRARINO G, JACKSON JR JH (1970) Calcification of the ductus arteriosus and ligamentum Botalli. *Radiology*, 94: 139-142.

DAVENDRALINGAM N, SHELMERDINE SC, HUTCHINSON JC, CHOPRA M, BARRETT H, AGAHI A, HALLIDAY K, DRINKWATER K, HOWLETT D, PALM L, ARTHURS OJ (2021) Ligamentum arteriosum calcification on paediatric postmortem computed tomography. *Pediatr Radiol*, 51(3): 385-391.

HALLIDAY K, DRINKWATER K, HOWLETT DC (2016) Evaluation of paediatric radiology services in hospitals in the UK. *Clin Radiol*, 71:1263-1267.

HONG G-S, GOO HW, SONG J-W (2012) Prevalence of ligamentum arteriosum calcification on multi-section spiral CT and digital radiography. *Int J Cardiovasc Imaging*, 28: 61-67.

KAUSHIK N, COHEN RA, HELTON JG (2004) 3-D CT angiographic demonstration of a neonatal ductus arteriosus aneurysm with development of ductal calcification: are the "ductus bump", ductus arteriosus aneurysm, and ductal calcification related? *Pediatr Radiol*, 34: 738-741.

KEET K, GUNSTON G, ALEXANDER R (2018) Variation in the anatomy of the ligamentum arteriosum in a South African sample. *Eur J Anat*, 22: 119-125.

KEYS A, SHAPIRO MJ (1943) Patency of the ductus arteriosus in adults. *Am Heart J*, 25: 158-186.

MURPHY PJ (2005) The fetal circulation. Continuing Education in Anaesthesia, Critical Care & Pain, 5: 107-112.

PROISY M, LOGET P, BOUVET R, ROUSSEY M, PELÉ F, ROZEL C, TREGUIER C, DARNAULT P, BRUNEAU B (2015) Non-specific post-mortem modifications on whole-body post-mortem computed tomography in sudden unexpected death in infancy. *J Forensic Radiol Imaging*, 3: 16-23.

SLOVIS TL, BERDON WE (2004) A new explanation for an old finding: the ductus bump. *Pediatr Radiol*, 34(9): 737.

WIMPFHEIMER O, HARAMATI LB, HARAMATI N (1996) Calcification of the ligamentum arteriosum in adults: CT features. *J Comput Assist Tomogr*, 20(1): 34-37.

Clinical reflection of anatomical evaluation in coccydynia

Emel Guler[1], Ilkay Guler[2], Ayla Arslan[3], Gökçe Bagci Uzun[4]

[1] *Sivas Cumhuriyet University Faculty of Medicine, Department of Physical Medicine and Rehabilitation, Algology, Sivas, Turkey*
[2] *General Surgery, Republic of Türkiye, Ministry of Health, General Directorate of Public Hospitals, Ankara, Turkey*
[3] *Ağrı İbrahim Çeçen University Faculty of Medicine, Department of Anatomy, 04200, Ağrı, Turkey*
[4] *Malatya Turgut Özal University, Faculty of Medicine, Department of Anatomy, Malatya, Turkey*

SUMMARY

Coccydynia is a pain in the coccyx and the surrounding anatomical structures. Our aim in the study was to evaluate whether the disease duration, pain assessment, and coccyx morphological type had an effect on this clinic in patients with a diagnosis of coccydynia. A total of 68 coccyx Magnetic Resonance Imaging (MRI) results were evaluated. Coccyx segment number, morphological typing, lumbosacral, sacrococcygeal, and intercoccygeal angle measurements were made. Disease duration, day and night movement and the rest of Numerical Pain Scale (NRS) values were recorded from existing records of patients with a diagnosis of coccydynia. When the morphological typing was evaluated, type 4 subluxation was found to be high in the group with coccydynia. Pain complaint duration was 13.94 ± 12.22 months, sitting time was 16.82 ± 14.22 minutes, and the numerical pain scale was 7.62 ± 1.48. Morphologically, type 1;14 (3 coccydynia), type 2;22 (9 coccydynia), type 3;14 (6 coccydynia), type 4;18 (16 coccydynia) images were also detected. A moderately statistically significant positive correlation was found between the sacrococcygeal and intercoccygeal angles ($p<0.05$). We believe that evaluating clinical data and anatomical measurements together will contribute to the treatment of coccydynia, which is especially difficult to treat.

Key words: Coccydynia – Sacrum – Pain – MRI

ABBREVIATIONS

MRI: Magnetic Resonance Imaging

NRS: Numerical Pain Scale

INTRODUCTION

Coccydynia is also known as coccygodynia or coccygeal neuralgia (Malik et al., 2014). Coccydynia was first defined by Simpson in 1859 as pain in the coccyx and surrounding anatomical structures (Lirette et al., 2014; Mabrouk et al., 2023). The coccyx consists of the union of the last 3-5 vertebrae that are not well developed. Its posterior surface is slightly convex, while its anterior surface is slightly concave (Nelson, 1991). There is a synarthrosis joint between the coccyx seg-

Shared corresponding authors:
Assist Prof. Dr. Emel Guler. Sivas Cumhuriyet University Faculty of Medicine, Department of Physical Medicine and Rehabilitation. Algology, Sivas, Turkey. Phone: +90 535 6492951; Fax: +90 346 487 00 00. E-mail: dremelguler@gmail.com - Orcid: 0000-0002-5049-8770

Submitted: January 5, 2024. **Accepted:** February 9, 2024

https://doi.org/10.52083/BKHP8714

ments. The sacrococcygeal and intercoccygeal joints forms are surrounded by ligaments (Andrés and Chaves, 2003). The coccyx has very important functions by carrying the weight of a person in a sitting position, helping voluntary bowel control, and supporting the anus positionally due to its anatomical neighbourhoods (Lirette et al., 2014). Although factors such as trauma, malignancy, and difficult delivery are listed in the etiology of coccydynia, one third of the cases are idiopathic. In patients with idiopathic etiology, there are radiology studies showing that pain is caused by anatomical changes in the coccyx and adjacent ligament structures (Maigne et al., 2006; Woon et al., 2013). Although coccydynia most commonly affects middle-aged women, it may be found in both sexes and in all age groups (White et al., 2022). In coccydynia, patients complain of pain, especially when sitting on hard places.

Internal and external trauma are significant etiological factors in the formation of coccydynia. While internal trauma occurs in difficult birth, external trauma is trauma caused by coccyx dislocation, coccyx fracture and supine fall. Anatomical knowledge of coccydynia is essential and its combination with radiological evaluation has a very important place in patients receiving appropriate treatment.

The goal of this work was to investigate the number of coccyx segments, morphological typing, lumbosacral, sacrococcygeal and intercoccygeal angle measurements and morphometric features, duration of complaints and pain in coccydynia.

MATERIALS AND METHODS

In our study, the images of patients who consulted to School of Medicine Physical Therapy and Rehabilitation clinic among 01/01/2021 and 31/12/2021 and were determined with coccydynia and healthy volunteers who were not diagnosed with coccydynia but had pelvic MRI images between the same dates were included. Consent was obtained with the consent forms prepared from the accessible patient and control groups.

In our study, a total of 68 coccyx Magnetic Resonance Imaging (MRI) results, 19 of women and 49 of men, were evaluated. Of these 68 coccyx MRIs, 34 were from patients with a diagnosis of coccydynia, and 34 were from healthy volunteers. In our retrospective study, the number of coccyx segments, morphological typing, lumbosacral, sacrococcygeal and intercoccygeal angle measurements were made in the current coccyx MRI. Disease duration was recorded from the existing records of patients with a diagnosis of coccydynia.

Inclusion criteria for the study: to be diagnosed with coccydynia, to have a history of trauma to the coccyx region, to be between the ages of 18-70, to accept the evaluation of their current images in the study

Exclusion criteria are: those under the age of 18 or over the age of 70, those with pilonidal sinus, those who underwent local surgery, and those who did not accept the evaluation of their current images.

Evaluation scales to be used during patient records:

Numerical pain scale (NRS): It is used to measure pain intensity and monitor pain. It provides a measurement from 0 to 10 (0 = no pain, 10 = most severe pain). The measurement was made by asking the patients to mark the number corresponding to their pain intensity.

Radiological evaluation: During the evaluation of coccyx bone anatomy, the classification created by Postacchini and Massobrio was used for segment number morphological typing. This grading showed that the morphology and morphometry of the coccyx can play a role in the formation of coccydynia. For instance,, the risk of developing coccygeal pain is higher in people who have a distinctly arcuate and forward-facing, sharply angled anterior coccyx or spicule and a posteriorly directed coccyx, scoliotic deformity or subluxation of the intercoccygeal or sacrococcygeal joints (Maigne et al., 2000; Nathan et al., 2010).

Classifications were made as follows:

- Type I: The coccyx is slightly arcuate anteriorly and the apex is directed downward.
- Type II: Increased coccyx tilt angle and apex forward.
- Type III: The coccyx is sharply angled.
- Type IV: It is in the form of subluxation at the

sacrococcygeal and first intercoccygeal joints (Nathan et al., 2010; Postacchini and Massobrio 1983).

In addition, lumbosacral, sacrococcygeal, and intercoccygeal angles were measured. In our study, three angle measurements were made (Figs. 1, 2):

1- Lumbosacral angle: The angle between the line passing entirely the middle of the 5th lumbar vertebra and the lines passing through the middle of the first sacral vertebra was calculated by measuring (Okpala, 2014).

2- Sacrococcygeal angle: The angle between the line passing entirely through the middle of the 1st coccygeal vertebra and the lines passing through the middle of the first sacral vertebra was calculated by measuring.

3- Intercoccygeal angle: The angle between the line passing entirely through the middle of the first coccygeal vertebra and the line passing through the middle of the other coccygeal vertebrae was calculated by measuring (Woon et al., 2013).

Ethics Committee Approval

This work was implemented with the approval School of Medicine Non-Invasive Clinical Research Ethics Committee dated 16.02.2022 and verdict number 2022-02/44. Informed assent forms were received from the control groups and patients included in the study.

Statistical analysis

The analysis of the data in the research was done with the SPSS (Statistical Program in Social Sciences) 25 program. Descriptive statistics were calculated as mean, number, median, percentage, min-max, and standard deviation. The Mann-Whitney U test was used for data that did not fit the normal distribution, and the t-test was used for the comparisons of the two groups in the data that fit the normal distribution. Kruskal Wallis analysis was used in multiple groups that did not show normal distribution. In the comparison of categorical data, the chi-square test was applied by composing cross tables. The significance value (p) was taken as 0.05. In the analysis of the relations between the variables, the Spearman rank correlation coefficient was used because normal distribution could not be achieved.

RESULTS

A statistically substantial dissimilarity was observed among coccydynia and healthy groups according to age and gender in the participants included in the study ($p<0.05$). The mean age was 36.62 ± 12.84 years in the coccydynia patient

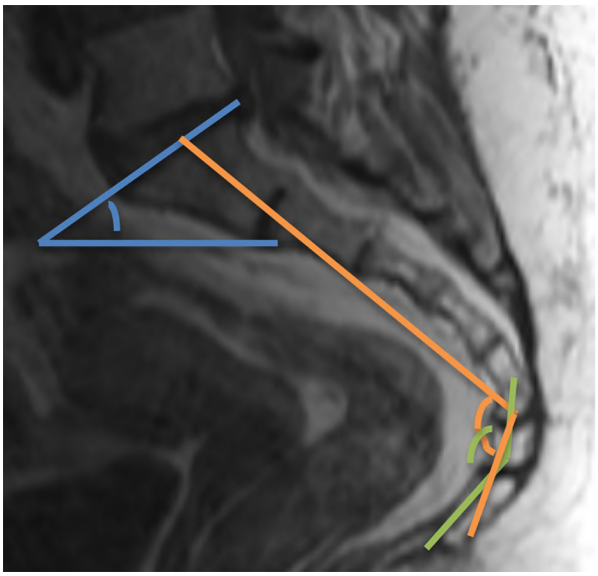

Fig. 1.- Angle measurement methods. Green line: Intercoccygeal angle. Blue line: Lumbosacral angle. Orange line: Sacrococcygeal angle.

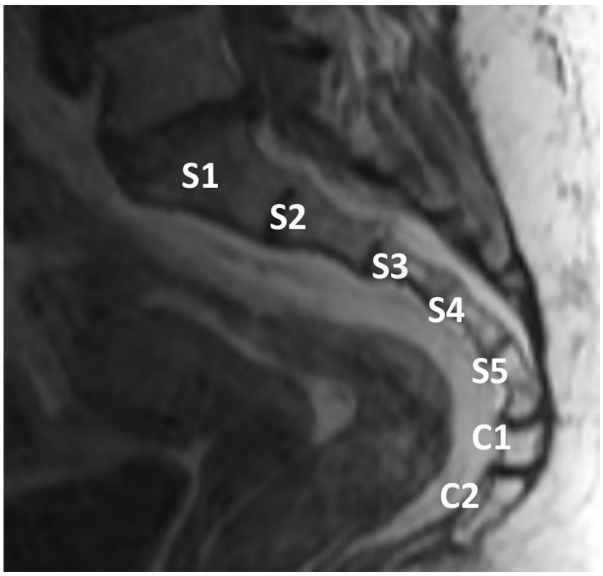

Fig. 2.- Sacrum and coccyx bone anatomy. S: Sacrum, C: Coccyx.

group and 44.35 ± 14.04 years in the healthy control group (Table 1). The duration of pain complaint was 13.94 ± 12.22 months, the sitting time was 16.82 ± 14.22 minutes, and the Numerical Pain Scale (NRS) was 7.62 ± 1.48 (Table 2). A statistically substantial difference was found among coccydynia and healthy groups according to morphological types (type I, type II, type III, and type IV) (p=0.001<0.05). Morphologically, type I;14 (3 coccydynia), type II;22 (9 coccydynia), type III;14 (6 coccydynia), type IV;18 (16 coccydynia) images were also detected (Table 3). When the morphological typing was evaluated, type IV with subluxation (partial dislocation) was found to be high in the coccydynia group. There was no statistically substantial dissimilarity among coccydynia and healthy groups according to the number of segments in the participants included in the study (p> 0.05). The number of segments was found to be 1 in 1 image, 2 in 16 images, 3 in 34 images, 4 in 16 images, and 5 in 16 images (Table 4). A statistically substantial dissimilarity was found among the groups (coccydynia and healthy) according to the measurement of sacrococcygeal angle (p=0.001<0.05, Table 5). A statistically substantial dissimilarity was found among the coccydynia and healthy groups according to the measurement of intercoccygeal angle (p=0.020<0.05, Table 5). In the coccydynia group, no statistically meaningful difference was found according to the morphological types (type I, type II, type III, and type IV) in point of duration of complaint, sitting time, and NRS variables (p>0.05, Table 4). A statistically important relationship was found between age and the number of segments in the negative direction (r =-0.365) and statistically meaningful

Table 1. Comparison of morphological types between groups.

Variable	Group	Value	coccydynia	healthy	Total	χ^2 Value	p Value
morphological type	Type I	n	3	11	14	0,492	0,001*
		%	8,8%	32,4%	20,6%		
	Type II	n	9	13	22		
		%	26,5%	38,2%	32,4%		
	Type III	n	6	8	14		
		%	17,6%	23,5%	20,6%		
	Type IV	n	16	2	18		
		%	47,1%	5,9%	26,5%		

n; number of samples, %; percent, p; Chi-square Test value (χ^2), *p<0.05; There is a statistically significant difference between the groups.

Table 2. Comparison of coccyx segment numbers between groups.

Variable	number	n %	group		Total	χ^2 Value	p Value
			coccydynia	healthy			
segment_number	1	n	1	0	1	4,152	0,386
		%	2,9%	0,0%	1,5%		
	2	n	9	7	16		
		%	26,5%	20,6%	23,5%		
	3	n	18	16	34		
		%	52,9%	47,1%	50,0%		
	4	n	6	10	16		
		%	17,6%	29,4%	23,5%		
	5	n	0	1	1		
		%	0,0%	2,9%	1,5%		
Total		**n**	**34**	**34**	**68**		
		100,0%	**100,0%**	**100,0%**	**100,00%**		

n; number of samples, %; percent, p; Chi-square Test value (χ^2),

Table 3. Comparison of number of segments and angles between groups.

Variable	Groups	Mean ± ss	Test	p Value
segment number	**coccydynia**	2,85 ± 0,74	-1,591	0,121
	healthy	3,15 ± 0,78		
lumbosacral angle	**coccydynia**	40,19 ± 10,64	0,303	0,772
	healthy	39,47 ± 9,46		
sacrococcygeal angle	**coccydynia**	96,82 ± 14,36	***-4,941***	***0,001****
	healthy	113,39 ± 13,26		
intercoccygeal angle	**coccydynia**	130,7 ± 26,63	***-2,472***	***0,020****
	healthy	143,71 ± 15,25		

Cover; mean, ss; standard deviation, Min; lowest score, max; highest score, test value; t Test Value, p value; statistical significance, *p<0.05; There is a statistically significant difference between the groups.

Table 4. Comparisons by morphological types for complaints, residence times and NRS in the coccydynia group.

Variable	Groups	M (Min - Max)	Test	p Value
complaint period	Type I	24(2-24)	0,758	0,859
	Type II	12(1-36)		
	Type III	15(1-48)		
	Type IV	10(1-36)		
sitting time	Type I	15(10-30)	3,528	0,317
	Type II	15(1-30)		
	Type III	22,5(10-60)		
	Type IV	10(3-60)		
NRS	Type I	6(6-8)	4,468	0,215
	Type II	7(6-10)		
	Type III	7(6-9)		
	Type IV	8(5-10)		

Cover; mean, ss; standard deviation, M; Median, Min; lowest score, max; highest score, test value; Kruskal Wallis Test Value, p value; statistical significance.

Table 5. Correlation analysis of the relationships between the variables in the coccydynia group.

Variable		complaint period	sitting time	NRS	segment number	lumbosacral angle	sacrococcygeal angle	intercoccygeal angle
age	r	0,293	-0,060	-0,026	***-0,365***	0,261	0,300	0,241
	p	0,093	0,738	0,886	***0,034****	0,136	0,085	0,170
complaint period	r		0,050	0,010	0,069	0,234	0,145	0,154
	p		0,780	0,953	0,698	0,182	0,414	0,386
sitting time	r			***-0,624***	-0,226	-0,088	0,160	***0,338***
	p			***0,001****	0,199	0,620	0,365	***0,049****
NRS	r				0,251	0,056	***-0,471***	-0,422
	p				0,153	0,752	***0,005****	0,013
segment number	r					0,016	-0,329	***-0,420***
	p					0,929	0,058	***0,013****
lumbosacral angle	r						-0,268	-0,002
	p						0,126	0,990
sacrococcygeal angle	r							***0,349***
	p							***0,043****

r; spearman rank correlation coefficient, p value; statistical significance, *p<0.05; There is a statistically significant relationship between the variables.

($p<0.05$). There was a moderate ($r=-0.624$) statistically significant negative correlation between sitting time and NRS ($p<0.05$, Table 5). A positive moderate ($r = 0.338$) significant correlation was found between sitting time and intercoccygeal angle ($p<0.05$, Table 5). A moderate ($r =-0.471$) statistically important negative connection was found between NRS and sacrococcygeal angle ($p<0.05$, Table 5). A moderate ($r =-0.420$) statistically important negative relationship was found between the number of segments and the intercoccygeal angle ($p<=0.05$, Table 5). A moderate ($r = 0.349$) statistically substantial positive relationship was observed between the sacrococcygeal angle and the intercoccygeal angle ($p<=0.05$, Table 5).

DISCUSSION

The anatomy of the coccyx, its neighbourhood with the surrounding anatomical structures, and the angle it makes with them are important for coccydynia. It has been reported that the coccyx has a highly variant structure, considering its morphology, inclusive of the number and segments of the coccygeal vertebrae (White and Folkens, 2005). Karayol et al. (2019) before this compared coccyx types as a morphological feature only in terms of the number of coccygeal vertebrae and determined a significant dissimilarity among the types. Guneri and Gungor (2021), according to the morphological shapes of the coccyx in their study, found type 1 and type 2 at the highest rate. In another study, type 2 was higher according to the Postacchini classification. In addition, pain intensity generally increased with higher angulation (Dalbayrak et al., 2014). Shams et al. (2023) found the most common coccygeal segment number to be 3 in both groups. Also, Shams et al. (2023) the most common coccygeal type in the coccydynia group was type 2. The most common in the control group was type 2, followed by type 3 and type 1. They found no statistically meaningful difference between the 2 groups in terms of intercoccygeal joint fusions. In our study, however, we found the highest number of segments to be 3 in the coccygodynia and healthy group. We found the highest morphological type to be type 4 in the coccydynia group, and the highest type 2 in the healthy group. Intercoccygeal joint subluxation was more common in the coccydynia groups than in the control group.

There are many studies in the literature evaluating changes in sacral, sacrococcygeal, and intercoccygeal angles, which are thought to cause disease in patients presenting with the diagnosis of coccydynia. Woon et al. (2013) found the sacral angle to be remarkably lower in coccydynia patients of both sexes compared to the control group, and they found the coccygeal curvature to be significantly lower in female patients with coccydynia. In addition, they did not find a remarkably significant dissimilarity in terms of sacrococcygeal curvature index in both genders in patients with coccydynia (Woon et al., 2013). Gupta et al. (2018) evaluated MRI to compare sacrococcygeal and intercoccygeal angles in their study, which included 10 volunteers with coccydynia and 106 volunteers in the control group. No statistically important difference was determined among the groups in sacrococcygeal and intercoccygeal angles. They observed that the intercoccygeal angle decreases with age. In another study, they found both intercoccygeal and sacral-angle coccydynia to be lower in the group than in the control group. There was no differentiation among the groups in the sacrococcygeal angle (Shams et al., 2023). Woon et al. (2013) found that the sacrococcygeal angle was not remarkably different between the coccydynia and control groups. In our study, we detected a statistically meaningful difference between the groups (coccydynia and healthy) according to the measurement of intercoccygeal angle and sacrococcygeal angle.

Ozkal et al. (2020) found a significant difference between the intercoccygeal angle and the sacrococcygeal angle and the number of segments in their study. They stated that 57 of the patients participating in the study had 3 segments and 98 had 4 segments, and type 1 was the most common morphological type.

Pain in coccydynia is the main symptom affecting the sitting time of patients. In the study conducted by Gonnade et al. (2017). The NRS worths were recorded after and before interventional treatment in 31 patients with coccydynia complaints, and they found the mean score before treatment was 7.90 ± 0.16. Similarly, in our study,

we found the NRS score to be 7.62 ± 1.48 (Gonnade et al., 2017). There are studies on the static and dynamic measurements of joint angles and the angles they make with neighbouring joints. However, there is no study in which patients' complaint duration and pain were evaluated together with all these parameters (Maigne et al., 2000). In addition, in our study, we found that the prolongation of sitting time was proportional to the decrease in NRS and that the increase in the intercoccygeal angle was correlated with the increase in the sitting time. Again, we found that the sacrococcygeal angle decreased with the increase in NRS value. We found that as the number of segments increases, the intercoccygeal angle decreases, and as the sacrococcygeal angle increases, the intercoccygeal angle increases. In the literature review, we did not find any study on this subject in which the number of segments, sitting time, pain scale, and angles were evaluated together.

CONCLUSION

Morphological typing of the coccyx has also gained more importance in terms of dynamic imaging studies, patient follow-up, and evaluation of the efficacy of treatment methods. There are few studies in the literature in which patients' pain, trauma history, and radiological images are evaluated. As a result, we believe that the evaluation of clinical data and anatomical measurements together will contribute to the treatment of the disease, especially in coccydynia, which is difficult to treat.

Study limitations

Our present study has some limitations: 1) This is not a sequential series of coccydynia patients. Because MR treatment was difficult and was done in serious cases. 2) The number of our patients is low due to the patients who do not want to have an MRI. Since it is difficult to find coccydynia patients, we do not have many patients.

Authors' contributions

Study concept and design: E.G. and I.G. Acquisition of data: E.G. Analysis and interpretation of data: E.G., I.G., A.A. and G.B.U. Drafting of the manuscript: E.G., I.G., A.A. and G.B.U. Critical revision of the manuscript for important intellectual content: E.G., I.G., A.A. and G.B.U Statistical analysis: E.G., I.G., A.A. and G.B.U. Administrative, technical, and material support: E.G., I.G., A.A. and G.B.U Study supervision: E.G.

Ethical approval

This work was implemented with the approval of Non-Invasive Clinical Research Ethics Committee dated 16.02.2022 and verdict number 2022-02/44.

REFERENCES

ANDRÉS JD, CHAVES S (2003) Coccygodynia: a proposal for an algorithm for treatment. *J Pain*, 4(5): 257-266.

DALBAYRAK S, YAMAN O, YILMAZ T, YILMAZ M (2014) Treatment principles for coccygodynia. *Turkish Neurosurg*, 24(4): 532-537.

GUNERI B, GUNGOR G (2021) Morphological features of the coccyx in the Turkish population and ınterrelationships among the parameters: a computerized tomography-based analysis. *Cureus*, 13(11): e19687.

GUPTA V, AGARWAL N, BARUAH BP (2018) Magnetic resonance measurements of sacrococcygeal and intercoccygeal angles in normal participants and those with idiopathic coccydynia. *Indian J Orthop*, 52: 353-357.

KARAYOL SS, KARAYOL KC, DOKUMACI DS (2019) Anatomic and morphometric evaluation of the coccyx in the adult population. *Harran Üniversitesi Tıp Fakültesi Dergisi*, 16(2): 221-226.

LIRETTE LS, CHAIBAN G, TOLBA R, EISSA H (2014) Coccydynia: an overview of the anatomy, etiology, and treatment of coccyx pain. *Ochsner J*, 14(1): 84-87.

MABROUK A, ALLOUSH A, FOYE P (2023) Coccyx Pain. In: StatPearls. Treasure Island (FL): StatPearls Publishing. http://www.ncbi.nlm.nih.gov/books/NBK563139/

MAIGNE JY, DOURSOUNIAN L, CHATELLIER G (2000) Causes and mechanisms of common coccydynia: role of body mass index and coccygeal trauma. *Spine*, 25(23): 3072-3079.

MAIGNE JY, CHATELLIER G, LE FAOU M, ARCHAMBEAU M (2006) The treatment of chronic coccydynia with intrarectal manipulation: a randomized controlled study. *Spine*, 31(18): E621-627.

MALIK SH, AHMAD K, ALI L (2023) Ganglion ımpar block for chronic coccydynia. *J Ayub Med Coll Abbottabad: JAMC*, 35(1): 123-126.

NATHAN ST, FISHER BE, ROBERTS CS (2010) Coccydynia: a review of pathoanatomy, aetiology, treatment and outcome. *J Bone Joint Surg British*, 92(12): 1622-1627.

NELSON DA (1991) Coccydynia and lumbar disk disease—historical correlations and clinical cautions. *Perspect Biol Med*, 34(2): 229-238.

OKPALA F (2014) Measurement of lumbosacral angle in normal radiographs: a retrospective study in Southeast Nigeria. *Ann Med Health Sci Res*, 4(5): 757-762.

OZKAL B, AVNIOGLU S, CANDAN B (2020) Morphometric evaluation of coccyx in patients with coccydynia and classification. *Acta Medica Alanya*, 4(1): 61-67.

POSTACCHINI F, MASSOBRIO M (1983) Idiopathic coccygodynia. Analysis of fifty-one operative cases and a radiographic study of the normal coccyx. *J Bone Joint Surg Am*, 65(8): 1116-1124.

RAJAGOPAL R, SHARMA PK (2017) Ganglion impar block in patients with chronic coccydynia. *Indian J Radiol Imaging*, 27(03): 324-328.

SHAMS A, GAMAL O, MESREGAH MK (2023) Sacrococcygeal morphologic and morphometric risk factors for idiopathic coccydynia: a magnetic resonance imaging study. Global Spine J, 13(1): 140-148.

WHITE WD, AVERY M, JONELY H, MANSFIELD JT, SAYAL PK, DESAI MJ (2022) The interdisciplinary management of coccydynia: A narrative review. *PM & R*, 14(9): 1143-1154.

WHITE T, FOLKENS P (2005) Pelvic girdle: sacrum, coccyx, & os coxae. In: *The Human Bone Manual*, Chapter 14. Elsevier, pp 241-253.

WOON JT, MAIGNE JY, PERUMAL V, STRINGER MD (2013) Magnetic resonance imaging morphology and morphometry of the coccyx in coccydynia. *Spine*, 38(23): E1437-1445.

Effects of endurance resistance exercise on knee joint cartilages in young male rats – a randomized controlled trial

Kiran Yameen[1], Kevin J.J. Borges[2], Sumaira I. Farooqui[1], Jaza Rizvi[1], Amna A Khan[1], Syed N.N. Shah[2]

[1] Ziauddin College of Rehabilitation Sciences, Ziauddin University, Karachi, Pakistan

[2] Ziauddin Medical College, Karachi, Pakistan

SUMMARY

To study the effects of endurance resistance exercise on the cellularity of knee joint hyaline cartilages and fibrocartilage in young male rats, twelve healthy young male Sprague Dawley rats were equally divided into Endurance resistance training (ERT) and Sedentary or Control (C). ERT group climbed a ladder carrying 5% of body weight with 3 sets for adaptation. From week 2, 10% and 3 sets then progressed to 20% and 4 sets, 30% and 5 sets, and 40% of the body weight and 6 sets every week till week 5 with 12-15 repetitions per set and 2-minute intervals and 5 days per week. Each training session's duration was 30 minutes. The effects on the number of chondrocytes per lacuna of fibrocartilage and tibial hyaline cartilage were found to be significantly better in ERT group. For the number of chondrocytes per lacuna of femoral hyaline cartilage, no significant difference was observed between the group analyses. These results collectively imply that endurance resistance training has potential for enhancing cartilage integrity and general health, specifically the fibrocartilage and tibial hyaline cartilage.

Key words: Endurance – Resistance – Exercise – Hyaline cartilage – Fibrocartilage

INTRODUCTION

Cartilage is a pliable, smooth, elastic tissue that is firm and less flexible than soft tissues like muscle, ligament, and tendon, but not as stiff and solid as bone (Zhang et al., 2018). Hyaline (e.g., articular cartilage), elastic (e.g., ear cartilage), and fibrous (e.g., intervertebral disc) cartilage are the types present in the human body (Lin and Klein, 2021). Hyaline cartilage, or articular cartilage (AC), is a highly specialized connective tissue that lines the articular surfaces of bones (Branly et al., 2017). AC lacks vascularity, lymphatics and nerve supply (Nie et al., 2020). AC enables bones to move over one another, reduces friction and protects from damage in lubricated joint movements (Costa et al., 2018). The fibrocartilage plates in the knee joint are known as the menisci. These circular wedge-shaped cartilages are located in pairs between the tibial plateaus and the femoral condyles, laterally and medially, respectively (Murphy et al., 2019). Due to meniscal

Shared corresponding authors:
Sumaira Imran Farooqui. Ziauddin College of Rehabilitation Sciences, Ziauddin University, Karachi, Pakistan. Phone: +92300-2375813. E-mail: sumaira.farooqui@zu.edu.pk - Orcid: 0000-0001-9263-8033

Submitted: November 24, 2023. **Accepted:** February 11, 2024

https://doi.org/10.52083/EWDP6111

injury, articular cartilage may be subjected to excessive biomechanical pressures (Favero et al., 2019). Deprivation of the meniscus puts the knee joint at risk of degeneration (Rhim et al., 2021). The mainstay of treatment in degenerative cartilage disorders is prevention via exercise and physiotherapy (Colella et al., 2020). Traditional exercise programs, including resistance, aerobic and flexibility training, and non-traditional exercises, including tai chi, yoga, and aquatic exercise programs, have successfully demonstrated relief (Wellsandt and Golightly, 2018). The morphological effects of therapeutic exercise on the individual components of articular cartilage of the knee joint need to be better recognized (Bricca et al., 2019). Although exercise is extensively suggested for preventing joint deterioration, the diversity of exercise choices evaluated is far broader. There is inadequate literature to advocate a particular exercise over another; thus, patients and clinicians are looking for guidelines on the "optimal" exercise and its frequency, intensity, time and type (FITT) (Kolasinski et al., 2019).

Zhou (2004) studied knee joint articular cartilages of male Sprague-Dawley (SD) rats using low, medium and high-intensity exercises for 8 weeks, 1 hour per day. The results showed that moderate-intensity active exercise can enhance cartilage repair and delay degeneration, while high intensity may increase damage (Zhou, 2004). In addition, Yao et al. (2019) investigated that running at high speed or intensity, rather than long-distance running, may cause cartilage degeneration in female mice (Yao et al., 2019). Furthermore, Moshtagh et al. (2018) added that intense running can result in mild cartilage degeneration and the study was done in male Wistar rats (Moshtagh et al., 2018). On the other side, Lee et al. (2011) studied the histology of medial knee joints of treadmill-running Wistar rats using a modified Mankin system (MMS) and Osteoarthritis Research Society International (OARSI) scores. MMS scores showed a greater prevalence of mild OA at 6 weeks and moderate OA at 10 weeks in the exercise group than in the control group. There were significantly higher OARSI scores in the exercise group than the control group at 10 weeks for both femoral and tibial cartilages. Therefore, this literature recognized that treadmill-running exercise can lead to the development of OA in rats (Lee et al., 2011). As the evidence regarding the effects of exercises on cartilage is enormous, literature on improving chondrocytes number is limited. Therefore, this study aims to determine the effects of endurance resistance exercise on the cellularity of knee joint hyaline cartilages and fibrocartilage in young male rats.

MATERIALS AND METHODS

Animal model selection and study setting

Young male Sprague Dawley rats were obtained from the Animal House of the International Centre for Chemical and Biological Sciences, University of Karachi. They were kept in cages at room temperature while maintaining a day and night cycle and were given ad libitum water and feed at Ziauddin College of Rehabilitation Sciences. The rats performed the exercise training at the same location. The histological procedures and microscopic examination of slides were performed at the Cell Biology and Histology Lab, MDRL-2, Ziauddin University, Clifton Campus. Sprague Dawley healthy young growing male rats and rats weighing 200 to 300 grams were included. Unhealthy rats having ambulation problems or any injury were excluded.

Randomization

A total of n=12 healthy young male Sprague Dawley rats weighing 200 to 300 grams were equally divided into two groups: Endurance resistance training (ERT) and Sedentary or Control (C) through simple random sampling technique (Charan and Biswas, 2013; Luciano et al., 2017).

Interventions Protocol

Generally, all the male rats enrolled in the ERT climbed the ladder carrying the load, which was tied to the proximal end of the tail. Height was 110 cm with 80° inclination and 2 cm distance between the steps (Neto et al., 2019). For ERT, initially, a one-week adaptation period was completed carrying 5% of individual body weight with 3 sets. The initial load to be carried and sets from week 2 were 10% and 3 sets, then progressed to 20% and

4 sets, 30% and 5 sets, and 40% of the body weight and 6 sets every week till week 5. There were 12-15 repetitions per set and 2-minute intervals in between. For Control, no training was done. At the end of the 5th week, all rats were euthanized within 48 hours. The total training protocol period was 5 weeks, including an initial one-week adaptation period for the exercise group (Mazor et al., 2019). The frequency of exercise training was 5 days per week, excluding weekends. Each training session's duration was 30 minutes.

Histological Evaluation

The knee joints were harvested en bloc by dissecting the shaft of lower limbs from the shaft of the femur to the shaft of the tibia/fibula. The harvested cartilage tissues were kept in a sealed plastic jar containing Bouin's fixative, and bone decalcification was done. The tissues were dehydrated with alcohol, cleared with xylene and fixed in paraffin. 0.4 um sections were taken on glass slides, and Haematoxylin and Eosin (H&E) staining was performed. After mounting the tissue, the slides were examined under a Nikon INTENSE LIGHT C-HGFI microscope. Microscopic images were analysed, and morphometry was performed by using NIS Elements software. The number of chondrocytes per lacuna was assessed in fibrocartilage and hyaline cartilages of the femur and tibia.

Data Analysis

The analysis was performed on SPSS (Statistical Package for Social Sciences) version 25. All numerical variables were expressed in mean and standard deviation. An independent sample t-test was applied to compare numerical variables. A p-value of <0.05 was considered significant in all statistical values.

Ethical Considerations

Ethical approval was obtained from the Animal Ethics Committee of Ziauddin University (Protocol No#2022-06/KY/ZCRS) before starting research. The protocols of animal ethics were followed throughout the intervention.

RESULTS

The effects of exercises on fibrocartilages were identified, and the findings were analysed on the number of chondrocytes per lacuna. The results provided evidence that the outcome measure was significantly $p<0.05$ better in the experimental group. (Table 1, Figs. 1a and 2).

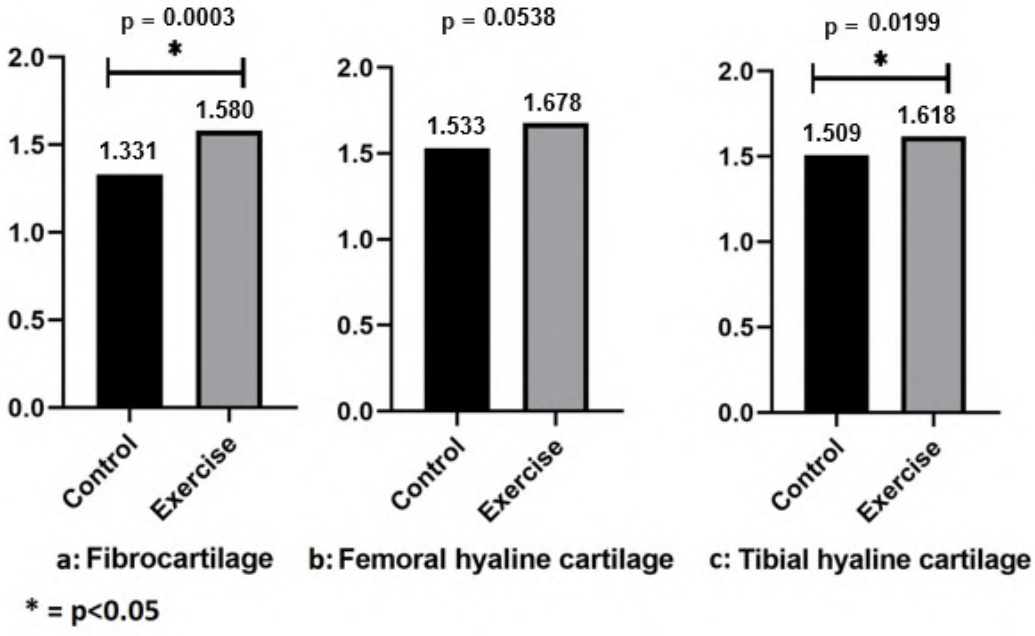

Fig. 1.- Graphically depicts the significant difference between the number of chondrocytes in fibrocartilage and tibial hyaline cartilage between the two groups (**a, c**). It also shows the no significant difference in number of chondrocytes per lacuna in femoral hyaline cartilage between the two groups (**b**).

Table 1. Represents the number of chondrocytes per lacuna in fibrocartilage, femoral hyaline cartilage and tibial hyaline cartilage. It was found to be significantly greater in the fibrocartilages and tibial hyaline cartilages of the exercise group. No significant differences were noted in the number of chondrocytes of femoral hyaline cartilages between the two groups.

Effects of Endurance Resistance Exercises on Knee Cartilage				
Variables	**Sample Size (n)**	**No. of Chondrocytes**		**p-value**
		Exercise Group (Mean±S.D)	**Control Group** (Mean±S.D)	
Fibrocartilage	12	1.580 ± 0.19	1.331 ± 0.04	0.0003*
Femoral Hyaline Cartilage	12	1.678 ± 0.18	1.533 ± 0.17	0.0538
Tibial Hyaline Cartilage	12	1.618 ± 0.09	1.509 ± 0.1	0.0199*

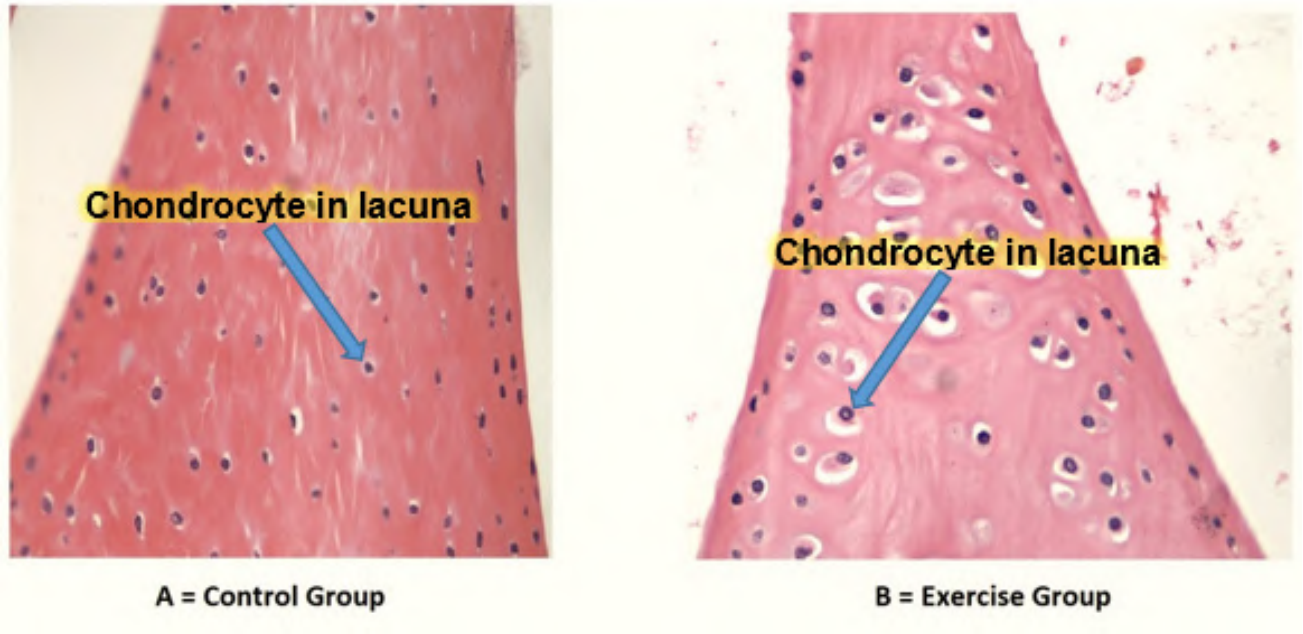

Fig. 2.- Shows difference between the number of chondrocytes per lacuna in knee joint fibrocartilage between the two groups (**A, B**).

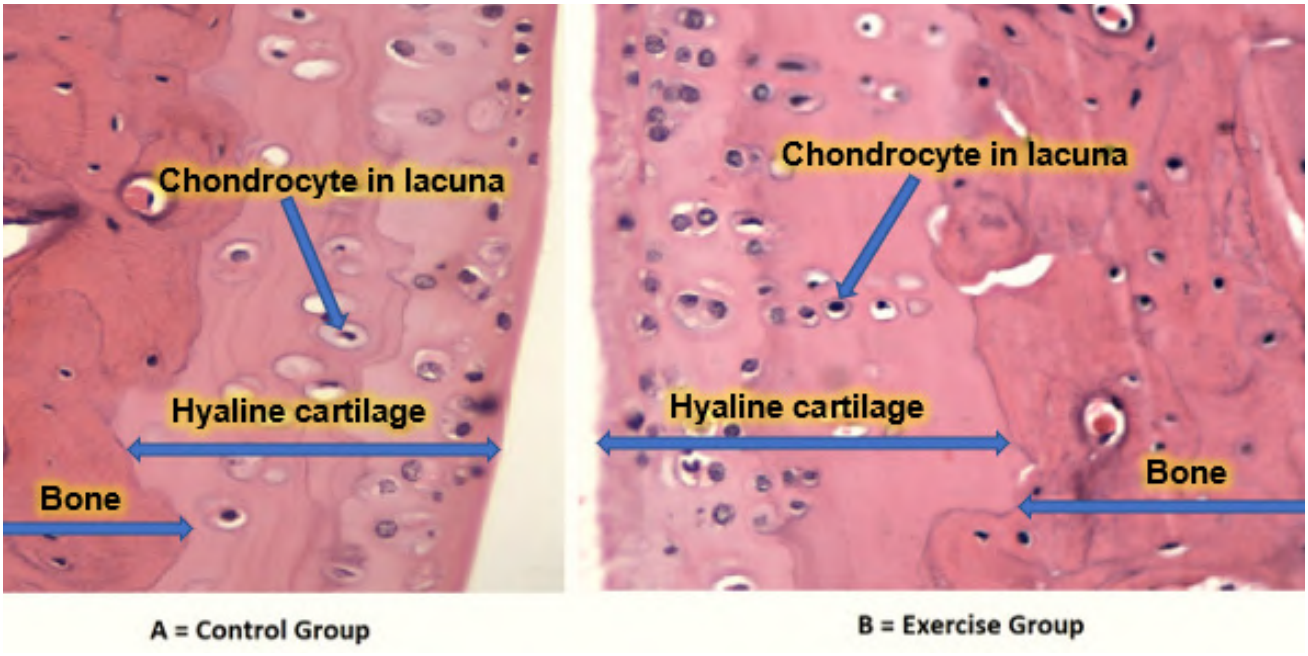

Fig. 3.- Shows difference between the number of chondrocytes per lacuna in knee joint femoral hyaline cartilage between the two groups (**A, B**).

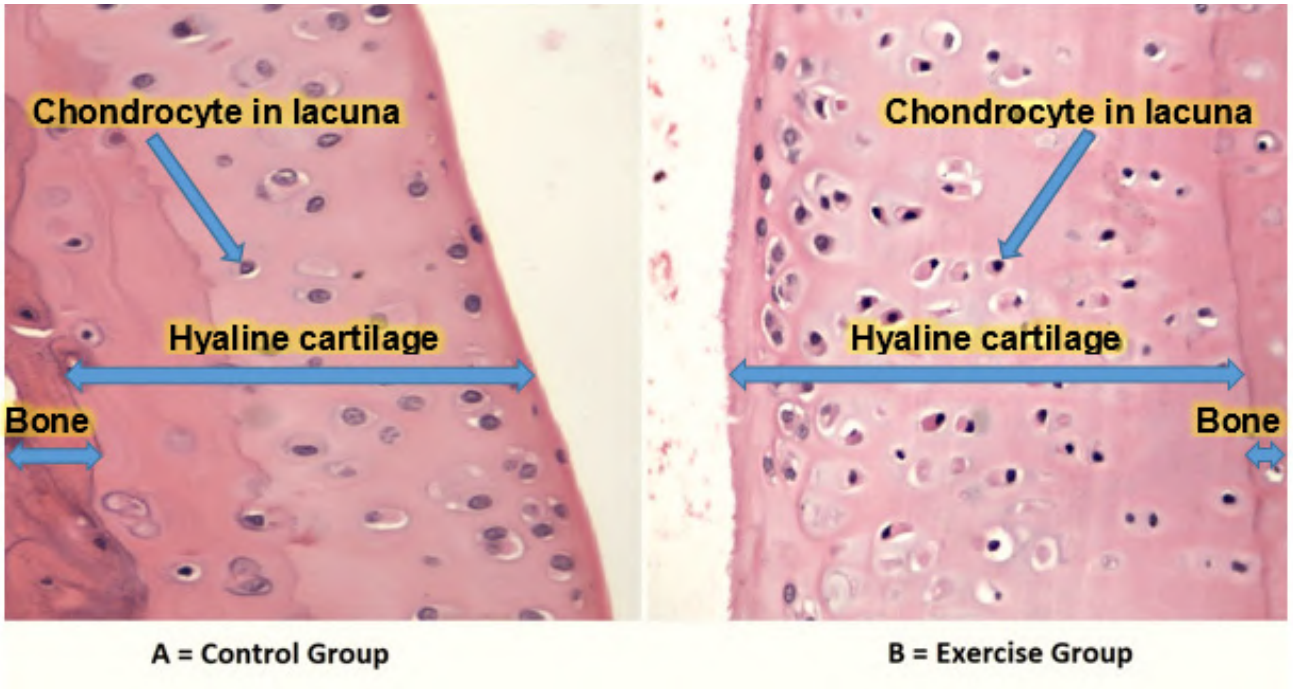

Fig. 4.- Shows difference between the number of chondrocytes per lacuna in knee joint tibial hyaline cartilage between the two groups (**A, B**).

Further femoral hyaline cartilage analyses were performed, and the findings revealed that for the number of chondrocytes per lacuna, an insignificant p-value was observed. (Table 1, Figs. 1b and 3).

Analyses of the effects of exercises on tibial hyaline cartilage were performed, and the findings revealed that a significant $p<0.05$ was observed in the number of chondrocytes per lacuna. (Table 1, Figs. 1c and 4).

DISCUSSION

We carried out this study to quantitatively analyse the effects of exercise on knee joint cartilage cellularity. The exercise group significantly outperformed the control group regarding the number of chondrocytes per lacuna in fibrocartilage. However, in the study of the femoral hyaline cartilage, the number of chondrocytes per lacuna did not differ between the groups. On the contrary, tibial hyaline cartilage examination showed significant changes in the number of chondrocytes per lacuna. Our results show potential advantages for cartilage health and integrity by showing that the endurance resistance exercise intervention favoured both fibrocartilage and hyaline cartilage in the tibia bones. The more enormous ramifications of these findings require more investigation, particularly about osteoarthritis and joint health, using both animal models and maybe human experiments.

A study examined the effects of two prevalent physical activities—walking on a treadmill and swimming—on a mechanical model of osteoarthritis (OA), and observed how both affected morphological factors associated with OA. Forty-eight male Wistar rats were used in the experiment, and they were divided into four groups for the study: Sham (no OA induction), Osteoarthritis (OA), OA + Treadmill (T), and OA + Swimming (S). The findings revealed that the number of chondrocytes per lacuna was significantly reduced in the OA and OA + S groups than in the Sham group ($p < 0.05$), pointing to a detrimental influence on the health of the cartilage. However, compared to the OA group, the OA + T group showed a significant increase in the number of chondrocytes per lacuna ($p<0.001$), indicating that treadmill exercise may have a positive effect on chondrocyte count in this OA model (da Silva et al., 2023). Similarly in our study, the number of chondrocytes within the fibrocartilages of both knees appears to have increased as a result of the exercise intervention,

which suggests that physical activity may enhance the integrity and health of knee fibrocartilage.

Another study found how Wistar rats with experimental rheumatoid arthritis (RA) responded to low-level laser treatment (LLLT), stair climbing exercise, and their combination. Eight groups of male Wistar rats were created: controls with LLLT, controls with exercise, controls with both LLLT and exercise, arthritis only, arthritis with LLLT, arthritis with exercise, and both LLLT and exercise for arthritis. There were five rats per group. According to the findings, the arthritis exercise group had more chondrocytes in its tibia and talus than the other groups (Retameiro et al., 2022). Comparatively, the number of chondrocytes in the femoral hyaline cartilage was not statistically significantly affected by exercise. Because of this, it does not seem that the exercise intervention in this study had the same effect on this specific type of cartilage as it did on the knee fibrocartilage.

Furthermore, researchers investigated how an 8-week, moderate-intensity treadmill aerobic training program affected rats with knee osteoarthritis (kOA)-like alterations caused by monosodium iodoacetate (MIA) in a study involving 27 rats. Three groups of rats were generated: SHAM (Control), kOA (induced), and kOA with aerobic exercise (OAE). According to the study, the number of chondrocytes in the rats in the OAE group decreased by 35%, showing that these crucial cells were preserved. Additionally, in rats with generated kOA-like alterations, aerobic training controlled inflammatory biomarkers and enhanced motor function. Overall, the results indicate a potential role for moderate-intensity aerobic exercise in preserving chondrocytes and improving kOA-like outcomes (Martins et al., 2019). However, exercise had a statistically significant impact on the number of chondrocytes in the tibial hyaline cartilage for this study.

Our study and the other studies show that the effects of exercise on chondrocyte count depend on many variables, including the type of exercise, the selected animal model (OA, RA, or kOA-like), and the kind of cartilage being studied (fibrocartilage or hyaline cartilage). Even though our study positively impacted the knee's fibrocartilage and tibial hyaline cartilage, other studies on OA, RA, and hyaline cartilage also reported favourable outcomes in different conditions. These variations emphasize the need for particular workout suggestions based on the state and type of cartilage. Additionally, they emphasize the potential advantages of exercise in maintaining the health of chondrocytes and cartilage in various arthritis-related disorders, but the underlying mechanisms may vary. More study is required to clarify these pathways and direct practical applicability for human patients.

The study has particular strengths, such as the use of young male rats as a controlled animal model, allowing researchers to evaluate the effects of exercise on knee joint cartilage histology without the difficulties of using human participants. In addition, the young rats were more likely to engage in physical activity. The investigator also conducted a thorough microscopic evaluation of the knee joint's cartilage that advances the knowledge of exercise effects, essential for developing exercise regimens and therapies for cartilage health. The study's conclusions are exclusive to the small sample of young male rats, which restricts the applicability of the findings to human populations. Also, there was no difference in age, gender, or species among the young male rats utilized in the study, making it difficult to extrapolate the results to a larger population.

Furthermore, the study's short length may not reflect the long-term effects of endurance resistance exercise on the viability of the identified changes. Since there was no activity-free control group in the study, it was not easy to separate the effects of exercise from other possible factors impacting cartilage health. Future studies may include functional tests that give a complete picture of how exercise affects cartilage with evidence-based trials with larger samples that might transfer into clinical recommendations for human exercise programs.

Endurance resistance exercise does increase the cellularity of knee joint cartilages. This increase is more prominently and specifically seen in fibrocartilage and tibial hyaline cartilage. This study implicates the protective role of resistance exercise on the morphology of these cartilages.

ACKNOWLEDGEMENTS

We want to express my appreciation to the Ziauddin College of Rehabilitation Sciences, Ziauddin University faculty and staff who have provided invaluable resources and a conducive environment for learning and research. Special thanks to Prof. Dr. Sumaira Imran Farooqui for her support and encouragement.

AUTHOR'S CONTRIBUTION

Following authors have made substantial contributions to the manuscript as indicated: **KY:** Concept and study design, acquisition, analysis and interpretation of data, drafting the manuscript. **KJJB:** Concept and study design, acquisition, analysis and interpretation of data. **SIF:** Concept and study design, critical review and approval of the final version to be published. **JR:** Concept and study design, drafting the manuscript. **AAK:** Critical review, approval of the final version to be published. **SNNS:** Critical review, approval of the final version to be published.

REFERENCES

BRANLY T, BERTONI L, CONTENTIN R, RAKIC R, GOMEZ-LEDUC T, DESANCÉ M, HERVIEU M, LEGENDRE F, JACQUET S, AUDIGIÉ F, DENOIX JM (2017) Characterization and use of equine bone marrow mesenchymal stem cells in equine cartilage engineering. Study of their hyaline cartilage forming potential when cultured under hypoxia within a biomaterial in the presence of BMP-2 and TGF-ß1. *Stem Cell Rev*, 13(5): 611-630.

BRICCA A, JUHL CB, STEULTJENS M, WIRTH W, ROOS EM (2019) Impact of exercise on articular cartilage in people at risk of, or with established, knee osteoarthritis: a systematic review of randomised controlled trials. *BJSM*, 53(15): 940-947.

CHARAN J, BISWAS T (2013) How to calculate sample size for different study designs in medical research? *Indian J Psychol Med*, 35(2): 121-126.

COLELLA F, GARCIA JP, SORBONA M, LOLLI A, ANTUNES B, D'ATRI D, BARRÉ FP, OIENI J, VAINIERI ML, ZERRILLO L, CAPAR S (2020) Drug delivery in intervertebral disc degeneration and osteoarthritis: Selecting the optimal platform for the delivery of disease-modifying agents. *JCR*, 328: 985-999.

COSTA JB, SILVA-CORREIA J, REIS RL, OLIVEIRA JM (2018) Recent advances on 3D printing of patient-specific implants for fibrocartilage tissue regeneration. 3D Print. *Med*, 2(3): 129-140.

DA SILVA LA, THIRUPATHI A, COLARES MC, HAUPENTHAL DP, VENTURINI LM, CORRÊA ME, SILVEIRA GD, HAUPENTHAL A, DO BOMFIM FR, DE ANDRADE TA, GU Y (2023) The effectiveness of treadmill and swimming exercise in an animal model of osteoarthritis. *Front Physiol*, 14: 1101159.

FAVERO M, BELLUZZI E, TRISOLINO G, GOLDRING MB, GOLDRING SR, CIGOLOTTI A, POZZUOLI A, RUGGIERI P, RAMONDA R, GRIGOLO B, PUNZI L (2019) Inflammatory molecules produced by meniscus and synovium in early and end-stage osteoarthritis: a coculture study. *J Cell Physiol*, 234(7): 11176-11187.

KOLASINSKI SL, NEOGI T, HOCHBERG MC, OATIS C, GUYATT G, BLOCK J, CALLAHAN L, COPENHAVER C, DODGE C, FELSON D, GELLAR K (2020) 2019 American College of Rheumatology/Arthritis Foundation guideline for the management of osteoarthritis of the hand, hip, and knee. *A&R*, 72(2): 220-233.

LEE YJ, PARK JA, YANG SH, KIM KY, KIM BK, LEE EY, LEE EB, SEO JW, ECHTERMEYER F, PAP T, SONG YW (2011) Evaluation of osteoarthritis induced by treadmill-running exercise using the modified Mankin and the new OARSI assessment system. *Rheumatol Int*, 31: 1571-1576.

LIN W, KLEIN J (2021) Recent progress in cartilage lubrication. *Adv Mater*, 33(18): 2005513.

LUCIANO TF, MARQUES SO, PIERI BL, DE SOUZA DR, ARAÚJO LV, NESI RT, SCHEFFER DL, COMIN VH, PINHO RA, MULLER AP, DE SOUZA CT (2017) Responses of skeletal muscle hypertrophy in Wistar rats to different resistance exercise models. *Physiol Res*, 66(2): 317-323.

MARTINS JB, MENDONÇA VA, AGUIAR GC, FONSECA SF, SANTOS JM, TOSSIGE-GOMES R, MELO DD, OLIVEIRA MX, LEITE HR, CAMARGOS AC, FERREIRA AJ (2019) Effect of a moderate-intensity aerobic training on joint biomarkers and functional adaptations in rats subjected to induced knee osteoarthritis. *Front Physiol*, 10: 1168.

MAZOR M, BEST TM, CESARO A, LESPESSAILLES E, TOUMI H (2019) Osteoarthritis biomarker responses and cartilage adaptation to exercise: A review of animal and human models. *Scand J Med Sci Sports*, 29(8): 1072-1082.

MOSHTAGH PR, KORTHAGEN NM, PLOMP SG, POURAN B, CASTELEIN RM, ZADPOOR AA, WEINANS H (2018) Early signs of bone and cartilage changes induced by treadmill exercise in rats. *JBMR plus*, 2(3): 134-142.

MURPHY CA, GARG AK, SILVA-CORREIA J, REIS RL, OLIVEIRA JM, COLLINS MN (2019) The meniscus in normal and osteoarthritic tissues: facing the structure property challenges and current treatment trends. *Annu Rev Biomed Eng*, 21: 495-521.

NETO WK, DE ASSIS SILVA W, DA SILVA AD, CIENA AP, DE SOUZA RR, CARBONE PO, ANARUMA CA, GAMA EF (2019) Testosterone is key to increase the muscle capillary density of old and trained rats. *J Morphol Sci*, 36(03): 182-189.

NIE X, CHUAH YJ, ZHU W, HE P, PECK Y, WANG DA (2020) Decellularized tissue engineered hyaline cartilage graft for articular cartilage repair. *Biomater*, 235: 119821.

RETAMEIRO AC, NEVES M, TAVARES AL, BOARO CD, RODRIGUEZ DF, STEIN T, COSTA RM, BERTOLINI GR, RIBEIRO LF (2022) Physical exercise and low-level laser therapy systemic effects on the ankle joint in an experimental rheumatoid arthritis model. *J Manipulative Physiol Ther*, 45(4): 248-260.

RHIM HC, JEON OH, HAN SB, BAE JH, SUH DW, JANG KM (2021) Mesenchymal stem cells for enhancing biological healing after meniscal injuries. *World J Stem Cells*, 13(8): 1005.

WELLSANDT E, GOLIGHTLY Y (2018) Exercise in the management of knee and hip osteoarthritis. *Curr Opin Rheumatol*, 30(2): 151-159.

YAO Z, CHEN P, WANG S, DENG G, HU Y, LIN Q, ZHANG X, YU B (2019) Reduced PDGF-AA in subchondral bone leads to articular cartilage degeneration after strenuous running. *J Cell Physiol*, 234(10): 17946-17958.

ZHANG J, DONG S, SIVAK WN, SUN HB, CHANG P (2018) Stem cells in cartilage diseases and repair 2018. *Stem Cells Int*, 2018: 3672890.

ZHOU L (2021) Cell metabolism under different intensity exercises in sports medicine. *Revista Brasileira de Medicina do Esporte*, 27: 682-685.

Investigating the volume of hippocampus and corpus callosum in Iranian multiple sclerosis patients using magnetic resonance imaging: a retrospective study

Soltani Reza[1], Aghajanpour Fakhroddin[2], Torabi Abolfazl[2], Afshar Azar[2], Kolivand Masoumeh[3], Dehghani Nejad Ali[4], Movassaghi Mahdiyeh[5], Mohammadzadeh Ibrahim[6], Kaedi Hossein[7], Norouzian Mohsen[2]

[1] Student Research Committee, Faculty of Medicine, Shahid Beheshti University of Medical Sciences, Tehran, Iran

[2] Department of Cell Biology and Anatomical Sciences, School of Medicine, Shahid Beheshti University of Medical Sciences, Tehran, Iran

[3] Department of Anatomical Sciences, School of Medicine, Kashan University of Medical Sciences, Kashan, Iran

[4] Department of Anatomical Sciences, School of Medicine, Qazvin University of Medical Sciences, Qazvin, Iran

[5] Master student of Clinical Psychology, Faculty of Clinical Psychology, Allameh Tabatabaei University, Tehran, Iran

[6] Skull Base Research Center, Shahid Beheshti University of Medical Sciences, Tehran, Iran

[7] Department of Radiology, Loghman Hakim Hospital, Shahid Beheshti University of Medical Sciences, Tehran, Iran

SUMMARY

Multiple Sclerosis (MS) is one of the most common forms of the acquired autoimmune demyelinating disorder affecting the brain. The neurological symptoms of MS are often presented in a relapsing-remitting manner. This study aims to investigate volume changes in the hippocampus and Corpus Callosum (CC). A cross-sectional study was conducted on 200 MS patients, 100 males and 100 females, aged 20-56 years. According to McDonald's 2017 criteria,100 patients were in the MS group, and 100 were in the control group. This study assessed volume changes in the hippocampus and CC with ITK-SNAP 4.0 software. Our study revealed that the volumes of the right Hippocampus ($P<0.0001$), left Hippocampus ($P<0.05$), and corpus callosum ($P<0.001$), were significantly decreased in MS group compared to control group, regardless of the sex of the patients. Additionally, our results showed that the volume of these three areas has no significant difference with the age of MS patients. This research shows that some brain regions, including the hippocampus and corpus callosum, can be essential landmarks in determining MS disease.

Key words: Multiple sclerosis – Hippocampus – Corpus callosum

Shared corresponding authors:
Dr Mohsen Norouzian. Department of Cell Biology and Anatomical Sciences, School of Medicine, Shahid Beheshti University of Medical Sciences, Tehran, Iran. E-mail: norozian93@gmail.com

Submitted: October 18, 2023. **Accepted:** February 20, 2024

https://doi.org/10.52083/VAFU2967

INTRODUCTION

Multiple Sclerosis (MS) is the most common form of the acquired autoimmune demyelinating disorder of the brain. In 2007, the global population of individuals with multiple sclerosis (MS) reached 2 million, and the prevalence of the disease has been on the rise in various regions across the world in recent years (Doerksen et al., 2007; Koch-Henriksen and Sorensen, 2011). The incidence rate of MS has shown an upward trend in many areas, including the Middle East and Iran. Ecological studies have estimated the prevalence to be 24.6/100,000 in Iran in 2006, increasing to 44.53/100,000 in 2011 (Dehghani et al., 2015). Urban lifestyle, and more significantly, smoking, have been identified as contributing factors (Dehghani et al., 2015). The neurological symptoms of MS are often presented in a relapsing-remitting pattern, encompassing a range of presentations, including blurred vision, diplopia, focal weakness, sensory disturbance, ataxia, bladder dysfunction, impaired cognitive abilities of the brain, or even psychiatric symptoms, which are common (Garg et al., 2015; Honeycutt and Smith, 1995).

Multiple Sclerosis (MS) is a chronic condition characterized by a variable natural history. In Relapsing-Remitting MS (RRMS), clinical relapses mark the onset, with subsequent periods of recovery that may be either complete or partial. However, over time, disability tends to accumulate, and the recoveries often become incomplete. Approximately 20% of individuals with RRMS eventually experience a transition to Secondary-Progressive MS (SPMS) during the course of the disease (Cree et al., 2016). In contrast, a minority of patients, around 15%, exhibit a progression of disability from the outset, a condition known as Primary-Progressive MS (PPMS). Notably, recent advancements in Disease-Modifying Treatments (DMTs) have contributed to an improvement in life expectancy and outcomes for individuals diagnosed with MS in more recent cohorts (McGinley et al., 2021; Marrie et al., 2015).

When a patient presents with neurological manifestations suggestive of MS, brain Magnetic Resonance Imaging (MRI) becomes pivotal for diagnosing and disease monitoring. This emphasis on MRI for diagnosis and monitoring has been underscored by the 2017 McDonald Criteria (Kalincik et al., 2012).

Among numerous diagnostic landmarks for MS, the Corpus Callosum (CC) holds a special place. CC is a commissural structure connecting the cortices of the two cerebral hemispheres. The CC is divided into rostrum, genu, body, and splenium in the sagittal plane from anterior to posterior. Recent advances in imaging technologies have revealed a lobe-specific structural connectivity gradient along the CC, reshaping our understanding of this brain region (Garg et al., 2015). The specific arterial supply to the CC renders it relatively resistant to chronic small vessel ischemia, as the many penetrating arterioles contributing to the circulation of CC show resistance to atherosclerosis (Garg et al., 2015). This makes the lesions in this region often specific to inflammatory processes, including MS. Abnormalities within the CC are observed in 55% to 95% of the patients. These CC lesions are diverse, but progressive CC atrophy in MS is known to correlate with disability and cognitive dysfunction (Garg et al., 2015; Kalincik et al., 2012; Llufriu et al., 2019; Honeycutt and Smith, 1995).

The hippocampus, situated in the temporal lobe, is a complex structure with distinct anatomical and functional features. It plays an important role in learning and memory (Anand and Dhikav, 2012). Studies utilizing MRI have enabled the specification of hippocampal morphology and its connections with other brain regions, linking these features to clinical and behavioural performances (Mey et al., 2023).

While there are relatively few studies investigating hippocampal alterations in MS, understanding the radiologic characteristics of the hippocampus in the progress of the disease may provide valuable insights into the relationships between hippocampal subfield changes and neurological presentations, particularly cognitive impairments. Furthermore, research has consistently demonstrated that age, sex, and race can influence various aspects of brain anatomy, including the hippocampus and corpus callosum (Caldito et al., 2018; Tokarska et al., 2023).

Given the limited number of studies conducted in the Iranian population, our study aims to com-

pare the volumes of the corpus callosum and hippocampus in the brain MRI of Iranian MS patients relative to healthy individuals. The results of this study may pave the way for future research, contributing to the development of radiological standards for accurate diagnosis and the assessment of MS severity while enhancing our understanding of the disease's nature.

MATERIALS AND METHODS

This cross-sectional study was conducted in the Radiology Department of Shahid Beheshti University of Medical Sciences. This study extended between March 2022 to March 2023 and received approval from the Student Research Committee at Shahid Beheshti University of Medical Sciences (IR.SBMU.RETECH.REC.1401.777).

Participants

We recruited a total number of 100 MS patients, maintaining an equal gender distribution, with participants aged between 20 and 56 years. Inclusion criteria encompassed individuals aged 18 years and older who met the McDonald's 2017 criteria. Exclusion criteria involved patients with positive imaging findings, as well as those with neurological or cognitive disorders stemming from conditions such as brain or spinal cord ischemia, tumours, infectious diseases impacting the neurological system, genetic disorders, systemic autoimmune disorders, brain or spinal trauma, or drug abuse affecting the neurological system. All images were reviewed and approved by experienced radiologists. The individuals responsible for brain region size measurement and image analysis were blinded to the disease, state, gender, and other personal information regarding the participants. Additionally, we randomly selected 100 healthy patients who had sought medical attention for headaches as the control group.

Magnetic Resonance Imaging (MRI) of the Brain

MRI scans were conducted in our Imaging Department using the Siemens 1.5T system from Siemens Medical Systems, Germany.

Routine brain MRI protocols included axial (T1WI and T2WI), coronal PDWI, and sagittal T1WI. A 3D T1WI sequence was performed with a slice thickness of 0.5 mm and slice spacing of 0 mm. The study images were converted into DICOM format and transferred to a personal computer (PC) workstation equipped with ITK-SNAP 4.0 software. ITK-SNAP 4.0 is an open-source software package designed for visualization and computation on medical images. It was developed by student teams led by Guido Gerig at the University of North Carolina, in collaboration with NYU Tanden School of Engineering. Notably user-friendly, this tool finds specific application in the field of image segmentation. Its primary function is to facilitate the reliable morphometry of structures of interest through manual methods.

Image Analysis

The structures scrutinized in this study included the total part of Hippocampus and CC. Volumetric analysis was conducted on the 3D T1-weighted images in both axial and sagittal planes. Manual tracing was drawn around the boundaries of the hippocampi and CC (Fig. 1). These boundaries were established according to anatomical landmarks on each slice based on accepted conventions derived from those used in the literature and from comparison with standard brain atlases (Morelli et al., 2020). The area within the boundary was calculated and multiplied by slice thickness to obtain volumetric measurement (cm^3).

Statistical analysis

All statistical analyses were executed using SPSS version 23, and graphs were plotted with Graph Pad Prism 9. Data are presented as mean ± SD. The normality of all data was assessed using Kolmogorov–Smirnov test.

A two-way ANOVA and Tukey's post-hoc test was employed to evaluate mean differences between groups, categorized based on two independent variables, and to assess the interaction effect between these variables—specifically, sex and the state of disease. The correlation between variables, the volume of regions and the age of MS patients, were examined using the Pearson correlation coefficient (PCC). A significance level of $P < 0.05$ was considered to determine statistical significance in the analyses.

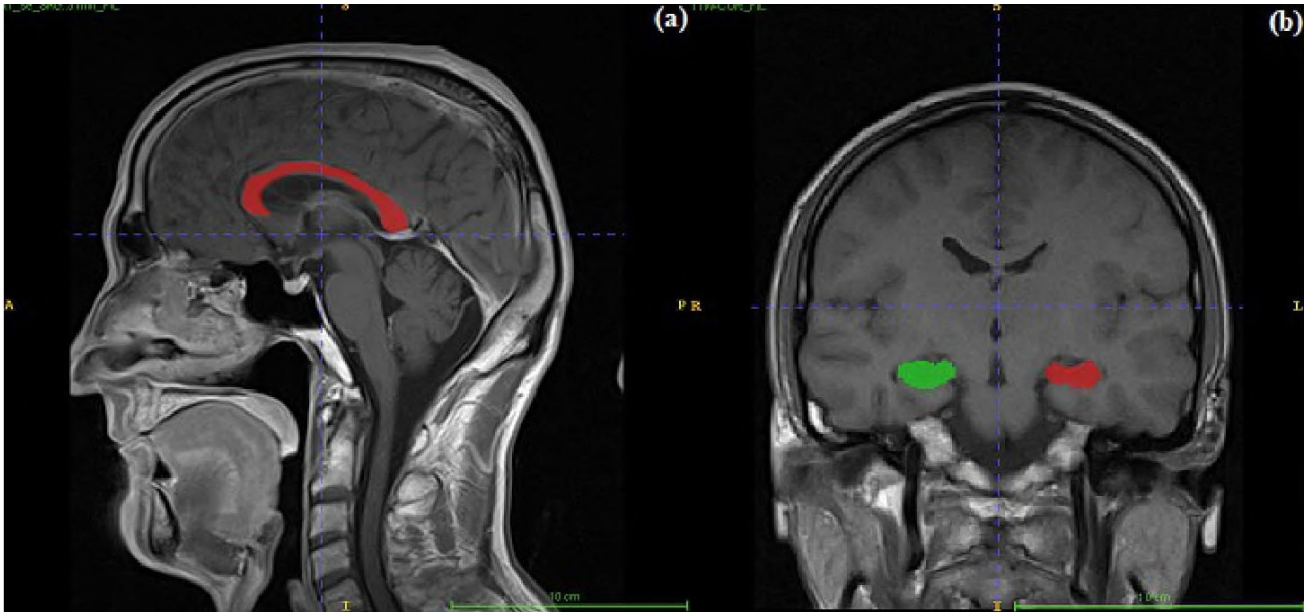

Fig. 1.- Example of manual segmentation in the control group. **a)** sagittal view of the corpus callosum segmentation. **b)** coronal view of the hippocampus segmentation.

RESULTS

Participants

All MS patients were included in the study based on McDonald's 2017 criteria. Th analysis included 100 healthy patients (50 males and 50 females) and 100 MS patients (50 males and 50 females) were analysed. The mean ± SD age of patients in the control and MS group was (39.02±11.87) and (39.46±9.67) years, respectively (Table1).

Table 1. Demographic statistics.

Variables		Mean±SD	
		Control	MS
Age		39.02±11.87	39.46±9.67
Gender	Male	50 (38.34±9.34)	50 (38.82±8.99)
	Female	50 (39.7±13.98)	50 (40.10±10.36)
Total		100	100

Volumetric assessment in experimental groups

In this study, the volume of the right hippocampus in the control and MS groups was (3.18±4.56) and (2.42±5.58) cm^3, respectively. Moreover, the volume of the left hippocampus in the control and MS group was (3.16±1.97) and (2.75±4.52) cm^3, respectively. Also, the volume of the corpus callosum in the control and MS groups was (16.54±5.30) and (12.40±10.4) cm^3, respectively. The Results from the volumetric assessment indicated a significant decrease in the volume of the right hippocampus (F=140.767, df=1, P=0.000), left hippocampus (F=4.083, df=1, P<0.045), and corpus callosum (F=12.668, df=1, P=0.000) in the MS group compared to the control group (Table 2).

Table 2. Results and comparison of mean volume three brain regions in experimental groups (cm^3).

Regions	Mean±SD		F (df=1)	p
	Control (n=100)	MS (n=100)		
Right Hippocampus Volume	3.18±4.56	2.42±5.58	140.767	0.000
Left Hippocampus Volume	3.16±1.97	2.75±4.52	4.083	<0.045
Corpus Callosum Volume	16.54±5.30	12.40±10.4	12.668	0.000

Volumetric assessment in both sexes

Volumetric assessment was done in both sexes. This assessment showed that the right hippocampus volume in the males and females was (3.07±45.63) and (2.53±45.63) cm^3, respectively. Moreover, the left hippocampus volume in the males and females was (3.01±14.40) and

(2.90±14.40) cm^3, respectively. Furthermore, the corpus callosum volume in males and females was (13.63±82.08) and (15.61±82.08) cm^3, respectively. A significant sex difference was observed in the volume of the right hippocampus (F=69.956, df=1, P=0.000) and corpus callosum (F=3.885, df=1, P<0.050), with the right hippocampus volume being lower in females and the corpus callosum volume being lower in males. However, no significant difference (F=0.340, df=1, P<0.561) was detected in the left hippocampus volume between males and females (Table 3).

Table 3. Results and comparison of mean volume three brain regions in both sexes (cm^3).

Regions	Mean±SD		F (df=1)	P
	Male (n=100)	Female (n=100)		
Right Hippocampus Volume	3.07±45.63	2.53±45.63	69.956	0.000
Left Hippocampus Volume	3.01±14.40	2.90±14.40	0.340	<0.561
Corpus Callosum Volume	13.33±82.08	15.61±82.08	3.885	<0.050

Interaction Effect of sex and pathology in Volume regions

The two-way ANOVA test results indicated no significant difference in the interaction effect of sex and pathology on the volume of the right (F=0.707, df=1, P<0.40) and left hippocampus (F=0.297, df=1, P<0.58) and corpus callosum (F=0.970, df=1, P<0.32; Table 4).

Assessment of the correlation between volume regions and age patients

This assessment aimed to determine the correlation between the volume of regions and the age of MS patients. The correlation between the volume of the right hippocampus (r= 0.0494), left hippocampus (r=0.0646), and corpus callosum (r=0.0016) with age patients was investigated using Pearson's correlation coefficient. This assessment showed that the volume of these three areas has no significant difference with the age of MS patients (P >0.05; Table 5).

Table 5. Pearson correlation between volume regions and age patients.

Regions	Age	
	R	P
Right Hippocampus Volume	0.0494	0.62
Left Hippocampus Volume	0.0646	0.52
Corpus Callosum Volume	0.0016	0.98

DISCUSSION

In this study, we did a volumetric analysis of brain images of patients with MS to investigate the sizes of two cortical brain structures, namely, the corpus callosum and the hippocampus, compared to those in healthy controls. In our current study, we had undertaken an analysis to explore the connection between the volume of the hippocampus and corpus callosum among individuals of varying ages and genders.

The findings of this study will provide some valuable intuitions into the alteration of these regions in the background of MS, shedding light on potential implications of the pathophysiology of the disease.

Table 4. Results of interaction effect of sex and pathology in volume regions (cm^3).

Regions	Mean±SD				F (df=1)	P
	Male (n=100)		Female (n=100)			
	Control (n=50)	MS (n=50)	Control (n=50)	MS (n=50)		
Right Hippocampus Volume	3.42±64.53	2.71±64.53	2.94±64.53	2.12±64.53	0.707	<0.40
Left Hippocampus Volume	3.17±20.36	2.86±20.36	3.16±20.36	2.63±20.36	0.297	<0.58
Corpus Callosum Volume	15.96±11.60	10.69±11.60	17.11±11.60	14.12±11.60	0.970	<0.32

A pivotal finding in our study was the notable reduction in the measure of the right and the left hippocampus in the MS group, which aligns with many other previous researches (Mey et al., 2023; Morelli et al., 2020; Naghavi et al., 2023). The observed hippocampal atrophy signifies the intrinsic neural alterations, encompassing demyelination and neural degeneration, that transpire throughout the progression of multiple sclerosis (Mey et al., 2023).

Pelletier et al. (2001) demonstrated that hippocampal atrophy may indicate a progressive cognitive decline, particularly in the left hippocampus. The hippocampal volume is linked to cognitive reserve measurements. Throughout the disease, the correlation between atrophy in hippocampal subfields and Information Processing Speed (IPS) appears to intensify (Planche et al., 2018; Platten et al., 2022; Sotgiu et al., 2022).

Another notable finding from our investigation was the shrinkage of the corpus callosum. This outcome also aligns with the existing body of evidence (Sparaco et al., 2021; Llufriu et al., 2019). Prompt identification of callosal atrophy in patients during their initial demyelination episode can predict their progression to MS (Sumowski et al., 2016; Thompson et al., 2018). The precise impact of corpus callosum (CC) atrophy on the disability of patients with MS remains elusive. While specific studies posit a correlation between CC atrophy and disability, contrasting perspectives exist (Yaldizli et al., 2010).

The fundamental mechanisms underlying hippocampal atrophy in the brains of patients with MS are intricately complex, involving factors such as the depletion of synaptic proteins and microglial responses triggered by complement activation in response to axonal demyelination and injury, among other contributing elements. This notable hippocampal atrophy, particularly in the CA1 region, has been observed to align with a decline in performance on memory-related tasks. The capacity of learning is also compromised (Zhao et al., 2021). Corpus callosum atrophy is also attributed to distinct inflammatory cellular responses, which precipitate the demise of oligodendrocytes (Zheng et al., 2022).

Our study found that the volume of the right hippocampi differed significantly between males and females. Specifically, the hippocampi in males were larger than those in females. Indeed, this discovery aligns with the findings of other studies that have explored sex-specific differences in the brains (Ruigrok et al., 2014). Researchers have identified that factors, including menstrual cycle, hormonal therapy, genotype, and testosterone levels, can affect the hippocampus volume in males and females (Lisofsky et al., 2015; Everaerd et al., 2012). However, we have not found significant differences in the left hippocampus volume between males and females.

Our study results indicated that CC volume in females was more significant than in males. This discovery aligns with other research finding that CC volume in females was more significant than in males (Shiino et al., 2017). However, Luders et al. (2014) have shown the opposite results. Several studies have shown that the gender difference in the volume of the corpus callosum can be due to the size of the brain (Ardekani et al., 2013).

The results of the literature corroborate our findings, suggesting that compromised hippocampal tissue integrity early in the course of MS results in diminished whole and regional hippocampal volumes, although our study specifically assessed the whole hippocampal volume (Sicotte et al., 2008; Longoni et al., 2015; Ciolac et al., 2021).

When assessing the interaction effect of sex and the disease state (MS or control) on the volume of the regions of interest, our statistical analysis revealed no significant differences in the volume of the right and left hippocampus, as well as the corpus callosum. In simpler terms, within our study cohort, there was no significant difference in the impact of disease status on regional volumes between females and males.

Studies on sex differences in corpus callosum volumetric indices in patients with MS are currently lacking.

In a paper published in 2021, Ciolac et al. evaluated the morphometric networks of the hippocampus, its anatomic compartments, and their impact on cognitive performance in both gen-

ders. The results of their study indicate a more clustered architecture in females with MS compared to males, both at baseline and after a 2-year follow-up. Interestingly, other available studies on sex differences in brain networks in MS patients did not report any significant distinctions between males and females (Ciolac et al., 2021; Schoonheim et al., 2012). It is worth noting that there may be regional, sex-specific changes in the hippocampus for both males and females, as highlighted by Ciolac et al. (2021).

Notably, there is a gap in the literature regarding studies on sex differences in callosal volume in MS patients. Among the limited research available, the results have shown a consistent pattern of similarity in terms of sex differences in the corpus callosum among MS patients with our study (Khasawneh, 2023).

Regarding age, our research found no significant correlation between the volume of the three areas of interest in MS patients. The relationship between a patient's age and the size of the brain regions involved in the disease is not established. Further investigations are needed to explore this relationship, as there is currently a lack of comprehensive literature on the subject.

While our study offers valuable insights into the volumetric measurements of the hippocampus and corpus callosum in patients with MS compared to a healthy population, we acknowledge the limitations inherent to our study design. Firstly, the small sample size may limit the generalizability of our results. Additionally, our study exclusively focused on size measurements of the regions of interest, potentially constraining our understanding of the underlying pathophysiology driving these changes.

Unfortunately, our study did not specifically explore subregional variations within the hippocampus. Furthermore, exploring the natural progression of the disease would enhance our insights into the relationship between Multiple Sclerosis and the morphological changes in the hippocampus and corpus callosum.

Conducting longitudinal studies with larger and more diverse cohorts and delving into molecular and cellular-level investigations could significantly enhance our comprehension of the underlying nature of the disease in the future.

In summary, it is evident that patients with MS exhibit a decrease in the volume of both the Hippocampus and Corpus Callosum. The outcomes of this study, in conjunction with findings from other investigations, contribute to the advancement of our comprehension regarding the underlying disease mechanisms. This collective knowledge holds the potential to refine prognostic assessments and pave the way for innovative therapeutic approaches.

CONCLUSION

The results of our study show that some of the brain regions, including the hippocampus and corpus callosum, can be essential landmarks in determining MS disease. These structures can relate to variables including age and sex, which can give doctors a better view of the disease. Moreover, it can provide neurologists with comprehensive information about some diseases, including Alzheimer's.

ACKNOWLEDGEMENTS

This study relates to project NO 1401/59304 From the Student Research Committee, Shahid Beheshti University of Medical Sciences, Tehran, Iran. We also appreciate the "Student Research Committee" and "Research & Technology Chancellor" at Shahid Beheshti University of Medical Sciences for their financial support of this study.

REFERENCES

ANAND KS, DHIKAV V (2012) Hippocampus in health and disease: An overview. *Ann Indian Acad Neurol*, 15: 239.

ARDEKANI BA, FIGARSKY K, SIDTIS JJ (2013) Sexual dimorphism in the human corpus callosum: an MRI study using the OASIS brain database. *Cereb Cortex*, 23(10): 2514-2520.

CALDITO NG, SAIDHA S, SOTIRCHOS ES, DEWEY BE, COWLEY NJ, GLAISTER J, FITZGERALD KC, AL-LOUZI O, NGUYEN J, ROTHMAN A (2018) Brain and retinal atrophy in African-Americans versus Caucasian-Americans with multiple sclerosis: a longitudinal study. *Brain*, 141: 3115-3129.

CIOLAC D, GONZALEZ-ESCAMILLA G, RADETZ A, FLEISCHER V, PERSON M, JOHNEN A, LANDMEYER NC, KRÄMER J, MUTHURAMAN M, MEUTH SG, GROPPA S (2021) Sex-specific signatures of intrinsic hippocampal networks and regional integrity underlying cognitive status in multiple sclerosis. *Brain Commun*, 3(3): fcab198.

CREE BA, GOURRAUD PA, OKSENBERG JR, BEVAN C, CRABTREE-HARTMAN E, GELFAND JM, GOODIN DS, GRAVES J, GREEN AJ, MOWRY E, OKUDA DT, PELLETIER D, VON BUDINGEN HC, ZAMVIL SS, AGRAWAL A, CAILLIER S, CIOCCA C, GOMEZ R, KANNER R, LINCOLN R, LIZEE

A, QUALLEY P, SANTANIELLO A, SULEIMAN L, BUCCI M, PANARA V, PAPINUTTO N, STERN WA, ZHU AH, CUTTER GR, BARANZINI S, HENRY RG, HAUSER SL (2016) Long-term evolution of multiple sclerosis disability in the treatment era. *Ann Neurol*, 80: 499-510.

DEHGHANI R, YUNESIAN M, SAHRAIAN MA, GILASI HR, KAZEMI MOGHADDAM V (2015) The evaluation of multiple sclerosis dispersal in iran and its association with urbanization, life style and industry. *Iran J Public Health*, 44: 830-838.

DOERKSEN SE, MOTL RW, MCAULEY E (2007) Environmental correlates of physical activity in multiple sclerosis: a cross-sectional study. *Int J Behav Nutr Phys Act*, 4: 49.

EVERAERD D, GERRITSEN L, RIJPKEMA M, FRODL T, VAN OOSTROM I, FRANKE B, FERNÁNDEZ G, TENDOLKAR IJN (2012) Sex modulates the interactive effect of the serotonin transporter gene polymorphism and childhood adversity on hippocampal volume. *Neuropsychopharmacology*, 37(8): 1848-1855.

GARG N, REDDEL SW, MILLER DH, CHATAWAY J, RIMINTON DS, BARNETT Y, MASTERS L, BARNETT MH, HARDY TA (2015) The corpus callosum in the diagnosis of multiple sclerosis and other CNS demyelinating and inflammatory diseases. *J Neurol Neurosurg Psychiat*, 86: 1374-1382.

HONEYCUTT NA, SMITH CD (1995) Hippocampal volume measurements using magnetic resonance imaging in normal young adults. *J Neuroimaging*, 5: 95-100.

KALINCIK T, VANECKOVA M, TYBLOVA M, KRASENSKY J, SEIDL Z, HAVRDOVA E, HORAKOVA D (2012) Volumetric MRI markers and predictors of disease activity in early multiple sclerosis: a longitudinal cohort study. *PloS One*, 7: e50101.

KHASAWNEH R (2023) The impact of multiple sclerosis on the size and morphology of corpus callosum: an MRI-based retrospective study. *Int J Morphol*, 41: 422.

KOCH-HENRIKSEN N, SORENSEN PS (2011) Why does the north-south gradient of incidence of multiple sclerosis seem to have disappeared on the northern hemisphere? *J Neurol Sci*, 311: 58-63.

LISOFSKY N, MÅRTENSSON J, ECKERT A, LINDENBERGER U, GALLINAT J, KUHN SJN (2015) Hippocampal volume and functional connectivity changes during the female menstrual cycle. *Neuroimage*, 118: 154-162.

LLUFRIU S, ROCCA MA, PAGANI E, RICCITELLI GC, SOLANA E, COLOMBO B, RODEGHER M, FALINI A, COMI G, FILIPPI M (2019) Hippocampal-related memory network in multiple sclerosis: a structural connectivity analysis. *Mult Scler J*, 25: 801-810.

LONGONI G, ROCCA MA, PAGANI E, RICCITELLI GC, COLOMBO B, RODEGHER M, FALINI A, COMI G, FILIPPI M (2015) Deficits in memory and visuospatial learning correlate with regional hippocampal atrophy in MS. *Brain Struct Funct*, 220: 435-444.

LUDERS E, TOGA AW, THOMPSON PM (2014) Why size matters: differences in brain volume account for apparent sex differences in callosal anatomy: the sexual dimorphism of the corpus callosum. *Neuroimage*, 84: 820-824.

MARRIE RA, ELLIOTT L, MARRIOTT J, COSSOY M, BLANCHARD J, LEUNG S, YU N (2015) Effect of comorbidity on mortality in multiple sclerosis. *Neurology*, 85: 240-247.

MCGINLEY MP, GOLDSCHMIDT CH, RAE-GRANT AD (2021) Diagnosis and treatment of multiple sclerosis: a review. *JAMA*, 325: 765-779.

MEY GM, MAHAJAN KR, DESILVA TM (2023) Neurodegeneration in multiple sclerosis. *WIREs Mech Disease*, 15: e1583.

MORELLI ME, BALDINI S, SARTORI A, D'ACUNTO L, DINOTO A, BOSCO A, BRATINA A, MANGANOTTI P (2020) Early putamen hypertrophy and ongoing hippocampus atrophy predict cognitive performance in the first ten years of relapsing-remitting multiple sclerosis. *Neurol Sci*, 41: 2893-2904.

NAGHAVI S, ASHTARI F, ADIBI I, SHAYGANNEJAD V, RAMEZANI N, POURMOHAMMADI A, DAVANIAN F, KARIMI Z, KHALIGH-RAZAVI S-M, SANAYEI M (2023) Effect of deep gray matter atrophy on information processing speed in early relapsing-remitting multiple sclerosis. *Mult Scler Relat Disord*, 71: 104560.

PELLETIER J, SUCHET L, WITJAS T, HABIB M, GUTTMANN C, SALAMON G, LYON-CAEN O, CHERIF AA (2001) A longitudinal study of callosal atrophy and interhemispheric dysfunction in relapsing-remitting multiple sclerosis. *Arch Neurol*, 58: 105-111.

PLANCHE V, KOUBIYR I, ROMERO JE, MANJON JV, COUPE P, DELOIRE M, DOUSSET V, BROCHET B, RUET A, TOURDIAS T (2018) Regional hippocampal vulnerability in early multiple sclerosis: Dynamic pathological spreading from dentate gyrus to CA 1. *Human Brain Mapping*, 39: 1814-1824.

PLATTEN M, OUELLETTE R, HERRANZ E, BARLETTA V, TREABA CA, MAINERO C, GRANBERG T (2022) Cortical and white matter lesion topology influences focal corpus callosum atrophy in multiple sclerosis. *J Neuroimaging*, 32: 471-479.

RUIGROK AN, SALIMI-KHORSHIDI G, LAI M-C, BARON-COHEN S, LOMBARDO MV, TAIT RJ, SUCKLING J (2014) A meta-analysis of sex differences in human brain structure. *Neurosci Biobehav Rev*, 39(100): 34-50.

SCHOONHEIM MM, HULST HE, LANDI D, CICCARELLI O, ROOSENDAAL SD, SANZ-ARIGITA EJ, VRENKEN H, POLMAN CH, STAM CJ, BARKHOF F, GEURTS JJ (2012) Gender-related differences in functional connectivity in multiple sclerosis. *Mult Scler*, 18:164-173.

SHIINO A, CHEN Y, TANIGAKI K (2017) Sex-related difference in human white matter volumes studied: inspection of the corpus callosum and other white matter by VBM. *Sci Rep*, 7: 3-9.

SICOTTE NL, KERN KC, GIESSER BS, ARSHANAPALLI A, SCHULTZ A, MONTAG M, WANG H, BOOKHEIMER SY (2008) Regional hippocampal atrophy in multiple sclerosis. *Brain*, 131: 1134-1141.

SOTGIU M, PIGA G, MAZZARELLO V, ZARBO I, CARTA A, SADERI L, SOTGIU S, CONTI M, SABA L, CRIVELLI P (2022) Corpus callosum volumetrics and clinical progression in early multiple sclerosis. *Eur Rev Med Pharmacol Sci*, 26(1): 225-231.

SPARACO M, LAVORGNA L, BONAVITA S (2021) Psychiatric disorders in multiple sclerosis. *J Neurol*, 268: 45-60.

SUMOWSKI JF, ROCCA MA, LEAVITT VM, RICCITELLI G, SANDRY J, DELUCA J, COMI G, FILIPPI M (2016) Searching for the neural basis of reserve against memory decline: intellectual enrichment linked to larger hippocampal volume in multiple sclerosis. *Eur J Neurol*, 23: 39-44.

THOMPSON AJ, BANWELL BL, BARKHOF F, CARROLL WM, COETZEE T, COMI G, CORREALE J, FAZEKAS F, FILIPPI M, FREEDMAN MS (2018) Diagnosis of multiple sclerosis: 2017 revisions of the McDonald criteria. *Lancet Neurology*, 17: 162-173.

TOKARSKA N, TOTTENHAM I, BAAKLINI C, GAWRYLUK JR (2023) How does the brain age in individuals with multiple sclerosis? A systematic review. *Front Neurol*, 14: 1207626.

YALDIZLI Ö, ATEFY R, GASS A, STURM D, GLASSL S, TETTENBORN B, PUTZKI N (2010) Corpus callosum index and long-term disability in multiple sclerosis patients. *J Neurol*, 257: 1256-1264.

ZHAO Z, LI T, DONG X, WANG X, ZHANG Z, ZHAO C, KANG X, ZHENG R, LI X (2021) Untargeted metabolomic profiling of cuprizone-induced demyelination in mouse corpus callosum by UPLC-orbitrap/ms reveals potential metabolic biomarkers of CNS demyelination disorders. *Oxid Med Cell Longev*, 2021: 7093844.

ZHENG F, LI Y, ZHUO Z, DUAN Y, CAO G, TIAN D, ZHANG X, LI K, ZHOU F, HUANG M (2022) Structural and functional hippocampal alterations in multiple sclerosis and neuromyelitis optica spectrum disorder. *Mult Scler J*, 28: 707-717.

Variations in pelvic floor thickness in relation to bony dimensions in South African women: using computed tomography scans

Ruth Kobedi[1], Suvasha Jagesur[1], Zeelha Abdool[2], Jacobus Oettlé[1], Anna C. Oettlé[1]

[1] *Department of Anatomy and Histology, Sefako Makgatho Health Sciences University (SA)*

[2] *Department of Obstetrics and Gynaecology, University of Pretoria (SA)*

SUMMARY

Pelvic floor disorders (PFDs) are a common reason for urogynaecological consultation around the world, especially in elderly women. These disorders have been associated with disruption to the structural integrity of the pelvic floor. This study explored whether there are variations in pelvic floor muscle (PFM) thickness in relation to parity, population group and age. Additionally, the study explored whether there were any correlations between PFM thickness and the bony pelvic parameters measured. This was a quantitative retrospective analysis of computerised tomography (CT) scans. A total of 125 CT scans of women belonging to black and white South African population groups were sampled from a tertiary hospital in Pretoria, South Africa. Statistical analyses were performed using Paleontological Statistics (PAST). A thicker pelvic floor was noted in black compared to white women. Pelvic floor thickness decreased with parity and age in both population groups. The intertuberous diameter, as well as the surface areas of the urogenital triangle and the perineum, were statistically significantly larger in white than in black women. Correlations between PFM thickness and bony dimensions were statistically significant for anteroposterior (AP) pelvic outlet diameter, where a greater AP outlet was associated with thinner PFMs in black women. Bony correlations with parity showed that the interspinous diameter in black women increased significantly with parity. The variations in bony pelvic dimensions and pelvic floor muscle thicknesses noted between population groups, in addition to the co-factors of parity and aging, will contribute to a better understanding of the anatomical reasons for incontinence.

Key words: Bony pelvic outlet – Clinical anatomy – Obstetrics and gynaecology – Pelvic floor – Pelvic floor disorders

INTRODUCTION

The pelvic floor is functionally important for the support of pelvic organs (García del Salto et al., 2014; Muro et al., 2024), as well as the maintenance of faecal and urinary continence (Miller et al., 2010; Betschart et al., 2014). Studies have shown that thicker pelvic floor muscles are relat-

Shared corresponding authors:
Ruth Kobedi. Department of Anatomy and Histology, Room 110, BMS Building, Sefako Makgatho Health Sciences University, Molotlegi Street, Ga-Rankuwa Pretoria, Gauteng, PO Box 232, Medunsa, 0204, South Africa. Phone: +2778 2977 289. E-mail: deekobedi@gmail.com

Submitted: December 27, 2023. **Accepted:** March 1, 2024

https://doi.org/10.52083/LDQK3229

ed to stronger muscle strength and, consequently, stronger pelvic support (Brækken et al., 2010, 2014). Weakness of these supporting structures may lead to pelvic floor disorders (PFDs) such as pelvic organ prolapse, faecal and urinary incontinence (Fielding, 2008; Dufour et al., 2018; Law and Blomquist et al., 2020). The integrity of pelvic floor support structures has been found to be influenced by various factors such as age (Wente and Dolan, 2018), parity (Özdemır et al., 2015; Hwang et al., 2019) and population group (Handa et al., 2008).

Anatomical variations in the dimensions of the bony pelvic outlet linked to the incidence of PFDs have been reported (Handa et al., 2008). These variations have been noted between different population groups: white American compared with African American women (Handa et al., 2008) and between South African (SA) white compared with SA black women (Jagesur, 2022). These bony dimensions include subpubic angles, interspinous diameters and the anteroposterior (AP) pelvic outlet. The subpubic angles and interspinous diameters were reportedly greater in white SA when compared to black SA women (Jagesur et al., 2017) and in white American when compared to African American women (Handa et al., 2008). The AP pelvic outlet distance was smaller in white SA compared to black SA women (Jagesur et al., 2017) and in white American compared to African American women (Handa et al., 2008).

Other population variations contributing to the pathophysiology of PFDs have been reported. A study by Abdool et al. (2017) reported that there exist significant variations in levator hiatal area and pelvic organ mobility between South Asian, Black and those from western European ancestry, where black nulliparous women showed increased levator hiatal dimensions and pelvic organ mobility compared with other population groups. They also observed significant variations between populations in stages of pelvic organ prolapse, where South Asians had a lower levator ani avulsion rate than the other two population groups. This is the first study evaluating bony pelvic dimensions versus pelvic floor muscle thickness between population groups.

This study aimed to explore whether there is an association between bony pelvic outlet dimensions and the thickness of the pelvic floor, and to ascertain whether there is any variation with co-factors (age, population group or parity). Population group assignment was based on the patient's surname (Morales, 2021) and verified by photo identification, as population group is not routinely collected and was therefore not available in retrospective records. These relationships were investigated using computerised tomography (CT) scans. Computerised tomography scans have been reported to be sufficient for the illustration of pelvic floor anatomy (Jorge and Bustamante-Lopez, 2022).

The results of this study are envisaged to provide crucial information towards a better understanding of the morphological factors influencing PFDs such as skeletal and muscular factors, with reference to parity, population group and aging.

MATERIALS AND METHODS

A total of 125 retrospectively collected pelvic CT scans of female patients were sampled from Steve Biko Academic Hospital, a tertiary hospital in Pretoria, South Africa. The sample was distributed according to parity and population group: 75 SA black women (28 nulliparous, 47 multiparous) and 50 SA white women (10 nulliparous, 40 multiparous). Parity subgroups were also considered where the sample was further categorised based on the number of children they had. The ages of women included in the study ranged between 18 years and 90 years. Patients that demonstrated any pelvic pathology, surgical alteration, skeletal abnormality or deformity were excluded.

Mevislab software (Heckel et al., 2009) was used to create 3D models of the imported CT scan data and to capture 3D points. The bony landmarks used for the parameters of interest were: tips of the ischial spine left (IS_L) and ischial spine right (IS_R), most inferior points of the ischial tuberosity left (IT_L) and ischial tuberosity right (IT_R), mid-ischiopubic ramus left (MIP_L) and mid-ischiopubic ramus right (MIP_R), pubic symphysis (PS), as well as the coccyx (C). The bony parameters that were measured were: 1) interspinous diameter between IS_L and IS_R; 2) intertuberous diameter between IT_L and IT_R; 3) subpubic angle (angle of

Fig. 1.- Horizontal section of computerised tomography (CT) scan showing pelvic floor muscle at the level of the urethra.

the subpubic arch), angle formed at inferior point of PS between MIP_L and MIP_R; 4) antero-posterior pelvic outlet (AP outlet), distance between the most inferior PS and tip of coccyx; 5) urogenital triangle, formed between PS and intertuberous diameter and lastly, 6) perineum, formed between PS and intertuberous diameter and tip of coccyx.

Distances between two 3D landmarks ($x_1y_1z_1$ and $x_2y_2z_2$) were calculated using the Pythagorean theorem (Katherine-Spradley and Jantz, 2016):

$$distance = \sqrt{(x_2 - x_1)^2 + (y_2 - y_1)^2 + (z_2 - z_1)^2}$$

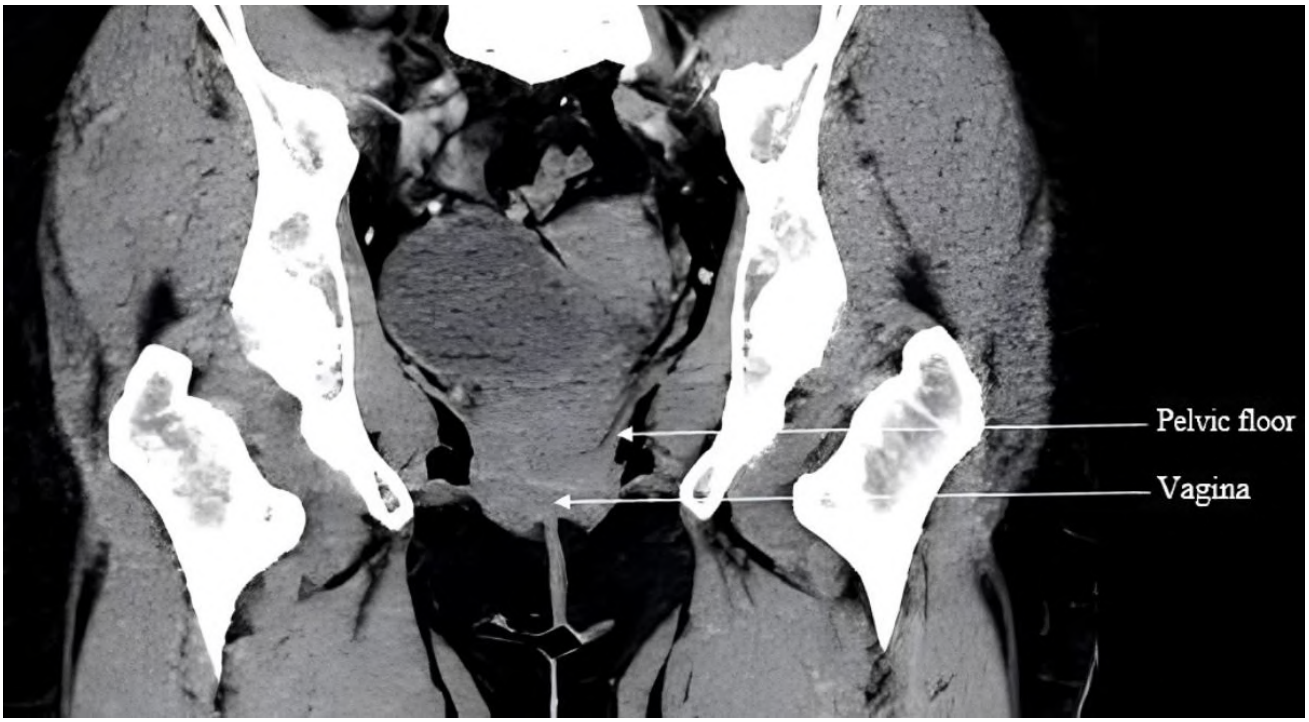

Fig. 2.- Coronal section of computerised tomography (CT) scan showing pelvic floor muscle at the level of the vagina.

The dot product formula (see annexure A1) was used to determine the angle between three 3D landmarks ($x_3y_3z_3$, $x_2y_2z_2$ and $x_1y_1z_1$) (Dumas, 2008). The surface area of the perineum was calculated as a composite of the urogenital triangle and the anal triangle, using the cross-product formula (Kuchel et al., 2021) (see annexure A2).

The thicknesses of the pelvic floor muscles from the CT scans were measured on Mevislab software (in millimetres). On a horizontal section, the thicknesses were measured at the level of the urethra (Fig. 1) and coronally at the level of the vagina (Fig. 2). The measurements were taken perpendicularly at the shortest distance across.

Statistical analyses were performed using Paleontological Statistics (PAST) (Hammer et al., 2001). Firstly, descriptive analysis was performed on all data, after which tests for normality were performed. To determine the extent of variation between groups, ANOVA, followed by Tukey's pairwise tests, were performed when samples were normally distributed, while the non-paramet-

Table 1. Univariate analysis of bony dimensions and pelvic floor thicknesses and statistical significance between group comparisons.

	Interspinous diameter (mm)	Intertuberous diameter (mm)	AP pelvic outlet (mm)	Subpubic angle (°)	Urogenital triangle mm²	Perineum mm²	Left Axial thickness (mm)	Left coronal thickness (mm)
SAB N = 75	**109.67** *8.49* (74.60-135.26)	**123.55**[a] *10.88* (95.13-152.91)	**112.04** *11.60* (80.83-139.17)	**89.49** *7.32* (75.25-106.38)	**3847.97**[a] *514.11* (2429.30-4966.13)	**8117.65**[a] *1113.74* (4562.81-11040.18)	**4.87**[a] *0.91* (3.05-6.97)	**4.92**[a] *0.93* (3.22-7.28)
SAB0 N = 28	**107.34**[a] *9.21* (74.60-120.16)	**124.02**[b] *12.53* (95.13-144.29)	**108.44** *13.00* (80.83-131.83)	**90.82** *6.16* (79.75-103.81)	**3784.06**[b] *555.1545* (2429.298-4860.127)	**7956.71**[b] *1237.86* (4562.81-9652.97)	**5.53**[bcdefg] *0.78* (4.13-6.97)	**5.56**[bcdef] *0.78* (4.11-7.27)
SABm N=47	**111.06** *7.80* (97.30-135.26)	**123.26**[c] *9.90* (99.84-152.91)	**114.19** *10.24* (94.21-139.17)	**88.70** *7.90* (75.25-106.38)	**3886.05**[c] *490.227* (2827.993-4966.135)	**8213.53** *1034.86* (5984.05-11040.18)	**4.47**[bh] *0.74* (3.05-6.54)	**4.53**[bg] *0.79* (3.22-7.12)
SAB1,2 N = 16	**109.13**[b] *6.12* (98.61-120.95)	**122.96** *8.50* (110.46-135.56)	**114.44** *8.55* (98.82-128.08)	**90.03** *9.67* (78.53-106.38)	**3774.92** *374.546* (2997.42-4500.33)	**8213.02** *810.46* (6822.81-9720.46)	**4.94**[eij] *0.72* (3.98-6.54)	**4.95**[h] *0.82* (3.90-7.12)
SAB3 N=16	**109.05**[c] *5.86* (98.98-116.51)	**123.10** *6.27* (110.69-132.00)	**111.69** *7.35* (94.21-125.74)	**87.33** *6.30* (77.36-99.56)	**3969.08** *364.75* (3345.67-4576.31)	**8051.32** *661.13* (6892.30-9123.76)	**4.35**[fi] *0.57* (3.55-5.54)	**4.38**[e] *0.67* (3.22-5.79)
SAB4+ N=15	**115.28**[abc] *9.75* (97.30-135.26)	**123.75** *14.21* (99.84-152.91)	**116.59** *13.97* (96.96-139.17)	**88.75** *7.60* (75.23-103.66)	**3916.03** *688.35* (2827.99-4966.14)	**8387.11** *1511.41* (5984.05-11040.18)	**4.11**[gj] *0.71* (3.05-5.91)	**4.24**[fh] *0.73* (3.23-5.79)
SAW N = 50	**109.36** *12.14* (48.32-135.05)	**130.37**[a] *17.32* (48.32-161.33)	**111.93** *11.58* (83.18-141.42)	**91.44** *6.97* (76.22-106.72)	**4213.07**[a] *604.39* (3084.10-5737.72)	**8739.8**[a] *1283.25* (6409.77-12160.12)	**3.52**[a] *0.94* (1.90-5.64)	**3.56**[a] *0.91* (1.88-5.22)
SAW0 N = 10	**106.51** *7.79* (95.44-117.56)	**128.70** *16.02* (109.93-161.33)	**108.03** *13.37* (92.84-129.35)	**93.63** *6.65* (85.13-106.72)	**3850.32**[d] *603.2742* (3146.752-4938.189)	**8466.29** *1672.08* (6816.48-12160.12)	**4.33**[cqklm] *0.56* (3.10-4.94)	**4.38**[cijk] *0.56* (3.12-5.00)
SAWm N=40	**109.36** *12.14* (48.32-135.05)	**130.37**[b,c] *17.32* (48.32-161.33)	**111.93** *11.58* (83.18-141.42)	**91.44** *6.97* (76.22-106.72)	**4303.76**[b,c,d] *576.8728* (3084.103-5737.716)	**8808.19**[b] *1183.13* (6409.77-11149.50)	**3.10**[dhq] *0.84* (1.90-5.00)	**3.15**[dgi] *0.82* (1.88-5.22)
SAW1,2 N= 21	**112.16** *10.50* (96.61-135.05)	**132.34** *13.22* (105.45-158.21)	**114.61** *9.25* (83.18-127.02)	**90.72** *7.56* (76.22-105.68)	**4312.68** *627.01* (3398.95-90566.25)	**8984.55** *1265.06* (6409.77-11149.50)	**3.69**[kno] *0.86* (2.23-5.64)	**3.78**[lm] *0.77* (2.88-5.22)
SAW3 N=11	**109.61** *6.12* (101.76-122.59)	**133.19** *12.48* (116.92-155.12)	**104.52** *9.52* (92.158-122.90)	**91.46** *7.24* (80.14-102.64)	**4319.39** *545.50* (3084.10-47513.23)	**8425.05** *1225.32* (6799.88-10966.95)	**3.01**[ln] *0.79* (2.00-5.00)	**2.98**[jl] *0.81* (1.86-4.90)
SAW4+ N= 8	**112.16** *3.59* (106.59-117.43)	**131.12** *10.89* (115.27-152.39)	**113.87** *11.29* (99.87-127.42)	**90.56** *6.01* (80.35-99.22)	**4258.87** *550.2753* (3651.93-5143.51)	**8872.06** *867.63* (7327.91-10062.64)	**2.74**[mo] *0.77* (1.90-4.01)	**2.93**[km] *0.62* (2.01-4.00)

Alphabet letters in the superscript indicate statistical significant differences (p value < 0.05) between groups per column

number of women = N; mean values are indicated in bold standard deviation is indicated in *italics*; range is shown within the round (brackets)

SAB refers to South African Black women and SAW refers to South African white women, the number following refers to the number of live births and *m* refers to multiparous

ric test, Kruskal-Wallis, followed by Mann Whitney test were performed when samples were not normally distributed (Neideen and Brasel, 2007). Comparisons between black and white women, between nulliparous versus multiparous, as well as between stepwise parity groups within population groups were performed. This was followed by correlations between continuous variables, i.e. the bony dimensions versus the pelvic floor thicknesses, and age versus the pelvic floor thicknesses. A Pearson's correlation coefficient r was determined, where a value of +1 indicates perfect positive association and a value of –1 indicates perfect negative association, while a value of 0 indicates no linear association (Schober et al., 2018).

Intra- and inter-observer tests for measurement accuracy were run by two observers. Twenty individuals were randomly selected from the entire sample, and analysed twice by the principal researcher in order to assess the intra-observer reliability and once by co-author, SJ, for the inter-observer reliability. Intraclass correlations were performed on the analysis of these 20 cases.

RESULTS

The mean age in years for the entire sample was 51.35 ± 15.44. The mean parity for the entire sample was 1.95 ± 1.72. The mean age in years and mean parity in black women were 47.87 ± 14.78 and 1.92 ± 1.87, respectively, while the mean values for age in years and parity in the white women were 56.58 ± 15.06 and 2 ± 1.48, respectively.

For each patient, the pelvic floor muscle thickness was measured on both the left and right sides (for both the axial and coronal sections). As the data had a normal distribution, ANOVA tests were performed between left and right sides and no statistically significant differences between sides were observed (left axial versus right axial, p = 0,804; left coronal versus right coronal, p = 0,909). The measurements for the left side of the pelvic floor are tabulated in Table 1 (since there were no statistically significant differences between the left and right sides). Intraclass correlation coefficients (r) for intraobserver and interobsever repeatability approached 1, indicating excellent agreement for all the measurements taken on the left side (Table 2).

Table 2. Intraclass correlation coefficients.

Parameters	Intraobserver repeatability	Interobserver repeatability
Interspinous diameter	0.992	0.940
Intertuberous diameter	0.961	0.910
AP pelvic outlet	0.966	0.925
Subpubic angle	0.988	0.930
Urogenital triangle	0.993	0.937
Perineum	0.952	0.981
Left Axial thickness	0.981	0.976
Left coronal thickness	0.993	0.989

A1:

$$angle = \cos^{-1}\left(\frac{(x_2 - x_1)(x_3 - x_1) + (y_2 - y_1)(y_3 - y_1) + (z_2 - z_1)(z_3 - z_1)}{\left(\sqrt{(x_2 - x_1)^2 + (y_2 - y_1)^2 + (z_2 - z_1)^2}\right)\left(\sqrt{(x_3 - x_1)^2 + (y_3 - y_1)^2 + (z_3 - z_1)^2}\right)}\right)$$

A2:

$$area = \frac{\sqrt{((y_2 - y_1)(z_3 - z_1) - (z_2 - z_1)(y_3 - y_1))^2 + ((z_2 - z_1)(x_3 - x_1) - (x_2 - x_1)(z_3 - z_1))^2 + ((x_2 - x_1)(y_3 - y_1) - (y_2 - y_1)(x_3 - x_1))^2}}{2}$$

Annexure A1 y A2

Table 1 describes the comparison between population groups, bony pelvic outlet and pelvic floor thickness measurements. Alphabet letters in the superscript indicate statistically significant differences (p-value < 0.05) between groups per column. The intertuberous diameter, as well as the surface area of the urogenital triangle and the perineum, were statistically significantly larger (p: 0.0003; p: 0.0004 and p: 0.0047 respectively) in the entire sample of white women (N=50) compared to black women (N=75). The subpubic angle was larger in white women, while the interspinous and AP outlet diameters were larger in black women but they did not reach statistical significance.

When considering the stepwise parity groups as set out in Table 1, the bony dimensions (interspinous diameter, AP outlet diameter, surface areas of urogenital triangle and perineum) increased slightly with increasing parity in both population groups, and were statistically significant when considering the interspinous diameter in black women.

Comparative analyses showed statistically significantly thinner pelvic floor measurements (p< 0.0001) in white when compared to black women throughout, as indicated by the superscript [a] in the last two columns of Table 1.

The black nulliparous women (SAB0 on Table 1) displayed statistically significant thicker mean values for the pelvic floor muscles than white nulliparous women (SAW0). The black multiparous women (SAB*m*) displayed statistically significant thicker mean values for the pelvic floor muscles when compared to white multiparous women (SAW*m*). Pelvic floor thinning was observed as parity increased in the stepwise population group comparisons (became thinner with increasing parity in both population groups) and many of these comparisons were statistically significant (see Table 1).

Ordinary least square regressions performed between pelvic floor thickness and age showed that the thickness of the pelvic floor decreased with age in nulliparous women of both population groups, even though age correlations within the white nulliparous group were not significant. The pelvic floor also became significantly thinner with increasing age in multiparous women of both population groups. Hard tissue correlations with the PFM thickness were not significant, except PFM correlations with AP pelvic outlet and surface area of the perineum. Weak, but statistically significant negative relationships for the entire sample of black women were noted when correlating the AP pelvic outlet dimensions with the pelvic floor thickness on both the coronal and horizontal sections. Significant but negative correlation was noted in the small group of eight white women who had given birth to four or more live babies when correlating the surface area of the perineum with the coronal section of the pelvic floor.

DISCUSSION

Main findings and interpretation (in light of other evidence)

Despite the fact that population group was not indicated in the patient's records and assignments were based on surnames and photographic identification, very clear population group variations were noted in the measurements taken. The trends observed in the variations of the bony dimensions include a longer AP outlet diameter in the entire sample of black women when compared to the entire sample of white women, as well as a greater surface area of the urogenital triangle and the perineum, subpubic angle and the intertuberous diameter in the entire sample of white women than in the entire sample of black women. The only significant observations were those of the intertuberous diameter, as well as the surface areas of the urogenital triangle and the perineum. Similar findings were reported in African- American versus white-American women concerning the AP pelvic outlet diameter (Handa et al., 2008).

These variations in the pelvic diameters between population groups were not entirely unexpected (Jagesur, 2022). It is well known that populations who originated in colder climates, as noted in the white South African population group in this study, have relatively wider pelves in order to reduce heat loss. Narrower pelves associated with populations that originated in tropical climates, as

noted in black South Africans, would help reduce heat stress (Weaver and Hublin 2009; Sharma et al., 2016). The variation in the shape of the pelvis reflects genetic diversity based on ancient demographic events, as explained by neutral phenotypic evolution and are therefore useful in population history (Stull et al., 2014; Betti, 2017).

This was the first study to evaluate relationships between pelvic floor muscle thickness and pelvic bony dimensions, and between population groups with respect to the effect of age and parity on the measurements. Variations in the bony dimensions based on parity have been noted in an older study (Russell, 1969). For instance, similar to our study, the interspinous diameter increased with parity in a study performed by Russell (1969); however, the population group was not specified in their study. The mechanism of this increase was explained by the backward movement of the lower part of the sacroiliac joint occurring during childbirth, consequently leading to a separation of the ischial spines.

White American women have been reported to be at a higher risk for pelvic floor disorders (PFDs) compared to African American women (Graham and Mallett, 2001). Increased risk for PFDs could be explained by the observed thinner pelvic floor in white women as compared to African American women (Hoyte et al., 2005), as also noted in our groups, since thinner pelvic floors have been associated with weakness and as such, may be more susceptible to PFDs (Brækken et al., 2010, 2014;).

The thinning of the pelvic floor with increasing parity (Özdemır et al., 2015) and aging (Alperin et al., 2016) has been documented. In the stepwise population group comparisons, we observed that the pelvic floor became thinner with increasing parity in both population groups where many of these comparisons were statistically significant. Possible mechanisms influencing the thinning of the pelvic floor with parity may be explained by micro-architectural distortion of the pelvic floor muscles and elevated intra-abdominal pressure experienced by the pelvic floor during pregnancy and labour (Mørkved et al., 2004). It is plausible that vaginal birth might, over time, have an effect on the pelvic floor and might therefore not be distinguishable from the effect that aging would have. In our study, nulliparous groups in both population groups demonstrated a thinning of the pelvic floor with aging. This, however, was not significant in white nulliparous women, perhaps due to the small sample number (N=10).

Although no studies were found which directly correlated the pelvic bony dimensions measured with pelvic floor thicknesses, greater dimensions of interspinous and intertuberous diameters, subpubic angles, as well as smaller dimensions in AP pelvic outlets were reportedly associated with PFDs (Handa et al., 2003). In our study, increasing AP pelvic outlet diameter was associated with thinner PFMs (in the entire group of black women). A possibility exists that the increased risk for PFDs noted when certain pelvic dimensions were increased could be linked to population group differences in pelvic dimensions rather than the differences in the dimensions themselves. For instance, a greater intertuberous dimension as noted in the white population group may be associated with an increased chance for PFD, while a greater AP outlet dimension as noted in the black population group may be associated with a smaller risk for PFD. Finally, South African white women may be particularly disadvantaged early on for possible PFDs, as they have greater bony dimensions and thinner pelvic floors, compounded by structural distortion of pelvic floor musculature by childbirth and aging.

Limitations

Possible limitations of this study are the factors that could have contributed to the variations in the pelvic floor thicknesses other than those noted with parity, population group and aging. These factors include the type of childbirth (vaginal or caesarean), body mass index (BMI), patient involvement in high impact physical activity or genetic factors. None of these factors were known in this retrospectively studied scan sample. It is crucial to recognise that the findings of this study, which are derived from Black and White patients at a Pretoria hospital, should be interpreted with an awareness that interethnic differences may exist in other regions of South Africa and beyond (Sapo, 2021).

CONCLUSION

This study has demonstrated that there exist population group variations between pelvic floor thickness and bony pelvic dimensions, in addition to the co-factors of age and parity. Black nulliparous women displayed statistically significant thicker mean values for the pelvic floor muscles than white nulliparous women. Ordinary least square regressions performed between pelvic floor thickness and age showed that pelvic floor thickness decreased with age in nulliparous women of both population groups, although age correlations within the white nulliparous group were not significant. The intertuberous diameter, as well as the surface area of the urogenital triangle and the perineum were statistically significantly greater in the entire sample of white women compared to black women. Bony correlations with parity were significant for the interspinous diameter, which increased with parity in black women. Bony pelvic correlations with pelvic floor muscle thickness were significant for AP pelvic outlet, where the increasing diameter of the AP pelvic outlet was associated with thinner PFMs in the entire sample of black women. It is therefore important in clinical practice to consider the variations noted in pelvic bony dimensions and pelvic floor muscles between women of varying populations groups, ages and parity in association to pelvic floor disorders. These conditions affect quality of lives, and therefore better understanding of mechanisms involved can lead to advancement of treatment options or even prevention where possible. The results of this study add to the paucity of data on the effect of population group on pelvic floor morphology.

Recommendations

Future research using greater sample sizes could confirm or disprove the non-significant relationships noted. Data where the mode of childbirth is known, e.g. vaginal or caesarean section, could be helpful to ascertain whether mode of delivery has any effect on the bony dimensions and the thickness of the pelvic floor.

Details of ethics approval

This study was approved by the University of Pretoria (UP) as well as the National Health Research Database (NHRD) and finally by Sefako Makgatho Health Sciences University (SMU). Reference number: 54/2020. Committee: University of Pretoria Faculty of Health Sciences Research Ethics Committee. Approval date: 24 March 2020.

NHRD: Reference number: GP_202005_037. Committee: Steve Biko Hospital Research Committee. Approval date: 05 June 2020.

SMU: Reference number: SMUREC/M/326/2020. Committees: Sefako Makgatho University Research Ethics Committee (SMUREC). Approval date: 14 December 2020.

ACKNOWLEDGEMENTS

Institutions: Sefako Makgatho Health Sciences University, University of Pretoria, Steve Biko Academic Hospital. Thanks to anonymous patients who made this study possible. Mrs HF Swanepoel for providing Mevislab training. Prof Z Lockhat (Head of Department, Radiology, Steve Biko Academic Hospital) for granting permission to the CT scan data. Staff of Steve Biko Academic Hospital who assisted with the retrieval of patient records.

Funding: National Research Fund (NRF) and Bakeng se Afrika project 597924-EPP-1- 2018-1-ZA-EPPKA2-CBHE-JP, an Erasmus plus project of the EU.

REFERENCES

ABDOOL Z, DIETZ HP, LINDEQUE BG (2017) Ethnic differences in the levator hiatus and pelvic organ descent: a prospective observational study. *Ultrasound Obstet Gynecol*, 50(2): 242-246.

ALPERIN M, COOK M, TUTTLE LJ (2016) Impact of vaginal parity and aging on the architectural design of pelvic floor muscles. *Am J Obstet Gynecol*, 215(3): 312.e1-9.

BETTI L (2017) Human variation in pelvic shape and the effects of climate and past population history. *Anat Rec*, 300(4): 687-697.

BETSCHART C, KIM J, MILLER JM (2014) Comparison of muscle fiber directions between different levator ani muscle subdivisions: in vivo MRI measurements in women. *Int Urogynecol J*, 25: 1263-1268.

BLOMQUIST JL, CARROLL M, MUÑOZ A, HANDA VL (2020) Pelvic floor muscle strength and the incidence of pelvic floor disorders after vaginal and cesarean delivery. *Am J Obstet Gynecol*, 222(1): 62.e1-62.e8.

BRÆKKEN IH, MAJIDA M, ENGH ME (2010) Morphological changes after pelvic floor muscle training measured by 3-dimensional ultrasonography: a randomized controlled trial. *Obstet Gynecol*, 115(2 Part 1): 317-324.

BRÆKKEN IH, MAJIDA M, ENGH ME (2014) Are pelvic floor muscle thickness and size of levator hiatus associated with pelvic floor muscle strength, endurance and vaginal resting pressure in women with pelvic organ prolapse stages I–III? A cross sectional 3D ultrasound study. *Neurourol Urodynamics*, 33: 115-120.

DUFOUR S, HONDRONICOLS A, FLANIGAN K (2018) Conservative primary care of urinary incontinence and pelvic organ prolapse in primary health care. *Ann Reprod Med Treat*, 3(1): 1020.

DUMAS R (2008) Hip and knee joints are more stabilized than driven during the stance phase of gait: an analysis of the 3D angle between joint moment and joint angular velocity. *Gait Posture*, 28(2): 243-250.

GARCÍA DEL SALTO L, DE MIGUEL CRIADO J, AGUILERA DEL HOYO LF (2014) MR imaging based assessment of the female pelvic floor. *Radiographics*, 34(5): 1417-1439.

GRAHAM CA, MALLETT VT (2001) Race as a predictor of urinary incontinence and pelvic organ prolapse. *Obstet Gynecol*, 185(1): 116-120.

HAMMER Ø, HARPER DA, RYAN PD (2001) PAST: Paleontological statistics software package for education and data analysis. *Palaeontologia electronica.*

HANDA VL, PANNU HK, SIDDIQUE S, GUTMAN R, VANROOYEN J, CUNDIFF G (2003) Architectural differences in the bony pelvis of women with and without pelvic floor disorders. *Obstet Gynecol*, 102(6): 1283-1290.

HANDA VL, LOCKHART ME, FIELDING JR, BRADLEY CS, BRUBAKER L, CUNDIFF GW, YE W, RICHTER HE (2008) Racial differences in pelvic anatomy by magnetic resonance imaging. *Obstet Gynecol*, 111(4): 914-920.

HECKEL F, SCHWIER M, PEITGEN HO (2009) Object-oriented application development with MeVisLab and Python. *Informatik*, 154: 1338-1351.

HOYTE L, THOMAS J, FOSTER RT, SHOTT S, JAKAB M, WEIDNER AC (2005) Racial differences in pelvic morphology among asymptomatic nulliparous women as seen on three-dimensional magnetic resonance images. *Am J Obstet Gynecol*, 193(6): 2035-2040.

HWANG JY, KIM BI, SONG SH (2019) Parity: a risk factor for decreased pelvic floor muscle strength and endurance in middle-aged women. *Int Urogynecol J*, 30: 933-938.

JAGESUR S (2022) Variations in pelvic canal and skull dimensions in South Africans: possible relationships and implications (Doctoral dissertation, University of Pretoria).

JAGESUR S, WIID A, PRETORIUS S, BOSMAN MC, OETTLE AC (2017) Assessment of the variability in the dimensions of the intact pelvic canal in South Africans: A pilot study. *J Homo Comp Human Biol*, 68(1): 30-37.

JORGE JMN, BUSTAMANTE-LOPEZ LA (2022) Pelvic floor anatomy. *Ann Laparosc Endosc Surg*, 7: 20.

KATHERINE-SPRADLEY M, JANTZ RL (2016) Ancestry estimation in forensic anthropology: geometric morphometric versus standard and nonstandard interlandmark distances. *J Forensic Sci*, 61(4): 892-897.

KUCHEL PW, COX CD, DANERS D (2021) Surface model of the human red blood cell simulating changes in membrane curvature under strain. *Sci Rep*, 11(1): 1-18.

LAW YM, FIELDING JR (2008) MRI of pelvic floor dysfunction. *Am J Roentgenol*, 191 Suppl 6: 45-53.

MILLER JM, BRANDON C, JACOBSON JA, LOW LK, ZIELINSKI R, ASHTON-MILLER J, DELANCEY JOL (2010) MRI findings in patients considered high risk for pelvic floor injury studied serially post vaginal childbirth. *Am J Roentgenol*, 195(3): 786-791.

MØRKVED S, SALVESEN KÅ, BØ K, EIK-NES S (2004) Pelvic floor muscle strength and thickness in continent and incontinent nulliparous pregnant women. *Int Urogynecol J*, 15(6): 384-390.

MURO S, MOUE S, AKITA K (2024) Twisted orientation of the muscle bundles in the levator ani functional parts in women: Implications for pelvic floor support mechanism. *J Anat*, 244(3): 486-496.

NEIDEEN T, BRASEL K (2007) Understanding statistical tests. *J Surg Educ*, 64(2): 93-96.

ÖZDEMIR ÖÇ, BAKAR Y, ÖZENGIN N, DURAN B (2015) The effect of parity on pelvic floor muscle strength and quality of life in women with urinary incontinence: a cross sectional study. *J Phys Ther Sci*, 27(7): 2133-2137.

RUSSELL JG (1969) Moulding of the pelvic outlet. *Int J Obstet Gynaecol*, 76(9): 817-820.

SAPO O (2021) Estimating ancestry among South African ethnic groups (Masters dissertation, University of Pretoria).

SCHOBER P, BOER C, SCHWARTE LA (2018) Correlation coefficients: appropriate use and interpretation. *Anesth Analg*, 126(5): 1763-1768.

SHARMA K, GUPTA P, SHANDILYA S (2016) Age related changes in pelvis size among adolescent and adult females with reference to parturition from Naraingarh, Haryana (India). *Homo*, 67(4): 273-293.

STULL KE, KENYHERCZ MW, L'ABBÉ EN (2014) Ancestry estimation in South Africa using craniometrics and geometric morphometrics. *Forensic Sci Int*, 245: 206.e1-7.

WEAVER TD, HUBLIN JJ (2009) Neandertal birth canal shape and the evolution of human childbirth. *Proc Natl Acad Sci*, 106(20): 8151-8156.

WENTE K, DOLAN C (2018) Aging and the pelvic floor. *Curr Geriat Rep*, 7: 49-58.

Unilateral optic nerve aplasia associated with microphthalmia: a rare cadaveric report

Arthur T. Manjatika[1,2], Joshua G. Davimes[1], Erin F. Hutchinson[1], Amadi O. Ihunwo[1]

[1] *School of Anatomical Sciences, University of the Witwatersrand, Parktown, Johannesburg, South Africa*

[2] *School of Life Sciences and Allied Health Professions, Anatomy Division, Kamuzu University of Health Sciences, Blantyre, Malawi*

SUMMARY

This case report describes the anatomical presentation of the anomalous optic nerve (cranial nerve II). Cranial nerve II developmental anomalies encompass both optic nerve hypoplasia and aplasia. While most studies on optic nerve anomalies rely on radiological imaging, anatomical presentation and nerve course are rarely described. The current case reveals a complete absence of the right optic nerve and its connection to the optic chiasma, resembling radiological presentation of optic nerve aplasia. In addition, the right-sided bony orbit and eyeball were smaller than the left, accompanied by a poorly developed cornea and iris with a calcified mass, resembling clinical presentation of microphthalmia. Having a thorough understanding of the gross anatomical presentation and course of optic nerve anomalies can facilitate precise diagnosis and management of visual impairments associated with these anomalies. Furthermore, such knowledge can provide valuable insights into the actual prevalence of optic nerve aplasia and further substantiate the literature.

Key words: Optic nerve aplasia – Microphthalmia – Cadaver – Anomaly

INTRODUCTION

Anomalies of the optic nerve are a significant cause of visual impairments (Taylor, 2007), and include optic nerve hypoplasia and aplasia (Margo et al., 1992). Optic nerve hypoplasia is common and presents with a smaller number of optic nerve fibres (Martín-Begué and Saint- Gerons, 2016). In contrast, optic nerve aplasia is a rare complete absence of optic nerve fibres, either unilaterally or bilaterally (Margo et al., 1992; Martín-Begué and Saint-Gerons, 2016; Taylor, 2007). Developmentally, the eye forms from the neural ectoderm, mesoderm and neural crest cells. The derivative of the neural ectoderm includes the optic nerve, retina and iris smooth muscles. The neural crest cells contribute to the formation of the stroma of the iris, ciliary muscles, choroid and vitreous part, and the endothelium and stroma of the cornea, while the mesoderm is interposed between the ectodermal tissues forming the cornea, choroid and vitreous substances, and sclera (Ohuchi et al., 2016; Taylor, 2007).

Corresponding author:
Joshua Gabriel Davimes. School of Anatomical Sciences, Faculty of Health Sciences, University of the Witwatersrand, 7 York Road, Parktown, 2193, Johannesburg, South Africa. Phone: +27 11 717 1337. E-mail: joshua.davimes@wits.ac.za - Orcid: 0000-0001-9808-5249

Submitted: December 13, 2023. **Accepted:** January 12, 2024

https://doi.org/10.52083/TRRU3034

An adult human optic nerve (cranial nerve II or CNII) is approximately 40 to 50 mm in length (Zeiss et al., 2017). CNII is a continuation of the optic tract which originates from the optic chiasma and courses about 10mm intracranially before taking an extracranial course (about 30 mm) by passing through the optic canal of the sphenoid bone to reach the posterior aspect of the eyeball to receive visual impulses from the neural retina. Developmentally, CNII is a derivative of the forebrain and, due to the complexity of the coordinated events during the development of the eye, optic nerve aplasia may be associated with other central nervous system or ocular anomalies (Martín-Begué and Saint-Gerons, 2016). The majority of these anomalies have been reported through radiological imaging studies that do not provide the comprehensive anatomical presentation and course of the anomalous optic nerve (Handley et al., 2021; Martín-Begué and Saint-Gerons, 2016; Taylor, 2007; Zhou et al., 2020). Herein, a case of unilateral optic nerve aplasia associated with microphthalmia is reported on following an incidental cadaveric dissection finding. Cadaveric dissections are exploratory in nature, and offer a comprehensive way to describe the anomalous course of any variation, an advantage that cannot be adequately achieved in living individuals when using radiological imaging studies.

CASE REPORT

This cadaveric study was conducted under the ethical clearance waiver number W-CBP- 220504-01 and was covered by the Human Tissue Act (No. 65 of 1983) and the National Health Act (No. 61 of 2003) on the use of human specimens for research and teaching purposes. During the routine dissection of the head and neck region in a female cadaver, South African of European descent, aged 52, the right eye appeared smaller and underde-

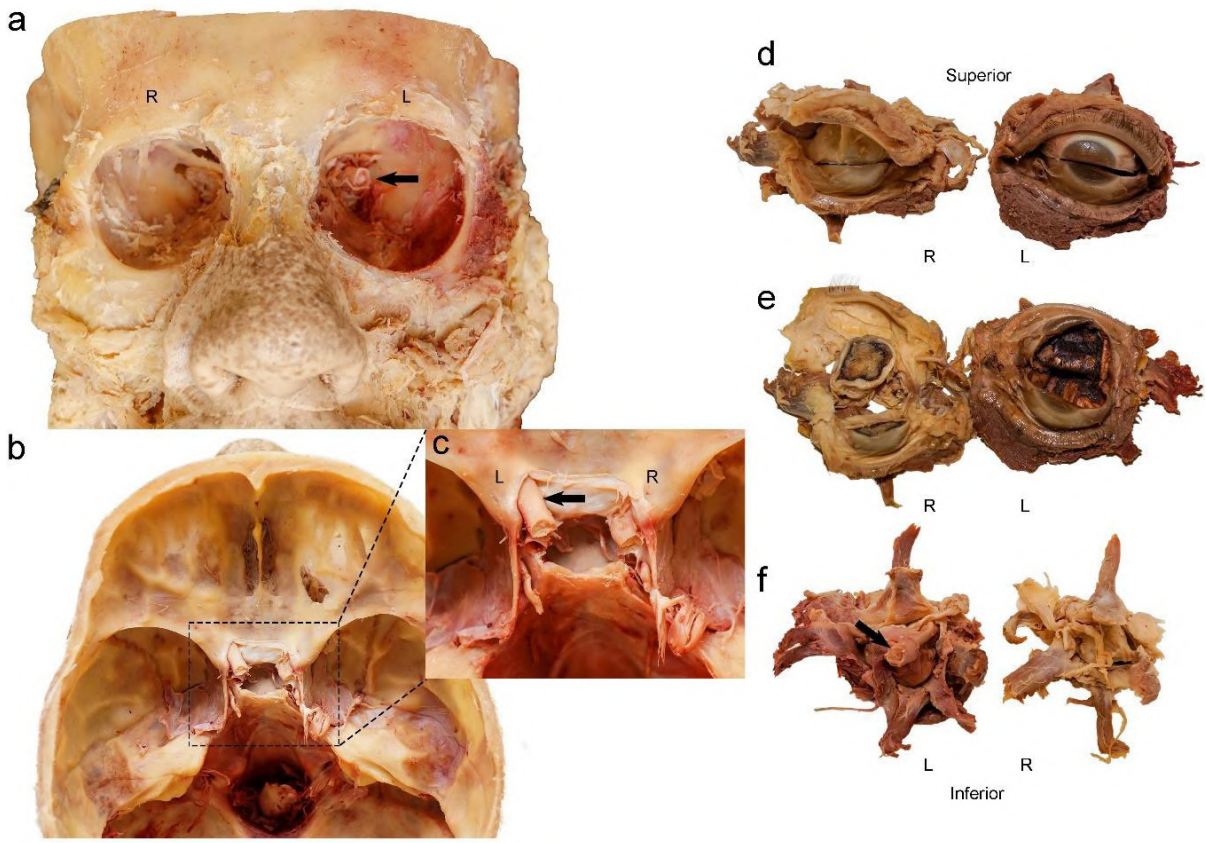

Fig. 1.- External and internal features of the skull and eyeballs. (**a**), anterior view of the skull showing a smaller right orbit and a larger left orbit, black arrow indicating the present left optic nerve. (**b**), Superior view of the intra-cranial fossa showing the central part of the mid-cranial fossa (Sella turcica) and its related structures. (**c**), Inset from b, with a magnified view showing the left optic nerve (black arrow) passing through the optic canal and the right ophthalmic artery passing through the right optic canal. (**d**), anterior view of the eyeballs, note the poorly developed cornea and iris of the right eye. (**e**), a transverse section of the eyeballs showing a calcified mass in the right eyeball and normal vitreous body and retina in the left eyeball. (**f**), posterior view of the eyeballs showing extraocular muscles, black arrow indicating left optic nerve as it enters the left eyeball, and fat and fibrous tissue on the right eyeball. R=Right side, L=Left side.

veloped when compared to the left eye. The eyes were then excised as part of the dissection protocol from the orbital sockets and inspected for abnormalities, where only the left optic nerve was present (Figs. 1 and 2). After the excision of the eyes, the brain was removed from the skull, where additional inspections of the neural tissues were conducted. These included gross inspections of the whole brain, followed by sagittal, horizontal and coronal sectioning.

In addition to a complete absence of the right optic nerve (Figs. 1 and 2), the bony orbit of the right side was smaller (orbital breadth 36.13 mm, orbital height 32.20 mm) when compared to the left (orbital breadth 40.60 mm, orbital height 36.24 mm). The right eyeball was also smaller with a poorly developed cornea and iris (Fig. 1D). A transverse section of the right eyeball showed the presence of a calcified mass covering the interior spaces, while the left eyeball presented with a normal vitreous body and retinal appearance (Fig. 1E). The right eyeball showed the presence of all, albeit grossly atrophied, extra-ocular muscles with fibrous tissue and fat occupying the central posterior part of the eyeball. The left eyeball showed the normal presence of all extra-ocular muscles with the optic nerve entering the posterior aspect centrally (Fig. 1F). The right optic canal was only patent enough for the passage of the right ophthalmic artery, while the left optic canal was intact with the left optic nerve and left ophthalmic artery passing through it (Fig. 1A-C). Both the left and right oculomotor (CN III), trochlear (CN IV) and abducens (CN VI) nerves took their normal course to supply their respective extra-ocular muscles. Visual inspection of the inferior view of the intact whole brain showed the complete absence of the right optic nerve and its connection to the optic chiasma. The right and left optic tracts originated off-centre to the left but then continued along their normal paths as the left and right optic tracts on either side of the tuber cinereum and infundibulum (Fig. 2A and B). A relatively smaller right splenium of the corpus callosum (13.68 mm, measured at widest point) compared with the left (15.17 mm) was the only noticeable difference in the midsagittal view of the brain. Horizontal and coronal brain sections showed no gross differences between the right and left side optic radiations (geniculocalcarine tracts), lateral geniculate bodies and superior colliculi.

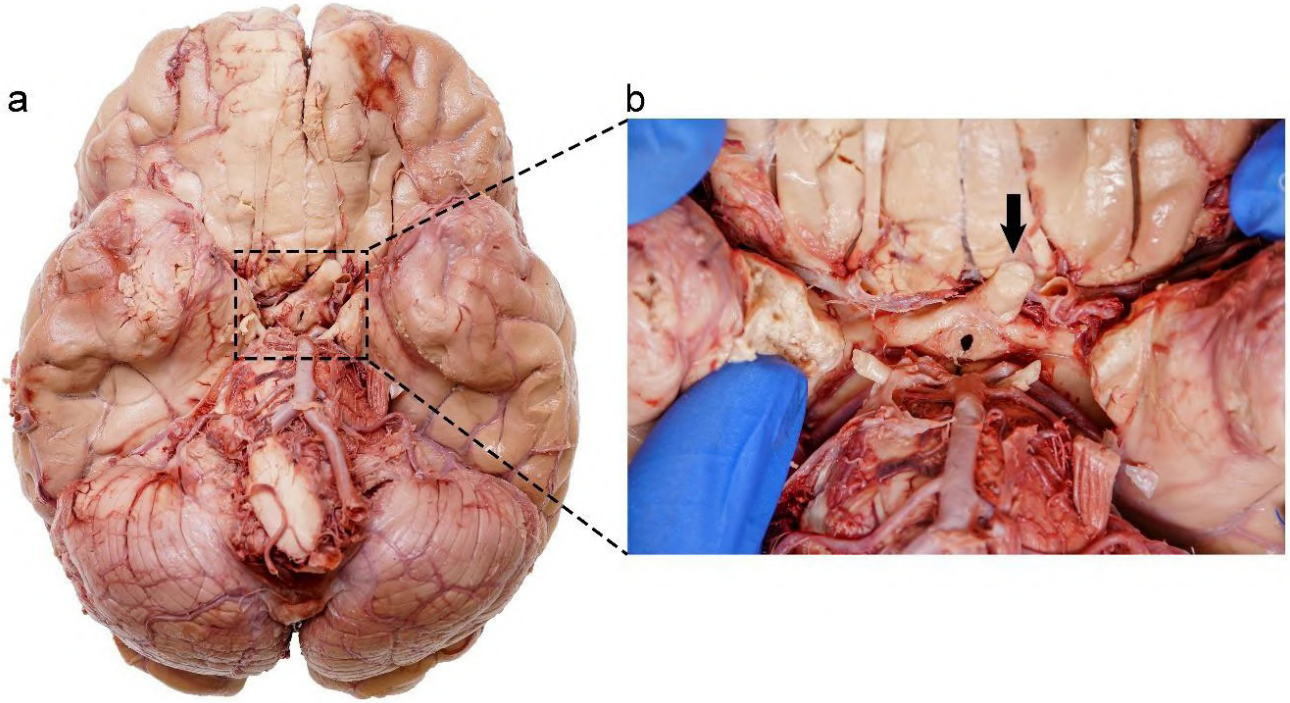

Fig. 2.- Inferior view of the brain. **(a)** presence of a cut left side optic nerve and absent right. **(b)** magnified inset showing convergence of left- and right-side optic tracts continuing as a single left optic nerve.

DISCUSSION

Optic nerve aplasia has been variably defined in the literature (Martín-Begué and Saint-Gerons, 2016; Ohuchi et al., 2016; Zhou et al., 2020). Diagnosis of optic nerve aplasia within the clinical setting is confirmed radiologically when a blind eye presents with a total absence of optic nerve fibres, optic disc, retinal ganglion cells and central retinal vessels (Martín- Begué and Saint-Gerons, 2016; Meire et al., 2011; Ohuchi et al., 2016; Taylor, 2007). The total absence of optic nerve fibres leading to the absence of the optic disc and central retina vessels in the case study presented concurs with radiological descriptions of optic nerve aplasia.

Ohuchi et al. (2016) reported a bilateral case of optic nerve aplasia observed during an autopsy. The optic nerve presented as a myelinated cotton-thread-like cord originating from the poorly developed optic chiasma and extending to the posterior pole of the eyeball (Ohuchi et al., 2016), which is consistent with an extreme case of hypoplasia presented in the literature (Margo et al., 1992). In contrast to Ohuchi et al. (2016), a complete unilateral absence of both the intracranial and extracranial course of the optic nerve is presented in the current case study.

The commonly used diagnostic imaging modalities for optic nerve aplasia include magnetic resonance imaging, computerized tomography, and brightness (B-Scan) ultrasonography. However, controversy still exists regarding the best imaging modalities to accurately diagnose true optic nerve aplasia (Martín-Begué and Saint-Gerons, 2016; Ohuchi et al., 2016; Zhou et al., 2020). As a result of differential diagnostic criteria being presented in imaging studies, optic nerve hypoplasia has been grossly misidentified as optic nerve aplasia in the literature and the incidence of true optic nerve aplasia remains unclear (Martín-Begué and Saint-Gerons, 2016).

While some patients with optic nerve hypoplasia may present with partial blindness, it should be noted that in true optic nerve aplasia patients usually present with complete blindness (Meire et al., 2011). Ocular anomalies associated with optic nerve aplasia include microphthalmia, iris anomalies, retinal dysplasia, cataracts, corneal oedema and sclerocornea (Handley et al., 2021; Martín-Begué and Saint-Gerons, 2016; Ohuchi et al., 2016).

Microphthalmia is the presence of an abnormally small eye with reduced axial length and corneal diameter measurements (Verma and FitzPatrick, 2007). The normal adult human eye presents with a mean axial length of 23.8 mm and a corneal diameter which ranges between 9.0-10.5 mm (Handley et al., 2021; Verma and FitzPatrick, 2007). In the clinical setting, any adult human eye with a mean axial length of less than 21 mm is considered microphthalmic (Verma and FitzPatrick, 2007). In the current case, eyeball measurements were not taken, as cadaveric soft tissues usually shrink after preservation with formalin. Instead, the measurements of the orbital socket taken to substantiate the gross appearance of the left and right eyeballs presented with an approximately 4mm smaller orbital height and breadth in the right eye. Thus, the size difference presented in the right eye when compared to the left in the current case may be considered within the spectrum of microphthalmia (Handley et al., 2021; Verma and FitzPatrick, 2007).

Optic nerve aplasia may also be associated with cardiovascular, endocrinological, gastrointestinal, vertebral and neurological anomalies (Ghassemi et al., 2015). While little is known about the lived state of health of the cadaver, presented in the current case study, a smaller right splenium of the corpus callosum was observed. The presence of a reduced splenium of the corpus callosum may be considered consistent with corpus callosum hypoplasia (Martín-Begué and Saint-Gerons, 2016). In contrast with the current case study, the radiological imaging of the brain in the case of optic nerve aplasia reported by Ohuchi et al. (2016) did not reveal any associated brain anomalies. Despite this finding, the existing evidence suggests that unilateral optic nerve aplasia associated with microphthalmia usually occurs without brain abnormalities, especially when the aplasia is due to single eye developmental interruptions (Martín-Begué and Saint-Gerons, 2016; Ohuchi et al., 2016; Taylor, 2007). In keeping with the varied embryological contributions of tissues to the

development of the eye previously reported, the absent right optic nerve in the current case may be due to developmental anomalies of the retinal ganglion cells (Ohuchi et al., 2016).

The calcified vitreous tissue may imply that the mesenchyme failed to develop properly (Margo et al., 1992; Ohuchi et al., 2016). In addition, there could be reduction in blood flow around the right eyeball, which could lead to proteins within the vitreous humor becoming sticky and hardening.

Potential contributing genetic factors are difficult to ascertain, as the family and genetic history was not available. There is also limited literature on the incidence and genetics of human optic nerve aplasia associated with microphthalmia (Ghassemi et al., 2015; Handley et al., 2021; Meire et al., 2011).

CONCLUSION

The current report includes the anatomical presentation of a true optic nerve aplasia associated with microphthalmia. Cadaveric reports may advance the understanding of optic nerve aplasia to the current sparse literature and substantiate clinical and radiological presentations, in turn, improving diagnosis and treatment.

ACKNOWLEDGEMENTS

The authors sincerely thank those who donated their bodies to science to perform anatomical research (Wits School of Anatomical Sciences Body Donation Programme). Such research can potentially increase humankind's overall knowledge to improve patient care. Therefore, these donors and their families deserve our highest gratitude.

REFERENCES

GHASSEMI F, BAZVAND F, HOSSEINI SS, KARKHANEH R, EBRAHIMIADIB N, SHEKARCHI B (2015) Optic nerve aplasia: Case report and literature review. *J Ophthalmic Vis Res*, 10: 187-192.

HANDLEY SE, MARMOY OR, GORE SK, MANKAD K, THOMPSON DA (2021) Case report: Unilateral optic nerve aplasia and developmental hemichiasmal dysplasia with vep misrouting. *Doc Ophthalmol*, 142: 247-255.

MARGO CE, HAMED LM, FANG E, DAWSON WW (1992) Optic nerve aplasia. *Arch Ophthalmol*, 110: 1610-1613.

MARTÍN-BEGUÉ N, SAINT-GERONS M (2016) Congenital optic nerve anomalies. *Arch Soc Esp Oftalmol (English Edition)*, 91: 577-588.

MEIRE F, DELPIERRE I, BRACHET C, ROULEZ F, VAN NECHEL C, DEPASSE F, CHRISTOPHE C, MENTEN B, DE BAERE E (2011) Nonsyndromic bilateral and unilateral optic nerve aplasia: First familial occurrence and potential implication of cyp26a1 and cyp26c1 genes. *Mol Vis*, 17: 2072.

OHUCHI H, TANIGUCHI K, MIYAISHI S, KONO H, FUJITA H, BANDO T, FUCHIZAWA C, OHTANI Y, OHTANI O (2016) Autopsy case of bilateral optic nerve aplasia with microphthalmia: Neural retina formation is required for the coordinated development of ocular tissues. *Acta Med Okayama*, 70: 131-137.

TAYLOR D (2007) Developmental abnormalities of the optic nerve and chiasm. *Eye*, 21: 1271-1284.

VERMA AS, FITZPATRICK DR (2007) Anophthalmia and microphthalmia. *Orphanet J Rare Dis*, 2: 1-8.

ZEISS CJ, TU DC, PHAN I, WONG R, TREUTING PM (2017) Special Senses: Eye. In: *Comparative Anatomy and Histology: A mouse, rat, and human atlas*, Second edition. Elsevier, pp 445-470.

ZHOU Y, RYAN ME, METS MB, YOON HH, RAHMANI B, KURUP SP (2020) Aplasia of the optic nerve: A report of seven cases. *Neuroophthalmology*, 44: 332-338.

Luschka's tubercle and snapping scapula syndrome: an anatomical and clinical discourse

Saad Ahmed[1], Panchal Hiten[2], Jain Prathmesh[3], Karthikeyan P. Iyengar[4], Rajesh Botchu[5]

[1] *Department of Orthopedics, Royal Orthopedic Hospital, Birmingham, UK*
[2] *Sanyapixel diagnostics, Ahmedabad, India*
[3] *Advance Hospital, Ahmedabad, India*
[4] *Department of Orthopaedics, Southport and Ormskirk Hospitals, Mersey and West Lancashire NHS Trust, Southport, UK*
[5] *Department of Musculoskeletal Radiology, Royal Orthopedic Hospital, Birmingham, UK*

SUMMARY

Snapping Scapula Syndrome (SSS) is an uncommon orthopaedic disorder characterised by audible crepitations and disrupted shoulder kinematics due to pathological interactions within the tissues between the scapula and ribcage. One rare cause of SSS is the presence of Luschka's Tubercle, a bony prominence located on the costal surface of the superior angle of the scapula. Diagnosis of SSS due to Luschka's Tubercle (LT) can be challenging, often eluding conventional imaging, potentially leading to mismanagement and worsening symptoms. This case series underscores the significance of LT detection, explores its role in SSS, and discusses treatment options.

This series presents five patients with posterior shoulder pain and a palpable click indicative of SSS over a six-month period. Three of these patients did not exhibit Luschka's Tubercle (LT) on 3D CT scans, while the remaining two patients had LT detected on the imaging. Arthroscopic resection successfully resolved symptoms in one of the two patients with LT.

SSS is characterised by scapular snapping during movement, often associated with anatomical abnormalities such as Luschka's Tubercle. A comprehensive approach to diagnosis and management, including imaging, conservative measures, and, when necessary, surgery, is crucial for alleviating symptoms and enhancing shoulder function in affected individuals.

Key words: Shoulder – Orthopaedics – Scapula – Shoulder pain – Ribs – Musculoskeletal diseases

INTRODUCTION

Snapping Scapula Syndrome (SSS) is an intriguing yet uncommon orthopaedic disorder characterised by audible crepitations and disrupted shoulder kinematics resulting from pathological interactions within the tissues located between the scapula and the ribcage (Lazar et al., 2009; Kuhne et al., 2009; Carvalho et al., 2019; Vidoni et al., 2022). The causes of SSS are diverse and can include morphological alterations of the scapula and rib cage, an imbalance in periscapular mus-

Shared corresponding authors:
Rajesh Botchur. Department of Musculoskeletal Radiology, Royal Orthopedic Hospital, Birmingham, UK. E-mail: drbrajesh@yahoo.com

Submitted: October 14, 2023 **Accepted:** January 22, 2024

https://doi.org/10.52083/HVJP6884

culature forces (dyskinesia), or neoplasia (bone tumours or soft tissue tumours) (Carvalho et al., 2019). This condition predominantly affects young, active individuals, often with a history of pain stemming from overuse, rapid shoulder movements, or participation in sports activities (Gaskill and Millett, 2013).

Among the rare causes of SSS is the presence of Luschka's Tubercle (Carvalho et al., 2019; Gallien, 1985; Estwanik, 1989; Dietrich et al., 2017; Somerson et al., 2024). Luschka's tubercle, first described and illustrated by Gruber, Luschka and Sauser in the years 1864, 1870 and 1936, is a bony protuberance found on the costal surface of the superior angle of the scapula (Sauser, 1936). The tubercle is distinct due to its hook-shaped morphology and discreet location at the superomedial aspect of the scapula. It occurs in approximately 3% of the general population and significantly influences the dynamics of the scapulothoracic articulation (Totlis et al., 2014). LTs can restrict normal shoulder mobility, contributing to the symptomatic expression of SSS by reducing the scapular interspace and increasing friction, thereby causing discomfort (Dietrich et al., 2017).

Diagnosis of SSS due to Luschka's Tubercle (LT) can be challenging, as it are often missed on conventional imaging, potentially leading to mismanagement of SSS and worsening symptoms in affected patients (Kuhne et al., 2009). This case series aims to emphasise the importance of detecting Luschka's Tubercle (LT), to explore its role within the context of SSS and to discuss the different treatment options.

CASE SERIES

In this series, we report on five patients with a mean age of 40 years (ranging from 26 to 46), comprising three females and two males. All patients presented with posterior shoulder pain, associated with pain on passive movements of adduction and forward flexion, and a palpable click, typical of Snapping Scapula Syndrome, over a six-month period. There was no history of trauma. The overlying skin over the scapula was normal. Cross-sectional imaging was performed to evaluate this further. Three out of the five patients did not exhibit Luschka's Tubercle (LT) on a 3D CT scan (15 slice ACT revolution, GE) and further assessment by Magnetic Resonance Imaging (MRI) (1.5T HDXT, GE MRI, T1 and STIR axial, coronal and sagittal), and there was no oedema in the scapulothoracic interval. The remaining two patients, a 26- and a 39-year-old male, presented with similar symptoms, with LT being detected on the 3D CT scan. There was oedema of the soft tissues between the LT and thoracic wall on MRI (Fig. 1).

They were initially managed with analgesics and physiotherapy. The 39-year-old male patient had recalcitrant pain despite these, and hence underwent arthroscopic resection of the tubercle with complete resolution of symptoms at a six-month follow up (Fig. 2). The other patient was also offered surgical resection; however, he could not proceed due to financial constraints. Other three out of the five patients with LT were managed conservatively, involving analgesia and steroid injections.

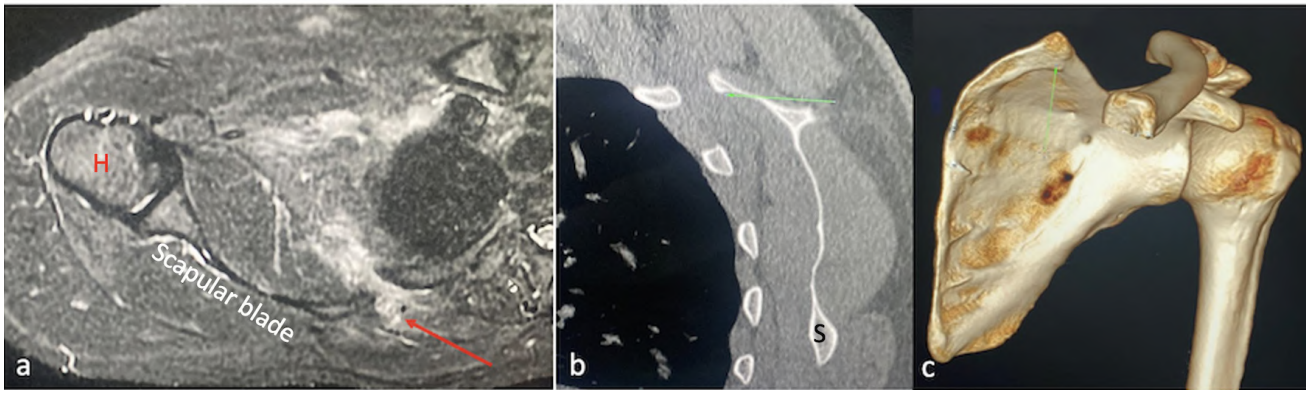

Fig. 1.- Axial STIR (**a**) showing edema between the Luschka's tubercle and posterior chest wall (arrow). Sagittal CT showing Luschka's tubercle (**b**) (arrow) and 3D reconstruction showing Luschka's tubercle (**c**). H (humeral head), S (scapula).

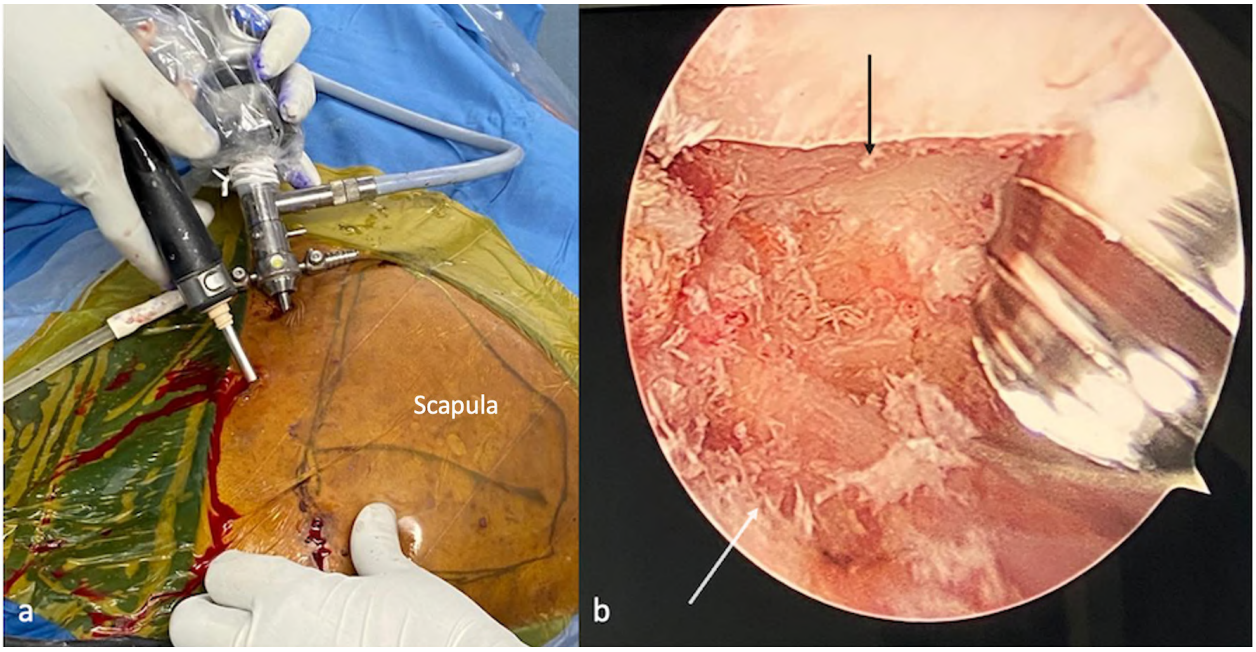

Fig. 2.- Arthroscopy images (**a, b**) showing surface marking of scapula, insertion of arthroscopic ports (**a**) and image after resection of Luschka's tubercle (**b**), highlighted area between the arrows.

DISCUSSION

Snapping Scapula Syndrome (SSS) is a fascinating condition thought to originate from an abnormal scapulothoracic articulation (Lazar et al., 2009; Carvalho et al., 2019). The scapula, a triangular bone situated between the second and seventh ribs, exhibits distinctive surfaces, borders, and angles. Its connection with the ribcage lacks conventional joint structures and is instead surrounded by a complex array of muscles, categorised into superficial, intermediate, and deep layers (Kuhne et al., 2009; Lazar et al., 2009; Carvalho et al., 2019). These encompass the trapezius, latissimus dorsi, rhomboids, levator scapulae, serratus anterior and subscapularis. Precise scapular positioning and control are essential for optimal glenohumeral joint function, necessitating synchronised actions of various scapular muscles (Lazar et al., 2009; Carvalho et al., 2019). These muscles collaborate to enable a range of movements, including abduction, adduction, elevation, depression, and rotation. Any disruption to the biomechanics of scapulothoracic movements can give rise to SSS.

SSS is characterised by an audible pop or clicking of the scapula during scapulothoracic joint movements, often associated with inflammation and irritation of the bursa in the serratus anterior space (Vidoni et al., 2022). Patients with SSS typically present with painful snapping, grinding, or popping of the shoulder during adduction, flexion or extension movements, often accompanied by crepitus and feelings of fullness in the posterior shoulder region. The pain worsens with overhead movements, heavy lifting, and repetitive use (Gaskill and Millett, 2013; Vidoni et al., 2022).

SSS has diverse causes, encompassing scapulothoracic bursitis, ribcage or scapula deformities, and congenital anomalies such as Sprengel's deformity. Occupational factors, particularly repetitive overhead motions, can also contribute to SSS (Kuhne et al., 2009). Notably, Luschka's Tubercle (LT) plays a pivotal role in SSS. LT, characterised as a unique bony protrusion with a distinctive hook-shaped structure located along the superomedial edge of the scapula, often proves challenging to detect by conventional imaging, posing a diagnostic challenge (Sauser, 1936; Lehtinen et al., 2005; Totlis et al., 2014; Dietrich et al., 2017). Despite the surrounding musculature providing support to the scapulothoracic joint, it is crucial to recognise that specific scapular areas, including the superomedial and inferomedial angles, along with the medial border, possess relatively less muscular and bursal coverage. LT develops around the superior angle of the scapu-

la, remaining unsupported by musculature, thus disrupting significantly normal shoulder movement. This disruption leads to the development of SSS by narrowing the space between the scapula and ribcage, resulting in heightened friction and accompanying symptoms (Totlis et al., 2014; Dietrich et al., 2017).

Understanding the embryological development of Luschka's Tubercle (LT) presents challenges due to its rarity in reported literature. The process begins with undifferentiated mesenchymal tissue, and the scapula's primary ossification centre emerges around the seventh week of gestation. During this intricate process, various areas of the scapula undergo differentiation, including the area where Luschka's tubercle eventually forms (Huang et al., 2006). Osteoblasts play a crucial role in depositing bone matrix in this specific region, giving rise to the tubercle. Secondary ossification centres also develop in other scapular areas, further contributing to its growth and maturation. As postnatal growth ensues, and the scapula continues to transform in shape and structure, with Luschka's tubercle becoming more distinct (Totlis et al., 2014). It is important to note that genetic factors and the complex processes of bone formation during embryonic development can influence the presence and characteristics of this anatomical feature.

Diagnosing snapping scapula primarily relies on patient history and physical examination. Some researchers have suggested the use of CT scans as a helpful adjunct in the diagnostic process for snapping scapula cases (Mozes et al., 1999; Kuhne et al., 2009). CT images can provide supplementary information to support clinical assessment. Nevertheless, due to the limited clarity in existing literature regarding the scapular morphology in individuals with snapping scapula, diagnosing this syndrome remains challenging for diagnostic radiologists. In our study, detection for LT was made through CT scans (Mozes et al., 1999). MRI is crucial in the visualisation of surroundings soft tissues but often misses bony anomalies. The use of ultrasound in these cases can be challenging (Conduah et al., 2010).

The treatment approach for Snapping Scapula Syndrome (SSS) associated with Luschka's Tubercle (LT) remains variable and subject to controversy. While some studies have found no conclusive link between LT and SSS (Dietrich et al., 2017), our case series highlights the diversity in management strategies. In our study, two patients with SSS and LT were managed differently. One patient opted for conservative treatment, which involved pain management through analgesia and steroid injections, coupled with physiotherapy to restore scapular control and muscle strength. However, in cases where symptoms persist, surgical intervention may become necessary, as demonstrated in one of our patients. In this instance, arthroscopic debridement of Luschka's Tubercle resulted in the complete resolution of the patient's symptoms, highlighting the potential efficacy of surgical intervention in selected cases. Scapulothoracic arthroscopy offers several advantages, including safe and straightforward access to the superomedial corner of the scapula, improved visibility for bursa and superomedial corner resection, enhanced cosmesis compared to open procedures, and minimal muscle dissection, resulting in reduced pain and quicker rehabilitation. Various approaches can be employed for this procedure. However, the chicken wing position, with the patient in a prone posture and utilizing the 3-portal technique (comprising superior, medial, and inferior portals with blunt trocars for scapular access), is notably effective. Initial access to the scapulothoracic space involves two superiorly positioned portals, one proximal and one medial to the superomedial angle of the scapula. Gaining access to the superomedial corner of the scapulothoracic interspace is a procedure that can be carried out in a straightforward and reproducible manner. However, it is crucial to be aware of the potential complications, such as the risk of injuring the dorsal scapular nerve or vessels, as well as the possibility of iatrogenic damage to the suprascapular nerve. Failing to insert the portal trocars toward the costal surface of the scapula may lead to perpendicular insertion into the thoracic wall and cavity (Saper et al., 2015).

CONCLUSION

SSS is a condition characterised by scapular snapping during movement, often linked to anatomical abnormalities like Luschka's Tuber-

cle. Proper diagnosis and management involve a multidisciplinary approach, including imaging, conservative measures, and, in some cases, surgery, to alleviate symptoms and improve shoulder function in affected individuals.

REFERENCES

CARVALHO SC DE, CASTRO A DO A E, RODRIGUES JC, CERQUEIRA WS, SANTOS D DO CB, ROSEMBERG LA (2019) Snapping scapula syndrome: pictorial essay. *Radiol Bras*, 52(4): 262-267.

CONDUAH AH, BAKER CL, BAKER CL (2010) Clinical management of scapulothoracic bursitis and the snapping scapula. *Sports Health*, 2(2): 147-155.

DIETRICH TJ, AGTEN CA, FÜRNSTAHL P, VLACHOPOULOS L, PFIRRMANN CWA (2017) The legend of the Luschka tubercle and its association with snapping scapulae: osseous morphology of snapping scapulae on CT images. *Am J Roentgenol*, 209(1): 159-166.

ESTWANIK JJ (1989) Levator scapulae syndrome. Phys Sportsmed, 17(10): 57-68.

GALLIEN R (1985) Accessory bone at the insertion of the levator scapulae muscle in a Sprengel deformity. *J Pediatr Orthop*, 5(3): 352-353.

GASKILL T, MILLETT PJ (2013) Snapping scapula syndrome: diagnosis and management. *J Am Acad Orthop Surg*, 21(4): 214-224.

HUANG R, CHRIST B, PATEL K (2006) Regulation of scapula development. *Brain Struct Funct*, 211(S1): 65-71.

KUHNE M, BONIQUIT N, GHODADRA N, ROMEO AA, PROVENCHER MT (2009) The snapping scapula: diagnosis and treatment. *Arthroscopy*, 25(11): 1298-1311.

LAZAR MA, KWON YW, ROKITO AS (2009) Snapping scapula syndrome. *J Bone Joint Surg*, 91(9): 2251-2262.

LEHTINEN JT, TINGART MJ, APRELEVA M, WARNER JJP (2005) Quantitative morphology of the scapula: normal variation of the superomedial scapular angle, and superior and inferior pole thickness. *Orthopedics*, 28(5): 481-486.

MOZES G, BICKELS J, OVADIA D, DEKEL S (1999) The use of three-dimensional computed tomography in evaluating snapping scapula syndrome. *Orthopedics*, 22(11): 1029-1033.

SAPER M, KASIK C, DIETZEL D (2015) Arthroscopic scapulothoracic decompression for snapping scapula syndrome. *Arthrosc Tech*, 4(6): e631-636.

SAUSER G (1936) Tuberculum hemi-articulare scapulae. *Z Anat Entwicklungsgesch*, 106(1): 80-84.

SOMERSON JS, JUNG B, STEGINK-JANSEN CW (2024) Regarding a human costoscapular joint by Prof. Dr. H. von Luschka (1870): A translation. *Clin Anat*, 37(3): 278-283.

TOTLIS T, KONSTANTINIDIS GA, KARANASSOS MT, SOFIDIS G, ANASTASOPOULOS N, NATSIS K (2014) Bony structures related to snapping scapula: correlation to gender, side and age. *Surg Radiol Anat*, 36(1): 3-9.

VIDONI A, DAVIES M, JAMES S, BOTCHU R (2022) Relevance of scapulothoracic joint assessment for unknown shoulder pain. *Indian J Musculoskel Radiol*, 4: 61.

Computed-tomography assessment of the lumbar spine body/canal index and review of the literature

Rodrigo Teran-Garza[1β], Santos Guzman-Lopez[1β], Kouatzin Aguilar-Morales[1], Yehuda Jesus Garcia-Gutierrez[2], Ricardo Pinales-Razo[2], José Félix Vilchez-Cavazos[3], Alejandro Quiroga-Garza[1], Javier Humberto Martinez-Garza[1], Jorge Gutierrez-de la O[1], Rodrigo Enrique Elizondo-Omaña[1]

[1] Universidad Autonoma de Nuevo Leon, School of Medicine, Human Anatomy Department, Monterrey, México

[2] Universidad Autonoma de Nuevo Leon, University Hospital "Dr. José Eleuterio González", Department of Radiology and Diagnostic Imaging, Monterrey, México

[3] Universidad Autonoma de Nuevo Leon, Hospital Universitario "Dr. José Eleuterio González", Department of Traumatology and Orthopedics, Monterrey, México

[β] both authors participated equally, and are both in the position of first author.

SUMMARY

Lumbar spinal stenosis (LSS) involves narrowing of the lumbar spinal space due to various factors. Torg-Pavlov Index measures predict LSS. The objective was to define the mean characteristics of the lumbar spine body/canal index in a Hispanic population stratified by age and sex. A retrospective, observational, transverse, and descriptive study was performed. Imaging studies included consecutive bone window full abdominal CT scans, in adult patients (≥18 years), without evidence of bone disease, musculoskeletal pathology, or traumatic event and a fully visible lumbar spine (L1-L5). The anteroposterior diameter (APD) and midsagittal diameter (MSD) of each vertebral level were measured using the Carestream image reformatting program at each lumbar vertebral level from L1 to L5 of the CT scan.

A total of 400 CTs of subjects with a mean age of 47.7±14.8 (range 18-80 years) were evaluated, of which 59.3% (n 237/400) were women. The presence of a ≤0.5 body/canal index was 31.6% (n 126). The MSD/APD lumbar index did not differ significantly between age groups in any of the vertebrae. However, there was a tendency to decrease with age. An mean index higher than 0.5 was the mean found in the patients evaluated where there was no previous data of spinal cord involvement. This study provides an accurate description of the normal morphometric parameters of the lumbar body/canal ratio in a Mexican population to assess clinical scenarios of lumbar spinal stenosis. Few studies evaluate the use of cut-off points to define an LSS.

Key words: Torg-Pavlov – Lumbar spinal stenosis – Computed tomography – Hispanic population

Shared corresponding authors:
Rodrigo E. Elizondo Omaña M.D. Ph.D. and Jorge Gutierrez-de la O M.D., Ph.D. Department of Human Anatomy, Faculty of Medicine and University Hospital "Dr. José Eleuterio González", Universidad Autónoma de Nuevo León (U.A.N.L.), Avenida Francisco I. Madero y Gonzalitos s/n Colonia Mitras Centro C.P. 64460, Monterrey, Nuevo León, México. Phone: +52 81 8329 4171. E-mails: rod_omana@yahoo.com / jorgegdelao@yahoo.com

Submitted: January 18, 2024 **Accepted:** February 9, 2024

https://doi.org/10.52083/KNGA7524

INTRODUCTION

Lumbar spinal stenosis (LSS) is defined as a narrowing of the spinal space at the lumbar level due to anatomical changes as a cascade of events including degeneration of the intervertebral disc, facet joint osteoarthritis, and hypertrophy of the ligamentum flavum (Verbiest, 1950; Jensen et al., 2020). LSS is classified into two types: Congenital and Acquired. Congenital or primary LSS can be mainly attributed to either a congenital abnormality or a postnatal development disorder, contrary to acquired or secondary LSS, which results from degenerative changes, trauma, infections, or surgical origin. (Genevay et al., 2010) Symptoms associated with this stenosis mainly include lower back pain, lower extremities weakness, paresthesia, and numbness (Jensen et al., 2020). Spinal stenosis increases the risk of neurological injuries in traumatic, degenerative, and inflammatory conditions (Zhang et al., 2012).

The measurement of the sagittal diameter of the lumbar canal has traditionally been considered the best predictor of lumbar stenosis (Eisenstein, 1977; Gepstein et al., 1991; Visuri et al., 2005). In the setting of the cervical spine the Torg-Pavlov method was developed to classify stenosis. This method calculates an index between the sagittal diameter of the body and the canal of the spine of the cervical vertebrae to determine stenosis (Pavlov et al., 1987). Some studies have correlated having cervical stenosis with having lumbar spinal stenosis (Iizuka et al., 2012). The measurement of the Torg-Pavlov Index in lumbar vertebrae in a cadaveric study proposed that it could be a useful technique for predicting lumbar stenosis (Bajwa et al., 2013). Based on their findings, the authors concluded a Torg ratio <0.5 predicted LSS. The primary objective of this study was to define the mean characteristics of the lumbar spine body/canal index in a Hispanic population stratified by age and sex, with comparison to other populations found in the literature.

MATERIAL AND METHODS

A retrospective, observational, transverse, and descriptive study was performed. Imaging studies included consecutive bone window full abdominal CT scans obtained from the Radiology and Imaging Department of the University Hospital in Monterrey, Mexico. All studies were performed using a General Electric CT99 LightSpeed VCT 64-slice Scanner ® (rotation 0.4s helicoidal acquisition, 20 mm detector covering, 120 Kv, 400+, 0.625 mm width slices).

Inclusion criteria were studies from adult patients (≥18 years), without gender distinction, who had a full abdominal CT performed without evidence of bone disease, musculoskeletal pathology, or traumatic event as an indication, and a fully visible lumbar spine (L1-L5). Exclusion criteria included studies that were part of a pre-surgical evaluation, or follow-up of an underlying disease with a diagnosis involving bone structures or the lumbar spine.

The anteroposterior diameter (APD) and midsagittal diameter (MSD) of each vertebral level were measured using the Carestream image reformatting program at each lumbar vertebral level from L1 to L5 of the CT scan. (Fig. 1) Using

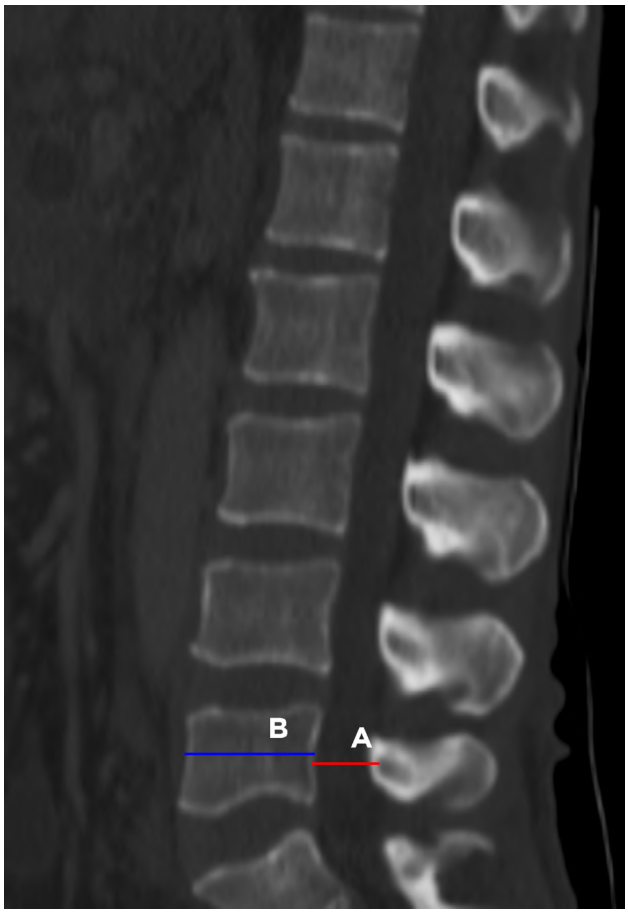

Fig. 1.- Midsagittal CT slice of vertebral column. The midsagittal diameter (A) and the antero-posterior diameter (B) of the vertebral body.

a mid-sagittal plane, the sagittal diameters of the body and canal of the lumbar spine at its 5 levels were taken to determine the lumbar ratio. Studies were evaluated by two non-blinded independent observers with experience in radiology and anatomy to establish measurements.

A sample size calculation was performed estimating the mean in a finite population, with a confidence of 95% and a margin of error of 5%, resulting in a total of 400. Normality tests were carried out using the Kolmogorov-Smirnov test. Central tendency and dispersion data were obtained, expressed as mean with standard deviation, frequencies, and percentages. Comparisons between the different groups obtained from the sample (sex, age) of the study were performed using a bilateral t-student test and One-Way ANOVA or with Mann-Whitney *U* test and Wilcoxon test, depending on the result of the normality tests. A value of p <0.05 was considered statistically significant. SPSS Statistics version 22 (IBM, Armonk, NY, USA) was used for Windows 10.

The study was previously reviewed and approved by the University's Ethics and Research Committees with the registration code AH19-00001, certifying that it adheres to the guidelines of the General Health Law on Health Research in Human Beings of our country and the Helsinki Declaration. None of the CT scans were performed for the purposes of this study.

RESULTS

A total of 400 CTs were evaluated with a mean age of 47.7 ± 14.8 (range 18-80 years), of which 59.3% (n 237/400) were women (Table 1). Men tended to have a statistically significantly larger APD than women, while MSD had no differences, except in L5. This in turn resulted in a larger vertebral body, while the vertebral canal remained similar when compared by sex, causing a statistically significant difference in the MSD/APD lumbar index, with women having the higher value (Table 1, Fig. 2).

Subcategorization was carried out stratified by age decades for comparison between the variables. A statistically significant difference was found for all groups of the lumbar vertebral body using the APD, with a clear increase with age (Table 2, Fig. 3). A post hoc statistical adjustment with Bonferroni a statistical change was noted

Table 1. Measurements of vertebrae from L1 to L5 with comparison between sex.

		General (n 400)		Men (n 163)	Women (n 237)	p
		Mean±SD	Range	Mean±SD	Mean±SD	
L1	MSD	16.3±1.5	11.9-20.5	16.3±1.5	16.3±1.4	0.784
	APD	28.2±2.9	22.0-36.6	30.3±2.5	26.8±2.2	<0.001*
	Index	0.58±0.08	0.38-0.86	0.54±0.07	0.61±0.08	<0.001*
L2	MSD	15.7±1.5	11.0-22.3	15.7±1.6	15.7±1.5	0.995
	APD	29.2±3.0	22.1-37.6	31.2±2.6	27.9±2.4	<0.001*
	Index	0.54±0.08	0.35-0.79	0.51±0.07	0.57±0.08	<0.001*
L3	MSD	15.2±1.8	10.0-29.3	15.3±2.0	15.2±1.6	0.972
	APD	30.3±3.1	14.1-40.0	32.2±3.1	28.9±2.4	<0.001*
	Index	0.51±0.11	0.32-2.08	0.48±0.15	0.53±0.08	<0.001*
L4	MSD	15.5±1.9	10.4-22.3	15.7±2.0	15.4±1.8	0.118
	APD	30.9±3.0	22.2-40.0	32.8±2.7	29.6±2.4	<0.001*
	Index	0.51±0.08	0.32-0.79	0.48±0.08	0.52±0.08	<0.001*
L5	MSD	16.4±2.6	10.4-31.0	16.8±2.9	16.1±2.4	0.014*
	APD	30.8±3.0	17.3-39.0	32.5±3.1	29.6±2.3	<0.001*
	Index	0.54±0.11	0.32-1.79	0.53±0.14	0.55±0.09	0.001*

Values expressed as millimeters. P value calculated for Statistical significance with Mann-Whitney U test for independent samples; significance set a p <0.05. n: sample size; MSD: Midsagittal diameter, APD: Anteroposterior diameter, SD: Standard deviation.

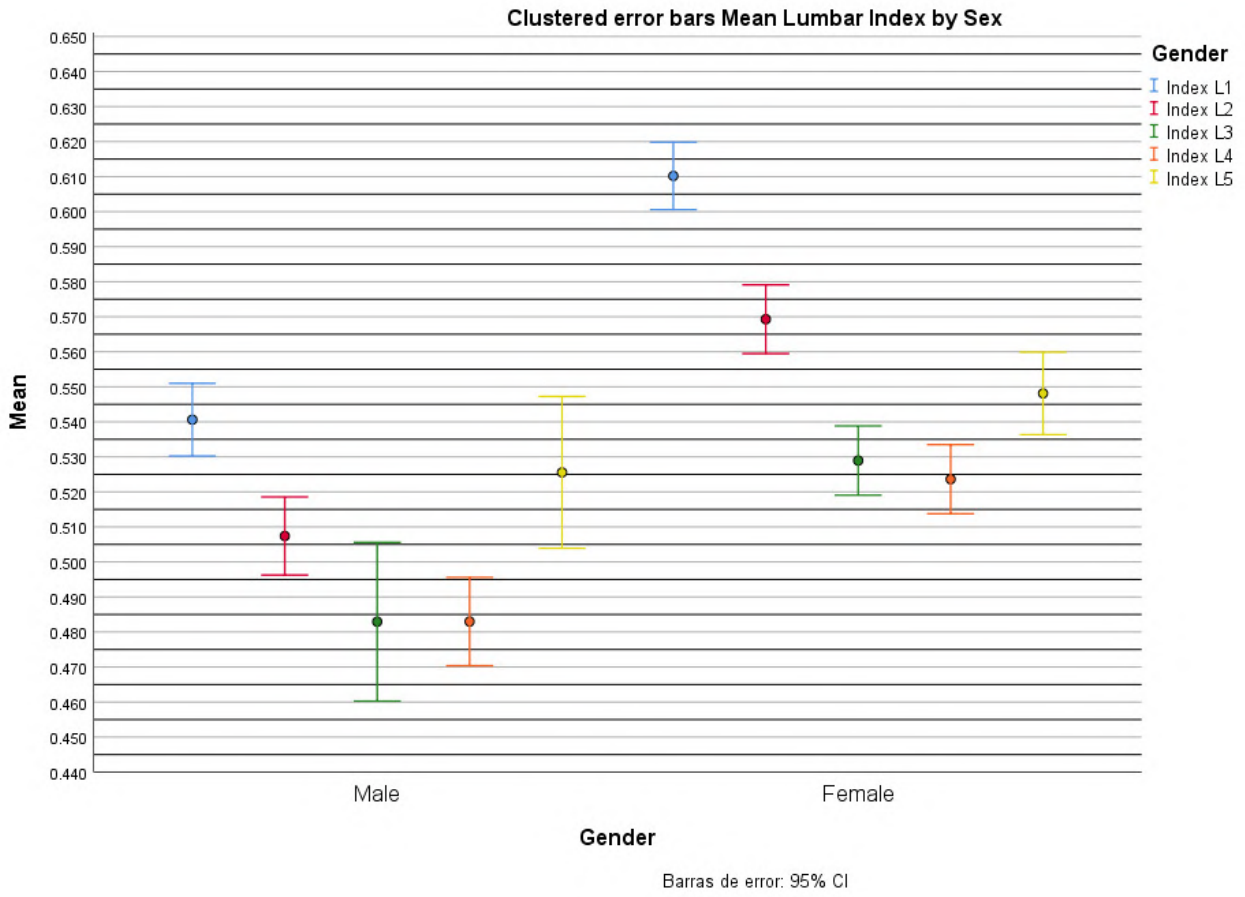

Fig. 2.- Pooled 95% error bar graph with mean MSD/APD ratio (y-axis) between men and women (x-axis).

Table 2. Measurements of vertebrae from L1 to L5 with comparison between categorical age groups.

		Mean±SD by Age groups						p
		≤29 (n)	30-39 (n)	40-49 (n)	50-59 (n)	60-69 (n)	≥70 (n)	
L1	MSD	16.3±1.6	16.2±1.3	16.1±1.4	16.3±1.5	16.3±1.3	16.3±1.7	0.879
	APD	27.3±2.9	28.3±2.9	28.0±3.1	28.2±2.5	29.0±2.7	29.5±2.7	0.004*
	Index	0.60±0.08	0.58±0.08	0.58±0.08	0.59±0.08	0.57±0.07	0.56±0.08	0.145
L2	MSD	15.6±1.3	15.4±1.3	15.6±1.5	15.9±1.7	16.0±1.6	16.1±1.6	0.171
	APD	28.4±2.8	29.3±2.9	29.1±3.2	29.2±2.8	29.8±3.2	30.3±2.6	0.035*
	Index	0.55±0.07	0.53±0.08	0.54±0.08	0.55±0.08	0.55±0.09	0.54±0.08	0.638
L3	MSD	15.2±1.5	14.9±1.4	15.2±2.2	15.2±1.7	15.5±1.9	15.6±1.9	0.375
	APD	29.1±2.9	30.3±3.0	30.0±3.5	30.4±2.8	31.2±3.2	31.7±3.0	0.001*
	Index	0.53±0.07	0.50±0.08	0.52±0.18	0.51±0.08	0.50±0.09	0.50±0.09	0.201
L4	MSD	15.7±1.9	15.4±1.7	15.4±1.8	15.4±1.9	15.7±2.1	15.8±1.9	0.697
	APD	29.7±2.9	30.7±2.7	30.6±3.1	31.0±2.6	32.0±3.1	32.5±2.9	0.000*
	Index	0.54±0.09	0.51±0.08	0.51±0.08	0.50±0.08	0.50±0.09	0.49±0.08	0.084
L5	MSD	16.5±2.9	16.6±2.6	16.1±2.4	16.3±2.9	17.0±2.6	16.3±1.7	0.414
	APD	29.7±3.0	30.8±2.8	30.4±3.0	30.9±2.9	31.7±2.9	32.2±2.6	0.002*
	Index	0.56±0.12	0.55±0.10	0.53±0.08	0.54±0.16	0.54±0.08	0.51±0.07	0.315

Values expressed as millimeters. P value calculated for Statistical significance with Kruskal-Wallis test for independent samples; significance set a p <0.05. n: sample size; MSD: Midsagittal diameter, APD: Anteroposterior diameter, SD: Standard deviation.

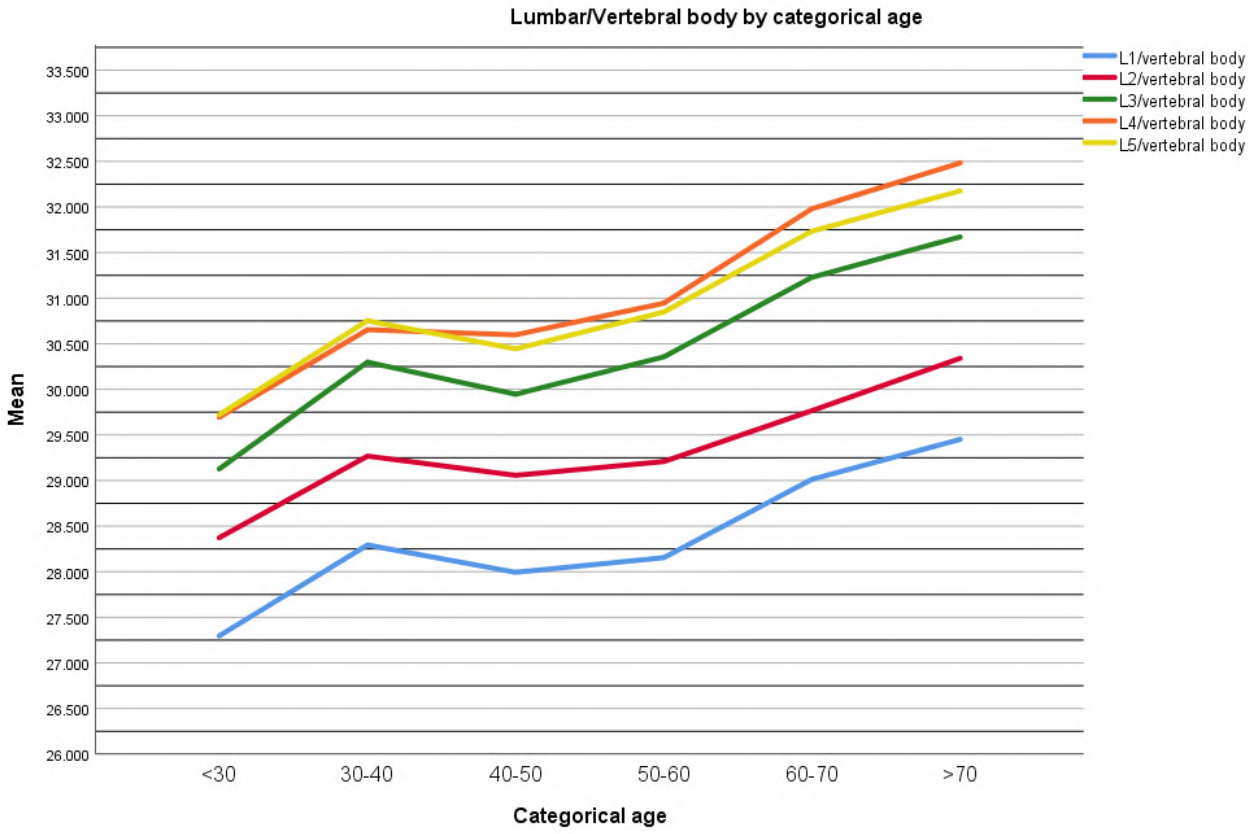

Fig. 3.- Comparison between categorical age groups of the APD ratio stratified by age decades.

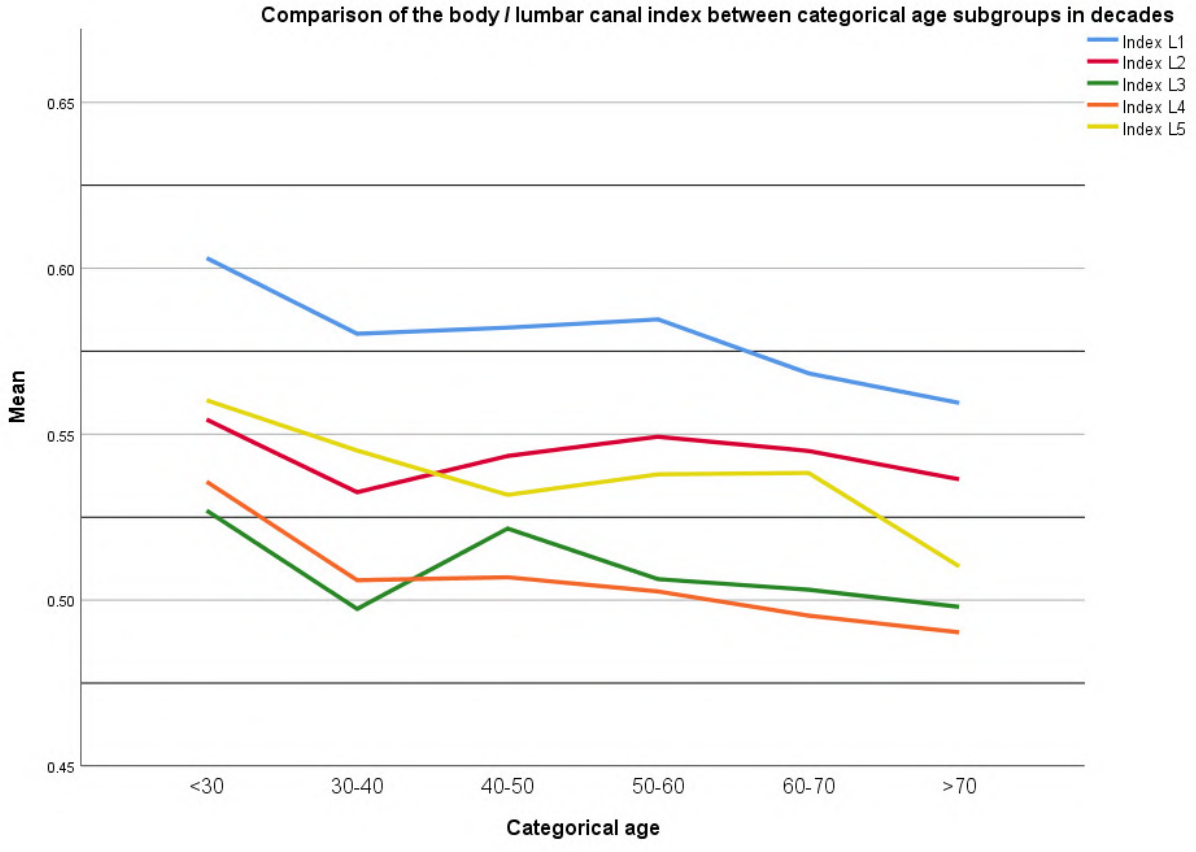

Fig. 4.- Comparison of the MSD/APD ratio between categorical age subgroups stratified by age decades.

between the groups of 50 to 60 years and older than 70 years with all the other age subgroups ($p < 0.05$). The MSD/APD lumbar index did not differ significantly between age groups in any of the vertebrae, however, there was a tendency to decrease with age (Fig. 4).

The presence of index lower than 0.5 was determined. In 126 (31.6%) of the patients the index was lower than 0.5, these patients being considered asymptomatic. In the case of women, 45 (35.7%) had an index lower than 0.5 while in men 81 patients (64.3%) had an index lower than 0.5.

DISCUSSION

Multiple morphometric studies focus on studying different measurements of the vertebral bones (Eisenstein et al., 1977; Gepstein et al., 1991; Bajwa et al., 2013; Amonoo-Kuofi et al., 1985; Azu et al., 2016). However, it's worth pointing out that vertebral anatomy goes beyond the bony structures, and involves a complex set of soft tissue structures that are vulnerable to many factors, both congenital and acquired, such as age, trauma, occupation, posture, etc (Genevay et al., 2010). Although LSS is defined as a narrowing of the spinal space at the lumbar level due to anatomical changes, there is no consensus on a strict measure to be able to identify it through imaging studies such as magnetic resonance imaging or computed tomography.

In a sample obtained from the Framingham Study of patients with LBP (Lower Back Pain), stenosis in the study population was defined as ≤12 mm ("relative" stenosis) and ≤10 mm ("absolute" stenosis). These cut-off points were arbitrarily obtained based on the cut-off points used in multiple studies (Kalichman et al., 2009).

Normal cut-off points for the MSD/APD lumbar index have not been described. Qudsieh et. al mentions in his study conducted in the Jordanian population, in patients without spinal pathology or LBP an average index of 0.45 (0.43-0.46) (Qudsieh et al., 2022)

In our population, we found a statistically significant difference in the vertebral body with age. The older populations had a greater APD. The spinal column functions as a shock-absorbent structure mainly by intervertebral discs, but involves skeletal structures as well, and gradually decreases its shock-absorbing capability with senescence (Brzuszkiewicz-Kuźmicka et al., 2018). The increase of APD with age may be hypothesized to be related to the decrease in shock absorption capability.

In turn, there is a decrease in the Torg-Pavlov index, associated with age, where for each decade of life this index decreases, especially when going from the fourth decade of life to the fifth, although this relationship was not statistically significant. The mean in the index in these patients without spinal pathology was not lower than 0.5 in any of the vertebral levels.

The importance of anatomy research with a clinical orientation is well established (Quiroga-Garza et al., 2020; Yammine, 2014; Tapia-Nañez et al., 2022). Anatomical understanding of the different clinical problems arising can guide clinical decisions and the learning of physicians (Garcia-Leal et al., 2021; Muñoz-Leija et al., 2018; Esparza-Hernández et al., 2017). Examples of how knowledge of morphometric characteristics in skeletal structures with the purpose of better understanding and predicting clinical outcomes can be found widely in medical literature, both in basic and clinical sciences (Muñoz-Leija et al., 2018; Vázquez-Barragán et al., 2016; Guzman-Lopez et al., 2019; Vazquez-Zorrilla et al., 2020). Bajwa et al. (2013) described 420 skeletal specimens and concluded that a ratio of lower than 0.5 could be associated with a probability of spinal stenosis. In our study, in the general measurements of the patients, evaluated by each one of the vertebral levels, an index higher than 0.5 was observed, taking into account that these patients did not present previous alterations at the lumbar spinal cord level before performing the imaging study.

In 126 patients (31.6%), when performing a mean of the vertebral level indices, these were classified with an index of lower than 0.5, although these patients did not have spinal cord compromise when they were chosen for the study.

However, they state the limitation of not considering the soft tissue component in the pathogenesis of disease. (Bajwa et al., 2013) The use of CT

not only improves the quality of the evidence, it allows the inclusion of ligaments and other musculoskeletal structures. (Bajwa et al., 2013; Javid et al., 2013).

It is important to emphasize that there is no standard measure in the index that can predict the presence of LSS. Studies in Jordanian patients without lumbar pathology showed an index lower than the means obtained in our population (Table 3) and where the presence of symptoms associated with LSS was not reported (Qudsieh et al., 2022).

Geographic and ethnic characteristic of different populations influences the anatomy (Teran-Garza et al., 2021). Morphometric studies have reported different mean indexes for the lumbar spine, with the highest index among Nepalese (Table 3). However, methodological techniques may influence, such as the use of dry bones (some may have deteriorated), incomplete samples, and lack of inter- and intra-observer confidence coefficients (Bajwa et al., 2013; Azu et al., 2016; Mansur et al., 2020). All studies were also limited by the lack of height and weight of the individuals.

LSS pathophysiology has not been completely understood.N, it has been shown that posture, disc pathology, vascular flow obstruction, and cerebrospinal fluid are influencing factors (Genevay et al., 2010). However, the evaluation of these is limited through imaging techniques, and therefore the relevance of the MSD/APD ratio will continue to be an objective tool, limited for considering only the skeletal structures.

Limitations

Our study has the limitation of being an observational morphometric imaging study that does not consider the clinical characteristics of the patient such as the presence of LBP. Therefore, the clinical correlation of the imaging studies remains the most important assessment of the patient.

CONCLUSIONS

This study provides an accurate description of the normal morphometric parameters of the lumbar body/canal ratio in a Mexican population to assess clinical scenarios of LSS. Few studies evaluate the use of cut-off points to define an LSS.

An index greater than 0.5 was the average found in the patients evaluated where there was no previous data on spinal cord involvement. Further studies are necessary to address both clinical characteristics and radiological characteristics to define the cut-off points associated with the presence of LSS.

Table 3. Torg-Pavlov MSD/APD Index for Lumbar column, differences in populations.

Author, year, country	Sample	L1	L2	L3	L4	L5
Azu et al., 2013 South Africa	107 Dry bone	0.65±0.09	0.52±0.07	0.53±0.07	0.52±0.05	0.53±0.06
Bajwa et al., 2014 USA	420 Dry bone	0.57±0.07	0.55±0.06	0.53±0.06	0.52±0.07	0.52±0.08
Mansur et al., 2020 Nepal	266 CT	0.60±NR	0.60±NR	0.58±NR	0.58±NR	0.54±NR
Qudsieh et al., 2021 Jordanian	68* MR	0.51±0.08	0.46±0.09	0.40±0.08	0.42±0.08	0.46±0.12
Teran-Garza et al., 2023 Mexico	400 CT	0.58±0.08	0.54±0.08	0.51±0.11	0.51±0.08	0.54±0.11

CT: computed tomography; SD: Standard deviation. NR: Not reported.
* Original study by Qudsieh et al. (2022) included 218 patients, however, the general measurements per vertebra were not reported, so the most extensive age group evaluated (50-59 years) was taken for comparison.

Ethical Approval

The study was previously reviewed and approved by the University's Ethics and Research Committees with the registration code AH19-00001, certifying that it adheres to the guidelines of the General Health Law on Health Research in Human Beings of our country and the Helsinki Declaration. None of the CT scans were performed for the purposes of this study.

Availability of data and materials

The data generated and analyzed during the current study are not publicly available but are available through the corresponding author on reasonable request.

REFERENCES

AMONOO-KUOFI HS (1985) The sagittal diameter of the lumbar vertebral canal in normal adult Nigerians. *J Anat*, 140(Pt 1): 69-78.

AZU OO, KOMOLAFE OA, OFUSORI DA, AJAYI SA, NAIDU ECS, ABIODUN AA (2016) Morphometric study of lumbar vertebrae in adult South African subjects. *Int J Morphol*, 34(4): 1345-1351.

BAJWA NS, TOY JO, AHN UN (2013) Application of a correlation between the lumbar Torg ratio and the area of the spinal canal to predict lumbar stenosis: A study of 420 postmortem subjects. *J Orthop Traumatol*, 14: 207-212.

BRZUSZKIEWICZ-KUŹMICKA G, SZCZEGIELNIAK J, BĄCZKOWICZ D (2018) Age-related changes in shock absorption capacity of the human spinal column. *Clin Interv Aging*, 13: 987-993.

EISENSTEIN S, SPINE L (1977) The morphometry and pathological anatomy of the lumbar spine in South African negroes and caucasoids with specific reference to spinal stenosis. *J Bone Joint Surg Br*, 59(2):173-180.

ESPARZA-HERNÁNDEZ CN, RAMÍREZ-GONZÁLEZ JM, CUÉLLAR-LOZANO RA, MORALES-AVALOS R, GONZÁLEZ-AROCHA CS, MARTÍNEZ-GONZÁLEZ B, QUIROGA-GARZA A, PINALES-RAZO R, ELIZONDO-RIOJAS G, ELIZONDO-OMAÑA RE, GUZMÁN-LÓPEZ S (2017) Morphological analysis of bronchial arteries and variants with computed tomography angiography. *Biomed Res Int*, 2017: 9785896.

GARCIA-LEAL M, GUZMAN-LOPEZ S, VERDINES-PEREZ AM, DE LEON-GUTIERREZ H, FERNANDEZ-RODARTE BA, ALVAREZ-VILLALOBOS NA, MARTINEZ-GARZA JH, QUIROGA-GARZA A, ELIZONDO-OMAÑA RE (2021) Trendelenburg position for internal jugular vein catheterization: A systematic review and meta-analysis. *J Vasc Access*, 24(2): 338-347.

GENEVAY S, PHYSICIAN A, ATLAS SJ (2010) Best practice & research clinical rheumatology lumbar spinal stenosis. *Best Pract Res Clin Rheumatol*, 24(2): 253-265.

GEPSTEIN R, FOLMAN Y, SAGIV P, BEN DAVID Y, HALLEL T (1991) Does the anteroposterior diameter of the bony spinal canal reflect its size? An anatomical study. *Surg Radiol Anat*, 13(4): 289-291.

GUZMAN-LOPEZ S, TERAN-GARZA R, QUIROGA-GARZA A, ELIZONDO-OMAÑA RE (2019) Anatomical variations of the sacroiliacal joint. *FASEB J*, 33(1 supplement): 616.2-616.2.

IIZUKA H, TAKAHASHI K, TANAKA S, KAWAMURA K, OKANO Y, ODA H (2012) Predictive factors of cervical spondylotic myelopathy in patients with lumbar spinal stenosis. *Arch Orthop Trauma Surg*, 132(5): 607-611.

JAVID M, OSTLERE S (2013) Radiculopathy. *Imaging*, 22(1): 22537980.

JENSEN RK, JENSEN TS, KOES B, HARTVIGSEN J (2020) Prevalence of lumbar spinal stenosis in general and clinical populations : a systematic review and meta-analysis. *Eur Spine J*, 29(9): 2143-2163.

KALICHMAN L, COLE R, KIM DH, LI L, SURI P, GUERMAZI A, HUNTER DJ (2009) Spinal stenosis prevalence and association with symptoms: the Framingham Study. *Spine J*, 9(7): 545-550.

MANSUR DI, KARKI S, MEHTA DK, SHRESTHA P, MASKEY S, SHRESTHA S (2020) Radiometric analysis of body and canal of lumbar vertebrae among population of central Nepal. *J Coll Med Sci*, 16(2): 57-61.

MUÑOZ-LEIJA MA, YAMAMOTO-RAMOS M, BARRERA-FLORES FJ, TREVIÑO-GONZÁLEZ JL, QUIROGA-GARZA A, MÉNDEZ-SÁENZ MA, CAMPOS-COY MA, ELIZONDO-ROJAS G, GUZMÁN-LÓPEZ S, ELIZONDO-OMAÑA RE (2018) Anatomical variations of the ethmoidal roof: differences between men and women. *Eur Arch Oto-Rhino-Laryngology*, 275(7): 1831-1836.

PAVLOV H, TORG JS, ROBIE B, JAHRE C (1987) Cervical spinal stenosis: Determination with vertebral body ratio method. *Radiology*, 164(3): 771-775.

QUDSIEH H, AL-RAWASHDEH I, DARADKEH A, ABUALNADI T, AL TAH B (2022) Variation of Torg-Pavlov ratio with age, gender, vertebral level, dural sac area, and ethnicity in lumbar magnetic resonance imaging. *J Clin Imaging Sci*, 12(53): 53.

QUIROGA-GARZA A, TERAN-GARZA R, ELIZONDO-OMAÑA RE, GUZMÁN-LÓPEZ S (2020) The use of clinical reasoning skills in the setting of uncertainty: a case of trial femoral head migration. *Anat Sci Educ*, 13(1): 102-106.

TAPIA-NAÑEZ M, QUIROGA-GARZA A, GUERRERO-MENDIVIL FD, SALINAS-ALVAREZ Y, JACOBO-BACA G, DE LA FUENTE-VILLARREAL D, GUZMAN-LOPEZ S, ELIZONDO-OMAÑA RE (2022) A review of the importance of research in Anatomy, an evidence-based science. Eur J Anat, 26(4): 477-486.

TERAN-GARZA R, VERDINES-PEREZ AM, TAMEZ-GARZA C, PINALES-RAZO R, VILCHEZ-CAVAZOS JF, GUTIERREZ-DE LA O J, QUIROGA-GARZA A, ELIZONDO-OMAÑA RE, GUZMAN-LOPEZ S (2021) Anatomical variations of the sacro-iliac joint: a computed tomography study. *Surg Radiol Anat*, 43(6): 819-825.

VÁZQUEZ-BARRAGÁN MÁ, GARZA-BÁEZ A, MORALES-AVALOS R, MARTÍNEZ-GONZÁLEZ B, JACOBO-BACA G, PINALES-RAZO R, QUIROGA-GARZA A, FUENTE-VILLARREAL D, ELIZONDO-ROJAS G, ELIZONDO-OMAÑA RE, GUZMÁN-LÓPEZ S (2016) Pelvimetría mediante tomografía computadorizada reformada sobre 290 pelvis femeninas. Variaciones morfométricas de acuerdo a la edad. *Int J Morphol*, 34(1): 298-304.

VAZQUEZ-ZORRILLA D, MILLAN-ALANIS JM, ALVAREZ-VILLALOBOS NA, ELIZONDO-OMAÑA RE, GUZMAN-LOPEZ S, VILCHEZ-CAVAZOS JF, FERNANDEZ-RODARTE BA, QUIROGA-GARZA A (2020) Anatomy of foot Compartments: a systematic review. *Ann Anat*, 229: 151465. https://doi.org/10.1016/j.aanat.2020.151465

VERBIEST H (1950) Primary stenosis of the lumbar spinal canal in adults, a new syndrome. *Ned Tijdschr Geneeskd*, 94(33): 2415-2433.

VISURI T, ULASKA J, ESKELIN M, PULKKINEN P (2005) Narrowing of lumbar spinal canal predicts chronic low back pain more accurately than intervertebral disc degeneration: a magnetic resonance imaging study in young finnish male conscripts. *Mil Med*, 170(11): 926-930.

YAMMINE K (2014) Evidence-based anatomy. *Clin Anat*, 27(6): 847-852.

ZHANG L, CHEN H-B, WANG Y, ZHANG L-Y, LIU J-C, WANG Z-G (2012) Cervical spinal canal narrowing and cervical neurological injuries. *Chinese J Traumatol*, 15(1): 36-41.

European Journal of Anatomy